Universität Stuttgart

Institut für Wasser- und Umweltsystemmodellierung

Mitteilungen

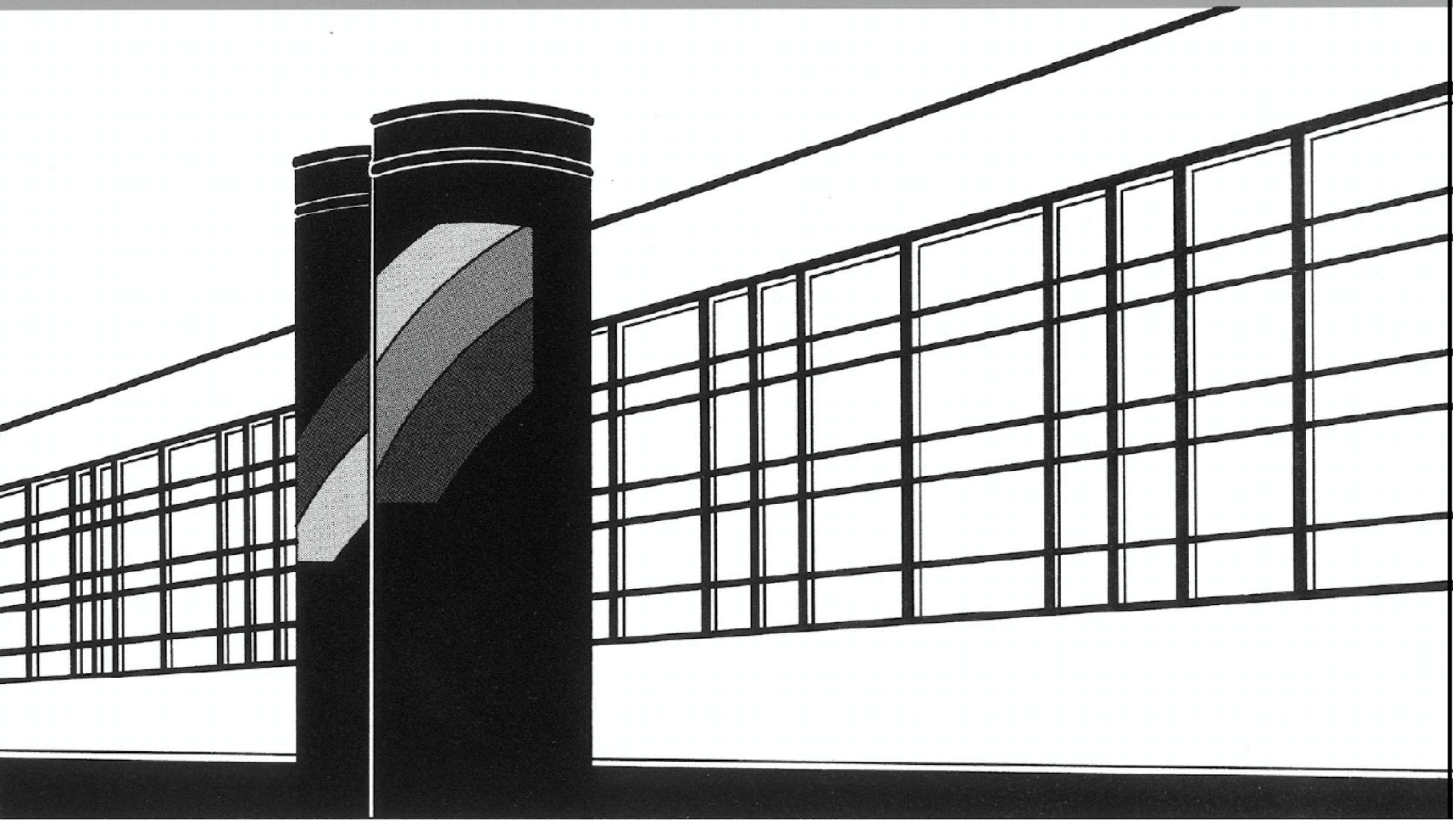

Heft 289 Mohammad Assem Mayar

High-resolution spatio-temporal measurements of the colmation phenomenon under laboratory conditions

High-resolution spatio-temporal measurements of the colmation phenomenon under laboratory conditions

von der Fakultät Bau- und Umweltingenieurwissenschaften der Universität Stuttgart zur Erlangung der Würde eines Doktor-Ingenieurs (Dr.-Ing.) genehmigte Abhandlung

vorgelegt von

Mohammad Assem Mayar

aus Wardak, Afghanistan

Hauptberichter:	Prof. Dr.-Ing. Silke Wieprecht
Mitberichter:	Prof. Dr. Maurizio Righetti
Mitberichter:	Prof. Dr.-Ing. Markus Noack

Tag der mündlichen Prüfung: 07. März 2022

Institut für Wasser- und Umweltsystemmodellierung
der Universität Stuttgart
2022

Heft 289

High-resolution spatio-temporal measurements of the colmation phenomenon under laboratory conditions

von
Dr.-Ing.
Mohammad Assem Mayar

Eigenverlag des Instituts für Wasser- und Umweltsystemmodellierung
der Universität Stuttgart

D93 High-resolution spatio-temporal measurements of the colmation phenomenon under laboratory conditions

Bibliografische Information der Deutschen Nationalbibliothek
Die Deutsche Nationalbibliothek verzeichnet diese Publikation in der Deutschen Nationalbibliografie; detaillierte bibliografische Daten sind im Internet über http://www.d-nb.de abrufbar

Mayar, Mohammad Assem:
High-resolution spatio-temporal measurements of the colmation phenomenon under laboratory conditions, Universität Stuttgart. - Stuttgart: Institut für Wasser- und Umweltsystemmodellierung, 2022

(Mitteilungen Institut für Wasser- und Umweltsystemmodellierung, Universität Stuttgart: H. 289)
Zugl.: Stuttgart, Univ., Diss., 2022
ISBN 978-3-942036-93-1

NE: Institut für Wasser- und Umweltsystemmodellierung <Stuttgart>: Mitteilungen

Herausgegeben 2022 vom Eigenverlag des Instituts für Wasser- und Umweltsystem-modellierung

Druck: DCC Kästl e.K., Ostfildern

Dedication

"To my family"

Declaration

I hereby declare that I have prepared the present work with the title of "High-resolution spatio-temporal measurements of the colmation phenomenon under laboratory conditions" independently and without unauthorized external assistance. There are no other sources and aids except those mentioned and which have identified passages taken verbatim or content-wise from the references used.

Stuttgart, April 07, 2021

Mohammad Assem Mayar

Acknowledgements

Throughout my research period at the University of Stuttgart, I received a great deal of support and assistance.

First, I would like to thank Prof. Dr.-Ing. Silke Wieprecht, head of the Department of Hydraulic Engineering and Water Resources Management at the University of Stuttgart, for accepting me as a Ph.D. student and later for my research and thesis supervision. Without her guidance, support, and encouragement, this thesis would not have been completed. I enjoyed my research work period at the University of Stuttgart and learned a lot through working at the laboratory of the Institute for Modelling Hydraulic and Environmental Systems (IWS).

Further, a special thanks goes to Prof. Dr.-Ing. Markus Noack, the co-supervisor of my thesis and head of the Research Institute for Hydraulic Engineering at the Karlsruhe University of Applied Sciences. He previously worked as Head of the Hydraulic Laboratory at the University of Stuttgart. I thank him for his dedication and continued support during my first years at the University of Stuttgart. I found him very professional, inspiring, and an ideal kind person. I will always remember his behavior and will try to follow him as a role model.

Moreover, I want to express my gratitude to Dr. Stefan Haun, the current head of the Hydraulic Laboratory, for his guidance and support during the recent years of my Ph.D. research work. I would also like to thank the laboratory staff, especially the Technical Scientific Assistant Dip.-Phys. Gerhard Schmid and the hydraulic laboratory's electrical engineer, Mr. Steffen Hägele, for their contribution in configuring the gamma-ray attenuation measurement system. I am also grateful to all my colleagues at the department of Hydraulic Engineering and Water Resources Management for having a pleasurable time in a friendly atmosphere.

In addition, I would like to thank the German academic exchange service (DAAD) for awarding me the scholarship for the Ph.D. research in Germany. Without their financial support, it would not have been feasible to conduct and complete this research.

In the end, I want to thank my parents for their support and prayers during my entire educational journey. It is beyond the words to express my gratitude to them. I also thank my wife, Safia, for her encouragement, patience, and love during my M.Sc. and Ph.D. studies. Finally, I want to thank my sons Mohammad Hamid and Mohammad Jahed for their patience and love during my educational period.

Thank you everyone!

Mohammad Assem Mayar

April 07, 2021

Stuttgart, Germany

The thesis may contain similar and/or identical formulations from my publications:

"Optimizing vertical profile measurements setup of gamma ray attenuation",
"Proof-of-concept for nonintrusive and undisturbed measurement of sediment infiltration masses using gamma-ray attenuation" and
"Measuring vertical distribution and dynamic development of infiltrated sediments under laboratory conditions".

I omit a clear identification for readability and use these parts from the articles with kind permission from the publisher. For the final version of the articles, readers are referred to journals through the DOI links provided in the metadata tables.

Contents

Notations

The following symbols are used in this thesis:

d	[m]	diameter of small spheres used in the bed configuration
D	[m]	diameter of large spheres used in the bed configuration
d_c	[m]	thickness of the colmation layer
d_m	[m]	mean grain size of the bed materials
d_{mix}	[mm]	diameter of mixed sediments supplied to experiments
d_s	[mm]	diameter of homogenous sediments supplied to experiments
Q	$[m^3/s]$	water discharge
t	[s]	time / duration
ρ_s	$[kg/m^3]$	density of the sediments
I_0	[counts per second - cps]	initial count rate emitted from the gamma source
I_x	[counts per second - cps]	transmitted count rate after passing the penetrating media
X	[m]	thickness of the measuring object through the Gamma-ray attenuation method
x	[-]	lateral / cross-sectional axis
y	[-]	longitudinal axis
z	[-]	vertical axis

Abbreviations

The following abbreviations are used in this thesis:

Al	Aluminum
GRA	Gamma-Ray Attenuation
PP	Polypropylene
PIV	Particle Image Velocimetry
PVC	Polyvinylchloride

List of Figures

List of Tables

Abstract

The fine sediment infiltration and accumulation into the gravel bed of rivers, the so-called colmation phenomenon, is a pernicious process exacerbated by anthropogenic activities. Owing to the importance and complexity of this phenomenon, it has been widely studied over the last decades. Various devices and methods have been developed to assess this phenomenon, where most of them are destructive and sample-based, resulting in an alteration of the natural conditions. Therefore, non-intrusive techniques, which provide spatial and temporal details with a high-resolution, are required to discretize the mechanisms involved in the colmation process. To address these issues, investigations under laboratory conditions may simplify the complexity of nature and enable individual and exactly defined boundary conditions to be investigated. Therefore, this thesis aims at (i) developing a non-intrusive and undisturbed measurement method for the high-resolution spatio-temporal measurements of the sediment infiltration processes and the development of sediment accumulation in an artificial river bed under laboratory conditions, (ii) applying this method to certain experiments for the assessment of the effects of different boundary conditions on sediment infiltration, and (iii) investigating the colmation phenomenon (also known as clogging) of gravel beds. For this purpose, the gamma-ray attenuation method is used together with an artificial gravel bed arranged from the spheres with various diameters and placed in a laboratory flume. This new method works based on the gamma radiation that passes through the infiltrated sediments, water, and bed spheres, in which the gamma-ray attenuation is linked to the variations of the infiltrated sediments' quantity. The main simplification of this approach is that gravel beds are represented by the combinations of different-sized spheres. This gives the opportunity to fully distinguish infiltrating sediments from the bed material, reduce the complexity of the natural environment, and allows for repetitive measurements of the same position with different boundary conditions.

From the results of this study, first, the gamma-ray attenuation measurement method was optimized to resolve the inconsistencies in the measurements. Subsequently, the concept of the non-intrusive and undisturbed measurement is proved through box experiments. Additional reproducibility experiments in the laboratory flume, for a similar bed structure, showed only small deviations between two experiments with the same setup. Consequently, the established technique was used in a series of experiments to evaluate the effects of different supply rates, total supply masses, and sediment particle size boundary conditions on the sediment infiltration and colmation processes. Vertical profiles of the infiltrated sediment were quantified through high spatial resolution measurements. Furthermore, to evaluate the infiltrating sediment accumulation development, and the temporal variations of the infiltrated sediments, the vertical profile measurements were first repeated after a specific time-period to track interval-averaged variations in all positions of the vertical axis. Next, a specific position of the vertical axis was measured continuously during the entire experiment in a high temporal resolution.

The measured vertical profiles illustrate the vertical distribution, colmation, and unimpeded percolation of the infiltrated sediments. The dynamic one-point measurement precisely identifies the three phases (the start of the pore-filling, the required time to fill the pore, and the final amount of infiltrated sediments including natural fluctuation during the ongoing experiments) of the sediment infiltration or the possible clogging.

As a limitation, the gamma-ray attenuation system's current configuration only works in artificial gravel beds because of the given density difference between infiltrated sediments and the artificial bed structure. Intense radiations that pass through the natural bed's thickness are capable of detecting a significant amount of infiltrated sediments. However, small amounts of infiltrated sediments will create only a minimal shift in attenuation, which might be confused with the statistical error. In addition, the legal restriction against using radioactive material in the natural environment is another reason for not applying it in the field. Furthermore, the gamma-ray attenuation method cannot resolve the sediment distribution in the measurement horizon and provides an integrative result for each measurement position. In addition, if a mixture of silt, clay, and sand is supplied to the experiment, the gamma-ray attenuation system will produce a bulk result of all the infiltrated materials.

To conclude, despite the limitations mentioned above, the gamma-ray attenuation method offers a unique opportunity for the non-intrusive and undisturbed measurements of the sediment infiltration or the special case of colmation, with a high spatio-temporal resolution. This method has the potential to quantify the investigated processes on a millimetric spatial scale, if the measurement time is not a constraint, or vice versa, in a high temporal resolution (seconds) for a specific position, if spatial scale is not important. Moreover, the gamma-ray attenuation approach can simultaneously measure the longitudinal distribution of the sedimentological processes, if multiple instruments or a single device with several radiation-emitting-holes is in operation. Last, but not least, rather than the spheres, artificial gravel beds could be made of any substance with a composition significantly different from the infiltrating sediments, and the boundary conditions of the experiments can be improved in order to attain conditions close to nature. Finally, the gamma-ray attenuation method can be integrated with advanced flow measurement instruments such as Particle Image Velocimetry (PIV) and other high-resolution endoscopic devices to track the behavior of fine sediment infiltration and its clogging process in the porous gravel beds as it occurs in nature.

Kurzfassung

Die Infiltration und Akkumulation von Feinsedimenten in das Kieslückensystem von Fließgewässern – auch bekannt unter dem Begriff der Kolmation – wirkt sich negativ auf die Gewässerökologie aus und wird durch anthropogene Aktivitäten noch verschärft. Aufgrund der Bedeutung und Komplexität ist das Phänomen Kolmation in den letzten Jahrzehnten in zahlreichen wissenschaftlichen Studien untersucht worden. Für die Bestimmung und Bewertung der Kolmation wurden hierfür verschiedenste Geräte und Methoden entwickelt, die zumeist auf Einzeluntersuchungen basieren und destruktiv funktionieren. Daher werden nicht-intrusive Techniken benötigt, die in der Lage sind sowohl räumlich als auch zeitlich hochauflösend die Entwicklung der an der Kolmation beteiligten Prozesse messtechnisch zu erfassen. Diesbezüglich bieten experimentelle Laboruntersuchungen die Möglichkeit die Komplexität der Natur auf einzelne diskrete Prozesse zu reduzieren und gezielt bestimmte Randbedingungen exakt einzustellen. Die Ziele dieser Arbeit umfassen daher (i) die Entwicklung einer nicht-intrusiven und nicht-destruktiven Messmethode für sowohl in Raum und Zeit hochauflösende Messungen von Infiltrationsprozessen, sowie die Akkumulation der infiltrierenden Feinsedimente („Verstopfung“) in künstlichen Gewässerbetten unter kontrollierten Laborbedingungen, (ii) die Anwendung der entwickelten Methode auf ausgewählte Experimente zur Abschätzung der Auswirkungen unterschiedlicher Randbedingungen auf die Sedimentinfiltrationsprozesse und (iii) die Verstopfung der Poren im Rahmen des Kolmationsprozesses zu untersuchen. Hierfür wird die Gamma-Absorptions-Methode gemeinsam mit einem künstlich hergestellten Gewässerbett verwendet. Das Gewässerbett besteht aus rundförmigen Kugeln mit unterschiedlichen Durchmessern und wird mit unterschiedlichen Lagerungsdichten aufgebaut. Die Gamma-Absorptions-Methode basiert auf der Abschwächung der Gamma-Strahlung beim Durchstrahlen des Laborgerinnes mit Gewässerbett, Wasser und infiltrierten Sedimenten, wobei aus dem Maß der Abschwächung auf die infiltrierten Sedimentmengen rückgeschlossen werden kann. Die größte Vereinfachung gegenüber dem natürlichen Prozess besteht in dem künstlichen Gewässerbett mit Kombinationen von Kugeln unterschiedlicher Größe, die mit Luft gefüllt sind und somit vollständig von den infiltrierenden Feinsedimenten unterschieden werden können. Dies reduziert die Komplexität des Kolmationsprozesses und ermöglicht Wiederholungsmessungen an identischen Stellen bei unterschiedlichen Randbedingungen.

Ausgehend von den Ergebnissen dieser Studie wurde zunächst die Methode zur Messung der Gammastrahlenabsorption optimiert, um Unstimmigkeiten bei den Messungen zu beseitigen. Anschließend wurde das Messkonzept der nicht-intrusiven und ungestörten Messung durch Box-Experimente verifiziert und nachgewiesen. Zusätzliche Wiederholungsexperimente in der Laborrinne mit vergleichbarem Aufbau des Gewässerbetts zeigten nur geringe Abweichungen zwischen zwei Experimenten. Daraufhin wurde die nun verifizierte Messtechnik in einer Versuchsreihe zur Untersuchung des Einflusses von Randbedingungen

(Sedimentzugaberaten, Zugabemassen, Partikelgrößen des zugegebenen Feinmaterials) eingesetzt, um die Auswirkungen auf die Sedimentinfiltrations- und -akkumulationsprozesse zu untersuchen. Vertikale Profile der infiltrierten Sedimentmengen wurden mittels räumlich hochauflösenden Messungen quantifiziert. Um die Entwicklung der infiltrierenden Sedimente und die zunehmende Verstopfung der Poren zu bewerten (zeitliche Kolmationsentwicklung) wurden die vertikalen Profilmessungen zunächst nach einem bestimmten Zeitraum wiederholt, um mögliche Variationen in allen Positionen der vertikalen Achse erfassen zu können. Zusätzlich wurde während der gesamten Experimentdauer an einer bestimmten Position der vertikalen Achse kontinuierlich und mit hoher zeitlicher Auflösung die Infiltrationsmasse gemessen (Ein-Punkt-Messung). Die gemessenen Vertikalprofile veranschaulichen die vertikale Verteilung, das Ausmaß der Porenverfüllung und die weitestgehend ungehinderte Infiltration der Feinsedimente. Die dynamische Ein-Punkt-Messung identifiziert präzise die drei Phasen: Beginn der Porenfüllung, die benötigte Zeit zum Füllen der Pore und die finale Infiltrationsmenge inklusive der natürlichen Fluktuationen während der Experimente.

Die derzeitige Konfiguration der Gamma-Absorptions-Methode funktioniert nur in künstlichen Gewässerbetten im Labor, da ein großer Dichteunterschied zwischen infiltrierenden Feinsedimenten und der künstlichen Bettstruktur benötigt wird. Eine starke Strahlung kann die Mächtigkeit eines natürlichen Gewässerbettes durchdringen und somit auch signifikante Mengen an infiltrierten Sedimenten detektieren, jedoch führen geringe Infiltrationsmengen nur zu einer minimalen Strahlenabsorption, was leicht mit einem statistischen Fehler der Gamma-Strahlung verwechselt werden könnte. Ein weiterer Grund für den Verzicht auf den Einsatz von radioaktivem Material in der Natur sind die gesetzlichen Beschränkungen für die Anwendung in der Praxis. Darüber hinaus kann die Gamma-Absorptionsmethode die horizontale Verteilung der Infiltrationsmengen nicht auflösen und liefert für jede vertikale Position lediglich ein integratives Ergebnis. Besteht das Zugabematerial aus verschiedenen Materialen (z. B. ein Gemisch aus Schluff, Ton und Sand) gibt die Gamma-Absorptions-Methode ebenfalls nur ein integratives Ergebnis der Strahlenabschwächung für alle infiltrierenden Materialien aus.

Zusammenfassend lässt sich schlussfolgern, dass die Gamma-Absorptions-Methode trotz der oben erwähnten Einschränkungen eine bisher einzigartige Möglichkeit zur nicht-intrusiven und ungestörten Messung der Sedimentinfiltration bzw. der Kolmation mit einer hohen räumlichen und zeitlichen Auflösung bietet. Diese Methode hat das Potenzial, die untersuchten Prozesse auf einer räumlichen Skala im Millimeterbereich zu quantifizieren, solange die Messdauer nicht limitierend ist. Andersherum können die Infiltrationsprozesse zeitlich hoch aufgelöst werden (Sekundenbereich), wenn der räumliche Aspekt nicht relevant ist. Darüber hinaus bietet die Gamma-Absorptions-Methode bei Verwendung mehrerer Geräte die Längsverteilung des Infiltrationsprozess messtechnisch zu erfassen. Weiterhin können anstelle von luftgefüllten Kugeln auch künstliche Gewässerbette aus beliebiger Substanz hergestellt werden, solange deren Dichte sich eindeutig von dem infiltrierenden Material unterscheidet. Außerdem können die Einstellungen der Randbedingungen für die Durchführung der Experimente noch optimiert bzw. an naturnähere Bedingungen angepasst werden. Ein weiterer Ausblick beinhaltet die Kombination der Gamma-Absorptionsmethode mit hochentwickelten mehrdimensionalen Strömungsmessungen (z. B. Particle Image Velocimetry, PIV) oder die Verwendung von endoskopischen Geräten, um das Verhalten der infiltrierenden Feinsedimente

sowie deren Akkumulation in Kieslückensystemen noch detaillierter zu erfassen.

1. Introduction

1.1. Background

Sediment transport in rivers is a natural phenomenon that conveys fine sediments as suspended and coarser material as bed loads from the upper reaches further downstream. This phenomenon affects the river morphology through the erosion and deposition processes that are in a dynamic balance in natural rivers. However, anthropogenic activities in the catchment and river disrupt this equilibrium conditions. For example, increased supplies of fine sediments to the river caused by deforestation, intensive agriculture, and urbanization in the basin, as well as river management measures conducted in the past, result in the fact that the stabilizing forces become larger than the driving forces of the transported sediments. Thus, the transported sediment particles deposit and infiltrate into the porous gravel bed of rivers. This process reduces the initial porosity of the gravel bed, and in a worst-case scenario, can entirely clog the river bed. As a result of the sediment infiltration into gravel beds, the reduction of permeability (Schälchli, 1992), the decrease of surface and subsurface flow exchange (Gayraud and Philippe, 2003), the degraded supply of dissolved oxygen to aquatic species living in the hyporheic zone, and the recession of reproduction of the gravel-spawning fishes (Tonina and Buffington, 2009; Noack et al., 2016) are observed. The whole process of fine sediment infiltration and accumulation in the gravel beds, which reduce the bed permeability and influence surface and subsurface exchange processes, is called colmation or clogging. The magnitude of sediment infiltration varies, on the one hand, spatially, as a result of the stream bed structures (pool, riffle), and, on the other hand, temporally, owing to the supply of fine sediments and the unsteady flow conditions. Hence, it is a highly complex and spatio-temporally dynamic phenomenon.

The colmation process depends on several physical, chemical, and biological factors. Physical parameters governing this phenomenon are the river bed characteristics, sediment particle size and shape, supply rate, type of infiltration, surface, and interstitial flow forces. The type and amount of organic materials and their residence time are the chemical factors. Similarly, biological factors include the variety of invertebrates, red algae, their commonness, and the extent of eutrophy of the water which makes a cohesive layer on the gravel surface that retains sediment particles (Schälchli 1992; Noack 2012). A classification of the influencing parameters and development processes divides colmation into physical, biological, and chemical types. Despite that, the position of clogged sediments also classifies this phenomenon into internal, intermediate, and external categories (Noack, 2012). More details about the colmation process, type, and influencing factors are described within the next chapter.

A decreased initial porosity of a river bed due to fine sediment infiltration may result in negative ecological consequences. For instance, it reduces the pore space, surface and subsurface exchange processes, and the supply of dissolved oxygen to the interstitial habitats, which hinder the reproduction of aquatic species (Noack, 2012). As a result, this species reduction, which is due to colmation, does not allow good ecological conditions to be achieved in the rivers. According to Pätzig et al. (2019), one significant aspect of the inability of the European water framework directive to achieve a good ecological status is the effect of the colmation process and its ecological consequences for interstitial ecosystems. Therefore, deeper understanding of this phenomenon is needed to seek a solution to minimize or avoid colmation in the rivers.

The complex phenomenon of colmation has been intensively studied in the field and laboratory. Sediment infiltration into the gravel bed of rivers, as a primary parameter of the colmation phenomenon, has been investigated by several researchers in the field (Beschta and Jackson 1979; Frostick et al. 1984; Zimmermann and Lapointe 2005; Evans and Wilcox 2014; Harper et al. 2017), in the laboratory (Einstein 1968; Wooster et al. 2008; Gibson et al. 2009a, 2011; Dudill et al. 2017; Mayar et al. 2020), or by using numerical simulations and mathematical models (Bui et al. 2020; Herrero and Berni 2016; Noack 2012; Schälchli 1995; Lisle and Lewis 1992). But there are still gaps in our knowledge due to the complex processes involved in colmation, resulting in a large number of involved variables, but also as result of the limitation of the current measurement methods. Colmation occurs in rivers, but due to the complexity of natural environment and the large number of parameters involved, it is difficult to investigate the phenomenon-involved mechanisms in situ. However, laboratory experiments allow the effects of various parameters and different boundary conditions to be examined distinctly. Thus, flume experiments decrease the complexity of the natural conditions in this study. For instance, the biological and chemical aspects of colmation are not considered, and artificial bed structures are designed for the investigation of the physical parameters of this phenomenon during this research.

Finally, to gain more knowledge of the infiltration processes, and precisely quantify the colmation, a high-resolution non-intrusive and undisturbed measurement method is required. Hence, this thesis first focuses on the development of a new non-destructive measurement method. During a second step, the spatio–temporal variation of the physical colmation is investigated under the laboratory conditions by using the developed high-resolution approach. To gain additional insight, several boundary conditions, including different sediment particle-size mixtures, supply rates, and total supplied sediment masses have been tested.

1.2. Motivation and objectives

The colmation of gravel bed rivers relies on a variety of physical, chemical, and biological factors. Physical parameters play a prominent role in the sediment infiltration and for accumulation processes. Thus, researchers have focused mainly in investigating the physical aspect of the colmation phenomenon (Einstein 1968; Beschta and Jackson 1979; Schälchli 1993; Wooster et al. 2008). However, biological and chemical aspects of the colmation process have also been studied (Beyer et al. 1975; Wood 1997; Schwarz et al. 2003) in order to define their impacts.

There are numerous methods and devices for the assessment of colmation. Seitz et al. (2019) identified, through a survey from experts, 35 approaches, which consider various single parameters for the assessment of colmation. Most of these approaches focus on the measurement of infiltrated sediments. Harper et al. (2017) suggested paying attention to the interpretation of findings obtained by various approaches due to the consideration of different parameters and device setups. Most of the existing methods are disruptive approaches that alter the natural conditions during the sampler installation and extraction. For example, sediment cylindrical sampling devices (Blomqvist and Abrahamsson 1985; Reikowski 2015), various types of built-in sediment traps (Frostick et al. 1984; Newson and Sear 1994; Wilcock et al. 1996), freeze coring (Noack, 2012), bulk-sampling and sediment bags (Evans and Wilcox 2014), are techniques that destroy the natural stream bed during extraction, which subsequently influence the quantification of sediment infiltration at this point. Furthermore, most of these methods present vertically averaged results and cannot evaluate the vertical distribution of infiltrated sediments. Additionally, they can only measure the infiltrated sediments at a particular location once. However, in some cases, the temporal changes are measured by installing several samplers together and extracting them at intervals ranging from 14 to 400 days (Harper et al. 2017). But these methods, based on sample extraction, alter the natural conditions and are not appropriate for detecting temporal variations of the infiltrated sediments exactly at the same position with a temporal resolution that enables the distinction of the mechanisms involved. An exception is a submersible linear displacement transducer placed under a sediment capture tray used by Fletcher et al. (1995) to track fine sediment intrusion into stable gravel stream beds. This device provides a depth-integrated result of the temporal variation but cannot consider the vertical distribution of infiltrated sediments.

In contrast, laboratory measurement techniques can provide more details. For example, the core and cubed sampling devices (Wooster et al. 2008; Gibson et al. 2009a,b, 2011) used in laboratory experiments provide the vertical distribution of the infiltrated sediments with a resolution depending on the bed gravel size and manual separation of the layers. Furthermore, Gibson et al. (2011) used a photometric approach to assess the distribution of colored sediments following the manual removal of the layers from sediment cores in the laboratory. However, these approaches are also disruptive and change the natural conditions through extracting the sample that limits the precision of measurements. Some indirect methods, such as tracking of suspended sediment concentration balance over time in the flume (Hamm et al. 2011; Herrero et al. 2015), monitoring water pressure and conductivity of the gravel bed (Schälchli 1992, 1995), and visual observation of infiltrated sediment height evolution captured by the camera through a transparent sidewall of the laboratory flume (Herrero et al. 2015) have been applied for infiltrated sediment measurements. However, these laboratory methods can have an integrative result for the entire experiment and cannot determine the infiltrated sediments at a given place and over time. In addition, Rosenbrand and Dijkstra (2012) and Niño et al. (2018) used imaging methods for quantifying suffusion and fine sediment transport in a transparent laboratory flume. But these approaches can only assess near-wall sediment flow that could be influenced by wall friction.

As described above, most of the conducted studies only consider the sum of infiltrated mass as a proxy parameter for the degree of colmation in the gravel beds. However, measurements of the infiltrated sediment masses, particularly as a sum parameter over depth, are not sufficient to understand the processes and interactions of the sediment infiltration. Therefore, it is necessary to gain further knowledge about the clogging and its underlying process by using new methods compatible with the current requirements. With the available technology of penetrating radiation, it is appropriate to move toward a non-intrusive and undisturbed measurement of the sediment infiltration and accumulation processes or their particular case of colmation.

For this reason, the Gamma-Ray Attenuation (GRA) method, which has so far been used for undisturbed measurements of material's physical properties in a static situation, e.g., soil bulk density, water content, porosity (Pires and Pereira 2014; Pires et al. 2009; Baytaş and Akbal 2002; Gerland and Villinger 1995; Reginato 1974; Cassel and Krueger 1972), soil columns hydraulic conductivity, and reservoir sediment's bulk density profiles measurements (Beckers et al. 2018; Moreira et al. 2011, 2007; Gerland and Villinger 1995), was used in a laboratory flume for the high-resolution spatio-temporal measurements of the physical parameters of the colmation phenomenon.

In order to achieve this goal, the objectives have been set as follows:

1. To optimize the GRA measurements setup for the best composition of spatial and temporal resolution with an acceptable statistical error.
2. To prove the concept of a non-intrusive and undisturbed measurement method for the infiltrated sediment masses and its high-resolution vertical distribution.
3. To investigate the effects of various boundary conditions on the spatial and temporal development of the sediment infiltration and accumulation (physical colmation) processes.

To fully distinguish the infiltrating sediment with gravels in the bed, the complexity of the natural gravel bed was reduced in order to achieve a high-resolution result. Additionally, the reproducibility of the experiments and different boundary conditions in exactly the same location were tested as well as artificial bed configurations in the laboratory flume were made from different-sized spheres in cubic and rhombohedral packings. More details about the flume setup and methods are given in Chapter 3.

1.3. Structure of the thesis

Besides three scientific peer-reviewed journal publications, this Ph.D. thesis gives additional information on the topic and applied methods within five chapters. The first chapter gives an introduction to the topic and discusses the background and motivation for this research work. The second chapter presents an overview of the fundamentals of the colmation phenomenon. Within this chapter, the basics of colmation process, influencing parameters, and the consequences of this phenomenon are summarized. Furthermore, this chapter discusses the limitations of the existing assessment methods as well as the necessity of a non-intrusive and undisturbed measurement method for the spatio-temporal investigation of sediment infiltration, accumulation and resulting colmation in the gravel bed. The third chapter discribes the developed approach in details. This chapter covers the optimization of the spatial and temporal resolution, including the accuracy of the measurements, the proof of concept for undisturbed measurements of infiltrated sediments, and gives details of the experimental setup and the investigated boundary conditions. The fourth chapter presents summaries of the published papers to get an overview of the published results. Finally, the fifth chapter concludes the results, discusses the limitations and gives an outlook and recommendations for further research in this field. At the end of this thesis, the manuscripts of the published papers are attached in the appendices I , II, and III.

2. Fundamentals of the colmation process

2.1. Colmation

Colmation is the process where fine sediments infiltrate porous gravel beds of rivers, with a comparable coarser matrix, and clog the river bed by forming a colmation layer. This process reduces the permeability of the porous gravel beds, compared to the initial conditions (Blaschke et al. 2003; Brunke and Gonser 1997; Schälchli 1993; Cunningham et al. 1987). Colmation occurs whenever stabilizing forces exceed the sediments conveyance forces in the river channels. Colmation is a complex process that occurs naturally in river systems during low flow, particularly when transporting fine particles which can be deposited and enter the gravel matrix of river beds (Brunke and Gonser 1997). The opposite process, such as suffusion or the resuspension of deposited fine particles, is called decolmation (Brunke, 1999), which occurs during high flow events, or due to up-welling of the groundwater (Blaschke et al., 2003). In active natural rivers, frequent peak flows erode the fine sediments and reopen the clogged river beds (Schälchli 1992). The degree of sediment resuspension depends on the erosion potential of the peak flow (Noack 2012). Both, colmation and decolmation processes, form a cycle in natural river beds (Blaschke et al., 2003; Brunke, 1998), because of the variations in the flow regime and sediment conditions. The balance between colmation and decolmation can be significantly influenced by the level of anthropogenic activities (Hancock, 2002; Baker et al., 2011).

2.2. Types of colmation

Due to multidisciplinary investigations of this phenomenon over the past decades, colmation is defined differently in literature. Terms such as embeddedness, colmation, clogging, infilling, and ingress are used, sometimes also with a reference to their position (i.e., internal, intermediate, and external colmation) to describe the deposition, infiltration, and accumulation of organic and inorganic fine materials in the gravel beds of rivers. A common understanding of all definitions is the resulting decrease in the initial porosity and permeability (Mohajeri 2015; Noack 2012). To date, there is no universal definition or criterion to distinguish between these terms. Similarly, these terms are often used synonymously in the scientific literature. For example, the term embeddedness is used for the degree to which coarser particles are surrounded by fine materials (Platts, 1982), and is mostly used by fish biologist to quantify the amount of fine sediments in the river (Bunte and Abt, 2001). This event occurs on the surface and subsurface of the gravel bed according to the infiltrating particle size, called outer and inner embeddedness, respectively. Furthermore, clogging is mostly used for the physical infiltration processes

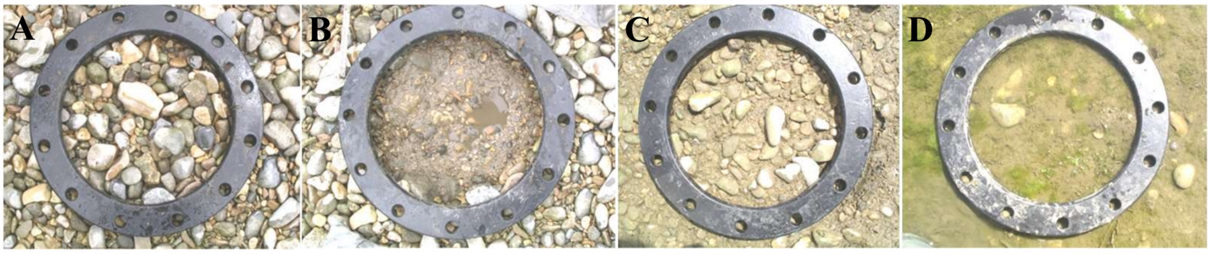

Figure 2.1. Types of the colmation observed in natural rivers: (A) No colmation, (B) internal colmation, (C) surface colmation, and (D) external colmation (Pictures: Eastman 2004)

(Blaschke et al., 2003), while colmation and clogging both include biological and chemical processes. The terms infilling and ingress are used in groundwater hydrology (McCloskey and Finnemore, 1996) and geomorphology, respectively. Here, the term colmation is used for the fine sediment infiltration and its clogging in the porous gravel beds.

Similarly, several authors have divided the colmation phenomenon into physical, biological, and chemical colmation (Baveye et al., 1998). The physical colmation addresses the fine sediment deposition, accumulation, and infiltration into porous gravel beds of rivers (Descloux et al., 2010). Biological colmation concentrates on microbial interactions contributing to interstitial biofilms with adhesive capacities that reduce the pore transects (Beyer et al., 1975). The chemical colmation is related to the iron clogging, redox potentials, ion exchange, and flocculation that alters the geometry of the canal pores by disaggregation and dispersion or swelling (Schwarz et al., 2003).

External colmation is very unstable and happens when fine material, which is larger than the pore size in the gravel-matrix of the river bed, is deposited as result of hydrodynamic forces, which are too small to transport fine materials further downstream (Beyer et al., 1975). This event can arise because of either an increase in fine sediment load, or a reduction in flow velocities. Sadid et al. (2017) observed external colmation in dryland rivers and streams with intensive fine sediment delivery, single peak flow regime, and prolonged dry periods. The abundance of fine sediments and the absence of base flows are considered to be the main drivers of external colmation in dryland intermittent rivers and streams (Sadid et al., 2016, 2017). Internal colmation happens when the suspended load is deposited into the interstitial pores lower than the armor layer in the river bed. A second possibility is that, fines move upward from the underlying layers, containing fine sediments, collect beneath the armor layer, and resulting in a distinctive colmation layer (Schälchli, 1992; Cunningham et al., 1987; Frostick et al., 1984). A third type of colmation is when fine sediments infiltrate and clog within the coarse top layer. This is called contact, intermediate, or armor layer colmation, which occurs in between external and internal colmation positions (Velickovic 2005; Blaschke et al. 2003). For a better understanding, three types of colmation in the natural rivers are shown in Figure 2.1.

Figure 2.1A depicts a river bed that is unclogged with larger pores and high permeability. Figure 2.1B represents internal or subsurface colmation, visible when the surface layer is removed. Figure 2.1C visualizes surface colmation or an embedded surface layer, while Figure 2.1D illustrates the external colmation or outer embeddedness with fine particles deposited on the surface of the river bed.

Furthermore, the conceptual diagrams of the external colmation, internal colmation, and decolmation processes are shown in Figure 2.2. Figure 2.2A shows the development of external colmation owing to the increased supply of fine sediments, reduced flow velocity and transport capacity. In this case, the larger particles first clog the gravel pores and, subsequently, fine and coarse sediments accumulate on the surface of the gravel bed. Figure 2.2B shows the internal colmation as result of fine particles infiltration into the gravel bed, because of the reduced flow velocity and transport capacity. Fine sediments penetrate the gravel matrix through the gaps in the armor layer and preferably accumulate near the filter layer. The boundary between the armor and filter layers serves as an interface between the coarse and the fine substrates and forms a thin colmation layer. Figure 2.2C indicates a special case of the internal colmation induced by the upward movement of the fines from underlying layers. In this case, the coarser gravels in the armor layer are tightly packed; suspended particles do not exist in the river flow to infiltrate. Hence, the upward moving fine particles form a colmation (seal) layer below the armor layer. Due to high flow conditions in Figure 2.2D, the velocity, transport capacity, and turbulence increase, which leads to erosion of the fine particles. Thus, the deposited fine particles are re-suspended, and is called the decolmation process.

2.2.1. Causes for colmation and parameters influencing and intensifying colmation

The key parameter of gravel bed colmation is the amount of fine sediments transported in the rivers. These sediments come from the catchment and upstream river sections as result of soil erosion. Although fine sediment infiltration itself does not have negative effects, hydromorphological changes (decolmation) occur. However, deposition of a high amount of fines into the gravel bed and the changing of the river's natural flow regime because of the anthropogenic activities can cause negative environmental effects (Seitz, 2020).

Furthermore, the colmation process can be exacerbated due to anthropogenic activities such as urbanization, deforestation (Frostick et al., 1984; Owens et al., 2005), and dam construction. For instance, the construction of barriers, dams, and reservoirs dramatically alters the natural flow regime, leading to a loss of peak flow and the modification of natural beds. This prevents the natural flushing of fine sediments from the river bed, which results in excessive deposition of fine sediments (Kondolf et al., 2014).

From an integrative point of view, the colmation layer's evolution is determined by a wide range of spatial and temporal variables interlinked in a dynamic framework of interactions shown in Figure 2.3.

Figure 2.3 shows the anthropogenic activities of agriculture, deforestation, and mining as examples for measures that intensify the erosion process in a basin, which later changes the river's flow and sediment regimes that cause colmation. Furthermore, the parameters are classified into physical, biological, and chemical groups, in which the physical parameters are subdivided into different sub-groups such as hydrology, geohydrology, hydraulics, and morphology.

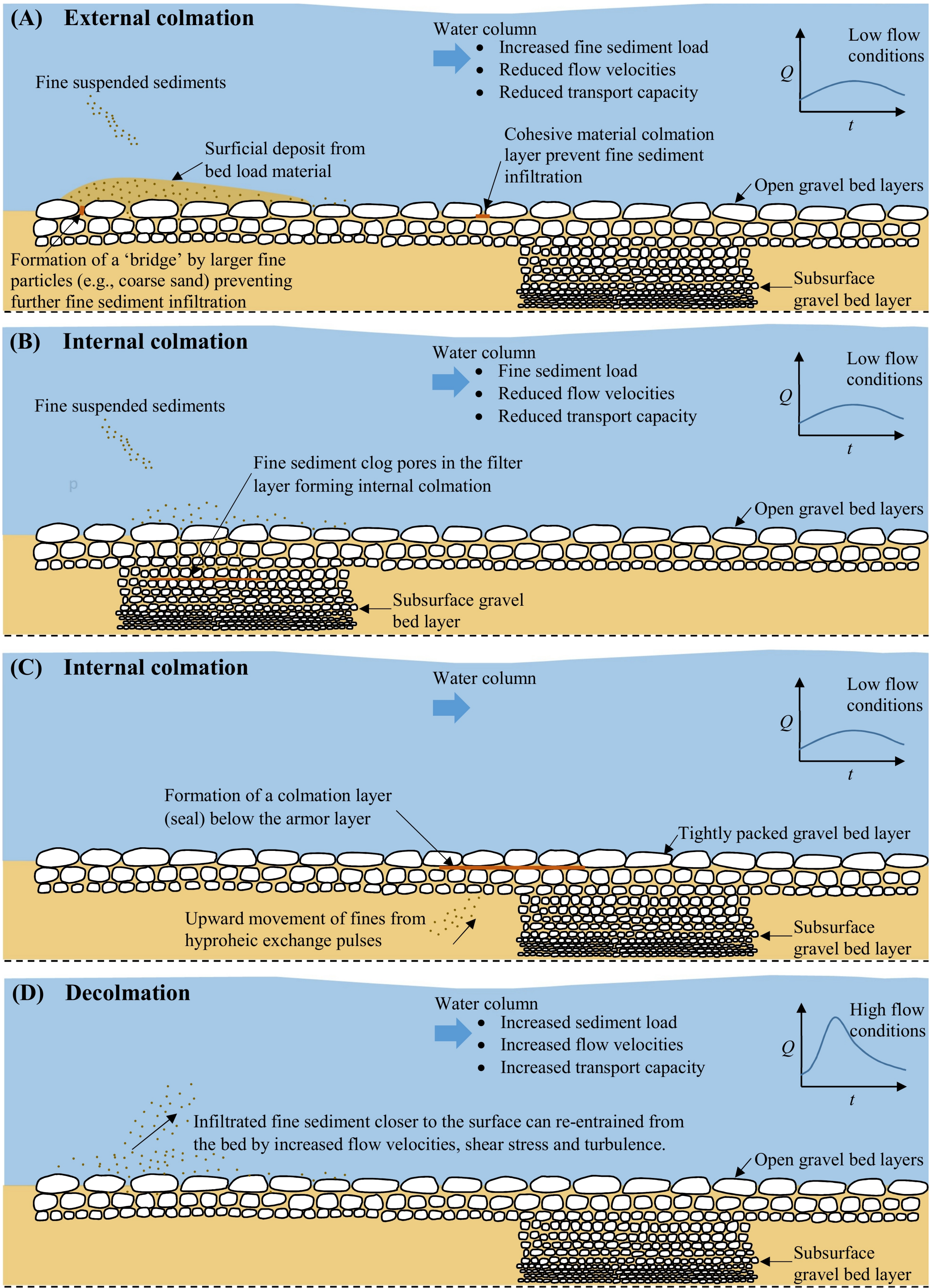

Figure 2.2. Conceptual diagram illustrating the processes of (A) external colmation (B) internal colmation due to the infiltration of suspended fine particles, (C) internal colmation because of the fine particles upward movement, and (D) the decolmation process development.

Despite the impact of the biological and chemical parameters on the infiltration and colmation of river beds, the focus of this thesis is set on the physical colmation induced by the sediment infiltration. Biological and chemical factors are therefore not discussed in the current work.

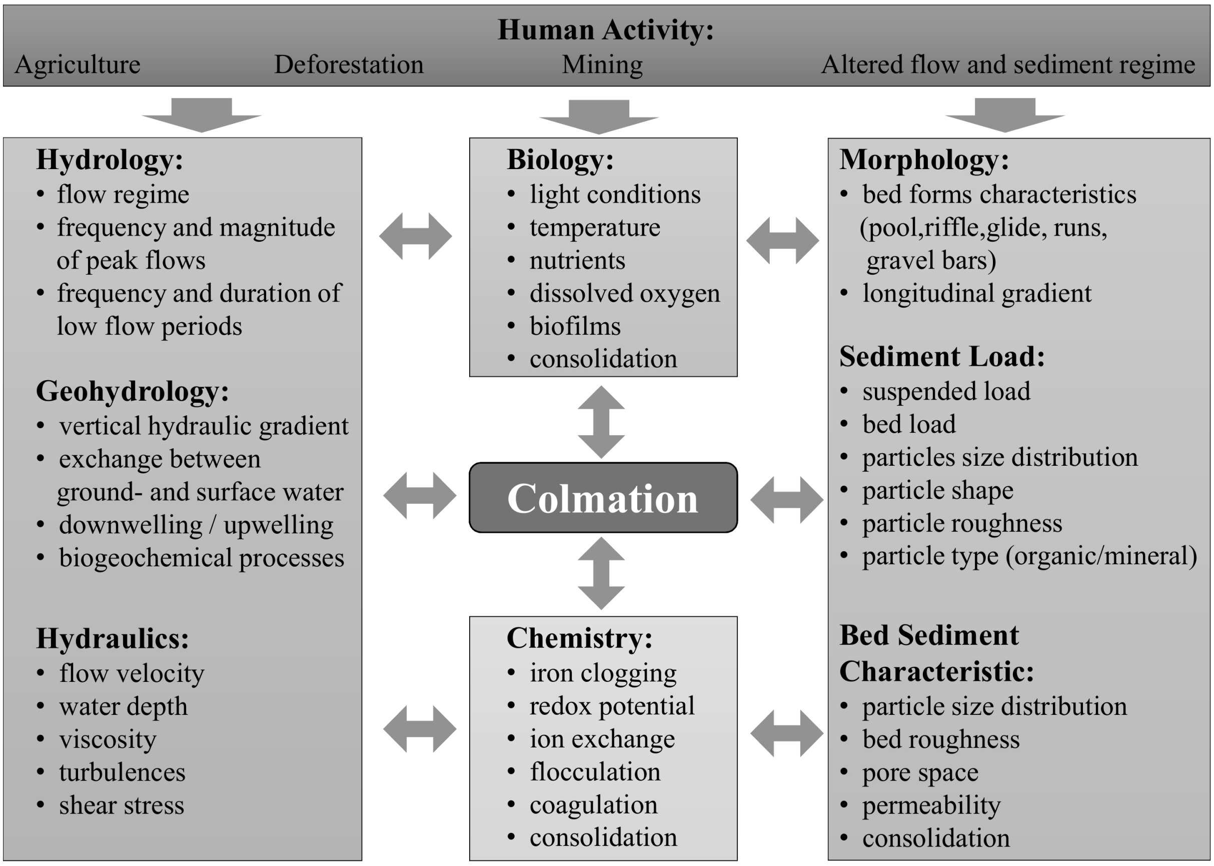

Figure 2.3. Factors and processes influencing the colmation phenomenon (Noack, 2012).

2.2.2. Structure of river beds

Typically, the vertical distribution of a river bed (Figure 2.4A) can be subdivided into three distinct layers, which play an important role for colmation (Schälchli, 1993). The top layer is called the armor layer, developed from the coarser materials that are resistant to high-flow conditions. Fine particles from the inistially fully mixed bed material are usually washed out during small to mean flow events. The filter and subsurface layers are the two layers located beneath the armor layer, respectively. Fine sediments penetrate the gravel matrix through the gaps in the armor layer and preferably accumulate near the filter layer. The boundary between the armor and filter layers serves as an interface between the coarse substrate and the fine substrate and forms a thin colmation layer. The filter layer is characterized by a lower porosity and a lower hydraulic conductivity than the subsurface layer (Seitz, 2020). In the case of very fine sediments such as suspended load and a coarse filter layer, fine sediments can infiltrate to the subsurface layer. The formation of a fourth layer (Figure 2.4B), called the skeleton layer, was also observed locally by Schälchli (1993). This layer grows beneath the armor layer and is as porous as the armor layer. Owing to the turbulence in this layer, there is no deposition of fine particles visible within it. Thus, it can be considered as an expansion of the top armor layer.

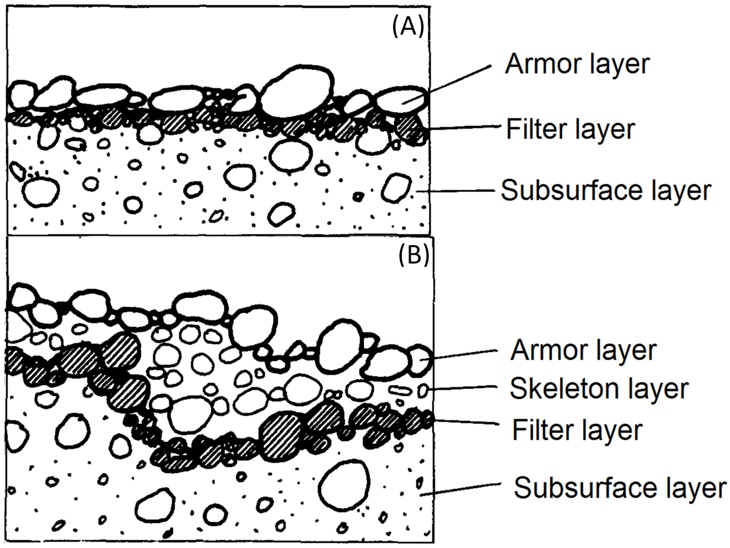

Figure 2.4. Different typical layers of the river bed. (A) River bed with typical armor, filter and subsurface layers. (B) River bed with a locally developed skeleton layer beneath the armor layer, which is also called the extension of armor layer (Schälchli, 1993).

2.2.3. Sediment infiltration and the evolution of colmation

Fine sediment infiltration into the gravel bed matrix has been investigated for decades. In contrast to colmation, for sediment infiltration, literature only considers the physical processes for occlusion of the gravel bed pores. Early researchers, e.g., Einstein (1968), observed the settling of fine particles on the bottom of the gravel framework (unimpeded static percolation) due to the gravity force acting on the very fine particles by penetrating coarser gravels. Later investigations revealed that despite gravity force, the supply rate of sediments to gravel bed (Carling, 1984), the pore size of the gravel bed matrix (Frostick et al., 1984), scour and fill sequences during the hydrological event (Schälchli, 1993), and river morphology (Diplas and Parker, 1992) are other factors influencing the fine sediment infiltration in the gravel bed.

The physical colmation of fine sediment in the top layers of the gravel bed is investigated by Schälchli (1992, 1993). Schälchli (1993) divided the development of colmation into three phases, as illustrated in Figure 2.5. Figure 2.5A shows the initial conditions of a natural gravel river bed without colmation. The first phase of colmation (Figure 2.5B) is a decisive process where coarser particles clog pores in the gravel matrix near the surface and develop a thin consolidated layer that prevents subsequent infiltration. This event is called bridging or clogging of sediments in the gravel bed. At this stage, infiltrating fine particles do not play an essential role since they are not filtered and intrude deeper into the river bed. The bridging and depositing process takes place in the upper portion of the filter and the armor layers. The clogged sediments reduce the porosity but do not significantly affect the hydraulic conductivity. In the

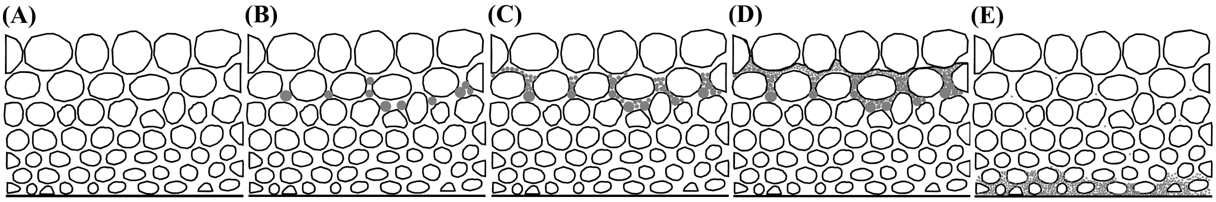

Figure 2.5. Fine sediment infiltration into a gravel bed of a river and subsequent accumulation processes. (A) No colmation (initial state); (B) first phase: clogging of the pores (bridging process) with coarse particles; (C) second phase: mean size particles clog smaller voids; (D) third phase: the finest particles fill the remaining spaces and complete the colmation process; (E) unimpeded static percolation of very fine sediments in the gravel bed.

second phase (Figure 2.5C), the mean size particles fill the voids between bridged sediments and play a vital role. A substantial reduction of the hydraulic conductivity is observed at this point. In the third phase (Figure 2.5D), the finest elements have a significant function by clogging the remained small pores. At this stage, the pores are fully clogged, and the exchange flow velocity as well as the permeability is significantly reduced. The subsurface flow below the colmation layer moves according to quasi-steady flow conditions until a decolmation process occurs (Seitz, 2020).

During low flow, very fine sediments such as suspended load (i.e., clay), absence of coarser particles in the supplied sediments, and coarse gravel bed, the first and decisive phase of colmation cannot be established. Thus, fine particles intrude into the gravel bed, and start filling from the bottom upward (Figure 2.5E). This case is called unimpeded static percolation, which is very unlikely in nature (Diplas and Parker, 1992).

Gibson et al. (2009a,b) established a threshold based on gravel bed and fine sediment grain (mainly sand) sizes for distinguishing unimpeded static percolation and the formation of a bridging layer close to the surface. According to Gibson et al. (2009b), experiments with the ratio $d_{15-gravel}/d_{85-sand}$ of 15.4 or larger, had unimpeded static percolation and fine sediment started filling uniformly from the bottom of the gravel layer to the top. However, infiltrating sediments having a ratio of 10.6 and smaller started to bridge. The clogging occurred near the surface in a thin layer, which prevented subsequent infiltration. Later, Huston and Fox (2016, 2015) revised this threshold by including the factor of geometric standard deviation of substrate material (σ_{ss}) to the bed-to-fine sediment grain sizes ratio. Therefore, according to Huston and Fox (2016, 2015) experiments with $d_{ss}/d_{fs}\sigma_{ss} < 27$ lead to bridging, while experiments with a value of $d_{ss}/d_{fs}\sigma_{ss} = 27$ initiate sediment bridging and the experiments with $d_{ss}/d_{fs}\sigma_{ss} > 27$ lead to percolation. Here d_{ss} represents mean diameter of substrate sediments and d_{fs} is the mean diameter of fine sediments.

The colmation layer thickness depends thereby on the grain size distribution of the bed material (Brunke, 1998). Schälchli (1993) has developed an empirical formula (equation 2.1) by using the mean grain size d_m of the bed material, which can be used for estimating the colmation layer thickness (d_c) in gravel bed rivers.

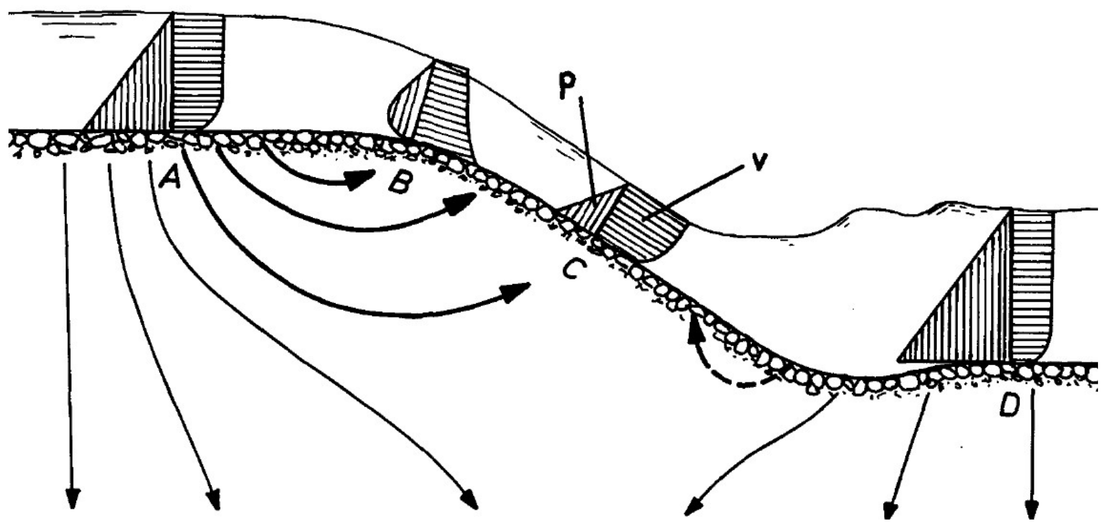

Figure 2.6. The distribution of vertical pressure and velocity in a riffle-pool sequence including interstitial flow path in the river bed (Schälchli, 1993).

$$d_c = 3d_m + 0.01[m] \tag{2.1}$$

Colmation happens heterogeneously in the river bed because fine sediments are preferably transported as suspended load and by the hyporheic interstitial flow (Boano et al., 2014). The infiltrated fine sediments prefer to follow pore water flow-paths, hence heterogeneities in colmation processes and the distinct pattern may also reach various bed types scales (Seitz, 2020). Sequences of pools and riffles for instance result in various interstitial flow paths on a longitudinal scale and thus have different clogging conditions. At the end of a pool (Figure 2.6; Position A), the pressure difference comparing to position B and C increases the seepage flow. Similarly, it may even happen from position D toward position C. This infiltration of flow enhances colmation due to increased interstitial flow. However, the flow's exfiltration restricts the entry of suspended sediment (Figure 2.6; Position B) and prevents colmation at a riffle sequence.

Due to the impact of certain parameters, the scale of colmation may vary from macro to meso and micro scale. As a proxy for the effectiveness of sediment infiltration, Zimmermann and Lapointe (2005) explained the impact of various scales on intra-gravel flow. Colmation on the macro-scale is influenced by the properties of the catchment, e.g., various sources of fine sediments, and by head variations due to effluent and influential discharges of groundwater. Pool-riffle-structures or gravel bars in meandering rivers can affect colmation on a meso-scale, resulting in different hydraulic heads, which is a significant driver for colmation processes (Schälchli, 1993). Micro-scale colmation is influenced by the passage of water through narrow beds leading to various pressure zones. Moreover, the ratio between settling and infiltration processes driven by gravity and turbulence is determined by the sediments surface's roughness. In comparison to the micro-scale impacts, the influence of head variations due to groundwater discharge could have less effect on local colmation processes (Zimmermann and Lapointe, 2005).

Furthermore, colmation can likewise change temporally because it may increase over time and establish a new route based on previously clogged paths. Or, it might change due to fluctuations in the flow conditions and bed load transport (Brunke and Gonser, 1997; Schälchli, 1993). In addition, high flow conditions can also destroy the developed colmation by flashing out the fine sediments.

2.3. Consequences of colmation

Colmation and decolmation processes are dynamically balanced in natural rivers. However, anthropogenic activities alter this equilibrium status by reduction of peak flows through water management as well as supplying more fine sediments, e.g. from the basin because of the land use changes and reservoir flushing, which intensify the sediment infiltration and accumulation processes. Physical colmation, or the fine sediment infiltration into gravels, changes the river bed relatively slow (Owens et al., 2005), but may negatively affect the ecology, hydraulics, and morphology of rivers. The sediment deposition and infiltration modify the composition and structure of the river bed. This in turn affects the characteristics of surface flow above the bed, the exchange of surface and subsurface flow, the quantity of interstitial pore water, the mechanisms in the hyporheic zone, the groundwater, the bio-geo-chemical functioning in these zones, and the connectivity between the river and floodplain environment (Wharton et al., 2017). Below these impacts on a river are subdivided into hydraulic, hydrologic and the ecological categories.

2.3.1. Hydraulic impacts

The infiltration of fine sediments into the streambed compacts the river substratum and increases cementation (Sternecker et al., 2013), which later changes the bed structure and morphology. Further, Smith and Nicholas (2005); Wren et al. (2011), and Mohajeri et al. (2016) showed by experiments how sediment infiltration significantly affects the flow structure and micro turbulence above the streambed by reducing the bed relief and effective roughness. Additionally, Kuhnle et al. (2013) exposed that the roughness geometry function (Nikora et al., 2001) decreases abruptly by increasing the sand level in the gravel bed. By homogenizing and smoothening the river bed, shear stress is reduced, and the hiding effect by coarse material increases. Thus, the erosion of fine material is reduced, which influences sediment transport mechanisms.

Despite the adverse effects, in some locations, colmation can help to preserve the groundwater environments and to enhance the process of bank infiltration (Mohajeri, 2015). Surface water in some locations carries a significant amount of pollutions owing to anthropogenic activities (Doussan et al., 1997). The colmated layers prevent pollutants from entering the groundwater (Brunke and Gonser, 1997)). Likewise, by reducing conductivity and increasing residence time, colmation can also improve the water purification by bank filtration processes (Doussan et al., 1997; Brunke and Gonser, 1997). In addition, clogged river beds in dry regions slow down the rate of evaporation (Sadid et al., 2017). This means that soil moisture is maintained longer in a colmated river bed compared to a natural gravel bed. Longer soil moisture in the river bed is necessary for the survival of the dryland flora and fauna.

2.3.2. Hydrologic impacts

Rivers interact with their subsurface environment through interflow via unsaturated and in-or exfiltration into saturated zones. The direction of the exchange processes alters with hydraulic head, whereas the flow depends on the bed permeability (Brunke and Gonser, 1997). Precipitation events can affect the hydraulic head, causing variations in flow direction. As a result, two flow directions of influent, in which surface water contributes to subsurface flow, and effluent, in which groundwater drains into the stream, could be differentiated. During periods of low precipitation, groundwater exfiltration yields base flow. In many rivers, this exfiltration makes up the discharge for most of the year (Hynes, 1983). However, during excessive precipitation, surface flow increases, leading to higher hydraulic pressure in the streams, causing the river to infiltrate and replenish the aquifer (Matthe and Ubell, 1983). Therefore, colmation of river beds on a large scale result in lowering the groundwater table (Brunke and Gonser, 1997) or a decline in the baseflow of rivers. Last but not least, colmation can even transform a perennial river into an ephemeral one (Webb and Leake, 2006). Finally, colmation in the beds of reservoirs reduces groundwater recharge.

2.3.3. Ecological impacts

Despite the hydraulic and hydrologic features, a river bed is a functional zone for many species of the river's ecosystem from invertebrates to fishes. Thus, the physical modifications of the streambed due to sediment infiltration directly influence the river ecology. Particularly, infiltration risks the river's health due to the loss of hydraulic conductivity (Brunke, 1998). Furthermore, colmation reduces the supply of dissolved oxygen as well as nutritions to the hyporheic zone depending on the stream conductivity and exchange processes. Likewise, colmation limits the refugial space for invertebrates and threatens the reproduction of spawning fishes (Noack, 2012). In addition, colmation affects the spatial distribution of instream vegetation by covering river bed roughness, disrupting subsurface nutrient concentration, and subsurface water flow (Eglin et al., 1997; Boulton et al., 1998). Finally, groundwater has a significant role in regulating the river temperature (Brunke and Gonser, 1997). Exfiltration of groundwater moderates the surface water temperature, which is vital for fish spawning and incubation, invertebrate development, and microbial activity in the hyporheic zone (Brunke and Gonser, 1997). Colmation reduces groundwater exfiltration and thus threatens the river temperature regulation.

2.4. Measurement methods

Despite understanding the various impacts of colmation, no universal method is available so far for a quantitative assessment of this phenomenon. This is a result of the complexity of involved processes and the overlaying scales. Hence, colmation is, regarding literature, measured differently, depending on the study (Descloux et al., 2010; Schälchli, 1992; Beschta and Jackson, 1979; Frostick et al., 1984). So far implemented methods can be divided into field and laboratory measurements, which are discussed below.

2.4.1. Field methods

Several methods, considering different parameters exist for the assessment of colmation. Seitz et al. (2019) identified 35 existing methods through a survey of experts in this field. Most of the methods measure the infiltrated sediments, based on visual inspection such as mapping, measuring hydraulic conductivity or by using tracer tests. Researchers also recommended methods on measuring the concentration of dissolved oxygen and water pressure reduction in the hyporheic zone. Seitz (2020) summarized the field colmation assessment methods, as in table 2.1.

The methods in Table 2.1 are distinguished into qualitative and quantitative groups, where the qualitative methods present the result as a ranking of colmation classes. Schälchli et al. (2002) developed a mapping method for the determination of the degree of internal colmation. Within this method, the top (armor) layer is removed, and the underlying layer is assessed on the basis of (i) the composition of underlying gravel bed layer's materials, especially the amount of cohesive sediments, (ii) the availability and distribution of large and small pores, and (iii) indictors on the river bed compaction. Accordingly, Schälchli et al. (2002) provided five classes for the classification of internal colmation ranging from no colmation (class 1) to complete colmation (class 5). This method can be applied in non-wetted areas of rivers by removing its top layer and evaluating the underlying material. A sample of these colmation classes with an external colmation sample is shown in Figure 2.7.

However, the quantitative methods in Table 2.1 present quantitative values for the measured and as characterstic defined specific parameters. These methods usually consider a single parameter, such as the particle size distribution, the amount of infiltrated sediments, dissolved oxygen, or the hydraulic conductivity. Seitz (2020) recently developed a multi-parameter approach to interactively determine colmation in the field by measuring four key parameters. These key parameters are grain size distribution, hydraulic conductivity, porosity, and dissolved oxygen. Although this multi-parameter method is labor-intensive and time-consuming, it allows for an adequate and high accuracy measurement of colmation at a certain spot.

Table 2.1. Summary of available colmation assessment methods (Seitz, 2020).

Method	Parameter	Reference
	Qualitative methods	
Visual mapping	Visible amount of fine particles, visible pore space, degree of pore clogging	(Schälchli et al. 2002; Descloux et al. 2010; Platts 1982)
Kick tests	Assessment of penetration resistance (bar or boots) and observation of sediment plume as result of erosion	(Schälchli et al. 2002; Thurmann and Zumbroich 2013)
Wooden sticks	Assessment of oxygenated conditions using wooden sticks	(Marmonier et al. 2004)
Shelter availability	Measurement of shelter depth using small rubber tubes	(Finstad et al. 2007)
	Quantitative methods	
Sediment samples using freeze-core or freeze-panel technique	Analysis of grain size distribution and the amount of fine sediments	(Bunte and Abt 2001)
Sediment traps and sediment buckets	Analysis of infiltrating sediment in a certain time interval	(Frostick et al. 1984; Mahoney and Erman 1984; Lachance and Dubé 2004; Heywood and Walling 2007; Franssen et al. 2014)
Tracer tests	Residual time of tracer in hyporheic interstitial and thus hydraulic conductivity	(Packman and MacKay 2003; Packman et al. 2004)
Mark IV Standpipe	Hydraulic conductivity	(Terhune 1958; Gustafson-Greenwood and Moring 1991)
Kolmameter	Hydraulic conductivity	(Zumbroich and Hahn 2018)

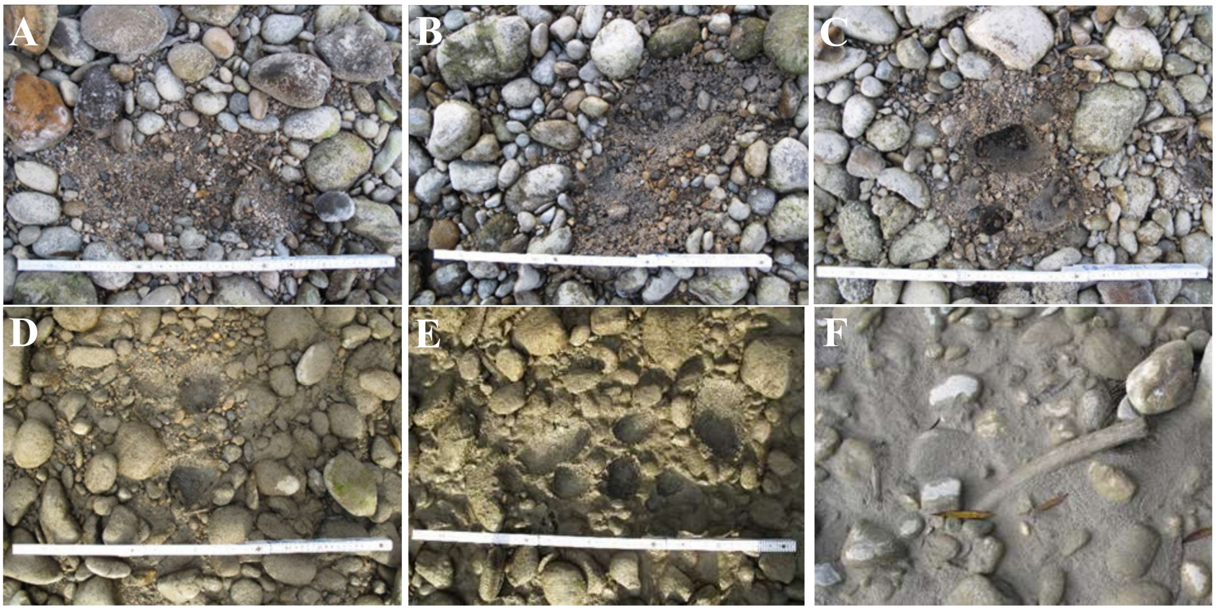

Figure 2.7. The five classes of internal colmation and one external colmation during assessment based on mapping method. (A) Class 1 - no colmation, (B) class 2 - weak colmation, (C) class 3 - moderate colmation, (D) class 4 - strong colmation, (E) class 5 - complate colmation, (F) external colmation. The photographs were taken from the original river bed between the Jettenbach weir and the Töging hydropower station on the river Inn in the German state of Bavaria.

2.4.2. Laboratory methods

In comparison to field survey, laboratory experiments help to reduce the level of complexity and the number of involved parameters through simplifications and allow for the investigation of specific boundary conditions. In the laboratory experiments, the analyzed parameters can be varied in order to understand the fundamental mechanisms involved in the colmation process. In addition, unlike natural conditions, the discharge and fine sediment supply variations can be regulated. Furthermore, laboratory experiments, despite providing more high-resolution spatial and temporal information than natural conditions measurements, allow testing the reproducibility of the same experimental conditions. Although the laboratory findings are not directly comparable to the natural conditions due to the required simplifications, it allows understanding the natural processes.

Many measurement techniques and instruments for assessing colmation in the laboratory are similar to field methods. In some cases, small-scale field instruments are used. For instance, small cylindrical samplers (Wooster et al. 2008; Gibson et al. 2009a,b; Herrero et al. 2015) and gravimetric methods, such as sieving and weighting for grain size distribution are used in the laboratory experiments for the infiltrated sediment measurements. The hydraulic conductivity and dissolved oxygen measurements also have similar principles, both in the field and in the laboratory. However, only a few approaches are solely applicable in the laboratory. For example, monitoring of the suspended sediment concentration balance over time (Hamm et al.

2011; Herrero et al. 2015), visual inspection of infiltrated sediment height evolution (Herrero et al., 2015), and photogrammetric analyses of fine sediment transport (Rosenbrand and Dijkstra 2012; Niño et al. 2018) observed through transparent sidewalls of the flume are not possible to achieve from observation of natural conditions. To increase knowledge about the colmation phenomenon, a combination of diverse methods in the assessment process is recommended (Noack et al., 2020).

In the following section, the need to establish a non-intrusive and undisturbed measurement method for achieving in-depth knowledge of the colmation phenomenon is discussed.

2.5. Toward a non-intrusive and undisturbed measurement method

Most of the methods mentioned in the previous sections are destructive and change the natural conditions during the sampling. Hence, it is only feasible to measure once the clogged sediments at a specific point. Thus, the results of sediment clogging obtained from existing methods are often vertically averaged over the sample depth and temporally averaged over the interval period and are often unable to monitor the temporal development of colmation at the same location, or continuously.

Some methods, such as continuous visual mapping, and monitoring of dissolved oxygen, which can temporally measure the degree of colmation in a certain spot, are unable to determine the amount and vertical distribution of the infiltrated sediments, especially on the small scale that is required for the discretization of the involved mechanisms in the colmation process. Although the multi-parameter measurement methods (e.g., Seitz 2020) consider the vertical profile of the involved parameters, the spatial resolution as well as their temporal resolution, are not detailed enough for the analysis of the colmation processes. Therefore, experimental investigations in the laboratory that reduce the complexity of the natural conditions are still very important for understanding the nature of this phenomenon.

Existing laboratory measurement methods provide only an integrative value per cross-section or vertical axis. Some approaches obtain values with a low vertical resolution. However, the quality and density of the data is strongly dependent on the bed material size, as these methods require manual separation of the vertical layer. Thus, most of the laboratory methods are also disruptive and cannot measure the dynamic behavior of the clogging process with a resolution that distinguishes the processes involved. Although there are a few methods (Rosenbrand and Dijkstra 2012; Niño et al. 2018) that non-intrusively assess the sediment infiltration and transport processes within the laboratory flume, these methods consider the processes from a transparent sidewall, and the internal variations are not considered.

To overcome these problems, and to better evaluate and understand phenomenon of colmation, a non-intrusive and undisturbed measurement method that considers all cross-sectional infiltrated or clogged sediments with a very high spatial and temporal resolution is required. For this purpose, the penetrating radiation technology available on the market and approved through relevant investigations (Beckers et al. 2018; Pires and Pereira 2014; Moreira et al. 2011;

Pires et al. 2009; Moreira et al. 2007; Baytaş and Akbal 2002), can facilitate the non-intrusive and undisturbed spatio-temporal measurements of the sediment infiltration and accumulation processes. The application of this method will allow in-depth knowledge of the involved mechanisms in the colmation phenomenon to be gained through further research. Therefore, the powerful gamma rays that pass through the cross-sectional materials (sediments, water, and glass walls) of a laboratory flume, are suitable for such measurements. The infiltrated sediments and its changes over time are measured using a repetitive measurement mechanism and considering the attenuation of passing radiation.

The next chapter presents the setup and procedure for the non-intrusive and undisturbed measurement method using the gamma-ray attenuation technique.

3. Materials and methods

3.1. Non-intrusive and undisturbed measurements of soil properties

The use of non-intrusive and undisturbed measurements began with the advent of X-ray at the end of the nineteenth century. Despite their application in the medical sector, penetrating rays gradually entered other scientific fields as a measuring technique. For instance, the Gamma-Ray Attenuation (GRA) method for measuring bulk density and soil water content, without physically disturbing the sample, was developed by Davidson et al. (1963). Subsequently, this method was applied to monitor the water content of large soil columns (Cassell and Nielson, 1971), the water content of soil-plant systems (Cassel and Krueger, 1972), water content and bulk density changes in a soil pedon (Reginato, 1974). Afterwards, the GRA method was widely applied to measure various physical properties of soil, e.g., soil bulk density, water content, porosity (Pires and Pereira, 2014; Pires et al., 2009; Baytaş and Akbal, 2002; Gerland and Villinger, 1995; Ferraz and Aguiar, 1985), soil column hydraulic conductivity (Moreira et al., 2011, 2007; Gerland and Villinger, 1995), and reservoir sediment's bulk density profile (Beckers et al., 2018).

In comparison to other penetrating techniques used for soil characteristic measurements (e.g., Electrical Resistivity Tomography - ERT, Time Domain Reflectometry - TDR, Ground Penetrating Radar - GPR), an advantage of the GRA method is that gamma-rays pass directly through an object whose attenuations are recognized in a high resolution.

In the above mentioned studies, the measuring element is soil, and the changes in water content or other sub-components are monitored through the GRA measurements. Thus, fine sediment infiltration into gravel bed was not investigated, due to the similar density of fine sediments and gravels in the natural river's bed. Therefore, the simplification of representing the bed gravels with an artificial element provides the opportunity to investigate fine sediment infiltration into porous media, with a non-intrusive and non-destructive measurement method.

In the Institute for Modelling Hydraulic and Environmental Systems (IWS) of the University of Stuttgart, the feasibility of using the non-destructive measurement of sediment infiltration and accumulation in an artificial gravel bed was investigated. Subsequently, various combinations of different boundary conditions were tested to gain further knowledge on the spatial and temporal development of this phenomenon. The following sections provides details about the GRA measurement system, the measurement procedures, and the experimental program used in this study.

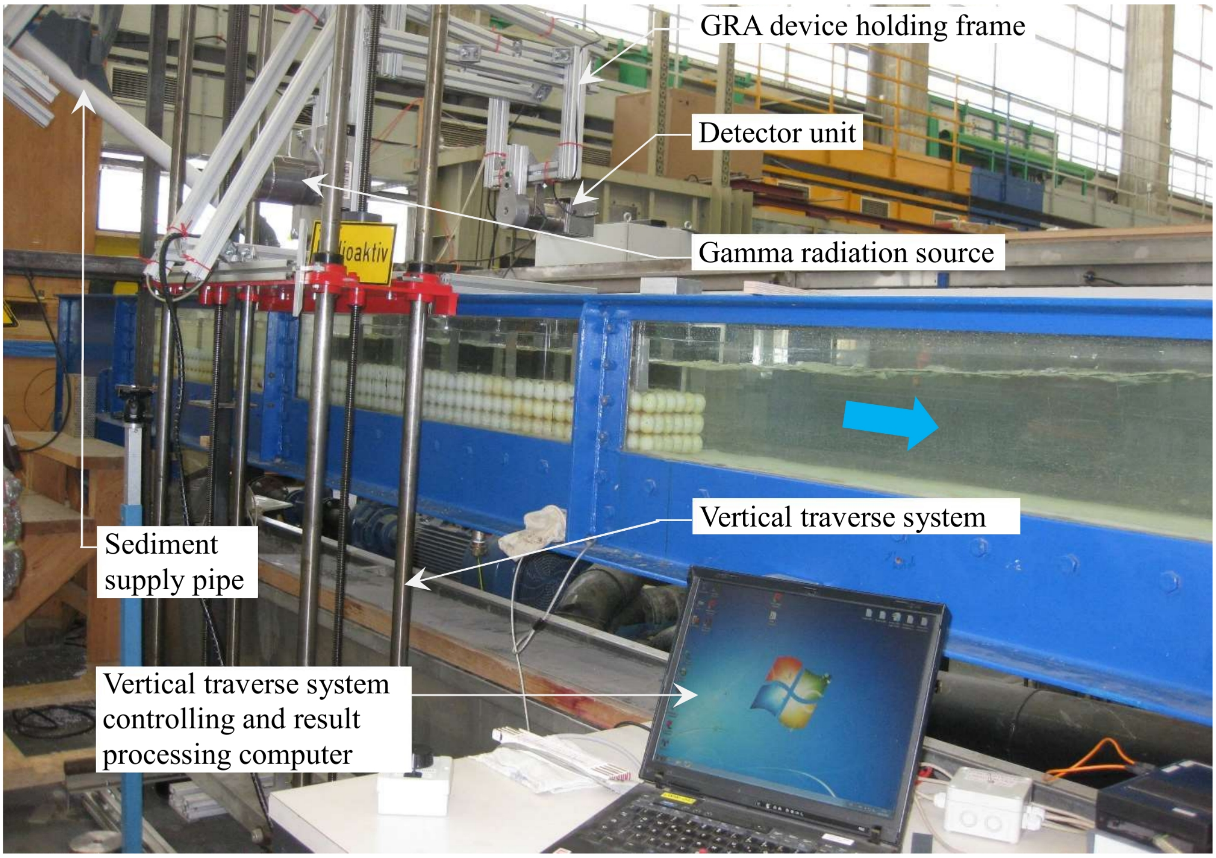

Figure 3.1. The experimental flume with the cubic configuration of the bed spheres, including measurement devices and system components.

3.2. Laboratory facilities

The investigations were conducted in a research flume, equipped with a sediment feeding machine, where the bed spheres are placed in different configurations. Figure 3.1 gives an overview of the flume, the measurement devices, and the system components.

3.2.1. Laboratory flume

The experimental flume is 8.00 m in length, 0.24 m in width, 0.30 m in height, and has a slope of 1.35 %. The flume is equipped with a recirculating flow pump to supply an almost steady flow up to 19 l/s. The longitudinal scheme of the laboratory flume is presented in Figure 3.2.

3.2.2. Gamma radiation source and detector

The radioactive source used in this study was Cs^{137} with a decay energy of 661 KeV. To measure the 0.24 m wide flume with 0.10 m thick framework at both sides, a detector unit with a 0.05

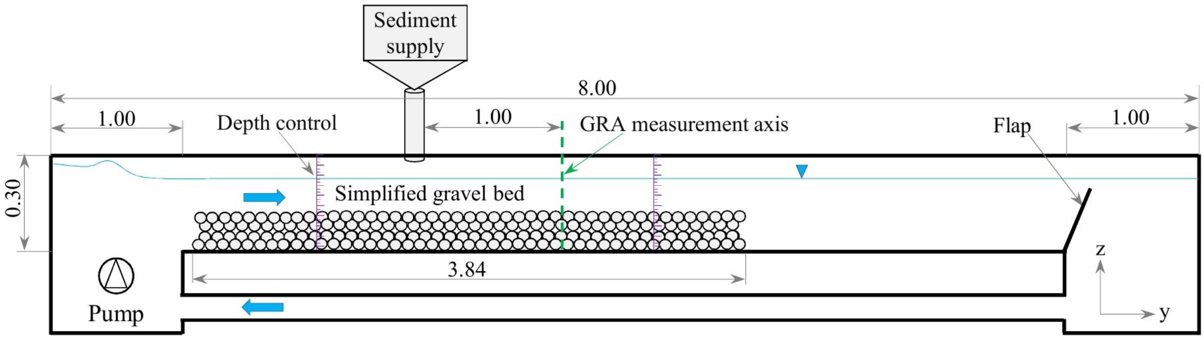

Figure 3.2. Longitudinal scheme of the recirculating laboratory flume for analyzing the vertical distribution and dynamic development of infiltrating sediments and their accumulation in an artificial bed. The lateral axis is nominated as x and represents the sediment thickness (all dimensions are in meter).

m diameter and 0.05 m thickness made of sodium iodide doped with Thallium [NaI(TI)] was positioned 0.49 m away from the source collimator. However, this distance was different (0.19 and 0.49 m) during the optimization process. As a radioactive source, the model FQG60 was used, where its technical information and operation instructions are available in Group (2015). The model, emission angle, and actual photograph of this radioactive source is shown in Figure 3.3. Furthermore, an automatic system was used in the experiments for the vertical movement of the GRA measurement setup as well as the recording of the results of each measurement for a determined interval and the entire profile.

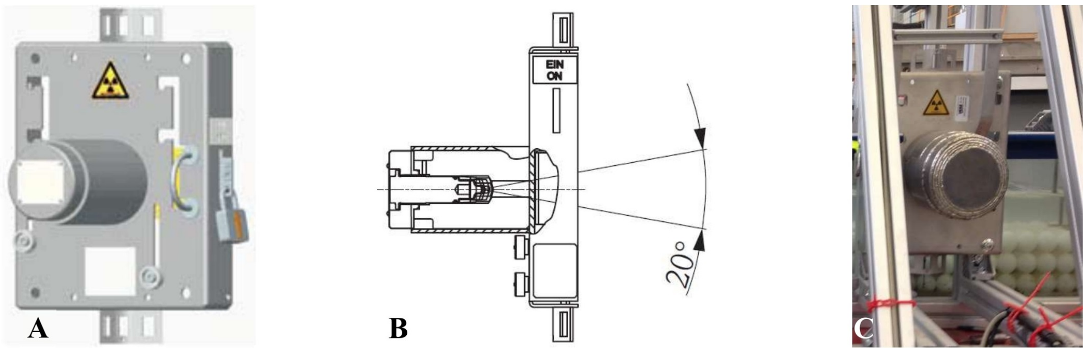

Figure 3.3. The FQG60 model of the GRA radioactive source, used for investigations (Group, 2015), (B) the emission angle of the source (Group, 2015), and (C) a photograph of the installed gamma radiation source with a view in direction of the flume.

3.2.3. Sediment feeding machine

A self-build apparatus that constantly and continuously supplies fine sediments to the flume was used in this study. The sediment feeding equipment, was already tested for various sediment particle sizes and supply rates by Benjamin (2016). The sediment supply rate was determined before the experiment by the machine controlling variables such as vibration, swirl rotation, and the size of the outlet opening for sediment release. Variations compared to the planned supply rates were observed that are discussed in Mayar et al. (2022). The scheme and dimensions of this feeding machine are shown in Figure 3.4.

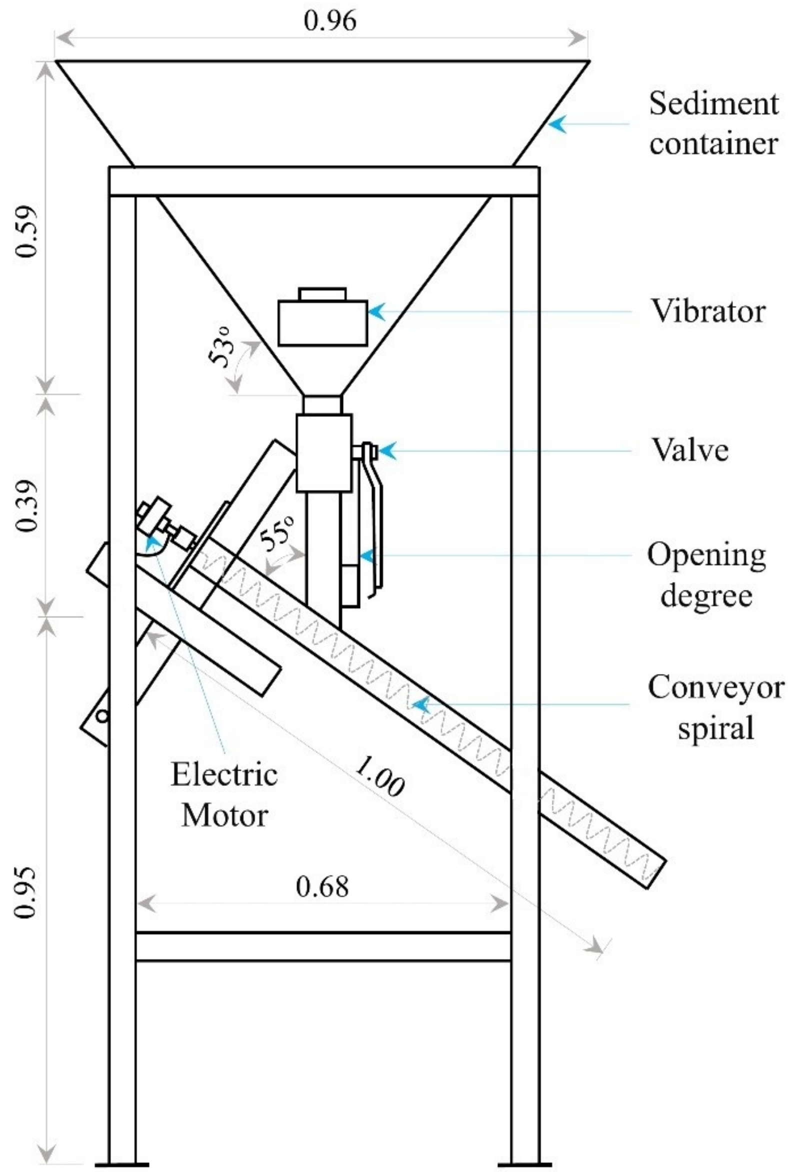

Figure 3.4. Schematic view and dimensions of the sediment feeding machine utilized for sediment supply in the experiments (all dimensions are in meters).

3.2.4. Fine sediment characteristics

The sediment mixtures used in this study are produced by merging round quartz particle shapes with a density of $\rho_s = 2,650 kg/m^3$ (Quarzsande GmbH). Three sediment mixtures of Dorsilit Nr.5 ($d_{S1} = 1.0–1.8 mm$), Dorsilit Nr.3 ($d_{S2} = 2.0–3.5 mm$), and an equal mass mixture (d_{mix}) of Dorsilit Nr.5 (d_{S2}) and Dorsilit Nr.7 ($d_S = 0.6–1.2 mm$) were employed in the experiments. The grain size distribution of these sediments are shown in Figure 3.5. More details about these sediments, their chemical composition, and technical details are available in the manual of Quarzsande GmbH and its website.

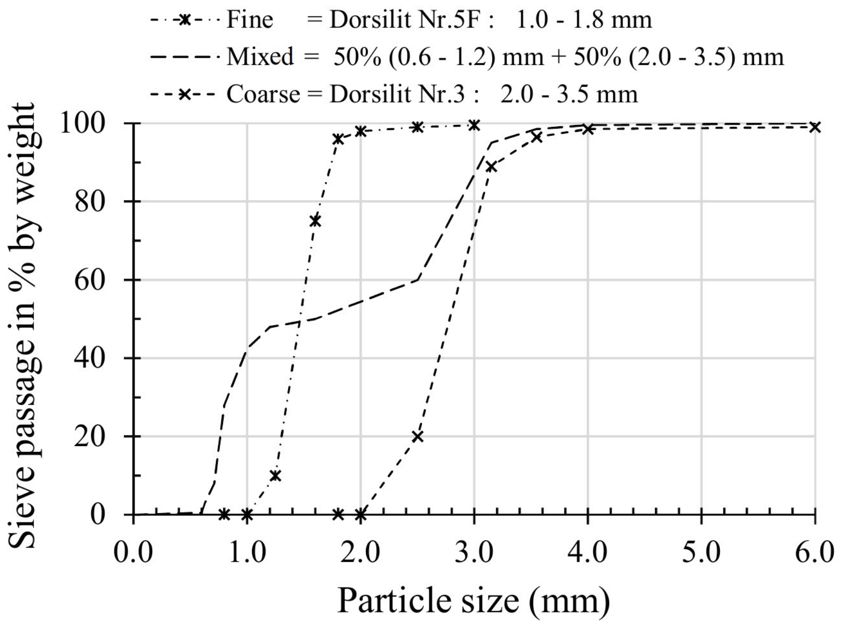

Figure 3.5. Particle size distribution of supplied sediment mixtures for infiltration into the artificial bed.

3.2.5. Artificial bed configuration

An artificial bed structure allows to precisely distinguish the infiltrating fine sediments from the bed gravels due to different densities. Furthermore, it reduces the complexity of natural conditions, and for several experiments, the same bed configuration can be ensured, means the reproducibility of the experiments at the exact same locations can be evaluated. In addition, the artificial bed enables the testing of various boundary conditions, which is vital for understanding the physical processes involved in colmation. Moreover, various bed designs representing the river's natural morphological structure can be conveniently set up and investigated.

Typically, six different bed configurations can be composed from spheres with the same diameter: Cubic, hexagonal, orthorhombic, tetragonal, triclinic and rhombohedral with initial porosities of 47.6 %, 39.5 %, 39.5 %, 30.2 %, 26.0 %, and 26.0 %, respectively. However, the combination of different size spheres can produce complex bed configurations. The cubic configuration of spheres has large and straightforward pores, which allows sediments to deeply infiltrate. However, the rhombohedral configuration of spheres has small and offset pores that increase the probability of clogging of the infiltrating sediments.

The spheres available in the Hydraulic Laboratory of the Institute for Modelling Hydraulic and Environmental Systems (IWS) of the University of Stuttgart for bed configurations, had two (0.04 m, 0.026 m) diameter sizes. In the feasibility experiments, a cubic configuration of 0.04 m spheres was used. While, for the subsequent experiments, a rather complex bed structure composed of both size spheres in a combination of cubic and rhombohedral arrangement was designed. The spheres of the feasibility experiments bed structure were glued manually in 0.24 m blocks. The artificial bed structure of the flume experiments contained 16 blocks of spheres, each with a length and width of 0.24 m, resulting a total length of 3.84 m. However, to ease the cleaning process, spheres of the rhombohedral packing in the complex bed structure were glued in horizontal layers, and the different diameter spheres, located in the cubic portion of this setup, were glued together to keep them in exact positions. The spheres blocks were fixed to the bottom of the flume with external fixation from the top at both ends of each block. The fixation system during the cubic configuration of the spheres is shown in Figure 3.6. The same fixation system was used for the subsequent experiments.

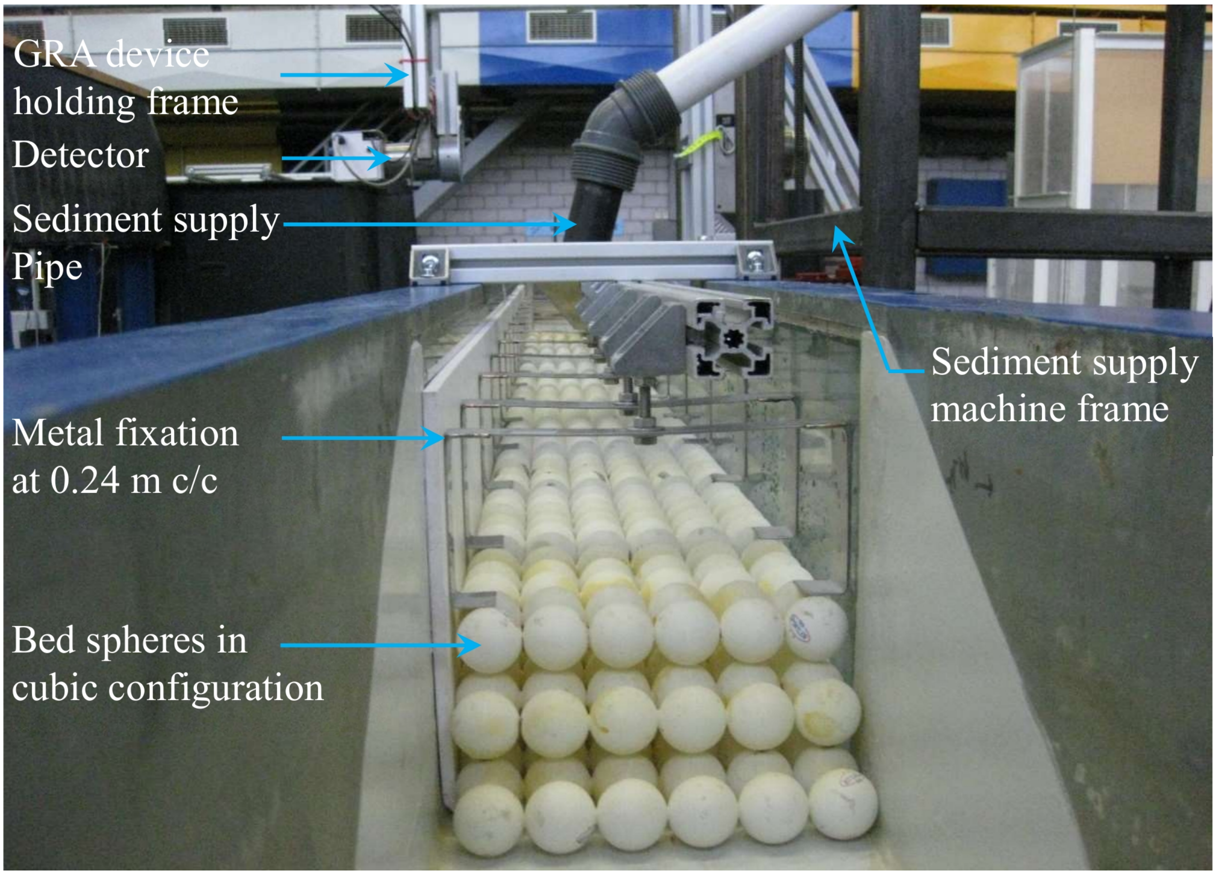

Figure 3.6. View into the flume from upstream, with spheres' in a cubic configuration and fixation system.

3.3. The GRA method measurement procedure

The key components of the GRA measurement system are the gamma radiation source, which emits a collimated beam of radiation that passes through an object, and a scintillator that detects the passed gamma quants. In the detector, the passed gamma quants produce photons that are optical signals and are eventually transformed to electrical signals by a photomultiplier. A discriminator and a counter finally process the electrical signals to present the numerical result in the computer (Mayar et al., 2020, 2022). The GRA measurement works based on the Beer-Lambert attenuation law that correlates the radiation attenuation to the object properties. A general concept of the GRA method is shown in Figure 3.7.

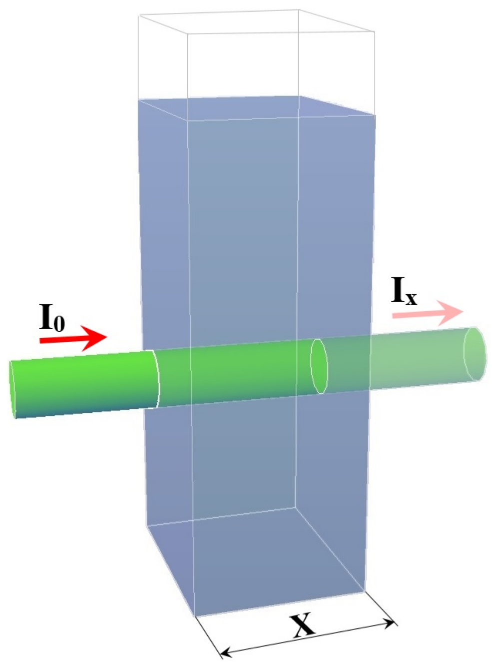

Figure 3.7. General concept of the GRA method showing the initial counts (I_0) emitted from the source, the transmitted counts (I_x) received by the detector and the thickness of the sample (X).

This measurement setup can be used once or repeated multiple times to obtain the desired results. For example, only one measurement for each collimator size was needed to determine the relationship between the collimator sizes and the initial count rates during the optimization process. However, for density and attenuation coefficient measurements, where the thickness of the material is known, two measurements are required: (i) the initial state (without object) and (ii) after passing through the object. The comparison of these two measurements determines the attenuation correlated to the characteristics of the measured object. In order to quantify the infiltrated sediment masses or the dynamic development of the clogging process, three measurements are needed (e.g., the three-fold measurement of the box experiment is shown in Figure 3.8): (i) initial state measurement for the background attenuation (walls and bed structure - Figure 3.8A), (ii) after filling the bed structure with water to identify the total available space for sediment infiltration (Figure 3.8B), and (iii) after sediment infiltration to determine the amount of infiltrated sediments (Figure 3.8C). In addition, due to being non-intrusive and undisturbed, measurements can be replicated multiple times in exactly the same location. Therefore, during the final experimental series, the vertical profile measurements were repeated for the flume experiments at a specific interval to determine interval-averaged temporal variations in all measurement positions of the vertical axis due to continued flow without further sediment supply. Besides, in order to track the dynamic development of sediments in a specific position of the vertical profile, the background and pore space profile measurements were carried out prior to the experiment, and the measurement of the third profile was conducted during the sediment infiltration only in one specific position. Owing to the single GRA instrument, only one position of the vertical profile was measured continuously during the experiment. However, the vertical profile measurements were possible to be repeated multiple times. More details about the theoretical basis and the measurement procedure of the GRA method, as well as structure of the samples are given in Mayar et al. (2020, 2022).

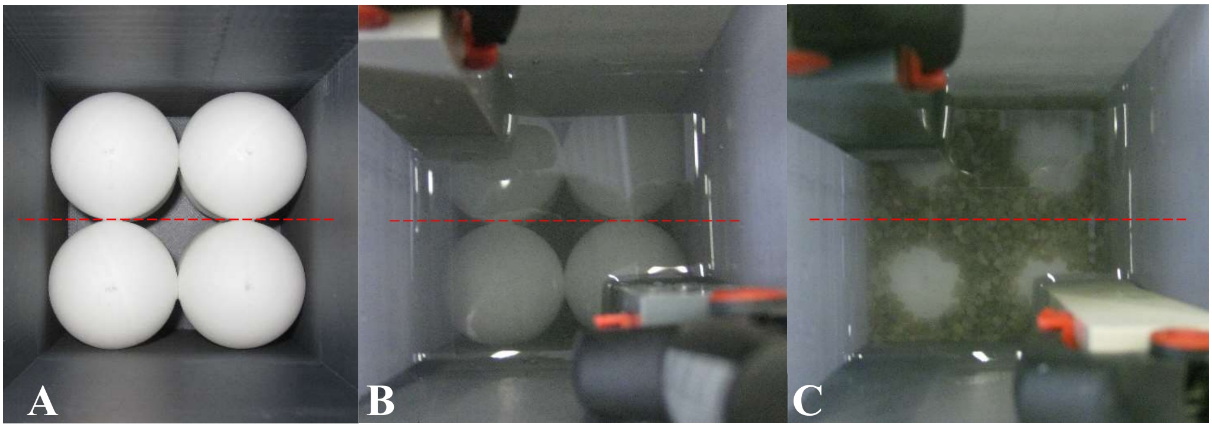

Figure 3.8. Three steps of the box experiment for comparing the infiltrated sediment gravimetric mass with the GRA-method measurement. (A) The empty box with bed structure (spheres) to quantify background attenuation, (B) the water-filled box, to obtain the total pore space available for sediment infiltration, and (C) the infiltrated sediments in the bed structure, with a water layer above, to determine the amount of infiltrated sediments. The horizontal centroid axis between the spheres represents the measurement axis.

3.4. Experimental program

In order to optimize the GRA measurement setup for the best composition of the spatial and temporal resolution, prove the concept of the non-intrusive and undisturbed measurement method for infiltrated sediment masses, and to investigate the effect of different boundary conditions on the spatial and temporal development of sediment infiltration and accumulation processes, various types of experiments were performed that are discussed below:

3.4.1. Optimization

Different combinations of collimator sizes, used measuring time-steps, and statistical errors have been reported for the GRA measurements in the literature (Pires and Pereira 2014; Moreira et al. 2011; Pires et al. 2009). Therefore, it was necessary to test and optimize the GRA measurement method to obtain the best spatial and temporal resolution associated with a statistical error in the range of previously conducted experiments before conducting the principle experiments.

Thus, first, the coverage of the vertical profile's cross-section through the combination of different collimator sizes was geometrically analyzed in order to choose a collimator combination that a top-to-bottom sequential measurement completely covers it. The analyses indicated that equal size collimators fully cover the vertical profile's cross-section in a consecutive top-to-bottom measurement, and present independent results from the upper and lower measuring horizons. Subsequently, two groups of experiments were performed. With the first set of experiments the relationship between the collimator's diameter and the initial count rates for an adequate collimator selection was found. For this reason, five equal size collimators (5, 7, 9, 12, and 15 mm) for the source and detector sides were tested. The achieved linear relationship allows determining the desired collimator based on two different collimator diameters initial count measurements.

The second experiment connects the measuring time, the collimator's diameter, and the collected total counts depending on the statistical error. To this end, six thicknesses of three materials: Aluminum (Al), Polyvinylchloride (PVC), and Polypropylene (PP), with known densities, were investigated. As a result, the obtained mathematical equation defines the boundary conditions for GRA measurements by using only the initial count rate, obtained before an experiment. A schematic view and a picture of the PVC sample from this experiment are shown in Figure 3.9.

3.4.2. Proof-of-concept for the GRA measurement

So far, only stationary measurements of different materials or soils were conducted. Due to the dynamic behavior of the sediment infiltration process, it was necessary to first prove the concept of the non-intrusive and undisturbed measurements for infiltrated sediment masses. Hence, two types of additional experiments were conducted in the laboratory. First, four box

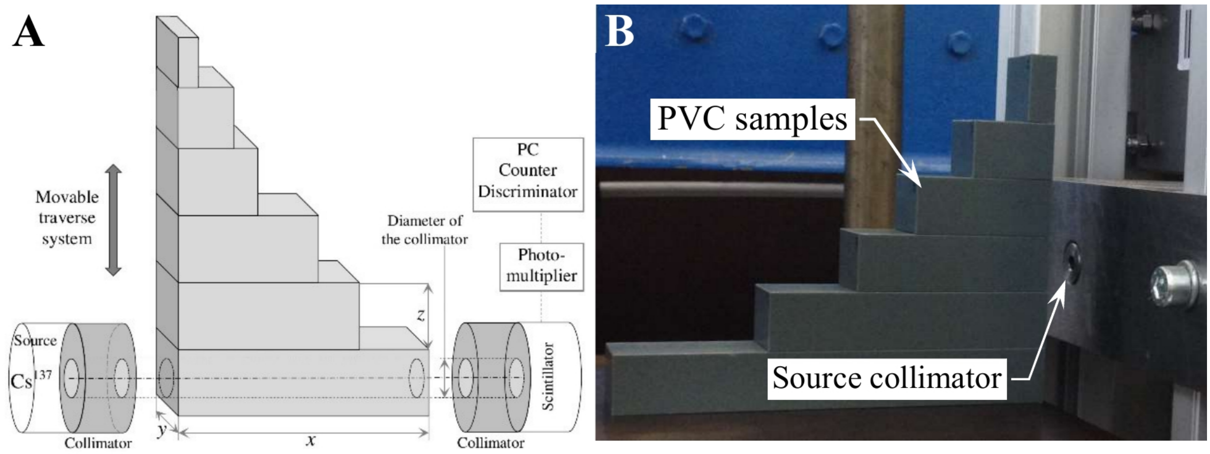

Figure 3.9. (A) The GRA attenuation measurement scheme for investigating various thicknesses of Al, PVC and PP samples (Mayar et al., 2019). (B) Photograph of the PVC sample measurement with a 5 mm collimator.

experiments, using a simplified bed structure of eight spheres packed in a two-layer cubic configuration (Figure 3.10), was tested to compare the GRA method measured results with the gravimetrically determined sediment masses. Known amounts of fine ($d_{S1} = 1.0$–$1.8mm$) and coarse ($d_{S2} = 2.0$–$3.5mm$) sediment mixtures were used. The vertical distribution of sediments in each sample was measured with a 7 mm collimator, selected through the optimization process, at the centroid axis of the two nearby spheres. However, the comparison of the GRA measurements with gravimetric values of the box model required a horizontal extrapolation of the GRA measurement to an equal width of the sample (box width = 0.08 m, 0.04 m extrapolation toward each corner). This was possible by assuming a horizontally uniform distribution of infiltrated sediments over the width. The measuring GRA beam in the strait of the spheres faces considerable thickness of sediment content. Thus, the uniform distribution hypothesis to a length of 0.08 m in the box experiments was valid for the bed's cubic configuration. An exemplary scheme of such a sediment distribution in the pore space, at the horizon with the minimum sediment content, 0.08 m width and the location of the penetrating collimated gamma beam is shown in Figure 3.10.

Subsequently, the cubic packing configuration was transferred into a flume to repeat the fine sediment infiltration experiments. The sediment mixtures were supplied with 1.4 kg/min and 3.7 kg/min supply rates, respectively. The total supplied mass of both sediment mixtures was 20 kg for each experiment. Both flume experiments were repeated and evaluated for reproducibility tests. Similar to the box experiments, the vertical profiles of infiltrated sediments were measured by a 7 mm collimator. However, the infiltrated sediment masses were calculated using an extrapolation to 0.04 m width (Figure 3.10B), in order to reduce the uncertainty. For more information about the experimental setup, boundary conditions and measurements of this series of experiments, refer to Mayar et al. (2020) in Appendix II.

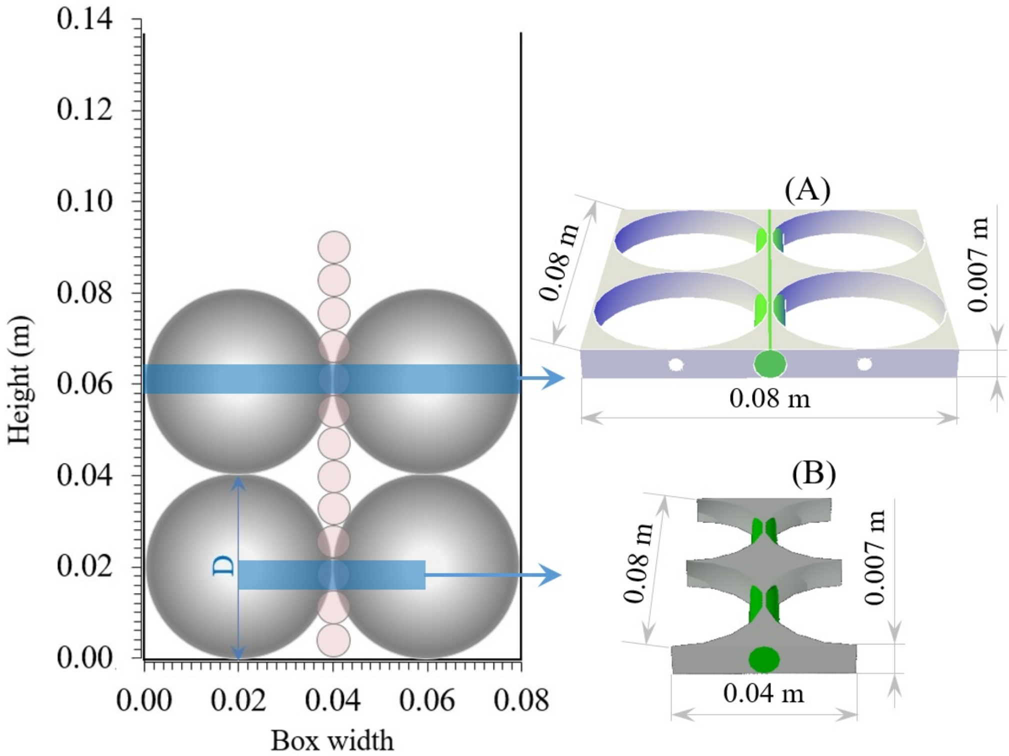

Figure 3.10. Schematic view of the pore space in the vertical profile of the cubic configuration of spheres for the bed. (A) The distribution of infiltrated sediments is assumed to be uniform in the box experiments for 0.08 m width, and (B) the distribution of infiltrated sediment in reproducibility flume experiments is assumed to be uniform in a 0.04 m width. The small light red circles on the bed spheres show the measurement positions (side view) of the GRA method in the vertical profile. The green cylinder in the (A) and (B) represents the gamma radiation beam.

Figure 3.11 gives a view of the distribution of infiltrated sediments during the reproducibility experiments after the supply phase. The supply rates were 1.4 kg/min with a total mass of 20 kg of (A) fine sediments ($d_{S1} = 1.0 - 1.8mm$), and 3.7 kg/min with a total mass of 20 kg of (B) the coarse sediments ($d_{S2} = 2.0\text{–}3.5mm$). The effects of different supply rates are clearly visible. The same discharge of water can transport fine sediments better with a supply rate of 1.4 kg/min than the coarse sediments with higher (3.7 kg/min) sediment supply rate. Thus, the upper layers in the fine sediment experiments are not filled, while the coarser sediments have filled the available pore volume.

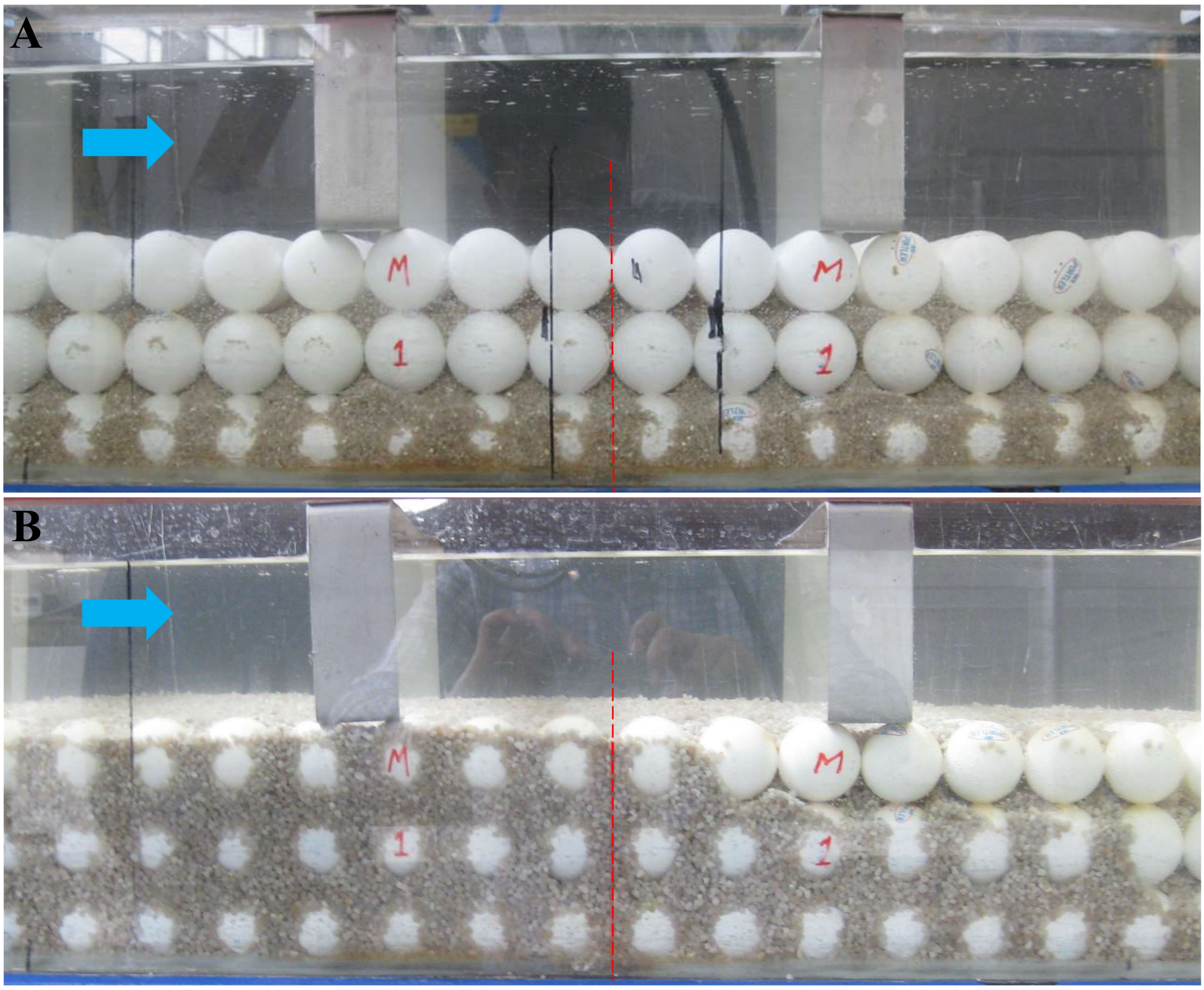

Figure 3.11. Infiltrated sediment distributions in the cubic bed configuration after finishing sediment supply for: (A) Fine sediments ($d_{S1} = 1.0$–$1.8mm$) with a supply rate of 1.4 kg/min, and (B) coarse sediments ($d_{S2} = 2.0$–$3.5mm$) with a supply rate of 3.7 kg/min. Both experiments had 20 kg supplied masses of sediments. The red dashed line shows the measurement axis for the vertical profile of GRA measurements.

3.4.3. The effect of boundary conditions and temporal development of the sediment infiltration and accumulation processes

A new series of experiments was designed to monitor the dynamic development of sediment infiltration and accumulation as well as to explore the effect of different boundary conditions on the sediment infiltration and accumulation (physical colmation) processes in a complex bed structure. A bed structure consisting of cubic and rhombohedral configurations of 0.040 m spheres as well as the 0.026 m spheres among the cubic packing of spheres (Figure 3.12), was designed. The bed structure and hydraulic conditions ($Q = 16l/s, Fr = 0.93$) of the flume were kept constant during the whole experimental period as well as for all subsequent experiments.

The boundary conditions consisted of two feeding masses of 10 and 20 kilograms, two supply rates of 1.4 kg/min and 3.7 kg/min, and three sediment mixtures of fine ($d_{S1} = 1.0$–$1.8mm$), coarse ($d_{S2} = 2.0$–$3.5mm$), and mixed (d_{mix}, which was obtained from equally mass mixing of d_{S2} and $d_S = 0.6 - 1.2mm$ particles in the laboratory). In total, twelve combinations of boundary conditions were tested.

In contrast to the cubic configuration, in complex geometries such as the rhombohedral configuration of the spheres or a bed structure developed from a composition of different sizes of spheres, which have smaller and offset pores, the probability of sediment clogging increases, and thus the assumption of a uniform, horizontal sediment distribution is not valid anymore. In addition, the measuring GRA beam also faces minimum thickness positions of the infiltrated sediments in the vertical profile, whereas its extrapolation to a 0.04 m width raises the uncertainty significantly. Particularly, during the coarse sediment experiments, particles cannot infiltrate to these small pore thicknesses. The scheme of the pore space in two positions of the vertical profile for the final configuration of the bed is outlined in Figure 3.12. These pore volumes are filled by infiltrating sediments during the experiment. Figure 3.12A shows the pore space at the strait of the 0.04 m spheres in the bed setup, which corresponds to the cubic configuration of the spheres. However, Figure 3.12B shows the pore space at the centroid of 0.04 m sphere in the bed setup, in which the current GRA method measures the minimum thickness of sediments, whereas the actual sediment distribution cannot be extrapolated from this position's measurement. Thus, the existance of such small thicknesses in the vertical profile restricts the horizontal extrapolation of sediments from a 7 mm collimator width to a substantial thickness. Therefore, in the final bed configuration, the infiltrated sediment masses are only considered in the collimating gamma beam (7 mm diameter) volume for the analyses. For a better understanding, the actual horizontal distributions of the infiltrated sediments (fine, coarse and mixed) in the final bed setup are shown in Figures 3.13, 3.14, 3.15, and 3.16 for each boundary condition. Here, the effect of infiltrating sediment particle sizes can be observed from the comparison of the infiltrated sediment distribution for different supplied sediment masses and rates. Similarly, the effect of different supply rates for each sediment mixture, on their infiltration and distribution behavior can be observed from the comparison of Figure 3.13 with Figure 3.14 for the 20 kg supplied sediments mass, and from the comparison of Figure 3.15 with Figure 3.16 for the 10 kg supplied sediments mass. Likewise, the supplied mass effects can be observed in the comparison of the Figures 3.13 and 3.15 for 1.4 kg/min supply rate and from the comparison of the Figure 3.14 and Figure 3.16 for 3.7 kg/min supply rate.

Each experiment of the final bed configuration was measured for the high-resolution (7 mm) vertical profiles in two time-steps (after sediment supply - T_{Exp}, then the experiment was resumed to complete a 28-minute period and subsequently measured - T_F) and a particular location with a 15 mm diameter for monitoring the sediment accumulation and its temporal development during the entire experimental period. The repetition of the vertical profile measurement at a specific time-step (T_F) was used to track the average fluctuations of the infiltrated sediments. This was carried out for each position of the vertical profile between the two time-steps. The one-point (15 mm diameter) measurements were used to capture almost real-time results for the temporal development of the sediment accumulation in the gravel bed. For more information about the experimental setup, boundary conditions, and measurements of this series of experiments, refer to Mayar et al. (2022) in Appendix III.

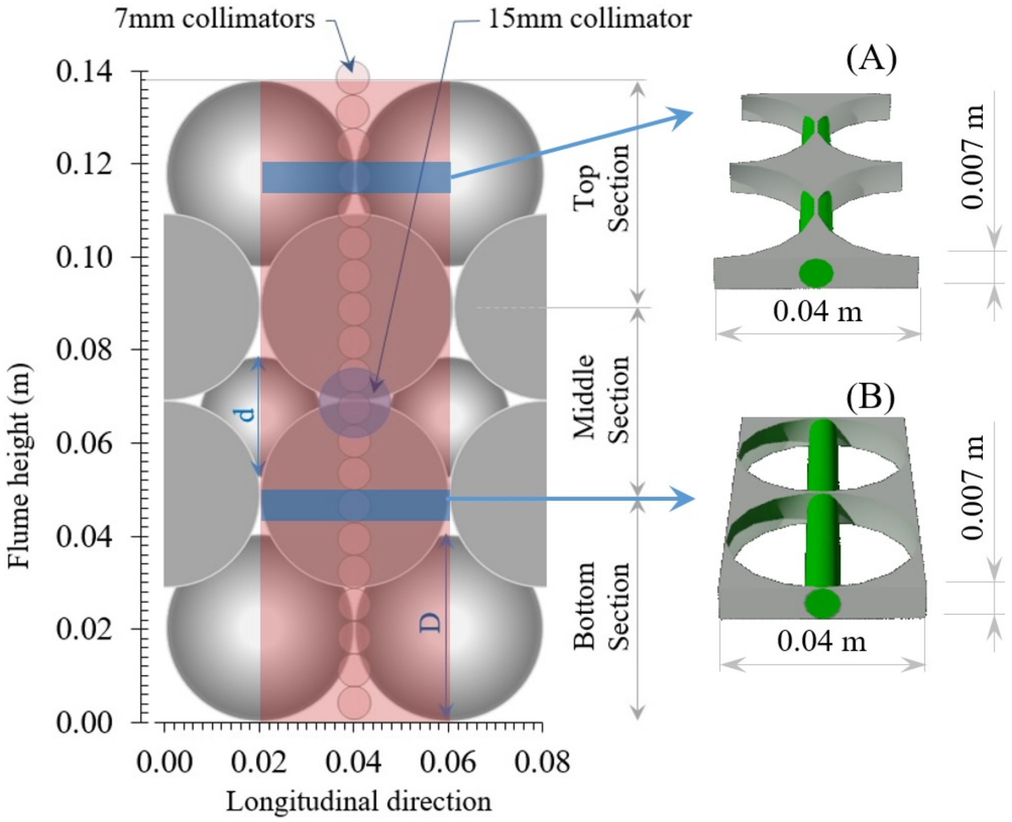

Figure 3.12. Schematic view of the pore space in two different positions of the vertical profile in the final configuration of spheres. (A) The scheme of sediment distribution in the measuring horizon at the strait of 0.04 m spheres, which is similar to cubic configuration of spheres. (B) The scheme of sediment distribution in the measuring horizon faced the centroid of 0.04 m sphere, in which the uniformly sediment distribution hypotheses (extrapolation to a 0.04 m width) is not valid, because the GRA method measures the minimum thickness of the infiltrated sediments. The small light red circles on the bed spheres show the measurement positions (side view) of the GRA method in the vertical profile. The green cylinders in (A) and (B) represent the gamma radiation beam in the measuring setup.

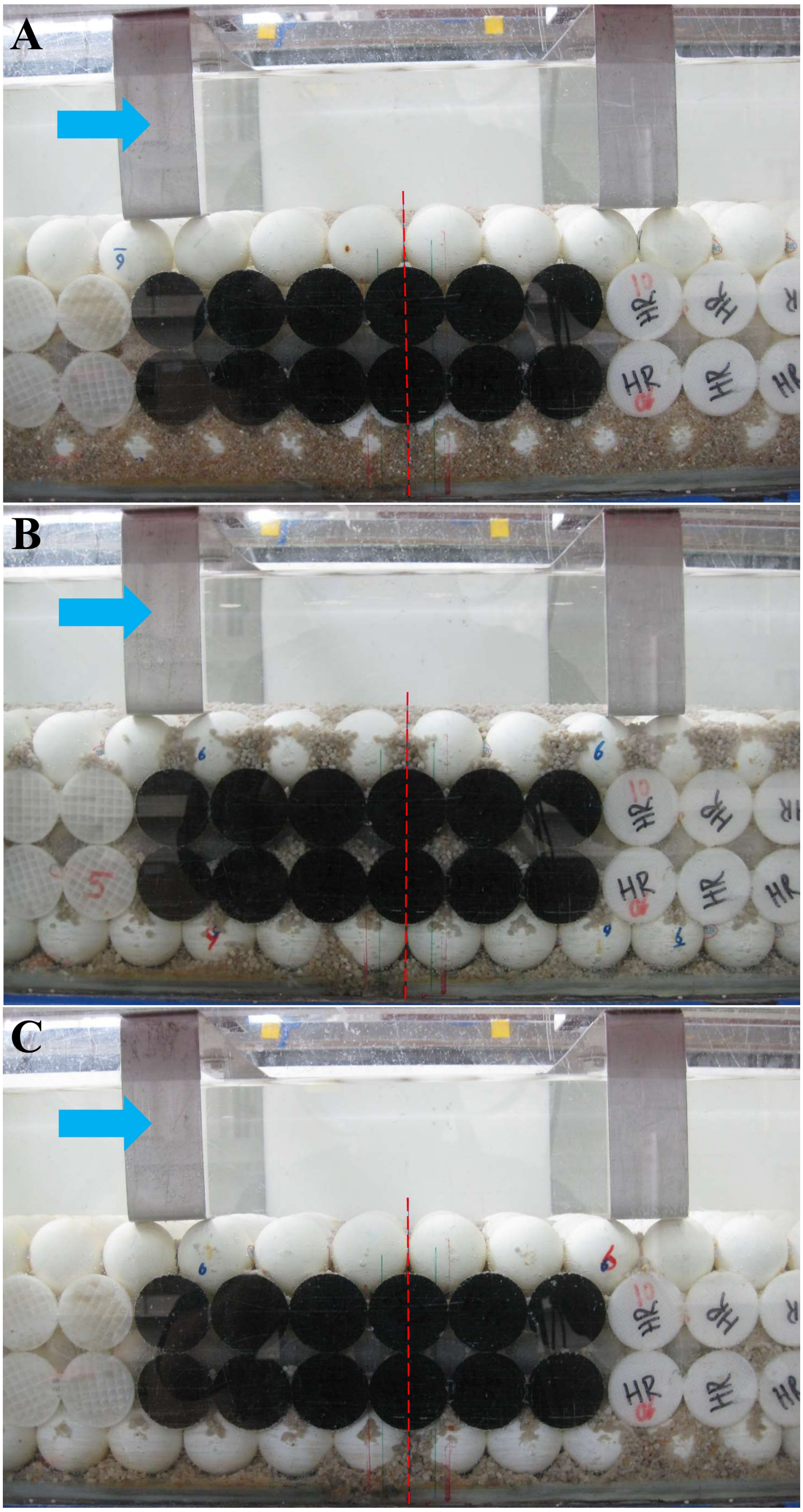

Figure 3.13. The infiltrated sediment distribution in the final bed configuration during T_{Exp} time-step for: (A) fine, (B) coarse, and (C) mixed sediments, with 20 kg supplied sediment mass and 1.4 kg/min supply rate. The red dashed line shows the measurement axis for the vertical profile of GRA measurements.

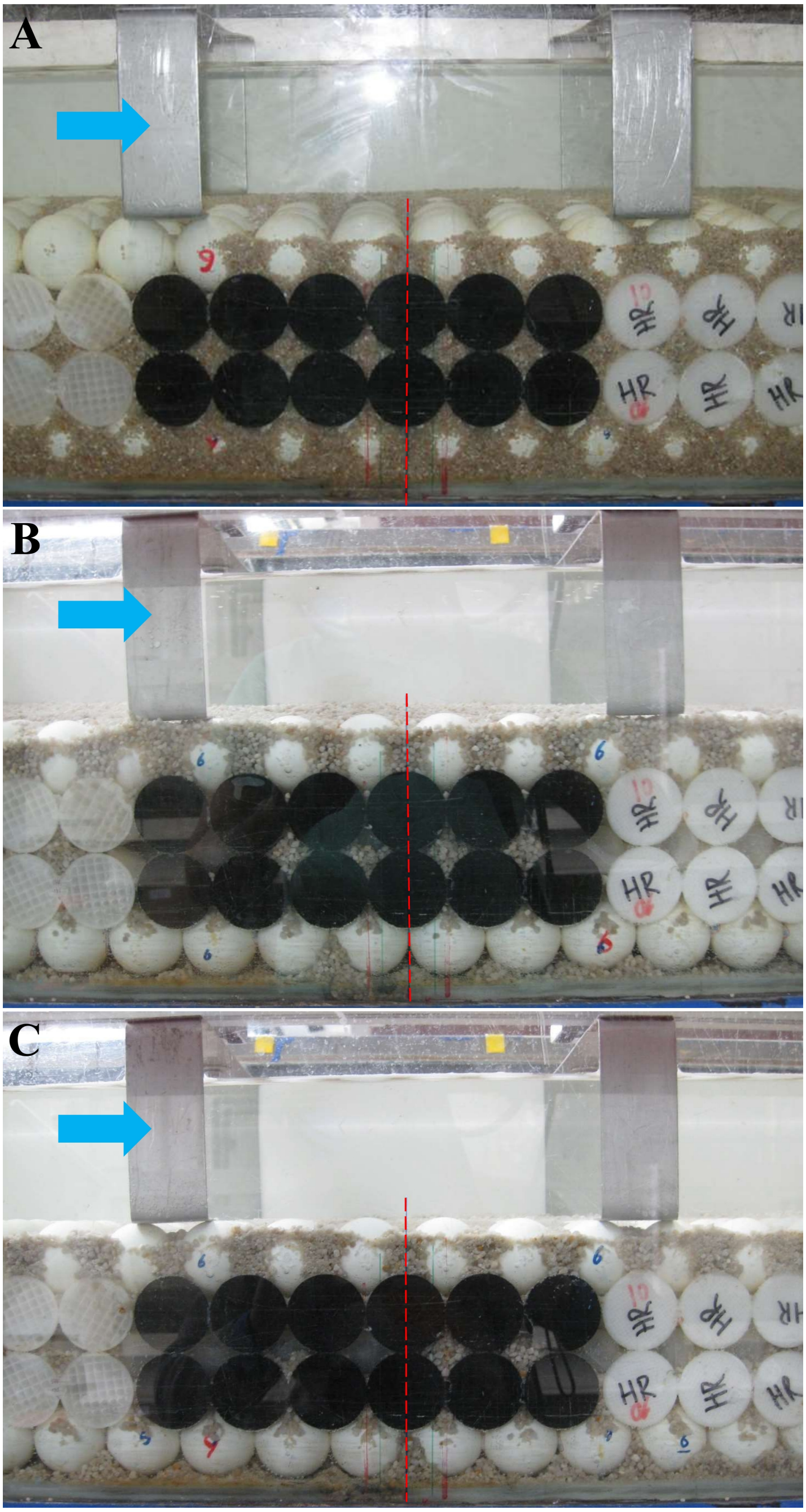

Figure 3.14. The infiltrated sediment distribution in the final bed configuration during T_{Exp} time-step for: (A) fine, (B) coarse, and (C) mixed sediments, with 20 kg supplied sediment mass and 3.7 kg/min supply rate. The red dashed line shows the measurement axis for the vertical profile of GRA measurements.

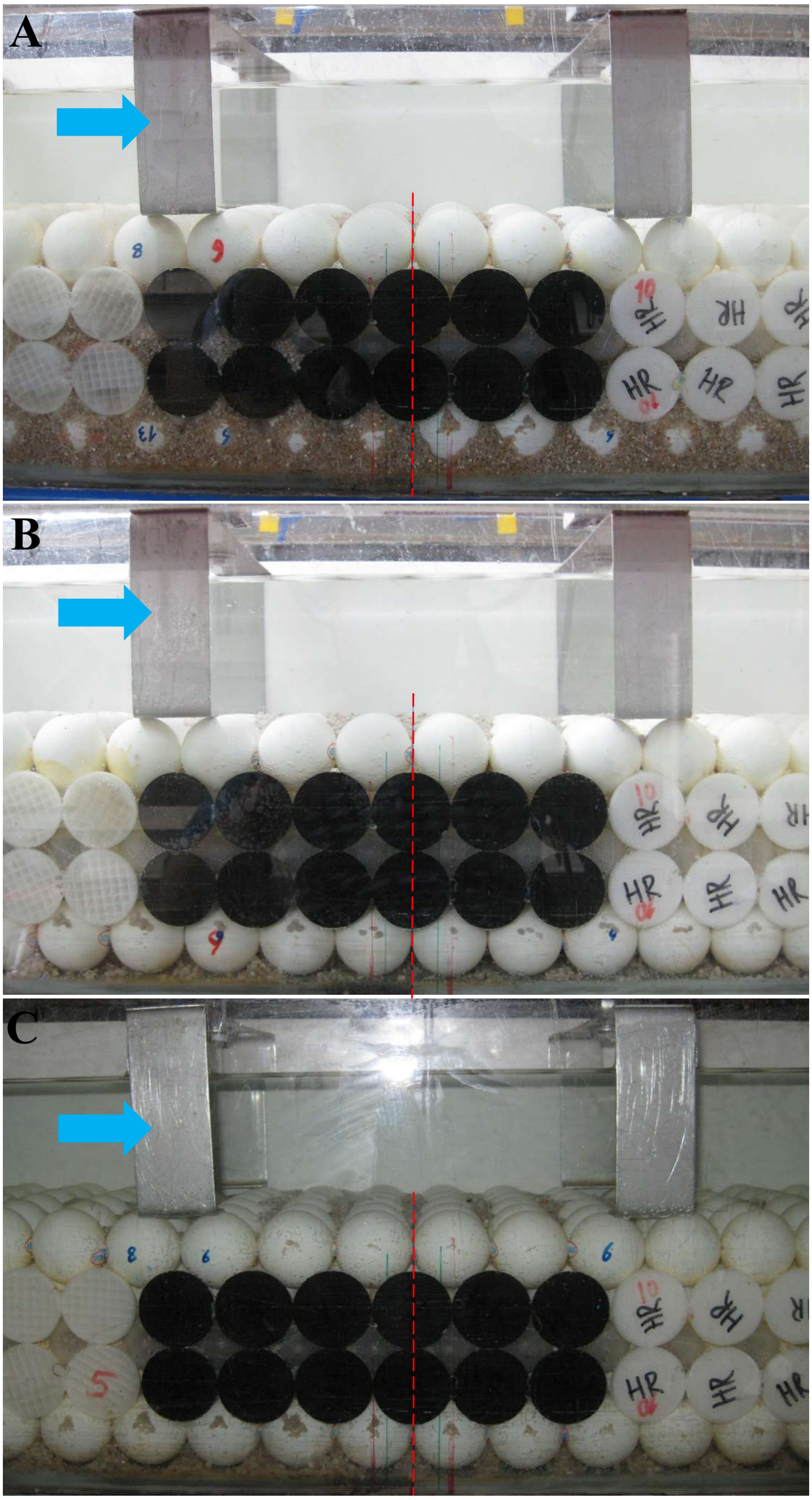

Figure 3.15. The infiltrated sediment distribution in the final bed configuration during T_{Exp} time-step for: (A) fine, (B) coarse, and (C) mixed sediments, with 10 kg supplied sediment mass and 1.4 kg/min supply rate. The red dashed line shows the measurement axis for the vertical profile of GRA measurements.

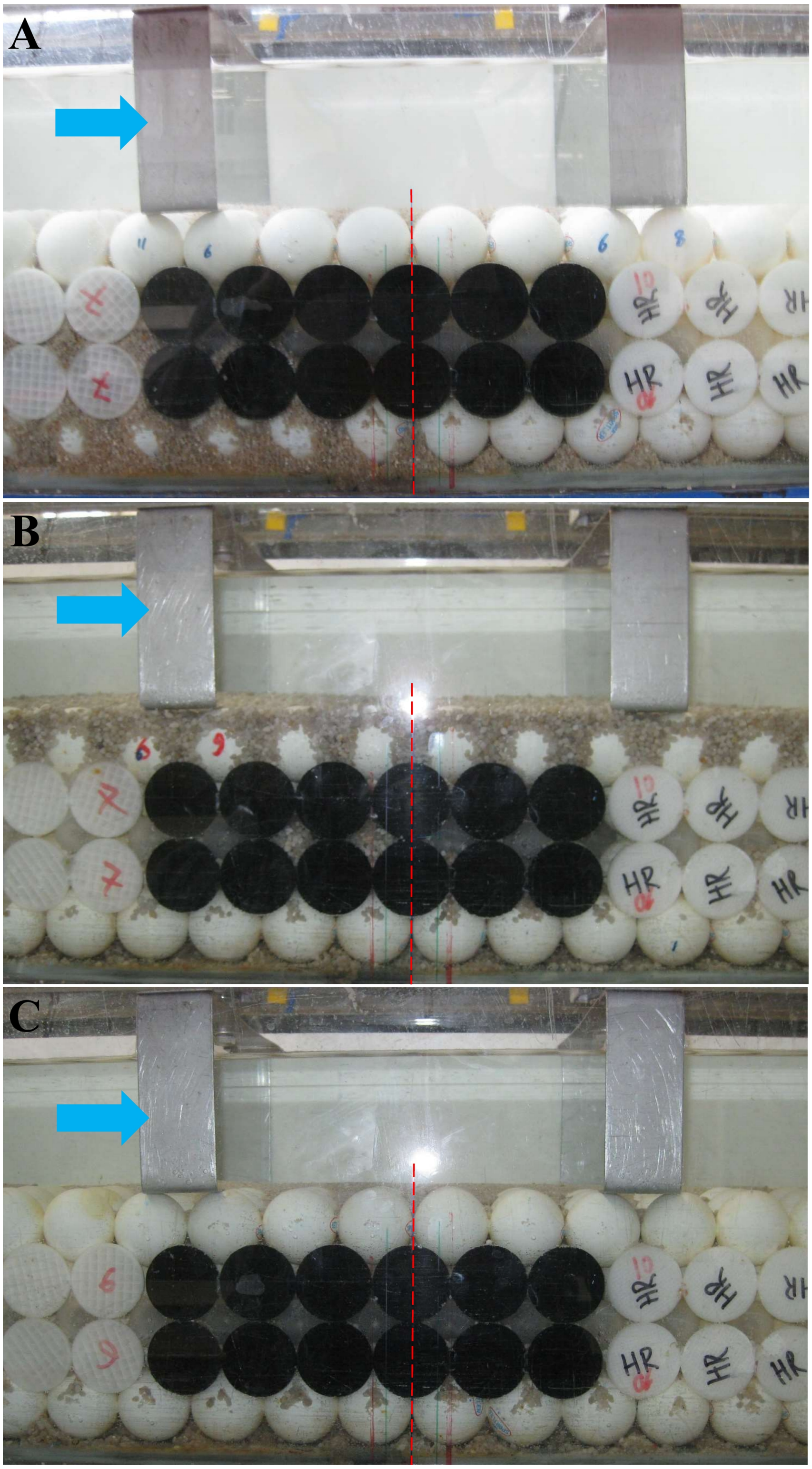

Figure 3.16. The infiltrated sediment distribution in the final bed configuration during T_{Exp} time-step for: (A) fine, (B) coarse, and (C) mixed sediments, with 10 kg supplied sediment mass and 3.7 kg/min supply rate. The red dashed line shows the measurement axis for the vertical profile of GRA measurements.

3.5. Uncertainty of GRA measurements

The measurement of infiltrated sediments with the GRA method has three sources of uncertainties. The first one is the statistical error associated with the GRA three-fold measurements. The gamma quants are created by a radioactive decay and are emitted with a probability, which shows a temporal statistical variation. This variation can be described by a Poisson distribution (Buczyk, 2009) with a standard deviation (δ) using equation 3.1 for the average number of received counts ($\bar{N}$).

$$\delta_{\%} = \pm \frac{1}{\sqrt{\bar{N}}} * 100 \tag{3.1}$$

According to equation 3.1, the statistical error solely depends on the number of collected counts at the detector. Due to the square root function in equation 3.1, the reduction of statistical error requires an increment of the collected counts in the power of two. This is achieved either by increasing the collimator size or by prolonging the measuring time, where the increment of the collimator size reduces the spatial resolution, and the measuring-time increment influences the temporal resolution, especially in the dynamic measurements. Therefore, a compromise between the resolution and the measurement time was found according to Mayar et al. (2019) for the subsequent experiments in this study.

During the calculation of the results, two standard deviation of the gamma count distribution is used from the statistical error. This means that according to the Gaussian distribution law 95.5 % of the GRA measurements will occur within the range of the considered statistical error. According to the equations discussed in Mayar et al. (2020) for the total pore space measurement, the statistical error of the measurement profiles (i) and (ii), while for the sediment thickness result, the statistical error of all three measurement profiles (i – iii), are combined. Finally, the total error of each measurement position is converted to the absolute thickness and is visualized in the relevant positions of the vertical profiles. To obtain the statistical error of the measured infiltrated mass in each section, the total error of all positions included in the section are summed up.

The second source of uncertainity is the inexact alignment of the measurement positions in the three-fold measurements, vertically for each position and horizontally for the entire profile. Initial measurements showed that owing to rapid variation of geometry, the positioning is very sensitive and can influence the final results. Therefore, the horizontal alignment was controlled through visual inspection in the measurement axis and the nearby positions. To keep the vertical positions accurate, spheres were glued into blocks. Further, an automatic vertical traversing system with a maximum error of 1.0 mm was used for the vertical positioning. However, the effect of this source of uncertainty could not be assessed quantitatively.

The third source of error is the performance of the sediment supply machine, which is not as precise for the coarse sediments as it is for the fine particles. Mayar et al. (2022) identified the variations between the planned and actual sediment supply rates, which need to be considered for the interpretation of results.

These three errors influenced the vertical profile results in the small total pore thickness positions of the final bed configuration (z = 0.046 m and z = 0.088 m), in which the collimator faced the centroid of the spheres, as well as in the surface layers, e.g. after washing away the sediments between the two stationary measurements (T_{Exp} and T_F), leading to a negative sediment thickness or a thickness that is higher than the available pore space. Therefore, the negative values were replaced with zero, and the latter was equalized to the pore space in this position. In the latter positions, the infiltrated sediments' porosity leads to zero, which is not realistic, but it is assumed that the actual porosity in such measurement positions is in the range of the statistical error (2.0 % - 3.0 %) because the statistical error resulted in a modification at these measurement points.

Furthermore, to verify the deflection of the gamma rays due to the diverse distribution of the infiltrated sediment in the measurement axis does not influence the sediment measurements results. The radiation after passing through the same thickness of Polyvinyl chloride (PVC) and Polypropylene (PP) samples in distributed and compacted forms were compared. The results showed a variation in the range of the statistical error. That means that different sediment distributions in the measurement axis do not cause contradictory deflection of the gamma rays.

4. Summary of the scientific papers

For the non-intrusive measurements of fine sediment infiltration and accumulation processes in the gravel beds or the particular case of colmation, in a first step, the existing GRA measurement approach was optimized by analyzing the vertical profile coverage and testing various combinations of collimators, time-steps, and statistical errors. In a second step, the concept of the non-intrusive and undisturbed measurement of infiltrated sediments was proved by comparing the GRA measured results of box experiments with the predefined amount of infiltrated sediments and reproducibility experiments in the flume. Finally, the established method was applied to experiments with various boundary conditions to investigate the spatial and temporal variation of the infiltrated sediments under laboratory conditions. The results of the three mentioned steps were published in three peer-reviewed articles. This chapter summarizes these three scientific articles to give an overview of the method developed, the proof-of-concept, and the investigation of the effects of different boundary conditions on the sediment infiltration and accumulation processes (colmation phenomenon). The three peer-reviewed articles can be found in Appendices I, II, and III, respectively.

4.1. Optimizing vertical profile measurements setup of gamma ray attenuation

This paper aimed to analyze the currently revealed discrepancies of the GRA measurements and to optimize this approach. Thus prior to the principle experiments, the existing GRA measurement approach was optimized to standardize the vertical profile measurements in terms of resolution and accuracy, which is influenced by the gamma radiation's statistical error.

This scientific article argued the problems of the currently applied GRA measurements. These issues include the utilization of different size collimators for source and detector, which either overlap the measurements or do not fully cover the cross-section of the vertical profile in a consecutive top-to-bottom measurement as well as measuring time-steps, and statistical errors for the GRA measurements. Therefore, it was necessary to optimize the GRA method for the best coverage of the vertical profile in a consecutive top-to-bottom measurement as well as to find the best combination of the spatial and temporal resolutions associated with an appropriately small statistical error. To address these issues, first, the coverage of the vertical profile measurements was analyzed by using different combinations of collimators. In a second step two sets of experiments were conducted. In the first set of experiments, five pairs of collimators were employed to quantify and correlate the scale of collimators' cross-sectional area to the initial count rates of the same collimators. Afterwards, the second group of experiments was conducted to find the relationship between measuring time, collimator size, and the sample's thickness including their statistical error. These experiments consisted of measurements of six thicknesses of three materials: Aluminum (Al), Polyvinylchloride (PVC), and Polypropylene (PP) with known densities using the GRA method. As a result, the first group of experiments resulted in a method for the optimal collimator selection, based on two initial measurements. Consequently, the second series of experiments resulted in a mathematical equation that defines the boundary conditions for the GRA measurements by using only the initial count rate, obtained before an experiment. This equation enables to find an optimal compromise between the resolution (collimator size) and the measurement time (needed for a predefined accuracy depending on the statistical error). In addition, the application of the same-size collimators for the source and the detector enhanced the GRA method to quantify the sediment content in the subsequent experiments.

4.2. Proof-of-concept for non-intrusive and undisturbed measurement of sediment infiltration masses using Gamma-Ray Attenuation

This paper proved the measurement principle of non-intrusive and undisturbed GRA measurements in order to obtain the infiltrated sediment masses. Hence, two sets of experiments were conducted to measure the vertical distribution of infiltrated sediments with a high spatial resolution.

The proof-of-concept for non-intrusive and undisturbed vertical profile measurements of the infiltrated sediments with high-resolution are reflected in this paper. At first, the article discusses the restrictions of the existing techniques and the need for a non-destructive measurement method of the infiltrated sediments. Consequently, the theoretical basis for the established approach, the experimental setup, and the calibration results with gravimetric measurements of the box experiments are given. Finally, the reproducibility tests in the flume experiments were clarified. As simplification, in the experiments, the natural gravel bed is represented by an artificial simplified bed structure consisting of 0.04 m spheres in a cubic configuration. This enables to clearly distinguish the infiltrating sediments from the bed. Hereby, first, a box model consisting of eight spheres in two layers with a cubic packing was designed. Next, gravimetrically weighted amounts of two different sediment mixtures ($d_{S1} = 1.0$–$1.8mm$, $d_{S2} = 2.0$–$3.5mm$) were added separately to the box, representing the infiltrating sediments in the gravel bed. Finally, the box model experiments were measured with a 7 mm collimator in accordance to the results of the optimization study. In order to assess their validity, both experiments were replicated. As a result, the comparison of the gravimetric and the GRA measurements' of the box experiments show deviations between 1.0 % and 5.0 %. After this, the box model was transformed into flume experiments. The same sediment mixtures with 20 kg mass, but two different supply rates (1.4 kg/min and 3.7 kg/min), were fed into the flow. Each experiment was repeated to test its reproducibility and showed deviations of 1.4 % and 7.7 % for the fine and coarse sediment mixtures in terms of total infiltrated mass in the measurement axis, respectively. The results of both sets of experiments also provided high-resolution vertical profiles of infiltrated sediment, porosity, and water content. Based on the results of this study, it was concluded that the GRA measurement approach offers a viable opportunity for the non-destructive quantification of infiltrated sediment masses and high-resolution vertical profiles of its porosity and water content under laboratory conditions. Therefore, in the subsequent experiments, a rather complex artificial bed was designed to analyze certain boundary conditions' effects on the sediment infiltration and accumulation processes as well as the development of the colmation phenomenon.

4.3. Measuring vertical distribution and dynamic development of sediment infiltration under laboratory conditions

The purpose of this publication was to present the effects of various boundary conditions on the spatial and temporal development of sediment infiltration and accumulation processes or the colmation phenomenon. Therefore, a rather complex bed structure was designed for the final experimental series of this study.

For this purpose, the so far optimized and tested method was applied in two ways. Firstly, the vertical profile measurements were repeated after a period of time to evaluate the changes in all positions of the vertical profile between the two measurements. The first measurement was performed at the end of sediment supply T_{Exp}. Then the experiment was continued without further sediment supply untill the end of the experimental period (28^{th} minute). Afterwards, the vertical profile measurement was repeated T_F. Secondly, a specific position in the vertical profile was continuously measured during the entire experimental duration to monitor the temporal development of sediment accumulation in almost real-time (one-point measurement). Due to the setup and availability of only one gamma-ray source with one collimating-radiation-hole, a single one-point measurement was carried out for each experiment. In addition, owing to the critical function of the vertical axis on the colmation process and the limitation of only one measuring device, the spatial measurement focused on the z-axis. A 7 mm collimator determined the vertical profile measurement resolution, while the one-point dynamic measurements were performed with a 15 mm collimator.

To analyze the clogging of fine sediment particles in the subsurface matrix pores, a bed structure, composed of cubic and rhombohedral packing of 0.040 m spheres with 0.026 m spheres in between the cubic portion, was designed for this experimental series. This configuration of spheres had smaller and offset pores compared to cubic and uniform packing of 0.04 m spheres. The combinations of three sediment mixtures, two sediment feeding masses, and two supply rates, resulted in twelve experiments.

The results showed that the amount and vertical distribution of infiltrated sediment highly depends on the particle size. The visual inspection during the experiments and the measurement results showed a high thickness of infiltrated fine sediments at the bottom of the flume, which proved that fine sediments had unimpeded percolation. Thus, colmation was not observed in fine sediment experiments. The reasons for fine sediment unimpeded percolation are the bed structure's pore size, and the small particle size of the supplied sediments. Gibson et al. (2009b) also observed unimpeded percolation when the ratio of bed gravels (0.04 m spheres in the current experiments) to the infiltrating sediments was greater than 15.6. The respective ratio for the fine sediment experiments in this study is equal to 23.5, which is even higher compared to the threshold given by Gibson et al. (2009b) for sediments bridging in the gravel beds. However, for the coarse sediment experiments, infiltrating particles were clogged in the bed's upper sections, which indicates the occurrence of colmation. The ratio of the diameter of bed gravels to the infiltrating coarse sediments is equal to 12.9, which is in the range of Gibson et al. (2009a,b) threshold for bridging sediments in the gravel bed. In the third series of experiments with mixed sediments the ratio is equal to 13.3, which is in the range of Gibson et al. (2009a,b). The mixed sediment due to bimodal sediment grain-size distribution did not develop a colmation layer near the surface. Thus, the very fine and some coarse particles penetrated to the bottom of the gravel bed.

Furthermore, the comparison of vertical profiles measured at T_{Exp} and T_F showed significant dynamic changes in the upper layers of the gravel bed due to the washing of sediments by the flow. In comparison to the upper section, the lower sections saw minor alterations as a consequence of re-distribution of infiltrated sediments and the resulting additional pore space filled by fine sediments infiltrating from the upper strata. The one-point measurements provided important information on the temporal development of the clogging processes. For example, it proved that higher supply rates lead to an earlier start of infiltration and rapid accumulation of the sediments, while a lower supply rate results in a later and gradual filling of the sediments.

To conclude, the high-resolution vertical profile measurements identified colmation as well as unimpeded percolation of infiltrating sediments. The repetition of vertical profile measurements showed the interval-averaged temporal variations for all measurement positions, which was significant in the top section due to flow forces acting on the particles to transport or infiltrate deeper. However, the lower position measurements, which had less variation in this study, might be important in some special interstitial flow cases. Moreover, the one-point measurements precisely determined the stages of the sediment infiltration and accumulation (the start of infiltration, the pore-filling period, and the final amount of infiltrated sediments including natural fluctuation during the ongoing experiments). Thus, for a comprehensive understanding of the colmation phenomenon or the overall sediment infiltration and accumulation processes, both the repetitive vertical profile and the one-point measurements, are required. Finally, the simultaneous application of multiple GRA devices will make it possible to evaluate the longitudinal distribution of infiltrating sediments in an experiment.

5. Conclusions and recommendations

The infiltration and accumulation of fine sediments in gravel beds rivers lead to serious adverse implications for aquatic species. Numerous field and laboratory methods have been developed for the assessment of these processes. However, most of them are destructive and do not allow for a high-resolution spatial and temporal measurement of the sediment infiltration and accumulation processes, required for understanding this phenomenon. Although colmation is observed in natural rivers, it is difficult to investigate this phenomenon in-situ due to the complexity of the physical, chemical, and biological processes and parameters involved. However, laboratory experiments help to determine the effect of distinct mechanisms involved in this natural phenomenon. Hence, this study focused on developing and applying a new non-intrusive and undisturbed measurement method for a high-resolution spatial and temporal measurement of the sediment infiltration, accumulation, and the colmation phenomenon under laboratory conditions.

For this purpose, several experiments were conducted to (i) refine and optimize the current GRA measurement system, (ii) prove the concept for non-intrusive and undisturbed spatial and temporal high-resolution measurements of the infiltrated sediments, and (iii) to apply this method to certain experiments for investigating boundary condition effects on the sediment infiltration and accumulation processes.

5.1. Conclusions

The optimization process of the GRA measurement resulted in a method, which enable the selection of an optimum collimator and in a mathematical equation for optimizing the measurement duration. These findings support users in defining the boundary conditions for the GRA measurements by applying an initial measurement before an experiment. This optimization method helps to achieve an optimal compromise between the resolution (collimator size) and measurement time (needed to achieve a statistical error that does not influence the precision and is in the range of previously conducted experiments). In addition, the equal size collimators proposed by this optimization enabled the GRA method to quantify the sediment content in all subsequent experiments.

Consequently, the concept of the measurements using the GRA method was verified with a cubic configuration of an artificial bed in a box model, and later the reproducibility was tested through flume experiments. The calibration of the measured total infiltrated sediment masses in the box with predefined amounts of sediments deviated from 1 % to 5 %. In comparison, the flume reproducibility experiments had differences of 1.4 % to 7.7 % in terms of the total infiltrated sediment mass in the measurement axis for fine and coarse sediments, respectively.

These variations originate from the statistical error of the GRA measurements, the exact alignment of the measurement positions correlated to the bed spheres as well as the performance of the sediment supply machine. Another potential source for the deviations in the cumulative masses of infiltrated sediments could result from the different vertical distributions during the reproducibility experiments, which is highly probable for the coarse particles compared to the fine sediments. Looking at the complexity of the sediment infiltration and accumulation processes and the existing destructive methods, the deviations observed in the conducted experiments were acceptable. Since the results of the proof-of-concept experiments were successful, it is concluded that the GRA measurement approach offers a viable opportunity for the non-destructive quantification of infiltrated sediment masses and high-resolution profiles of the sediment vertical distribution, porosity, and water content under laboratory conditions.

In addition, it is concluded that high-resolution, non-intrusive, and undisturbed vertical profile measurements identify the colmation and unimpeded percolation of infiltrating sediments. The measured vertical profiles result shows that the thickness of infiltrated sediment strongly depends on the sizes of supplied particles and the artificial bed structure's pore. Fine sediments infiltrated smoothly and started to accumulate from the bottom, continuing upward owing to unhindered infiltration. Thus, colmation was not observed in fine sediment experiments. The infiltration of coarse sediments leads to bridging and clogging effects within the bed's pores, preventing further downward infiltration, which indicates the occurrence of colmation. The mixed sediment also infiltrated to the bottom of the bed owing to the bimodal particle mixture and did not develope a colmation layer near the surface. The repetition of the vertical profile measurements at a specific interval shows the interval-averaged temporal variations for the entire measurement positions of the vertical profile. The comparison of these vertical profiles revealed that dynamic changes mainly occur in the upper section of the bed, as flow rinsed away the sediments. In contrast to the upper section, smaller changes in the lower parts were seen as a result of re-distribution of the infiltrated sediments and the ensuing additional pore space filled by fine sediments infiltrating from the upper layers. Furthermore, the one-point measurement precisely determines the decisive stages of the sediment infiltration and accumulation (start of the sediment infiltration, duration of the pore filling, cumulative sediment infiltration, and their subsequent variations). For instance, the continuous one-point measurements revealed that higher supply rates result in an earlier start and rapid filling of the pores than the lower supply rates. Thus, for a comprehensive understanding of the colmation phenomenon or the overall sediment infiltration process, both the repetitive vertical profiles and the one-point measurements are required.

5.2. Limitations

The GRA measurement method has certain restrictions. Firstly, the method is associated with a statistical error related to the decay of the radioactive source. Caution should be paid to balance this error with the spatial resolution as well as with the measurement time-step. This is to neither lose the variation that needs to be recorded nor to reduce the confidence level of the measurements by raising the level of statistical error. According to the resolution and measuring time-step relationship investigated by Mayar et al. (2019), it is revealed that the finer the resolution, the longer time-step is required to maintain the statistical error within an acceptable range. Therefore, optimization is essential in most of the measurements, except the experiments where the spatial (collimator size) or temporal resolution is irrelevant. Secondly, the GRA method is highly sensitive to the position of the measuring points during the repetitive measurements (horizontally for the entire profile and vertically for each measurement). Thus, it is advised to locate the bed spheres precisely and use an accurate vertical traverse system. Thirdly, a sediment feeder with a high accuracy is necessary to precisely provide coarse particles as fine sediments, which can affect the accuracy of the experiment's performance. In addition, the GRA method cannot address the horizontal distribution of infiltrated sediments along the measuring horizon and provides only net or bulk results. Moreover, the current setup of the GRA method is not appropriate for beds with natural gravels because of the similar density of infiltrating sediments. However, strong radiations that pass through the thickness of a natural bed are able to identify the significant amounts of infiltrated sediments. In comparison, small amounts of infiltrated sediments will produce only a minimal change of the attenuation that might be confused with the statistical error. Another important limitation in field measurements is the legal restrictions on the use of radioactive material in a natural environment. Group (2015) provided technical and safety guidelines for radioactive source applications. Hence, the maximum safety protection is recommended in compliance with laws and regulations of the respective country.

5.3. Outlook and recommendation

Despite the previously discussed restrictions, the GRA method offers a unique opportunity for an undisturbed and non-intrusive measurement of the sediment infiltration and accumulation processes in the laboratory. Notably, it opens the way for their time-resolved or dynamic investigation as well as exploration of the effects of different boundary conditions. In addition, the GRA approach can measure the vertical profile on a millimetric scale, if the measurements have no time constraints. Similarly, for the measurement of one position with a large collimator, the GRA method can provide a time-varying result with a resolution of a few seconds. Furthermore, the long-term one-point measurements may also determine the alternating period between colmation and decolmation processes.

The current investigations focus on the physical colmation under laboratory conditions through sediment infiltration and accumulation processes. But the GRA method can also measure the biological and chemical colmation individually or compositely, if those are developed in the laboratory experimental setup, and if their effects are larger than the statistical error of the GRA measurements. The GRA measurement approach will present a bulk result, if the physical, biological, and chemical colmation occur simultaneously.

Although the current GRA measurement setup is not appropriate for field conditions, the boundary conditions' setup and selection could be improved to become closer to the natural conditions. There are numerous morphological structures and condition in rivers, whose investigations were out of the scope of this thesis, but can be investigated by the GRA method in the laboratory. Thus, most of such bed structures can be represented in the laboratory flume by combining different sizes and configuration of the spheres or any material with a considerably different density compared to sediments, to investigate additioanl variables of the colmation process. The bed structure can be organized layer-wise to enable the cleaning of infiltrated sediments and for a repeated use. In other words, the natural gravel beds could be scanned layer-wise by a high-resolution device and reproduced from a light material (e.g., plastic, PVC, Polypropylene) to be distinguished from the infiltrating sediments. Using this technique, any natural configuration of a bed structure can be investigated by the GRA method for the vertical distribution and dynamic development purposes of the infiltrating sediments.

Furthermore, the GRA method allows for simultaneously distributed measurements in space and time. However, spatially (in the longitudinal direction) distributed measurements require the simultaneous application of multiple devices or different designs of the radiation-emitting source. Due to the recent development of numerical simulation techniques, some advanced computational models (e.g., Bui et al. 2020, 2019), have been developed to simulate and predict the fine sediment transport and infiltration in the gravel-beds. Such simulations can only be validated using non-intrusive and high-resolution measurements. Thus, the GRA technique is an appropriate option for such a task.

Finally, the GRA method can be coupled with the Particle Image Velocimetry (PIV) and endoscopic PIV measurement devices, which allow to measure the behavior of sediment infiltration and accumulation processes as it occurs in nature.

References

D. W. Baker, B. P. Bledsoe, C. M. Albano, and N. L. Poff. Downstream effects of diversion dams on sediment and hydraulic conditions of Rocky Mountain streams. *River Research and Applications*, 27(3):388–401, 2011. ISSN 1535-1467. doi: 10.1002/rra.1376. URL https://onlinelibrary.wiley.com/doi/abs/10.1002/rra.1376.

P. Baveye, P. Vandevivere, B. L. Hoyle, P. C. DeLeo, and D. S. de Lozada. Environmental Impact and Mechanisms of the Biological Clogging of Saturated Soils and Aquifer Materials. *Critical Reviews in Environmental Science and Technology*, 28(2):123–191, Apr. 1998. ISSN 1064-3389, 1547-6537. doi: 10.1080/10643389891254197. URL http://www.tandfonline.com/doi/abs/10.1080/10643389891254197.

A. F. Baytaş and S. Akbal. Determination of soil parameters by gamma-ray transmission. *Radiation Measurements*, 35(1):17–21, 2002. URL http://www.sciencedirect.com/science/article/pii/S1350448701002530.

F. Beckers, S. Haun, and M. Noack. Experimental investigation of reservoir sediments. *E3S Web of Conferences*, 40:03030, 2018. ISSN 2267-1242. doi: 10.1051/e3sconf/20184003030. URL https://www.e3s-conferences.org/10.1051/e3sconf/20184003030.

E. Benjamin. *Analyse eines Fördergerätes zur Geschiebezugabe in wasserbaulichen Modellversuchen*. B.Sc. Thesis, University of Stuttgart, Stuttgart, Germany, June 2016.

R. L. Beschta and W. L. Jackson. The Intrusion of Fine Sediments into a Stable Gravel Bed. *Journal of the Fisheries Research Board of Canada*, 36(2):204–210, Feb. 1979. ISSN 0015-296X. doi: 10.1139/f79-030. URL http://www.nrcresearchpress.com/doi/10.1139/f79-030.

W. Beyer, B. W, and B. E. ZUR KOLMATION DER GEWAESSERBETTEN BEI DER UFERFILTRATGEWINNUNG. *ZUR KOLMATION DER GEWAESSERBETTEN BEI DER UFERFILTRATGEWINNUNG.*, 1975.

A. P. Blaschke, K.-H. Steiner, R. Schmalfuss, D. Gutknecht, and D. Sengschmitt. Clogging processes in hyporheic interstices of an impounded river, the Danube at Vienna, Austria. *International Review of Hydrobiology*, 88(3-4):397–413, 2003. URL http://onlinelibrary.wiley.com/doi/10.1002/iroh.200390034/abstract.

S. Blomqvist and B. Abrahamsson. An improved Kajak-type gravity core sampler for soft bottom sediments. *Swiss Journal of Hydrology*, 47(1):81–84, Mar. 1985. ISSN 0036-7842, 1420-9055. doi: 10.1007/BF02538187. URL http://link.springer.com/10.1007/BF02538187.

F. Boano, J. W. Harvey, A. Marion, A. I. Packman, R. Revelli, L. Ridolfi, and A. Wörman. Hyporheic flow and transport processes: Mechanisms, models, and biogeochemical implications. *Reviews of Geophysics*, 52(4):603–679, 2014. ISSN 1944-9208. doi: 10.1002/2012RG000417. URL `https://agupubs.onlinelibrary.wiley.com/doi/abs/10.1002/2012RG000417`.

A. J. Boulton, S. Findlay, P. Marmonier, E. H. Stanley, and H. M. Valett. The functional significance of the hyporheic zone in streams and rivers. *Annual Review of Ecology and Systematics*, pages 59–81, 1998. URL `http://www.jstor.org/stable/221702`.

M. Brunke. *The influence of hydrological exchange patterns on environmental gradients and community ecology in hyporheic interstices of a prealpine river*. PhD thesis, ETH Zurich, 1998. URL `http://hdl.handle.net/20.500.11850/143794`.

M. Brunke. Colmation and depth filtration within streambeds: retention of particles in hyporheic interstices. *International Review of Hydrobiology*, 84(2):99–117, 1999. URL `http://onlinelibrary.wiley.com/doi/10.1002/iroh.199900014/abstract`.

M. Brunke and T. Gonser. The ecological significance of exchange processes between rivers and groundwater. *Freshwater Biology*, 37(1):1–33, 1997. ISSN 1365-2427. doi: 10.1046/j.1365-2427.1997.00143.x. URL `https://onlinelibrary.wiley.com/doi/abs/10.1046/j.1365-2427.1997.00143.x`.

B. Buczyk. Poisson Distribution of Radioactive Decay. *MIT Department of Physics, Cambridge*, page 4, 2009.

V. Bui, M. Bui, and P. Rutschmann. Advanced Numerical Modeling of Sediment Transport in Gravel-Bed Rivers. *Water*, 11(3):550, Mar. 2019. ISSN 2073-4441. doi: 10.3390/w11030550. URL `https://www.mdpi.com/2073-4441/11/3/550`.

V. H. Bui, M. D. Bui, and P. Rutschmann. The Prediction of Fine Sediment Distribution in Gravel-Bed Rivers Using a Combination of DEM and FNN. *Water*, 12(6):1515, June 2020. doi: 10.3390/w12061515. URL `https://www.mdpi.com/2073-4441/12/6/1515`.

K. Bunte and S. R. Abt. *Sampling Surface and Subsurface Particle-size Distributions in Wadable Gravel- and Cobble-bed Streams for Analyses in Sediment Transport, Hydraulics, and Streambed Monitoring*. U.S. Department of Agriculture, Forest Service, Rocky Mountain Research Station, 2001. Google-Books-ID: A1DUpYKJY94C.

P. A. Carling. Deposition of Fine and Coarse Sand in an Open-Work Gravel Bed. *Canadian Journal of Fisheries and Aquatic Sciences*, 41(2):263–270, Feb. 1984. ISSN 0706-652X, 1205-7533. doi: 10.1139/f84-030. URL `http://www.nrcresearchpress.com/doi/10.1139/f84-030`.

D. K. Cassel and T. H. Krueger. Gamma Rays Determine Soil Water Content of Soil-Plant Systems. 1972. URL `https://library.ndsu.edu/ir/bitstream/handle/10365/24424/ndfr_19720301_v29_iss04_003.pdf?sequence=1&isAllowed=y`.

D. K. Cassell and D. R. Nielson. A Gamma Attenuation Unit and Logistic System for Monitoring Water Content of Large Soil Columns. *Water Resources Research*, 7(3):731–733, 1971. ISSN 1944-7973. doi: 10.1029/WR007i003p00731. URL https://agupubs.onlinelibrary.wiley.com/doi/abs/10.1029/WR007i003p00731.

A. B. Cunningham, C. J. Anderson, and H. Bouwer. Effects of Sediment-Laden Flow on Channel Bed Clogging. *Journal of Irrigation and Drainage Engineering*, 113(1):106–118, Feb. 1987. ISSN 0733-9437, 1943-4774. doi: 10.1061/(ASCE)0733-9437(1987)113:1(106). URL http://ascelibrary.org/doi/10.1061/%28ASCE%290733-9437%281987%29113%3A1%28106%29.

J. M. Davidson, J. W. Biggar, and D. R. Nielsen. Gamma-radiation attenuation for measuring bulk density and transient water flow in porous materials. *Journal of Geophysical Research (1896-1977)*, 68(16):4777–4783, 1963. ISSN 2156-2202. doi: 10.1029/JZ068i016p04777. URL https://agupubs.onlinelibrary.wiley.com/doi/abs/10.1029/JZ068i016p04777.

S. Descloux, T. Datry, M. Philippe, and P. Marmonier. Comparison of Different Techniques to Assess Surface and Subsurface Streambed Colmation with Fine Sediments. *International Review of Hydrobiology*, 95(6):520–540, Dec. 2010. ISSN 14342944. doi: 10.1002/iroh.201011250. URL http://doi.wiley.com/10.1002/iroh.201011250.

P. Diplas and G. Parker. Deposition and removal of fines in gravel-bed streams. *Dynamics of gravel-bed rivers*, pages 313–329, 1992.

C. Doussan, G. Poitevin, E. Ledoux, and M. Detay. River bank filtration: modelling of the changes in water chemistry with emphasis on nitrogen species. *Journal of Contaminant Hydrology*, 25(1):129–156, Feb. 1997. ISSN 0169-7722. doi: 10.1016/S0169-7722(96)00024-1. URL http://www.sciencedirect.com/science/article/pii/S0169772296000241.

A. Dudill, P. Frey, and M. Church. Infiltration of fine sediment into a coarse mobile bed: a phenomenological study. *Earth Surface Processes and Landforms*, 42(8):1171–1185, June 2017. ISSN 1096-9837. doi: 10.1002/esp.4080. URL http://onlinelibrary.wiley.com/doi/10.1002/esp.4080/abstract.

K. Eastman. Effects of Embeddedness on Fish Habitats: An Approach for Implementation in the Habitat Simulation Model CASiMiR. Master's thesis, Institute of Hydraulic Engineering, University of Stuttgart, Germany, 2004.

I. Eglin, U. Roeck, F. Robach, and M. Tremolieres. Macrophyte biological methods used in the study of the exchange between the Rhine river and the groundwater. *Water Research*, 31(3):503–514, Mar. 1997. ISSN 0043-1354. doi: 10.1016/S0043-1354(96)00298-9. URL http://www.sciencedirect.com/science/article/pii/S0043135496002989.

H. A. Einstein. Deposition of Suspended Particles in a Gravel Bed. *Journal of the Hydraulics Division*, 94(5):1197–1206, 1968. URL http://cedb.asce.org/CEDBsearch/record.jsp?dockey=0015321.

E. Evans and A. C. Wilcox. Fine sediment infiltration dynamics in a gravel-bed river following a sediment pulse. *River Research and Applications*, 30(3):372–384, Mar. 2014. ISSN 15351459. doi: 10.1002/rra.2647. URL http://doi.wiley.com/10.1002/rra.2647.

E. S. B. Ferraz and O. Aguiar. Gamma-ray attenuation technique for determining density and water content of wood samples. *IPEF*, 30:9–12, 1985. URL http://ipef.br/publicacoes/scientia/nr30/cap01.pdf.

W. K. Fletcher, W. E. McLean, and T. Sweeten. An instrument to monitor infiltration of fine sediment into stable gravel stream beds. *Aquacultural Engineering*, 14(4):289–296, Jan. 1995. ISSN 0144-8609. doi: 10.1016/0144-8609(94)00007-N. URL http://www.sciencedirect.com/science/article/pii/014486099400007N.

L. Frostick, M. Lukas, and I. Reid. The infiltration of fine matrices into coarse-grained alluvial sediments and its implications for stratigraphical integration. *Journal of the Geological Society (London)*, 141:955–965, 1984.

S. Gayraud and M. Philippe. Influence of Bed-Sediment Features on the Interstitial Habitat Available for Macroinvertebrates in 15 French Streams. *International Review of Hydrobiology*, 88(1):77–93, Jan. 2003. ISSN 1522-2632. doi: 10.1002/iroh.200390007. URL https://onlinelibrary.wiley.com/doi/abs/10.1002/iroh.200390007.

S. Gerland and H. Villinger. Nondestructive density determination on marine sediment cores from gamma-ray attenuation measurements. *Geo-Marine Letters*, 15(2):111–118, 1995. URL http://link.springer.com/article/10.1007/BF01275415.

S. Gibson, D. Abraham, R. Heath, and D. Schoellhamer. Bridging process threshold for sediment infiltrating into a coarse substrate. *Journal of geotechnical and geoenvironmental engineering*, 136(2):402–406, 2009a. URL http://ascelibrary.org/doi/abs/10.1061/(ASCE)GT.1943-5606.0000219.

S. Gibson, D. Abraham, R. Heath, and D. Schoellhamer. Vertical gradational variability of fines deposited in a gravel framework. *Sedimentology*, 56(3):661–676, Apr. 2009b. ISSN 00370746, 13653091. doi: 10.1111/j.1365-3091.2008.00991.x. URL http://doi.wiley.com/10.1111/j.1365-3091.2008.00991.x.

S. Gibson, R. Heath, D. Abraham, and D. Schoellhamer. Visualization and analysis of temporal trends of sand infiltration into a gravel bed: TEMPORAL TRENDS OF SAND INFILTRATION INTO A GRAVEL BED. *Water Resources Research*, 47(12), Dec. 2011. ISSN 00431397. doi: 10.1029/2011WR010486. URL http://doi.wiley.com/10.1029/2011WR010486.

Q. GmbH. Kristallquarzsand feuergetrocknet - Quarzsande GmbH. URL http://www.quarzsande.at/produkte/kristallquarzsand_feuergetrocknet.php.

E. Group. Technical Information / Operating Instructions: Source container FQG60 Radiometric Measurement. Manual, Endress+Hauser Messtechnik GmbH+Co. KG, Germany, 2015. URL https://portal.endress.com/wa001/dla/5001016/7034/000/03/TI00445FEN_1615.pdf.

N. T. Hamm, W. B. Dade, and C. E. Renshaw. Fine particle deposition to porous beds. *Water Resources Research*, 47(11):W11508, Nov. 2011. ISSN 1944-7973. doi: 10.1029/2010WR010295. URL `http://onlinelibrary.wiley.com/doi/10.1029/2010WR010295/abstract`.

P. J. Hancock. Human Impacts on the Stream-Groundwater Exchange Zone. *Environmental Management*, 29(6):763–781, June 2002. ISSN 0364-152X, 1432-1009. doi: 10.1007/s00267-001-0064-5. URL `http://link.springer.com/10.1007/s00267-001-0064-5`.

S. Harper, I. Foster, D. Lawler, K. Mathers, M. McKenzie, and G. Petts. The complexities of measuring fine sediment accumulation within gravel-bed rivers. *River Research and Applications*, 33(10):1575–1584, Dec. 2017. ISSN 15351459. doi: 10.1002/rra.3198. URL `http://doi.wiley.com/10.1002/rra.3198`.

A. Herrero and C. Berni. Sand infiltration into a gravel bed: A mathematical model: SAND INFILTRATION INTO A GRAVEL BED. *Water Resources Research*, 52(11):8956–8969, Nov. 2016. ISSN 00431397. doi: 10.1002/2016WR019394. URL `http://doi.wiley.com/10.1002/2016WR019394`.

A. Herrero, C. Berni, and B. Cemenen. Laboratory Analysis on Silt Infiltration into Gravel Bed. In *E-proceedings of the 36th IAHR World Congress*, The Hague, Netherlands, 2015.

D. Huston and J. F. Fox. Momentum-Impulse Model of Fine Sand Clogging Depth in Gravel Streambeds for Turbulent Open-Channel Flow. *Journal of Hydraulic Engineering*, 142(2):04015055, Feb. 2016. ISSN 0733-9429, 1943-7900. doi: 10.1061/(ASCE)HY.1943-7900.0001092. URL `http://ascelibrary.org/doi/10.1061/%28ASCE%29HY.1943-7900.0001092`.

D. L. Huston and J. F. Fox. Clogging of Fine Sediment within Gravel Substrates: Dimensional Analysis and Macroanalysis of Experiments in Hydraulic Flumes. *Journal of Hydraulic Engineering*, 141(8):04015015, Aug. 2015. ISSN 0733-9429, 1943-7900. doi: 10.1061/(ASCE)HY.1943-7900.0001015. URL `http://ascelibrary.org/doi/10.1061/%28ASCE%29HY.1943-7900.0001015`.

H. B. N. Hynes. Groundwater and stream ecology. *Hydrobiologia*, 100(1):93–99, 1983. ISSN 0018-8158, 1573-5117. doi: 10.1007/BF00027424. URL `http://link.springer.com/10.1007/BF00027424`.

G. M. Kondolf, Y. Gao, G. W. Annandale, G. L. Morris, E. Jiang, J. Zhang, Y. Cao, P. Carling, K. Fu, Q. Guo, R. Hotchkiss, C. Peteuil, T. Sumi, H.-W. Wang, Z. Wang, Z. Wei, B. Wu, C. Wu, and C. T. Yang. Sustainable sediment management in reservoirs and regulated rivers: Experiences from five continents. *Earth's Future*, 2(5):256–280, 2014. ISSN 2328-4277. doi: 10.1002/2013EF000184. URL `https://agupubs.onlinelibrary.wiley.com/doi/abs/10.1002/2013EF000184`.

R. A. Kuhnle, D. G. Wren, E. J. Langendoen, and J. R. Rigby. Sand Transport over an Immobile Gravel Substrate. *Journal of Hydraulic Engineering*, 139(2):167–176, Feb. 2013. ISSN 1943-

7900. doi: 10.1061/(ASCE)HY.1943-7900.0000615. URL https://ascelibrary.org/doi/abs/10.1061/%28ASCE%29HY.1943-7900.0000615.

T. E. Lisle and J. Lewis. Effects of Sediment Transport on Survival of Salmonid Embryos in a Natural Stream: A Simulation Approach. *Canadian Journal of Fisheries and Aquatic Sciences*, 49(11):2337–2344, Nov. 1992. ISSN 0706-652X. doi: 10.1139/f92-257. URL https://www.nrcresearchpress.com/doi/abs/10.1139/f92-257.

G. Matthe and K. Ubell. Allgemeine Hydrogeologie, Grundwasserhaushalt, Gebr. *Borntraeger, Berlin*, 1983.

M. A. Mayar, G. Schmid, S. Wieprecht, and M. Noack. Optimizing vertical profile measurements setup of gamma ray attenuation. *Radiation Physics and Chemistry*, 164:108376, Nov. 2019. ISSN 0969806X. doi: 10.1016/j.radphyschem.2019.108376. URL https://linkinghub.elsevier.com/retrieve/pii/S0969806X18310740.

M. A. Mayar, G. Schmid, S. Wieprecht, and M. Noack. Proof-of-Concept for Nonintrusive and Undisturbed Measurement of Sediment Infiltration Masses Using Gamma-Ray Attenuation. *Journal of Hydraulic Engineering*, 146(5):04020032, May 2020. ISSN 0733-9429, 1943-7900. doi: 10.1061/(ASCE)HY.1943-7900.0001734. URL http://ascelibrary.org/doi/10.1061/%28ASCE%29HY.1943-7900.0001734.

M. A. Mayar, S. Haun, G. Schmid, S. Wieprecht, and M. Noack. Measuring vertical distribution and dynamic development of sediment infiltration under laboratory conditions. *Journal of Hydraulic Engineering*, (In press), 2022. doi: https://doi.org/10.1061/(ASCE)HY.1943-7900.0001980.

T. F. McCloskey and E. J. Finnemore. Estimating Hydraulic Conductivities in an Alluvial Basin from Sediment Facies Models. *Groundwater*, 34(6):1024–1032, 1996. ISSN 1745-6584. doi: 10.1111/j.1745-6584.1996.tb02168.x. URL https://ngwa.onlinelibrary.wiley.com/doi/abs/10.1111/j.1745-6584.1996.tb02168.x.

S. H. Mohajeri. *Hydrodynamics of Gravel Bed Flows (Implication on Colmation)*. PhD thesis, Queen Mary University of London, 2015. URL https://qmro.qmul.ac.uk/xmlui/handle/123456789/8770.

S. H. Mohajeri, M. Righetti, G. Wharton, and G. P. Romano. On the structure of turbulent gravel bed flow: Implications for sediment transport. *Advances in Water Resources*, 92:90–104, June 2016. ISSN 0309-1708. doi: 10.1016/j.advwatres.2016.04.001. URL http://www.sciencedirect.com/science/article/pii/S0309170816300847.

A. C. Moreira, O. Portezan Filho, F. H. M. Cavalcante, M. M. Coimbra, and C. R. Appoloni. Gamma ray transmission for hydraulic conductivity measurement of undisturbed soil columns. *Brazilian Archives of Biology and Technology*, 50(2):321–328, Mar. 2007. ISSN 1516-8913. doi: 10.1590/S1516-89132007000200017. URL http://www.scielo.br/scielo.php?script=sci_arttext&pid=S1516-89132007000200017&lng=en&tlng=en.

A. C. Moreira, O. P. Filho, F. H. d. M. Cavalcante, and C. R. Appoloni. Determination of Hydraulic Conductivity of Undisturbed Soil Column: a Measurement Accomplished with the Gamma Ray Transmission Technique. In O. Dikinya, editor, *Developments in Hydraulic Conductivity Research*. IntechOpen, Rijeka, 2011. doi: 10.5772/15866. URL https://doi.org/10.5772/15866.

M. Newson and D. Sear. Sediment and gravel transportation in rivers including the use of gravel traps. *Research and Development Note C*, 5, 1994.

V. Nikora, D. Goring, I. McEwan, and G. Griffiths. Spatially Averaged Open-Channel Flow over Rough Bed. *Journal of Hydraulic Engineering*, 127(2):123–133, Feb. 2001. ISSN 0733-9429. doi: 10.1061/(ASCE)0733-9429(2001)127:2(123). URL https://ascelibrary.org/doi/abs/10.1061/%28ASCE%290733-9429%282001%29127%3A2%28123%29.

Y. Niño, W. Licanqueo, C. Janampa, and A. Tamburrino. Front of unimpeded infiltrated sand moving as sediment transport through immobile coarse gravel. *Journal of Hydraulic Research*, 56(5):697–713, Sept. 2018. ISSN 0022-1686, 1814-2079. doi: 10.1080/00221686.2017.1402828. URL https://www.tandfonline.com/doi/full/10.1080/00221686.2017.1402828.

M. Noack. *Modelling Approach for Interstitial Sediment Dynamics and Reproduction of Gravel-Spawning Fish*. Dissertation No. 214, Institute for Modelling Hydraulic and Environmental Systems, University of Stuttgart, Stuttgart, Germany, 2012. URL https://elib.uni-stuttgart.de/handle/11682/485.

M. Noack, J. Ortlepp, and S. Wieprecht. An Approach to Simulate Interstitial Habitat Conditions During the Incubation Phase of Gravel-Spawning Fish. *River Research and Applications*, 33(2):192–201, Mar. 2016. ISSN 1535-1467. doi: 10.1002/rra.3012. URL https://onlinelibrary.wiley.com/doi/abs/10.1002/rra.3012.

M. Noack, L. Seitz, M. A. Mayar, S. Haun, and S. Wieprecht. How to address colmation best? – Field and laboratory investigations at different scales. page 8, 2020.

P. N. Owens, R. J. Batalla, A. J. Collins, B. Gomez, D. M. Hicks, A. J. Horowitz, G. M. Kondolf, M. Marden, M. J. Page, D. H. Peacock, E. L. Petticrew, W. Salomons, and N. A. Trustrum. Fine-grained sediment in river systems: environmental significance and management issues. *River Research and Applications*, 21(7):693–717, 2005. ISSN 1535-1467. doi: https://doi.org/10.1002/rra.878. URL https://onlinelibrary.wiley.com/doi/abs/10.1002/rra.878.

L. Pires, J. Rosa, A. Pereira, R. Arthur, and O. Bacchi. Gamma-ray attenuation method as an efficient tool to investigate soil bulk density spatial variability. *Annals of Nuclear Energy*, 36(11-12):1734–1739, Nov. 2009. ISSN 03064549. doi: 10.1016/j.anucene.2009.08.016. URL http://linkinghub.elsevier.com/retrieve/pii/S0306454909002771.

L. F. Pires and A. B. Pereira. Gamma-Ray Attenuation to Evaluate Soil Porosity: An Analysis of Methods. *The Scientific World Journal*, 2014:1–10, 2014. ISSN 2356-6140, 1537-744X. doi: 10.1155/2014/723041. URL http://www.hindawi.com/journals/tswj/2014/723041/.

W. S. Platts. *Methods for Evaluating Stream, Riparian, and Biotic Conditions*. U.S. Department of Agriculture, Forest Service, Intermountain Forest and Range Experiment Station, 1982. Google-Books-ID: kVrlw7GgI28C.

M. Pätzig, S. Kube, M. Labrenz, M. Stöck, S. U. Pauls, J. Dutz, F. Hölker, J. M. Jeschke, H.-P. Grossart, P. Haase, M. Gessner, K. Jürgens, A. Kremp, R. Arlinghaus, S. Jähnig, J. Freyhof, M. Pusch, and J. Piontek. Forschungsagenda zur biologischen Vielfalt der Binnen- und KüstengewässerLebendiges Wasser. 2019. doi: 10.4126/FRL01-006414368. URL https://repository.publisso.de/resource/frl:6414368.

R. J. Reginato. Water content and bulk density changes in a soil pedon measured with dual energy gamma-ray transmission. *Canadian journal of soil science*, 54(3):325–328, 1974. URL http://www.nrcresearchpress.com/doi/abs/10.4141/cjss74-042.

A. Reikowski. *Betriebsanleitung FRAHM-LOT*. MBT Underwater Technology, Kiel, 1.1 edition, 2015.

E. Rosenbrand and J. Dijkstra. Application of image subtraction data to quantify suffusion. *Géotechnique Letters*, 2(2):37–41, Apr. 2012. ISSN 2045-2543. doi: 10.1680/geolett.12.00006. URL http://www.icevirtuallibrary.com/doi/10.1680/geolett.12.00006.

N. Sadid, S. Haun, and S. Wieprecht. An overview of hydro-sedimentological characteristics of intermittent rivers in Kabul region of Kabul river basin. In *River Sedimentation: Proceedings of the 13th International Symposium on River Sedimentation (Stuttgart, Germany, 19-22 September, 2016)*, page 85. CRC Press, 2016.

N. Sadid, S. Haun, and S. Wieprecht. An overview of hydro-sedimentological characteristics of intermittent rivers in Kabul region of Kabul river basin. *International Journal of River Basin Management*, 15(4):387–399, Oct. 2017. ISSN 1571-5124, 1814-2060. doi: 10.1080/15715124.2017.1321004. URL https://www.tandfonline.com/doi/full/10.1080/15715124.2017.1321004.

U. Schälchli. The clogging of coarse gravel river beds by fine sediment. *Hydrobiologia*, 235(1):189–197, July 1992. ISSN 1573-5117. doi: 10.1007/BF00026211. URL https://doi.org/10.1007/BF00026211.

U. Schälchli. *DIE KOLMATION VON FLIESSGEWASSERSOHLEN: PROZESSE UND BERECHNUNGSGRUNDLAGEN*. PhD thesis, ETHZ, 1993.

U. Schälchli. Basic Equations for Siltation of Riverbeds. *Journal of Hydraulic Engineering*, 121(3):274–287, Mar. 1995. ISSN 0733-9429, 1943-7900. doi: 10.1061/(ASCE)0733-9429(1995)121:3(274). URL http://ascelibrary.org/doi/10.1061/%28ASCE%290733-9429%281995%29121%3A3%28274%29.

U. Schälchli, J. Abegg, and L. Hunzinger. Kolmation–Methoden zur Erkennung und Bewertung. *Eidg. Anstalt für Wasserversorgung, Abwasserreinigung und Gewässerschutz EAWAG, Dübendorf, Schweiz*, 2002.

M. Schwarz, S. Fuchs, and H. H. Hahn. Mikrobielle Kolmation und Dekolmation in Bodenfiltern. *Mikrobielle Kolmation und Dekolmation in Bodenfiltern*, 55(10):20–23, 2003. ISSN 0043-0951.

L. Seitz. *Development of new methods to apply a multi-parameter approach – A first step towards the determination of colmation*. PhD thesis, University of Stuttgart, Stuttgart, Germany, 2020.

L. Seitz, I. Lenz, M. Noack, S. Wieprecht, and C. Haas. Kolmation - Eine unterschätzte Größe in der Gewässerbewertung? *WASSERWIRTSCHAFT*, 109:41–46, Mar. 2019. doi: 10.1007/s35147-019-0005-y.

G. H. S. Smith and A. P. Nicholas. Effect on flow structure of sand deposition on a gravel bed: Results from a two-dimensional flume experiment. *Water Resources Research*, 41(10), 2005. ISSN 1944-7973. doi: 10.1029/2004WR003817. URL `https://agupubs.onlinelibrary.wiley.com/doi/abs/10.1029/2004WR003817`.

K. Sternecker, R. Wild, and J. Geist. Effects of substratum restoration on salmonid habitat quality in a subalpine stream. *Environmental Biology of Fishes*, 96(12):1341–1351, Dec. 2013. ISSN 1573-5133. doi: 10.1007/s10641-013-0111-0. URL `https://doi.org/10.1007/s10641-013-0111-0`.

D. Tonina and J. M. Buffington. Hyporheic Exchange in Mountain Rivers I: Mechanics and Environmental Effects. *Geography Compass*, 3(3):1063–1086, May 2009. ISSN 17498198, 17498198. doi: 10.1111/j.1749-8198.2009.00226.x. URL `http://doi.wiley.com/10.1111/j.1749-8198.2009.00226.x`.

B. Velickovic. Colmation as one of the processes in interaction between the groundwater and surface water. *Facta universitatis - series: Architecture and Civil Engineering*, 3(2):165–172, 2005. ISSN 0354-4605. doi: 10.2298/FUACE0502165V. URL `http://www.doiserbia.nb.rs/Article.aspx?ID=0354-46050502165V`.

R. H. Webb and S. A. Leake. Ground-water surface-water interactions and long-term change in riverine riparian vegetation in the southwestern United States. *Journal of Hydrology*, 320 (3-4):302–323, Apr. 2006. ISSN 00221694. doi: 10.1016/j.jhydrol.2005.07.022. URL `https://linkinghub.elsevier.com/retrieve/pii/S0022169405003525`.

G. Wharton, S. H. Mohajeri, and M. Righetti. The pernicious problem of streambed colmation: a multi-disciplinary reflection on the mechanisms, causes, impacts, and management challenges: The pernicious problem of streambed colmation. *Wiley Interdisciplinary Reviews: Water*, page e1231, July 2017. ISSN 20491948. doi: 10.1002/wat2.1231. URL `http://doi.wiley.com/10.1002/wat2.1231`.

P. R. Wilcock, A. F. Barta, C. C. Shea, G. M. Kondolf, W. V. G. Matthews, and J. Pitlick. Observations of Flow and Sediment Entrainment on a Large Gravel-Bed River. *Water Resources Research*, 32(9):2897–2909, Apr. 1996. ISSN 1944-7973. doi: 10.1029/96WR01628. URL `https://agupubs.onlinelibrary.wiley.com/doi/abs/10.1029/96WR01628`.

P. J. Wood. Biological Effects of Fine Sediment in the Lotic Environment. *Environmental Management*, 21(2):203–217, Mar. 1997. ISSN 0364-152X, 1432-1009. doi: 10.1007/s002679900019. URL `http://link.springer.com/10.1007/s002679900019`.

J. K. Wooster, S. R. Dusterhoff, Y. Cui, L. S. Sklar, W. E. Dietrich, and M. Malko. Sediment supply and relative size distribution effects on fine sediment infiltration into immobile gravels: Fine sediment infiltration into immobile gravels. *Water Resources Research*, 44(3):n/a–n/a, Mar. 2008. ISSN 00431397. doi: 10.1029/2006WR005815. URL `http://doi.wiley.com/10.1029/2006WR005815`.

D. G. Wren, E. J. Langendoen, and R. A. Kuhnle. Effects of sand addition on turbulent flow over an immobile gravel bed. *Journal of Geophysical Research: Earth Surface*, 116(F1), 2011. ISSN 2156-2202. doi: 10.1029/2010JF001859. URL https://agupubs.onlinelibrary.wiley.com/doi/abs/10.1029/2010JF001859.

A. E. Zimmermann and M. Lapointe. Intergranular flow velocity through salmonid redds: sensitivity to fines infiltration from low intensity sediment transport events. *River Research and Applications*, 21(8):865–881, 2005. ISSN 1535-1467. doi: 10.1002/rra.856. URL https://onlinelibrary.wiley.com/doi/abs/10.1002/rra.856.

Publication I.

Optimizing vertical profile measurements setup of gamma ray attenuation

Table 5.1. Metadata of publication I

Title	Optimizing vertical profile measurements setup of gamma ray attenuation
Authors	**M. A. Mayar**, G. Schmid, S. Wieprecht, M. Noack
Journal	Radiation Physics and Chemistry
Submitted	October 24, 2018
Accepted	June 20, 2019
Published	June 21, 2019
DOI	https://doi.org/10.1016/j.radphyschem.2019.108376

The final version of this article is accessed through the above DOI link.

Optimizing vertical profile measurements setup of gamma ray attenuation

M. A. Mayar[1, 2,*], G. Schmid[1], S. Wieprecht[1], M. Noack[1,3]

[1] *Institute for Modelling Hydraulic and Environmental Systems, University of Stuttgart, Stuttgart, Germany*

[2] *Environmental and Water Resources Engineering Faculty, Kabul Polytechnic University, Kabul, Afghanistan*

[3] *Faculty of Architecture and Civil Engineering, Karlsruhe University of Applied Science, Karlsruhe, Germany.*

* *Corresponding author: M.A. Mayar, Email: assem.mayar@iws.uni-stuttgart.de*

Abstract:

For undisturbed measurements of material properties, the gamma ray attenuation (GRA) method is a commonly used approach, e.g. in soil sciences. So far, various setups of the GRA method are applied depending on specific purposes. For accurate measurements, statistical error due to radioactive decay must be considered. In addition, a careful setting of the further involved parameters such as collimator size, the distance between source and detector as well as the measuring time need to be taken into account. In this study, a method to optimize GRA measurements is presented by relating measuring time and collimator selection to the statistical error of radiation. As a result, a method for choosing the optimum collimator size and a mathematical equation for optimizing the measuring time are derived, which is helpful for planning the vertical profile measurement in terms of required time and spatial resolution.

Keywords: gamma ray attenuation, optimization of the experimental setup, vertical profile measurements

1. Introduction:

Gamma Ray Attenuation (GRA) is a robust measuring technique for undisturbed measurements of materials' physical properties e.g. soil bulk density, water content, porosity, (Pires and Pereira 2014; Pires et al. 2009; Baytaş and Akbal 2002; Gerland and Villinger 1995; Reginato 1974; Cassel and Krueger 1972), particle size analysis (Elias 2004; Naime et al. 2001; Elias et al. 1999; Oliveira et al. 1997), soil column's hydraulic conductivity and density profile (Beckers et al. 2018; Moreira et al. 2011, 2007; Gerland and Villinger 1995).

To measure an accurate vertical profile of soil using gamma ray attenuation; the spatial resolution is a vital parameter and is basically determined by the collimator size. In previous studies, different combinations of collimators are used behind the gamma source and before detection. Early researchers utilized equal collimator sizes in both source and detector sides such as (Ferraz and Aguiar 1985) for density, (Naime et al. 2001; Oliveira et al. 1997) for particle size analyses and Gerland and Villinger (1995) for sediment core density profile. But, more recent studies apply different collimator sizes for the source and detector sides, whereby the detector collimator is predominantly larger to achieve a higher count rate (Saadi and Saadon 2012; Şahin et al. 2011; Moreira et al. 2011, 2007). However, continuous soil profile measurements with different collimators lead to uncovered or overlapping measuring areas. Besides, Singh et al. (2006) and Sidhu et al. (1999) also reported that increasing the detector collimator size will detect more scattered events, which might be out of computation and may affect the result.

Generally, the GRA measurements are based on the Beer-Lambert law that is shown in Equation 1.

$$I = I_0 \, e^{-(\mu\rho x)} \dots\dots\dots\dots\dots\dots 1$$

where I_0, I, μ, ρ and x are the count rate before and after passing the absorber, mass attenuation coefficient, density and net thickness of absorber, respectively. The absorber thickness x can simply be measured while the density ρ can be determined by measuring I_0 and I before and after passing the penetrating media. The mass attenuation coefficient μ can either be calculated from a precise geometry of the absorber or can be derived from the XCOM systems (Gerward et al. 2004; Berger et al. 1998; Berger and Hubbell 1987) by knowing the composition of the absorber.

In principle, the quantity of the transmitted count rate depends on radiating source energy, geometrical setup, collimator sizes, and measuring material properties. However, a lower limit for the count rate is also given by the natural environment radiation. The transmitted count rate should be significantly larger compared to the count rate of the natural environment radiation. For a given gamma source, geometrical setup (collimator sizes, distance between source and receiver, object thickness) and absorber properties (density), the number of transmitted counts and thus the accuracy of GRA measurements solely depend on the measuring time.

GRA measurements are associated with a statistical error given the radioactive decay that can be estimated using Poisson's statistics for the transmitted counts (Equation 2), where δ is the statistical error in percent and $\overline{N}$ is the average number of counts.

$$\delta_{\%} = \pm \frac{1}{\sqrt{\overline{N}}} * 100 \dots\dots\dots\dots\dots .2$$

Equation 2 shows that the statistical error is only a function of the number of collected counts at the detector. In literature, different measuring times are applied leading to transmitted counts with a statistical error between 1% and 5% (Pires and Pereira 2014; Moreira et al. 2011; Pires et al. 2009). However, this measuring time could be optimized for each collimator size and penetrated media to reduce the statistical error to a desired level.

So far, information about the relation between the governing variables for representative GRA measurements is rare in literature. Therefore, this study presents a method to optimize the GRA measurement setup by relating measuring time and collimator selection to the count rate depending on the statistical error.

2. Methods

The applied radioactive source in the conducted experiments is Cesium Cs^{137} with a decay energy of 661 KeV. A detector unit with 5cm diameter and 5cm thick scintillator made of Sodium Iodide doped with Thallium (NaI (TI)) is employed. To neglect any temperature effects, the room's temperature was kept constant (27°C) throughout the entire experiments. Two sets of experiments were performed to analyze the relation between collimator selection, measuring time and the count rate depending on the statistical error.

The first setup aimed at the selection of best sizes for the combination of source and detector collimators. According to the geometrical analyses of continuous measurements of a vertical profile, equal size collimators show the best coverage (**Figure 1**). A larger detector collimator creates an overlap or uncovered areas proportional to the size difference between the source and the detector collimator and dependent the result during overlap on the location of the upper and lower measurements in the vertical profile. Hence, equal size collimators for both sides were selected for further applications.

Subsequently, five diameters (5, 7, 9, 12, 15 mm) of identical source and detector collimators were employed to measure the initial count rate for distances of 19 and 49 cm between the source and the detector collimator. A measuring time of 120 to 30s was used depending on the applied collimator sizes. The longest measuring times were applied for the smallest collimator size to collect sufficient counts for reducing the statistical error effect. In addition, each measurement was repeated four times for further reduction of uncertainty. Based on this setup a relation between the initial count rates and the ratios of the collimators' cross-sectional areas were derived for the selection of the optimal collimator size.

The second experimental setup aims at analyzing the relation between the statistical error, the thickness of the penetrated media, collimator diameters and the measuring time (**Figure 2**). The penetrated media for this setup consisted of cuboids with six different thicknesses (1.0, 3.0, 5.0, 7.0, 10.0, 15.0 cm). The height and width of each sample were constant (z = 2.0 cm and y = 2.6 cm). Each cuboid was measured at a central position with four repetitions to determine the transmitted count rate. The distance between source and detector collimator of 19 cm was kept constant for all measurements, whereby the diameter of each investigated source and detector collimator was identical. In addition, various measuring times (30, 60, 90, 120 s) were utilized depending on the applied collimator sizes to evaluate the statistical error. The measurements were conducted for three different materials with known densities: Aluminum (Al) $\rho_{Al} = 2.65\ g/cm^3$, Polyvinylchloride (PVC) $\rho_{PVC} = 1.39\ g/cm^3$, and Polypropylene (PP) $\rho_{PP} = 0.91\ g/cm^3$.

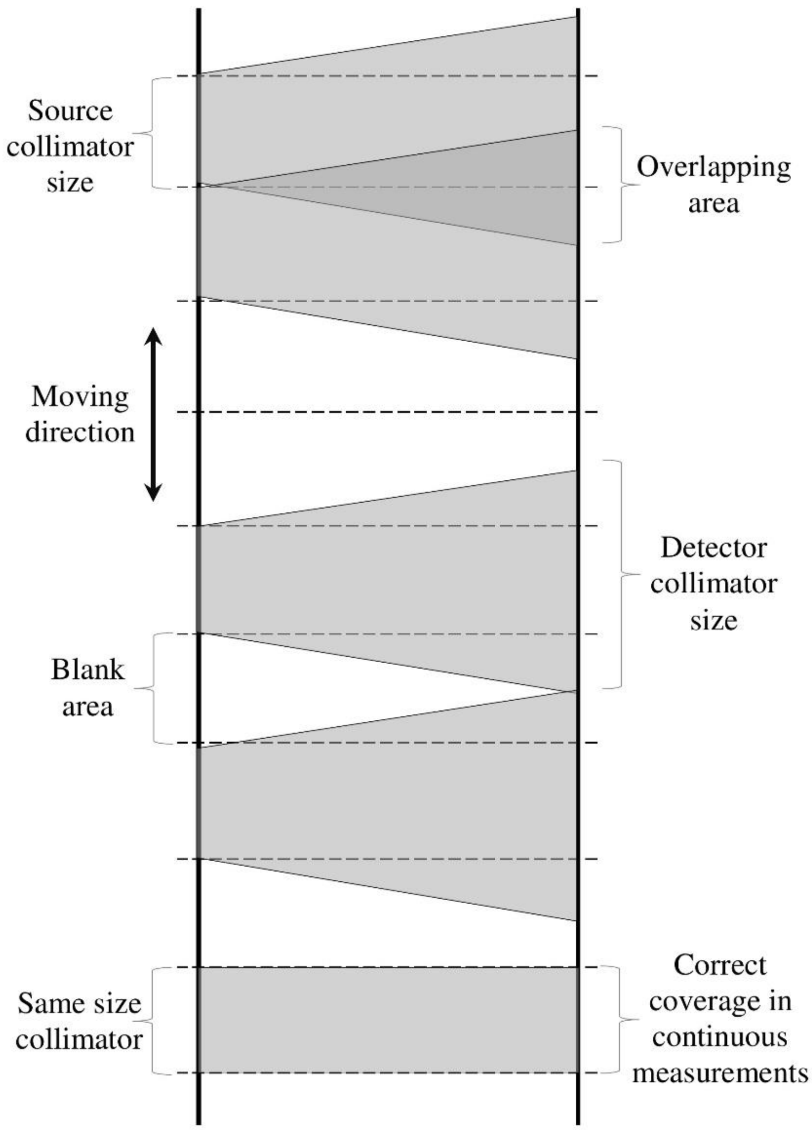

Figure 1: Collimator combination and profile coverage geometrical analyses

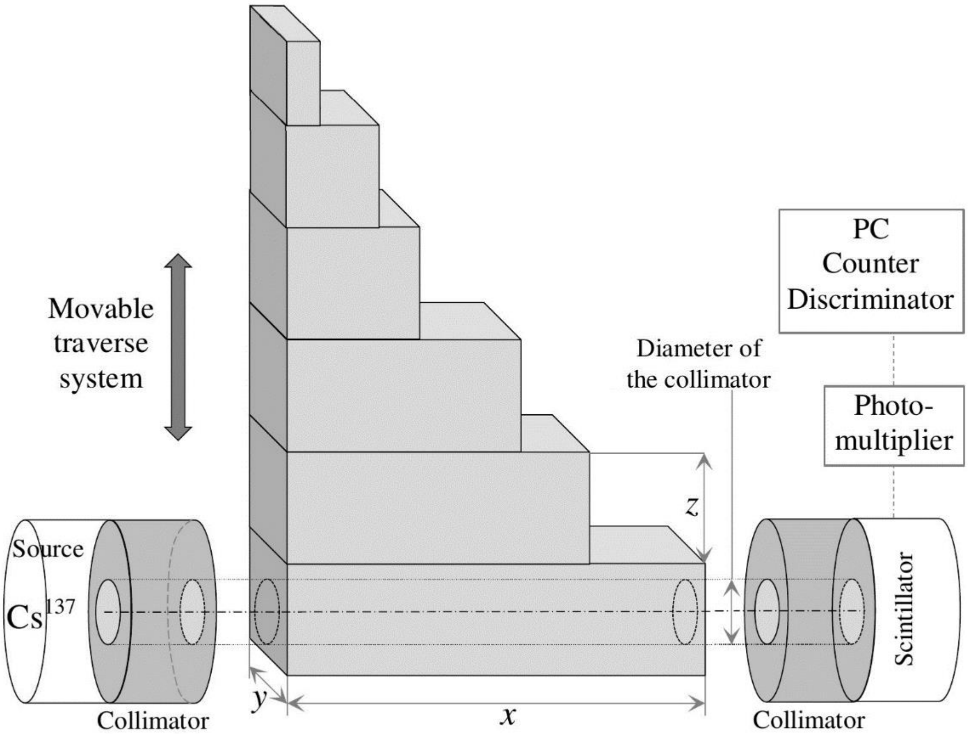

Figure 2: Scheme of the GRA measurement to relate statistical error, thickness of penetrated media, count rates and measuring time.

3. Results and discussion

The relation between the ratios of the different size identical collimators' cross sectional area and the ratios of the initial count rate (Equation 3) show a linear trend, as it can be indicated in

for two different distances between source and detector (19cm, 49cm). The slope of this relation is not only a function of the collimator size but depends also on radiation source characteristics and the distance between the source and the detector.

$$\frac{A_{\emptyset i}}{A_1} = \frac{I_{0_{\emptyset i}}}{I_{0_{\emptyset 1}}} \dots \dots (3)$$

where A_1, $A_{\emptyset i}$, $I_{0_{\emptyset 1}}$ and $I_{0_{\emptyset i}}$ are the cross-sectional areas and the initial count rates for the first and the $i-th$ collimator size respectively. The results of the initial count rate measurements for each collimator size and their related cross-sectional areas are shown in Table 1 for both distances.

Table 1: Measured initial count rates (counts per second, cps) for the different investigated collimator sizes (given in diameter and cross-sectional area) and different measuring times. *

Collimator diameter (mm)	5	7	9	12	15
Cross-sectional area (mm^2)	19.625	38.465	63.585	113.04	176.625
Area ratio (-)	1.00	1.96	3.24	5.76	9.00
Initial count rates at 19 cm - I_0 (cps)	48.20	90.00	153.50	262.46	400.00
Initial count rates at 49 cm - I_0 (cps)	17.218	27.029	39.688	-	88.570
Count rate ratio at 19 cm (-)	1.00	1.87	3.19	5.44	8.30
Count rate ratio at 49 cm (-)	1.00	1.57	2.31	-	5.14
Measuring time (s)	120	60	30	30	30

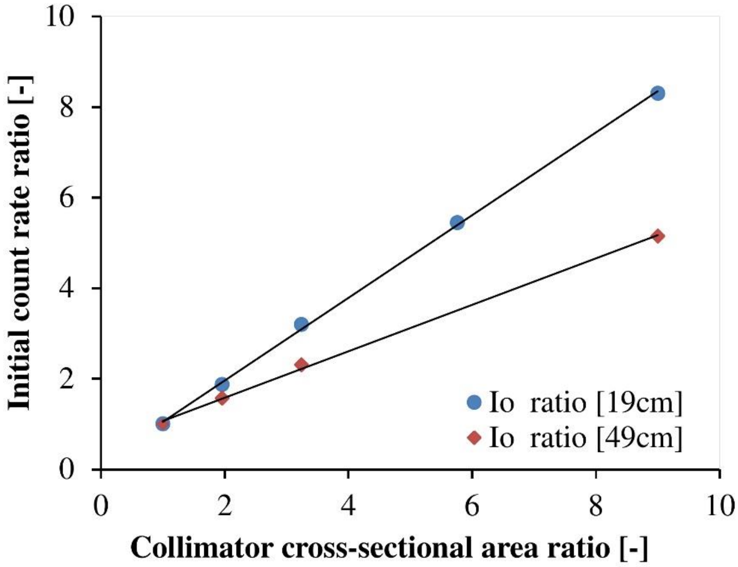

Figure 3: Linear relation between the collimator cross-sectional area ratios versus the initial count rate ratios.

The results show that for arbitrary experiments, at least the initial count rate of two collimators need to be measured to obtain a linear trend for a given distance between source and detector. After these pre-measurements, the optimal collimator size can be selected from the interpolation or extrapolation of Equation 3 in dependency of the count rate, which includes the statistical error of the pre-measurements. Hence, the statistical error of the initial conditions for a newly selected collimator can be estimated by the Poisson's statistics.

* The initial count rate for the collimator diameter = 12mm at 49 cm distance was not measured during experiment. However, this does not affect the final result.

Therefore, the count rate simply needs to be transferred back to absolute counts by multiplying the selected count rate with the desired measuring time.

The analyses of the second experimental setup showed that the smaller collimator sizes are inversely related to the count rate. For achieving a constant statistical error (required counts using Equation 2) for a specific material and geometrical setup, different measurement times are required for different collimator sizes. Hence, the measuring time for a specific collimator size is then only related to its count rate or equal to the required number of counts for the desired statistical error (Equation 2), divided by the collimator dependent count rate after passing the penetrated media. The transmitted count rate could be either measured directly or estimated by the Beer-Lambert law. After simplification, the required measuring time t [s] is equal to:

$$t = \frac{\overline{N_\delta}}{I} = \frac{10^4 * \delta^{-2}}{I} = \frac{10^4}{(I_0 * e^{-\mu\rho x})\delta^2} \ldots\ldots\ldots 4$$

where $\overline{N_\delta}, I_0, I, \mu, \rho, x$ are the average number of counts required for a specific statistical error, count rate (counts per second [cps]) before and after passing the absorber, mass attenuation coefficient [-], density [g/cm^3] and absorber thickness [cm] respectively.

To estimate the transmitted intensity I using Equation 1, I_0 must be measured in advance because it varies due to the source energy range, the distance between the source and the detector as well as the experimental conditions. The mass attenuation coefficient μ can be derived from the XCOM databases (Berger et al. 1998, Gerward et al. 2004), as it was used in this and many other studies in the literature.

The developed Equation 4 is used to compute the relation between measuring time, statistical error and thickness for each material type (PVC, Al and PP) resulting in three dimensional correlations, that are exemplarily shown in **Figure 4** for a collimator size of 9mm.

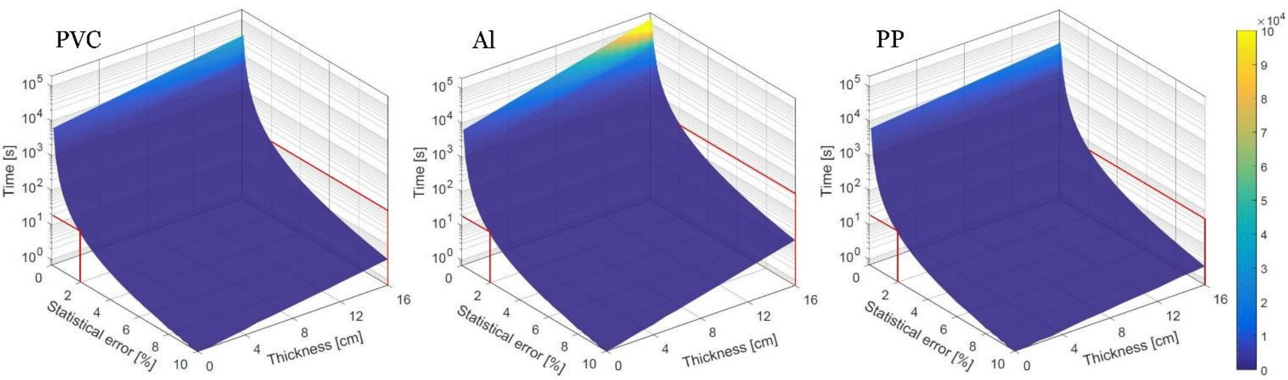

Figure 4: Computational results for the materials PVC, Al and PP relating thicknesses, statistical error and measuring time.

The graphs show that the required measuring times for a constant statistical error is changing given the different densities of each material type. In addition, it can be indicated that the density has a higher influence on the required measuring time compared to the thickness of a material type. As an example: the required measuring time for maintaining the statistical error to 2% in the initial condition (no absorber) gives 18 s (according to Equation 4), while for an absorber of 16.0 cm thickness of PVC, Equation 4 yields a required measured time of 95 s, for PP it is 60 s and for Al it is 385 s (the examples are marked with red lines in **Error! Reference source not found.**). Based on these results, Equation 4 provides a helpful tool to optimize the experimental setup for GRA measurements. If a certain statistical error should be achieved, Equation 4 could be used to estimate the required measuring time based on thickness and material properties of the penetrated media.

Figure 5 presents a comparison of measured (Equation 2) and computed (Equation 4) statistical errors for a constant measuring time of 30s. Exemplarily the result for collimator sizes of 9mm and 15mmalong with the corresponding measured count rates are shown for all three material types. In both cases, low thicknesses lead to high count rates and accordingly to a low statistical error. For the collimator size of 9mm, **Figure 5** indicates for the materials PVC and PP a high agreement of estimated and measured statistical errors for all investigated thicknesses. However, for Al the largest thickness of 15cm shows a significant deviation between the measured and calculated statistical error. The reason is the low count rate for this thickness. To achieve more reliable results either several repetitive measurements are required or the measuring time needs to be increased. A similar behavior can be observed for the collimator size of 15mm.

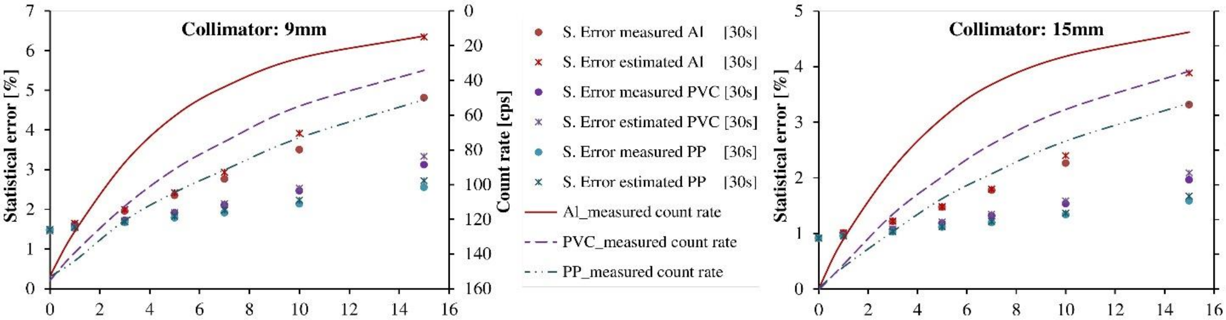

Figure 5: Comparison of estimated (Equation 4) and measured statistical error for all material types (dots, stars), while the lines represent the measured count rates of each material type.

Equation 4 allows for an estimation of the experimental boundary conditions for GRA measurements. By recording the initial intensity of GRA, the measuring time for a desired statistical error of each absorber can be optimized, or vice versa the statistical error for each measuring time could be predicted. Generally, the measuring time and the statistical error have an opposite relation for GRA measurements. Short measuring times are associated with a higher statistical error while longer measuring times have a lower statistical error. Temperature effects are sensitive in long-term measurements (Peyvandi et al. 2014), such as several hours or days. Therefore the temperature must be kept constant if smaller collimator sizes (lower count rates) and accordingly longer measuring times are desired.

4. Conclusions

Two sets of experiments were performed for optimizing the vertical profile measurements setup of GRA. The first experiment aims to find the relation between the collimator's cross-sectional area and the initial count rate ratio for a suitable collimator selection, while the second experiment intended to relate the measuring time, the collimator size and the count rate dependent statistical error. The first experiment resulted in a method for an optimal collimator selection based on two pre-measurements, while the second experiment resulted in an equation to predict the measuring time for a desired statistical error to support users in defining their boundary conditions for GRA measurements. The estimation of GRA accuracy (based on the statistical error) is in high agreement with measured values except for very low count rates. Finally, the developed relation is capable to determine boundary conditions using only initial count rate measurements before performing an experiment and thus helps to find an optimal compromise between the vertical resolution (depending on the collimator size) and required measuring time for a predefined accuracy based on the statistical error due to the source radioactive decay.

5. References

Baytaş, A. Filiz, and Sevgi Akbal. 2002. "Determination of Soil Parameters by Gamma-Ray Transmission." *Radiation Measurements* 35(1): 17–21.

Beckers, Felix, Stefan Haun, and Markus Noack. 2018. "Experimental Investigation of Reservoir Sediments" eds. A. Paquier and N. Rivière. *E3S Web of Conferences* 40: 03030.

Berger, Martin J, and JH Hubbell. 1987. *XCOM: Photon Cross Sections on a Personal Computer*. Washington DC: National Bureau of Standards. http://www.iaea.org/inis/collection/NCLCollectionStore/_Public/19/009/19009871.pdf?r=1 (August 3, 2018).

Berger, MJ et al. 1998. *XCOM: Photon Cross Sections Online Database*. NIST standard reference database. English. https://physics.nist.gov/PhysRefData/Xcom/html/xcom1.html (March 12, 2019).

Cassel, D. K., and T. H. Krueger. 1972. "Gamma Rays Determine Soil Water Content of Soil-Plant Systems." https://library.ndsu.edu/ir/bitstream/handle/10365/24424/ndfr_19720301_v29_iss04_003.pdf?sequence=1&isAllowed=y (March 12, 2019).

Elias, E. A., O. O. S. Bacchi, and K. Reichardt. 1999. "Alternative Soil Particle-Size Analysis by Gamma-Ray Attenuation." *Soil and Tillage Research* 52(1): 121–123.

Elias, Elimoel A. 2004. "A Simplified Analytical Procedure for Soil Particle-Size Analysis by Gamma-Ray Attenuation." *Computers and Electronics in Agriculture* 42(3): 181–84.

Ferraz, E. S. B., and O. Aguiar. 1985. "Gamma-Ray Attenuation Technique for Determining Density and Water Content of Wood Samples." *IPEF* 30: 9–12.

Gerland, Sebastian, and Heinrich Villinger. 1995. “Nondestructive Density Determination on Marine Sediment Cores from Gamma-Ray Attenuation Measurements.” *Geo-Marine Letters* 15(2): 111–118.

Gerward, L., N. Guilbert, K.B. Jensen, and H. Levring. 2004. “WinXCom—a Program for Calculating X-Ray Attenuation Coefficients.” *Radiation Physics and Chemistry* 71(3–4): 653–54.

Moreira, Anderson Camargo et al. 2007. “Gamma Ray Transmission for Hydraulic Conductivity Measurement of Undisturbed Soil Columns.” *Brazilian Archives of Biology and Technology* 50(2): 321–28.

Moreira, Anderson Camargo, Otávio Portezan Filho, Fábio Henrique de Moraes Cavalcante, and Carlos Roberto Appoloni. 2011. “Determination of Hydraulic Conductivity of Undisturbed Soil Column: A Measurement Accomplished with the Gamma Ray Transmission Technique.” In *Developments in Hydraulic Conductivity Research*, ed. Oagile Dikinya. Rijeka: IntechOpen. https://doi.org/10.5772/15866.

Naime, J. M., C. M. P. Vaz, and A. Macedo. 2001. “Automated Soil Particle Size Analyzer Based on Gamma-Ray Attenuation.” *Computers and electronics in agriculture* 31(3): 295–304.

Oliveira, J. C. M., K. Reichardt, C. M. P. Vaz, and D. Swartzendruber. 1997. “Improved Soil Particle-Size Analysis by Gamma-Ray Attenuation.” *Soil Science Society of America Journal* 61(1): 23–26.

Peyvandi, R. G., S. R. Tootkaleh, S. Z. Islami rad, and R. Hosseinzadeh. 2014. “Influence of Temperature on the Performance of Gamma Densitometer.” *Instruments and Experimental Techniques* 57(6): 667–70.

Pires, L.F. et al. 2009. “Gamma-Ray Attenuation Method as an Efficient Tool to Investigate Soil Bulk Density Spatial Variability.” *Annals of Nuclear Energy* 36(11–12): 1734–39.

Pires, Luiz F., and André B. Pereira. 2014. “Gamma-Ray Attenuation to Evaluate Soil Porosity: An Analysis of Methods.” *The Scientific World Journal* 2014: 1–10.

Reginato, R. J. 1974. “Water Content and Bulk Density Changes in a Soil Pedon Measured with Dual Energy Gamma-Ray Transmission.” *Canadian journal of soil science* 54(3): 325–328.

Saadi, A. J. Al, and A. K. Saadon. 2012. “Using Gamma Ray Transmission for Determination of Porosity in Doped Alumina Samples.” *Ibn Al-Haitham Journal for Pure and Applied Science* 25(1).

Şahin, Yusuf et al. 2011. “Measurement of Soil Water Using Compton Scattering.” *X-Ray Spectrometry* 40(4): 315–18.

Sidhu, Gurdeep S., Karamjit Singh, Parjit S. Singh, and Gurmel S. Mudahar. 1999. “Effect of Collimator Size and Absorber Thickness on Gamma Ray Attenuation Measurements.” *Radiation Physics and Chemistry* 56(5): 535–37.

Singh, Manpreet, Gurvinderjit Singh, B.S. Sandhu, and Bhajan Singh. 2006. “Effect of Detector Collimator and Sample Thickness on 0.662MeV Multiply Compton-Scattered Gamma Rays.” *Applied Radiation and Isotopes* 64(3): 373–78.

Publication II.

Proof-of-concept for nonintrusive and undisturbed measurement of sediment infiltration masses using gamma-ray attenuation

Table 5.2. Metadata of publication II

Title	Proof-of-concept for nonintrusive and undisturbed measurement of sediment infiltration masses using gamma-ray attenuation
Authors	**M. A. Mayar**, G. Schmid, S. Wieprecht, and M. Noack
Journal	ASCE Journal of Hydraulic Engineering
Submitted	April 01, 2019
Accepted	October 14, 2019
Published	March 03, 2020
DOI	https://doi.org/10.1061/(ASCE)HY.1943-7900.0001734

The final version of this article is accessed through the above DOI link.

Proof-of-concept for Non-intrusive and Undisturbed Measurement of Sediment Infiltration Masses Using Gamma Ray Attenuation

M.A. Mayar[1], G. Schmid[2], S. Wieprecht[3], and M. Noack[4]

[1]Ph.D. Candidate, Institute for Modelling Hydraulic and Environmental Systems, University of Stuttgart, Stuttgart, Germany; Lecturer, Environmental and Water Resources Engineering Faculty, Kabul Polytechnic University, Kabul, Afghanistan. Email: assem.mayar@iws.uni-stuttgart.de

[2]Technical Director of the Hydraulic Laboratory, Institute for Modelling Hydraulic and Environmental Systems, University of Stuttgart, Stuttgart, Germany. Email: gerhard.schmid@iws.uni-stuttgart.de

[3]Professor, Institute for Modelling Hydraulic and Environmental Systems, University of Stuttgart, Stuttgart, Germany. Email: silke.wieprecht@iws.uni-stuttgart.de

[4]Professor, Faculty of Architecture and Civil Engineering, University of Applied Science, Karlsruhe, Germany; Head of the Hydraulic Laboratory, Institute for Modelling Hydraulic and Environmental Systems, University of Stuttgart, Stuttgart, Germany. Email: markus.noack@hs-karlsruhe.de

ABSTRACT

Fine sediment infiltration into gravel riverbeds adversely affects the riverine ecology and influences hyporheic exchange processes. So far different sampling methods have been utilized to measure the amount of infiltrated sediment masses in the field and laboratory. Most of these methods disturb the sediment bed, and only few of them provide a vertical gradation of infiltrated sediment masses. Therefore, this study presents the proof-of-concept for a non-intrusive and non-destructive technique for measuring the masses of infiltrated fine sediments in high-resolution vertical profiles using the Gamma Ray Attenuation (GRA) method in laboratory flume experiments. Firstly, the

principal functionality of the GRA method is successfully tested on preliminary experiments, which consist of a box filled with spheres, known masses of infiltrated sediments and water. Afterwards, the GRA method is applied in a laboratory flume with a simplified gravel-bed to test the repeatability of the measuring concept under varying boundary conditions. The accuracy of the measured infiltration masses for the preliminary box tests show a deviation of less than 5% compared to gravimetrically determined masses, which proves the applicability of the GRA method. Furthermore, the repeatability tests of the flume experiments yielded deviations from 1.4% to 7.7%, which is still in an acceptable range, considering the complexity of the infiltration process. Based on the obtained results, the non-intrusive and non-destructive GRA method provides a profound basis for further in-depth investigations of fine sediment infiltration and accumulation in gravel riverbeds.

INTRODUCTION

Fine sediment infiltration into the interstices of a riverbed has been investigated intensively in both laboratory and field experiments given to the immense impact on riverine ecology. The infiltration and subsequent accumulation of fine sediments in the pores reduce the pore space, hydraulic conductivity and influence the exchange process between surface and subsurface waters (e.g. Schälchli 1992). The process also affects the supply of dissolved oxygen to aquatic species living in the hyporheic zone (e.g. Gayraud and Philippe 2003) and the reproduction habitats of gravel-spawning fish (e.g. Tonina and Buffington 2009; Noack et al. 2016).

So far, field and laboratory investigations have utilized different methods to measure sediment infiltration masses. In natural river, methods such as built-in sediment traps (Frostick et al. 1984; Newson and Sear 1994; Wilcock et al. 1996), plastic traps (Levasseur et al. 2006), cylindrical sediment cores (Blomqvist and Abrahamsson 1985; Reikowski 2015), freeze coring (Noack 2012), bulk sampling and sediment bags (Evans and Wilcox 2014) are applied. In addition, small-scale cylindrical samplers (Wooster et al. 2008; Gibson et al. 2009a,b, 2011; Herrero et al. 2015), and gravimetric methods (dry sieving and weighting for grain-size distribution analyses) are used in laboratory experiments for measuring infiltrated sediment masses. These methods are destructive, intrusive and change the natural conditions during the sample installation or extraction. Some sediment sampling methods (impermeable traps) only allow the vertical infiltration and neglect the lateral transport of particles and the change of surrounding conditions, which reduce their accuracy of measurement. Harper et al. (2017) identified significant differences between the vertical and lateral-and-vertical infiltration of fine sediments (<2mm) in substrate infiltration traps in natural rivers. Seydell et al. (2009) also observed 40% and 20% reduction of silt and sand in horizontally impermeable sampling pots respectively. Furthermore, Carling (1984) found a trap efficiency of 93.3% for permeable pots and 61.9% for solid walled pots compared to the surrounding bed materials during fine sand experiments. However, the disadvantage of horizontally permeable methods is that the measurement sample may lose or receive additional gravel and fine material from surrounding environment into the measurement sample during extraction and installation processes. Given the different available methods, Harper et al. (2017) suggest to take caution for interpretation of sediment infiltration data that are gained using different designs of sampling methods.

In addition, indirect methods such as interstitial water pressure and conductivity measurements are employed to investigate sediment infiltration (Schälchli 1992, 1995). The difference in suspended sediment concentration over time (Hamm et al. 2011; Herrero et al. 2015) and visual inspection of infiltrated sediment height evolution observed through transparent sidewalls (Herrero et al. 2015) are also used as an indicator for fine sediment infiltration in laboratory flumes. However, these methods are only applicable for very fine or suspended sediment infiltration cases under laboratory conditions, and cannot determine the infiltrated sediment mass in a specific location or at a specific time step as they provide an integrative result for the whole experiment. Furthermore, Rosenbrand and Dijkstra (2012) and Niño et al. (2018) used image analysis technique to quantify infiltrated sand movement and suffusion. This method only considers the fine sediment transport near the sidewall. Fletcher et al. (1995) developed an instrument using a submersible linear displacement transducer mounted beneath a sediment catch-tray to monitor infiltration of fine sediment into gravel bed in natural rivers, which only provides a depth integrated result and cannot present a profile of infiltrated sediments.

Among all the methods mentioned above, sediment cylindrical samplers (cores) allow for a vertical gradation of infiltrated sediments with a resolution depending on the bed gravel size (Wooster et al. 2008; Gibson et al. 2009b, 2011) and subsequent destructive separation of sediment layers under laboratory conditions. However, this technique destroys the sediment bed and the achievable accuracy of the vertical gradation is limited. Gibson et al. (2011) used a photometric method for identifying colored sediment distribution after the manual separation of sediment core samples collected from the laboratory experiment. Although this is an automatic particle separation method, the sample (core) extraction and layer separation alter the natural conditions. The main disadvantage of the destructive methods is that they only allow the assessment of fine sediment infiltration masses at one specific time-step and hence, are not suitable to detect the change of sediment characteristics over time. Therefore, a non-intrusive and non-destructive measurement method that provides high-resolution vertical distribution profiles of infiltrated sediments and allows for the temporal change detection is essential for further investigations in this field.

Penetrating rays are usually utilized for the non-destructive measurement of an object. Gamma ray is a radiation technique where the attenuation of emitting rays passing through the object is used for determining its physical characteristics. So far, the Gamma Ray Attenuation (GRA) method has been successfully used for measuring physical properties of soils, e.g. bulk density, porosity, soil water content, soil column's hydraulic conductivity and density profiles (Cassel and Krueger 1972; Reginato 1974; Gerland and Villinger 1995; Baytaş and Akbal 2002; Moreira et al. 2007; Pires et al. 2009; Moreira et al. 2011; Pires and Pereira 2014; Beckers et al. 2018).

The objective of this study is to provide a proof-of-concept for the development of the GRA method for the non-intrusive and non-destructive measurement of infiltrated fine sediment masses with a high vertical resolution profile for laboratory flume experiments. First, preliminary and simplified box experiments with known masses of infiltrated sediments are conducted to test and prove the principal functionality of the GRA-method for infiltration mass measurements. Afterwards, the GRA method is applied to a laboratory flume to test its reproducibility during fine sediment infiltration experiments using different boundary conditions, which represent a fundamental precondition to conduct further infiltration experiments using the GRA method.

MATERIAL AND METHODS

The general setup of GRA measurements includes a gamma source, which emits a collimated gamma beam penetrating through the media, and a scintillator to detect the gamma quants by creating photons. The optical signals are subsequently converted into electrical signals by a photomultiplier and further processed by a discriminator and a counter to produce the numerical results. The radioactive source in these experiments is Cesium Cs^{137} with a decay energy of 661 KeV. The detector unit has a diameter of 5.0 cm and a 5.0 cm thick scintillator made of Sodium Iodide doped with Thallium (NaI(TI)). The environmental temperature can influence the capability of the photomultiplier. Therefore, the temperature of the photomultiplier in the detection system is kept constant throughout each measurement period by installed heaters to neglect any temperature effects.

The measured sample profile contains three components: air, water, and spheres in a cubic packing arrangement to represent the simplified gravel bed. The reason for using cubic packing of empty spheres (table tennis balls) for representing the river gravel bed is to reduce the complexity, evaluate the repeatability and distinguish accurately the infiltrated sediment masses due to high densities differences of infiltrated sediments and 'empty' spheres.

In order to measure fine sediment infiltration masses, the GRA method requires three measurement profiles (I, II, III), where each profile can be divided into different zones (see also Figure 1). (I) The first step is to measure the vertical profile of an empty sample without water and infiltrated sediments for detecting background attenuation given to the side walls and bed structure (spheres). This profile is divided into two zones consisting of an air zone and the zone representing the bed structure (spheres) in which fine sediments can penetrate. (II) For the second measurement, the sample is filled with water to determine the linear attenuation coefficient in the pure water zone and the total pore space in the bed structure zone. (III) The third measurement is performed after sediment infiltration. Accordingly, this profile has three zones consisting of an air zone, a pure water zone and the zone of the bed structure with infiltrated fine sediments. The measurement profiles (I) and (II) are constant for all experiments of a sample due to identical geometry of the bed structure, while the measurement of third profile (III) is repeated for each experiment. During the measurement of the three profiles, caution should be paid that each measurement needs to be conducted exactly at the same position. The average radiation of the air section (zone 1) of all three steps is used to correct the temperature dependence of the detection system between the measurements.

It should be noted that the GRA method only allows for horizontally integrative results, which means that it cannot resolve the horizontal distribution of each component but only the net or the bulk thickness of each component.

The accuracy of GRA measurements mostly depends on the magnitude of the statistical error associated with the total counts of gamma quants collected after passing through an object. This error originates from the statistical variation of the emitted count rates of the gamma source by the radioactive decay. The statistic error follows the Poisson's law; this means, the higher the number of collected gamma quants or the longer the measuring time, the less will be the statistical error. Thus, a compromise between accuracy and resolution, which depends on the diameter of the collimator, exists. Mayar et al. (2019) investigated the optimization of GRA vertical profile measurements and suggested a mathematical equation for determining the optimal experimental boundary conditions.

Theoretical basis

Generally, the theory of the GRA method is based on the Beer-Lambert law that is shown in Equation 1 and relates the gamma ray attenuation to the properties of the penetrating material.

$$I = I_0 * exp(-\mu X) \tag{1}$$

where I_0, I, μ and X are the count rate before and after passing the absorber, the linear attenuation coefficient and the size of the absorber respectively. The I_0 is first measured without sample and later it is modified using the correction factor derived from measurement profile (I); which represents the background attenuation given to the side walls of the flume and the bed structure. Alternatively, the I_0 can also be measured directly from the measurement profile (I) to represent the background attenuation profile.

In Equation 1, the μ for elements, compounds and mixtures can be either extracted from the XCOM database (Berger and Hubbell 1987) or measured during the experiments. According to Sidhu et al. (1999); Jalali and Mohammadi (2008); Medhat et al. (2014) some deviation between the XCOM database and measured values of μ exist. Given the sensitivity of this parameter on the measuring result of fine sediment infiltration masses, the values of μ are calculated in this study based on experimental measurements. The linear attenuation coefficient of water μ_w is calculated in zone 2 as:

$$\mu_w = \frac{ln(\frac{I_0}{I_w})}{X_w} \tag{2}$$

where I_0 and I_w are the average initial and transmitted count rates from the pure water zone (2) in measurement profiles (I) and (II) respectively. The total thickness of water X_w in this section is equal to the entire horizontal width of the sample. Similarly, by achieving μ_w from Equation 2, the total pore space of each axis for the sediment penetration zone (4) is calculated as:

$$X_w = \frac{ln(\frac{I_0}{I_w})}{\mu_w} \tag{3}$$

where I_0 and I_w represent the initial and transmitted count rates of each horizontal axis of the penetration zone (4) in measurement profiles (I) and (II) respectively.

For the third measurement with infiltrated sediments (III), Equation 1 can be written as:

$$I = I_0 * exp - (\mu_w X_{w'} + \mu_s X_s) \tag{4}$$

where $X_{w'}$, μ_s and X_s are the net thickness of water content after sediment infiltration, linear attenuation coefficient and net thickness of the sediments respectively. The calculation of the linear attenuation coefficient of sediments μ_s, which are made of quartz (SiO_2), is not directly feasible because the sediment's exact thickness (X_s) and the net thickness of water content $X_{w'}$

are unknown. According to the XCOM database (Berger et al. 1998; Gerward et al. 2004), the linear attenuation coefficient of quartz (SiO_2), and Aluminum (Al) is very similar for the energy range of 0.1 – 3 MeV. Thus, a piece of Aluminum with a known geometry and equal density of sediments ($\rho_{Al} = \rho_s = 2650kg/m^3$) is placed on the top of the spheres (zone 3 - after finishing the experiments) and before the third measurement profile (III) to alternatively determine the value of μ_s with a measured linear attenuation coefficient from Aluminum (μ_{Al}). Therefore, Equation 1 can be written for this section (zone 3) as:

$$I = I_0 * exp - (\mu_w X_w + \mu_{Al} X_{Al}) \tag{5}$$

where X_{Al} is the thickness of Aluminum. The linear attenuation coefficient of water μ_w is already calculated using Equation 2 and the water thickness X_w in this section is equal to the difference of the total distance of the sample X and the Aluminum thickness X_{Al} ($X_w = X - X_{Al}$). From Equation 5 the μ_{Al} can be calculated as:

$$\mu_{Al} = \frac{ln(\frac{I_0}{I}) - \mu_w X_w}{X_{Al}} \tag{6}$$

where I_0 and I are the average initial and transmitted count rates of the horizontal positions occupied by Aluminum (zone 3) in the measurement profiles of (I) and (III) respectively. By substituting the linear attenuation coefficient of sediments with Aluminum ($\mu_s = \mu_{Al}$) for the penetration zone (4), the Equation 4 could be written as:

$$I = I_0 * exp - (\mu_w X_{w'} + \mu_{Al} X_s) \tag{7}$$

where I_0 and I are the initial and transmitted count rates of each horizontal axis of penetration zone (4) in measurement profiles (I) and (III) respectively. In this equation, the net thickness of water content ($X_{w'}$) and the net thickness of infiltrated sediments X_s are still unknown and a function of time. Where, the total thickness of each horizontal layer ($X = X_{w'} + X_s$) is equal to X_w derived by Equation 3. By substituting X_s with $X - X_{w'}$, and considering the ratio of the linear attenuation coefficients μ_s/μ_w by a parameter F, Equation 7 can be reorganized to calculate the net thickness of the water content ($X_{w'}$) for the bed structure section with the infiltrated sediments (zone 4):

$$X_{w'} = \frac{F * X - \frac{ln(\frac{I_0}{I})}{\mu_w}}{F - 1} \tag{8}$$

With the total pore space X from Equation 3 after the profile measurement (II) and the sediment water content $X_{w'}$ obtained from Equation 8, the net thickness of the infiltrated sediment content X_s in any horizontal layer of the bed structure (zone 4) is calculated as:

$$X_s = X - X_{w'} \tag{9}$$

By knowing the total pore space X equal to X_w from Equation 3 of each horizon in this zone and the remaining water content after sediment infiltration $X_{w'}$, the porosity $\varnothing$ can be calculated as:

$$\varnothing = (\frac{X_{w'}}{X})100\% \tag{10}$$

Alternatively, the porosity can be also rewritten as:

$$\varnothing = (1 - \frac{X_s}{X})100\% \tag{11}$$

With the known density of the infiltrated material ($\rho_s = 2650 kg/m^3$), the mass of the infiltrated sediment for each horizontal measurement can be derived by:

$$M_z = (\frac{X_s}{X}) * V_z * \rho_s \tag{12}$$

where $M_z(kg)$ and $V_z(m^3)$ are the mass and the available volume between the spheres in each horizontal position along the vertical profile respectively. Because of the cubic packing with regular geometric dimensions, the total available volume between the spheres can be calculated for each position along the vertical and horizontal axis. Assuming a uniform sediment distribution for the sections between two neighboring spheres, the mass of total infiltrated sediment $M_T(kg)$ is equal to the summation of all horizontal masses M_z.

$$M_T = \Sigma M_z \tag{13}$$

Preliminary experiments – Box setup

The concept of the GRA method to measure fine sediment infiltration masses is proved in preliminary box experiments in which a defined infiltration mass is added (gravimetrically) that can be subsequently compared to the measured fine sediment infiltration mass using the GRA method. The simplified experimental setup consists of a box with the following dimensions: (length L = 0.08 m, width W = 0.08 m and height H = 0.25 m). The box is partially filled with a central cubic packing of 8 spheres (table tennis balls with a diameter of $d_{sp} = 0.04$ m) that represent a highly simplified replica of a gravel bed (Figure 1a). The spheres are glued together and fixed to the bottom by a fixation at two sides of the box. The sample is measured according to the measurement profiles (I-III) procedure described earlier. Two different ranges of particle sizes of infiltrating material are tested: $d_{S1} = 1.0 - 1.8mm$ and $d_{S2} = 2.0 - 3.5mm$ during box experiments (B1.1 and B2.1). For validating the GRA concept in the box setup, measurements of profiles (I-III) were repeated for the same boundary conditions resulting in two additional box experiments (B1.2 and B2.2). During the sample filling, the sediments were compacted through shaking the box. Given the selection of a collimator with a diameter of 7.0 mm and a measuring time of 45 seconds, the maximum statistical errors, calculated by Poisson statistics law for the three measurement profiles (I-III) are approximately 1.60‰, 2.15‰, and 2.84‰ respectively. In addition, the distance between source and detector of gamma quants is 0.19 m. Figure 1 (a-c) illustrates setups for the different profile measurements. Figure 1C additionally shows the four zones of air, water, Aluminum, and bed structure with infiltrated sediments.

Flume experiments - setup

The measurement procedure of the box experiments is subsequently transferred to a laboratory flume. The flume is 8.00 m long, 0.24 m wide, 0.30 m high and has a slope of 1.35‰. In addition, the flume is equipped with a sediment feeding machine to continuously supply fine sediments into the center of flowing water. The sediment supply rate is controlled by vibration, swirl rotation and the opening for the sediment release, which allow for almost constant sediment supply rates. In a previous study, the feeder was tested for various sediment particle sizes and supply rates by Eckert (2016). The experimental setup of the flume consists of sixteen blocks, each of them with three vertical, six cross-sectional and six longitudinal layers of 0.04 m spheres (table tennis balls) in a cubic packing arrangement to represent a simplified river gravel bed (Figure 2). The spheres of each block are glued together and fixed to the bottom of the flume by a metal fixation at both ends. The spheres placement produces a continuous layer of 96 spheres in the stream-wise direction. After running an experiment and the measurements, the sediments are removed, blocks are extracted, washed and re-installed at the same position. The distance between source and detector collimator is in total 0.49 m due to 0.10 m mounted frames on both sides of the flume and the required space for the vertical traversal to move the devices for the GRA measurements. Figure 2 shows a cross-sectional view of the flume setup while Figure 3 represents a longitudinal view.

The simplified gravel bed has several advantages compared to natural gravel-matrices that have been used so far for sediment infiltrating and accumulation experiments. Firstly, the simplified geometry with variable but known bed characteristics (particle sizes, pore sizes, porosity etc.) allows for a detailed examination of the distinct contributions of the different processes involved in sediment infiltration and accumulation. Secondly, for several experimental runs with the same bed configuration, identical initial conditions can be guaranteed by simply washing out the infiltrated particles. Thirdly, different bed configurations can be easily installed to investigate different geometries.

Hence, this flume setup allows for many variations of boundary conditions including hydraulic (e.g. flow rate, water depth, Froude-Number) and sedimentary conditions (sediment supply, particle size, distribution of supplied sediments, different sphere sizes and mixes of sphere sizes to represent the bed material and different packing arrangements of the bed). However, the focus of this study is to test and prove the feasibility of the GRA method for fine sediment infiltration mass measurements and to test the repeatability of such experiments, which represents an indispensable precondition to conduct reliable and trustworthy sediment infiltration experiments.

Therefore, this study includes in total four flume experiments representing two repeatability tests (R1, R2) for two different boundary conditions. For both repeatability tests the hydraulic conditions are identical with a discharge of $Q = 0.015m^3/s$ and a water depth of $h = 0.08m$ resulting in a Froude-Number of $Fr = 0.79$ and a Reynolds-Number of $Re = 62,921$. The total mass of supplied sediments ($M_s = 20kg$) are also identical; however repetitions were carried out for experiments with two different sediment particle sizes of supplied materials ($d_{S1} = 1.0 - 1.8mm$ and $d_{S2} = 2.0 - 3.5mm$). Furthermore the feeding rate (Q_s) varies with $1.40kg/min$ for the d_{S1} sediments and $3.70kg/min$ for the d_{S2} sediments. After the complete amount of sediments having been supplied, the flow runs constantly for an additional time period of one supplied time (t_s) for $1.4kg/min$, and four supplied times (t_s) for $3,7kg/min$ feeding rates respectively to obtain identical experimental time for different supply rates. Table 1 provides an overview of the boundary conditions for the flume experiments.

According to the dimensions of the flume and the selected collimator size of 7.0 mm a measuring time step of 240 second is defined and results in a maximum statistical error for the three different measurement profiles I-III (background, water-filled and water and sediment-filled) of 1.70%, 3.30%, and 3.90% respectively. The measurement profiles I and II are conducted once before running the experiment, while the third profile (III) is measured after each experimental run is finished. Finally, the mass of infiltrated sediments for each point of the profile in the flume experiment is calculated and summed up to receive the total mass of fine sediment infiltration (for a 4.0 cm longitudinal section between two neighboring spheres).

RESULTS AND DISCUSSIONS

Preliminary box experiment

To test the feasibility of the GRA method for the box experiments, each measurement profile (I-III) is analyzed. Figure 4a shows the correction factor for the box experiments (B1.1, B2.1) with its repeatabilities (B1.2, B2.2) along the vertical measuring axis to account for the background attenuation of the box walls and spheres and Figure 4b represents the total pore space (X_w) for the box experiments (B1.1, B2.1) with its repeatabilities (B1.2, B2.2) in comparison to the geometrically determined pore space. Figure 4c represents a geometrical view of the measuring locations. Here, the small circles symbolize the diameter of the collimator.

The background attenuation profiles (Figure 4a) shows a lower value (0.93) at positions where the sphere's touching points face the Gamma emitting beam (e.g. box height 2.0 cm, 6.0 cm) because of higher absorption due to the fact that the Gamma beam hits the spheres compared to positions at the net pore (e.g. box height 4.0 cm, 7.5 cm) in which the corrections factor yields values of 1.0. The repeated measurement of this profile yields a deviation of 2.1% to the first profile measurement. The comparison of the measured total pore space (Figure 4b) with geometrically determined values shows a good agreement with a mean absolute deviation of 7.0%. The repeatability profile displays a better agreement with geometrically determined values and the mean absolute deviation is 3.7%. The pore space is maximum (8.0 cm) when the emitted gamma beam does not hit the spheres (e.g. box height 4.0 cm, 7.5 cm) and is minimum (5.0 cm) at box heights 2.0 cm, 6.0 cm, where the emitting beam (diameter 7.0 mm) hits the spheres at their touching positions. The identified correction factors and the total pore space profiles represent the initial conditions and thus apply for both box experiments (B1.1, B2.1). For the repeatability experiments (B1.2, B2.2) the repeated correction factor and total pore space profiles are used.

Figures 5 (a-c) and 6 (a-c) illustrate the measurement results of the box experiments for the sediment particle sizes of d_{S1} and d_{S2} along with the repeatability of each experiment respectively. Figures 5a and 6a show the net thicknesses of the infiltrated sediments (X_s) for both particle sizes. Figures 5b and 6b give the vertical profiles of the porosity ($\varnothing$), while Figures 5c and 6c present the vertical profiles of the measured net thicknesses for the water content ($X_{w'}$).

According to the available total pore space, the net sediment thickness in Figures 5a and 6a is high in horizons where the total pore space is high as well (e.g. 4.0 cm) and minimum at positions where spheres touch each other (e.g. 2.0 cm, 6.0 cm). Fine sediment particles produced higher thickness compared to the coarser sediments. The porosity and water content profiles in Figures 5 (b-c) and 6 (b-c) present non-similar profiles due to different sediment particle sizes (d_{S1} and d_{S2}), as well as compaction due to shaking the box. The fine sediments (d_{S1}) were better compacted, while the coarser sediments (d_{S2}) which contain less fines, were unable to be correctly compacted and produced higher porosity.

The measured results represent the expected vertical distribution of each measurement profile (I-III) and the shape of the spheres can be clearly identified in infiltrated sediment profiles. However, to prove the functionality of the GRA method, the total mass of infiltrated sediments as sum of all horizontal measurements (M_{GRA}) is compared to the previously gravimetrically determined infiltration mass M_{grav} (Table 2). However, it is important to note that this verification method assumes that, if the integral of the sediment masses matches the total gravimetric measurement, then the sediment masses at any elevation are correct. Because one cannot determine the mass of compacted sediments for each horizontal measurement to compare with GRA method.

The relative deviations between measured total infiltration mass (M_{GRA}) and gravimetrically determined total infiltration mass (M_{grav}) for B1.1, B2.1 and their repeatabilities (B1.2, B2.2) vary approximately between 1% and 5%. To evaluate the measuring results of the GRA method, both the statistical error of approximately 2.84% given to the chosen collimator diameters and the measuring time in measurement profile (III) need to be taken into account. This source of error could be reduced either by using a larger collimator diameter, or by increasing the measuring time. But a larger collimator diameter leads to a loss in vertical resolution and for the latter, an increase of measuring time to 340 seconds for each measuring point of the profile would be required to achieve a statistical error of 1%, because according to the Poisson's law a minimum of 10,000 quants is required (Mayar et al., 2019). Another potential source of error is the positioning of the measuring locations (horizontally for the entire profile and vertically for each horizontal measurement) for the three measuring profiles I-III. Previous tests showed that the positioning is highly sensitive in terms of measured correction factor and total pore space, which can lead to massive deviations in the measured total infiltration mass. Therefore, it is greatly recommended to use an accurate vertical traversal system to minimize the error due to positioning. The applied automatic traversal in this study has a maximum error of 1.0 mm in vertical positioning. Hence, slight differences between the three required measuring profiles can occur. Another aspect to be taken into account is the assumption of a uniform distribution of infiltrated sediment between the spheres. The GRA measurement covers the area equal to the diameter of the collimator (0.7 cm) while the width of each volume piece is equal to the width of the box (8.0 cm). Considering these potential sources of errors, the relative deviations (1% - 5%) between gravimetrically determined infiltration masses and measured masses with GRA can be interpreted to be acceptable, especially in comparison to existing destructive measuring techniques and their methods to derive a vertical gradation of infiltrated fine sediments.

Flume experiments

The aim of the flume experiments is to test the feasibility of the GRA setup for further infiltration experiments including variations of boundary conditions but also to investigate in future dynamic infiltration processes that is only feasible with non-destructive methods. For the proof of reliability, repeatability tests are indispensable. According to Table 1, two repeatability tests are conducted with different sediment supply rates for different particles sizes (R1, R2) resulting in four experiments in total. Given the identical hydraulic conditions and the same packing arrangement of the spheres, the measured vertical profiles for the correction factor (I) and the total pore space (II) are also identical for both repeatability tests shown in Figure 7 (a-b). Figure 7c represents the vertical distribution of the horizontal measuring locations with a collimator diameter of 7.0 mm.

The correction factor (Figure 7a) characterizes the expected fluctuations along the vertical profile due to the spheres. Compared to the box experiments, the minimum values of the correction factor for the flume experiments are smaller (0.86) due to the higher number of horizontally arranged spheres (six) and the longer width (0.24 m) of the flume along the horizontal measurement axis. However, Figure 7a displays that the profile's minimum and maximum values follow a similar pattern compared to the box model tests representing the shape of the spheres. The profile of the total pore space (X_w) shows again a similar pattern compared to the correction factor and indicates also the location of the spheres. The minimum values of the GRA measured total pore space are at flume heights 1.85, 6.05, 10.25 cm, while the maximum values occur at flume heights of 3.95, 8.15, 11.65 cm. Again a comparison to the geometrically determined total pore space is performed leading to mean absolute deviations of 5%, which is in the same range as for the box experiments and most probably due to correct vertical positioning with the automatic traversal.

Figure 8 represents the repeatability experiment R1 with a supply rate of $Q_{S1} = 1.4 kg/min$ and particle size of $d_{S1} = 1.0 - 1.8 mm$. Figure 8a displays the derived vertical profile for the net thicknesses of infiltrated sediments (X_s). Figure 8b gives the vertical profile of the porosity (∅) and Figure 8c presents the vertical profile of the measured net thicknesses of the water content ($X_{w'}$).

Comparing all profiles in Figure 8 (a-c), significant differences along the vertical axis can be identified. The vertical profile of the net thicknesses of infiltrated sediments (Figure 8a) shows results between 0.0 and 13.6 cm not reflecting the shape of the spheres and is characterized by comparable low variations along the vertical axis, except of the upper part at flume heights of 11.0 - 12.0 cm. The latter is due to the fact that the deposited and hardly infiltrated fine sediments are re-suspended. The uniform vertical distribution of net thicknesses of infiltrated sediments can be explained considering additionally the measured net thicknesses of the water content (Figure 8c). The measured net thickness of the water content as well as the total pore space reflect properly the shape of the spheres. As the net thickness of infiltrated sediments is the difference of total pore space and water content, the profile of the net thicknesses of infiltrated sediments is close to uniform. Physically, the varying water content reflects the different accumulation and compaction pattern of the infiltrated sediments which is high at the positions of pores (e.g. flume height 0.0, 4.0, 8.0 cm) and low at positions where spheres touch each other (e.g. flume height 2.0, 6.0 cm). At a flume height > 10.0 cm fine sediments are flushed by the flow. These obtained results become also visible in the vertical profiles of the porosity (Figure 8b). When the available pore space achieves minimum values also the porosity values yield lower values (e.g. flume height 2.0, 6.0 cm) compared to the position with maximum available pore space and high porosity (e.g. flume height 4.0, 8.0 cm). The reason for variation of the profiles with the box experiment is due to different filling process. The box was manually filled and compacted by shaking while the flume pores were filled by the sediments transported by the flow. Therefore, the profiles are not comparable.

In terms of repeatability, an overall good agreement can be observed for the net thicknesses of infiltrated sediments, the porosity as well as for the water content (Figure 8). Only at flume heights between 3.0 and 5.0 cm some minor deviations are visible that might occur given to different compaction processes during pore filling. The calculation of the total infiltration mass (M_{GRA}, Table 3) results for the experiment R1.1 in 620.41 g while for the repetition experiment (R.1.2) 611.44 g were measured. This means a relative deviation of 1.44% and can be interpreted as a very good repeatability. The general slight deviation of infiltrated sediment along the vertical profiles may originate from the statistical error or exact positioning of the measurement axes.

The results of the second flume experiment and its repeatability test (R2, $Q_{S2} = 3.7kg/min$, $d_{S2} = 2.0-3.5mm$) are represented in a similar way (Figure 9). Due to the identical initial conditions in terms of hydraulic conditions, sphere sizes and packing arrangement, the available total pore space is identical to R1. The vertical profiles for the net thicknesses of infiltrated sediments are characterized by small variations along the profile and again the top layers are represented by a low sediment thickness due to the flushing of fine sediment. However, the flushing effect is not as pronounced as in R1 given the larger particles (d_{S2}) and the higher feeding rate. In addition, the overall net sediment thickness with values around 0.0 to 9.8 cm is slightly lower compared to R1 with values between 0.0 and 13.6 cm. Hence, the resulting porosity of R2 is higher compared to R1.

The repeatability for all vertical profiles shows a sufficient agreement. Deviations are visible at the bottom of the flume (e.g. 1.0 cm to 3.0 cm) and at a flume height of 5.5 cm. However, the general patterns of the vertical profiles are repeated very well. In terms of total infiltrated mass (M_{GRA}), the second experiment R2.1 resulted in an infiltration mass of 564.90 g, while the repetition R2.2 sums up to in 521.18 g. This corresponds to a relative deviation of 7.7% and thus, is larger compared to the experiment R1 (Table 3). In addition to the already mentioned potential sources of error, such as the exact positioning of the measuring locations and the statistical error, another source of error results from the limited accuracy of the sediment feeding machine: the dosage of supply rate is less precise for the coarser sediments than for the finer sediments. Moreover, the probability of observing exactly the same infiltration pattern or the repeatability of all ingredients of an experiment with identical boundary conditions, for coarser sediment is lower compared to finer sediments due to larger sediment particles and limited space. The fine sediments may pass through the available space while clogging might occur differently for coarser sediments.

Furthermore, the current setup of GRA measurement is only applicable for the laboratory conditions with artificial gravel beds. This setup is not appropriate for beds with natural gravels due to similar density of infiltrating sediments with bed material. However, stronger radiation will be able to identify larger amounts of infiltrated fine sediments. Small amounts of infiltrated sediments will produce only a very small change of the attenuation that might be confused with the statistical error. Another critical limitation for field measurement is the legal restriction of using the radioactive material in the nature. EHG (2015) provides safety instructions for the source applications. Therefore, maximum safety protection is recommended according to each country's rules and regulations.

Despite of the mentioned limitations, the GRA method can be highly useful for in-depth investigations of sediment infiltration and accumulation, the temporal development and to provide data for development of numerical methods. In addition, the method is transferable to other flumes, but the geometry, energy, resolution, measuring time and other parameters need to be considered for the reliable results. Furthermore, the GRA method theoretically allow for distributed measurements in space and time. However, spatially distributed measurements requires application of multiple devices at the same time.

CONCLUSIONS

Two types of laboratory experiments were conducted to investigate the feasibility of non-intrusive and undisturbed measurements of fine sediment infiltration using the gamma ray attenuation method. First, the proof-of-concept for the GRA method to measure infiltration masses is shown on preliminary box experiments using a simplified bed structure of eight spheres in a central cubic packing arrangement. Subsequently, laboratory flume experiments are designed to test the repeatability of fine sediment infiltration experiments, which represent an indispensable precondition for further experiments with controlled variations of hydraulic and sedimentary boundary and initial conditions. The box experiments allowed for a comparison between known and measured infiltration masses and the obtained measuring results showed only marginal deviations between 1% and 5%. The repeatability tests of the flume experiments were conducted for two different setups and showed deviations of 1.4% and 7.7%. The main potential sources of error originate from the statistical error given to the radioactive decay, the requirement of highly exact positioning of the measuring locations in the sub-millimeter range and the capability and accuracy of the sediment feeding machine. Considering these potential errors and the general complexity of the infiltration and accumulation processes (surface and subsurface processes), the measured infiltration masses provide promising results for future fine sediment infiltration measurements. The GRA method is a non-intrusive and non-destructive method allowing also for time dependent investigations of the infiltration process, which provides vertical profiles of infiltration masses that have – compared to destructive methods – a high spatial resolution. In addition, further parameters can be obtained by the GRA measurements that are very helpful for the interpretation of riverbed composition, such as water content and porosity. However, two limitations are identified. Firstly, the GRA method cannot resolve the horizontal distribution of infiltration masses along the horizontal measuring axis and provides 'only' net or bulk results. The second limitation is the compromise between the collimator diameter and measuring time. The smaller the diameter of collimator the longer the required measuring time to keep the statistical error in an acceptable range. However, based on the promising results of the presented feasibility tests, it can be concluded that the GRA method represents a highly valuable opportunity to measure sediment infiltration masses without disturbing the riverbed in hydraulic laboratory conditions, especially because it opens the way for time-resolved or dynamic investigations of infiltration and accumulation processes and to investigate the effect of different boundary conditions.

DATA AVAILABILITY STATEMENT

Some or all data, models, or code generated or used during the study are available from the corresponding author by request.

APPENDIX I. NOTATION

The following symbols are used in this paper:

Al	=	Aluminum;
d_s	=	diameter of infiltrated sediment particles (m);
d_{sp}	=	diameter of sphere (m);
Fr	=	Froude number (-);
h	=	height (m);
I	=	count rate after passing penetrating media (cps - counts per second);
I_0	=	initial count rate / before passing penetrating media (cps - counts per second);
M_{grav}	=	mass of gravimetrically measured total infiltrated sediments (kg);
M_s	=	mass of total feeding sediments (kg);
M_T	=	mass of total infiltrated sediments (kg);
M_z	=	mass of infiltrated sediments of each measuring section in the vertical profile (kg);
Q	=	discharge (m^3/s);
Q_s	=	feeding rate of sediment (kg/min);
t_s	=	duration of supplying sediment to the flume (s);
V_z	=	volume of each measuring section along the vertical profile (m^3);
X	=	thickness (m);
X_{Al}	=	thickness of Aluminum (m);
X_s	=	thickness of sediments (m);
$X_{w'}$	=	thickness of soil water content (m);
X_w	=	thickness of water (m);
z	=	vertical axis;
μ	=	linear attenuation coefficient (-);
μ_{Al}	=	linear attenuation coefficient of Aluminum (-);
μ_s	=	linear attenuation coefficient of sediments (-);
μ_w	=	linear attenuation coefficient of water (-);
ρ_s	=	density of sediment (kg/m^3); and
$\varnothing$	=	porosity (%) ;

REFERENCES

Baytaş, A. F. and Akbal, S. (2002). “Determination of soil parameters by gamma-ray transmission.” *Radiation Measurements*, 35(1), 17–21.

Beckers, F., Haun, S., and Noack, M. (2018). “Experimental investigation of reservoir sediments.” *E3S Web of Conferences*, 40, 03030.

Berger, M., Hubbell, J., Seltzer, S., Chang, J., Coursey, J., Sukumar, R., Zucker, D., and Olsen, K. (1998). “XCOM: Photon cross sections online database, <https://physics.nist.gov/PhysRefData/Xcom/html/xcom1.html>.

Berger, M. J. and Hubbell, J. (1987). “XCOM: Photon cross sections on a personal computer.” *Report No. NBSIR–87-3597*, National Bureau of Standards, Washington DC, <http://www.iaea.org/inis/collection/NCLCollectionStore/$_{public}/19/009/19009871.pdf?r = 1$>.

Blomqvist, S. and Abrahamsson, B. (1985). “An improved Kajak-type gravity core sampler for soft bottom sediments.” *Swiss Journal of Hydrology*, 47(1), 81–84.

Carling, P. A. (1984). “Deposition of Fine and Coarse Sand in an Open-Work Gravel Bed.” *Canadian Journal of Fisheries and Aquatic Sciences*, 41(2), 263–270.

Cassel, D. K. and Krueger, T. H. (1972). “Gamma Rays Determine Soil Water Content of Soil-Plant Systems.

Eckert, B. (2016). “Analyse eines Fördergerätes zur Geschiebezugabe in wasserbaulichen Modellversuchen.” B.Sc. Thesis, University of Stuttgart, Stuttgart, Germany.

EHG, E. G. (2015). “Technical Information / Operating Instructions: Source container FQG60 Radiometric Measurement.” *Manual*, Endress+Hauser Messtechnik GmbH+Co. KG, Germany, <https://portal.endress.com/wa001/dla/5001016/7034/000/03/TI00445FEN$_1$615.pdf>.

Evans, E. and Wilcox, A. C. (2014). “Fine sediment infiltration dynamics in a gravel-bed river following a sediment pulse.” *River Research and Applications*, 30(3), 372–384.

Fletcher, W. K., McLean, W. E., and Sweeten, T. (1995). “An instrument to monitor infiltration of fine sediment into stable gravel stream beds.” *Aquacultural Engineering*, 14(4), 289–296.

Frostick, L., Lukas, M., and Reid, I. (1984). “The infiltration of fine matrices into coarse-grained alluvial sediments and its implications for stratigraphical integration.” *Journal of the Geological Society (London)*, 141, 955–965.

Gayraud, S. and Philippe, M. (2003). “Influence of Bed-Sediment Features on the Interstitial Habitat Available for Macroinvertebrates in 15 French Streams.” *International Review of Hydrobiology*, 88(1), 77–93.

Gerland, S. and Villinger, H. (1995). “Nondestructive density determination on marine sediment cores from gamma-ray attenuation measurements.” *Geo-Marine Letters*, 15(2), 111–118.

Gerward, L., Guilbert, N., Jensen, K., and Levring, H. (2004). “WinXCom—a program for calculating X-ray attenuation coefficients.” *Radiation Physics and Chemistry*, 71(3-4), 653–654.

Gibson, S., Abraham, D., Heath, R., and Schoellhamer, D. (2009a). “Bridging process threshold for sediment infiltrating into a coarse substrate.” *Journal of geotechnical and geoenvironmental engineering*, 136(2), 402–406.

Gibson, S., Abraham, D., Heath, R., and Schoellhamer, D. (2009b). “Vertical gradational variability of fines deposited in a gravel framework.” *Sedimentology*, 56(3), 661–676.

Gibson, S., Heath, R., Abraham, D., and Schoellhamer, D. (2011). “Visualization and analysis of temporal trends of sand infiltration into a gravel bed: TEMPORAL TRENDS OF SAND INFILTRATION INTO A GRAVEL BED.” *Water Resources Research*, 47(12).

Hamm, N. T., Dade, W. B., and Renshaw, C. E. (2011). “Fine particle deposition to porous beds.” *Water Resour. Res.*, 47(11), W11508.

Harper, S., Foster, I., Lawler, D., Mathers, K., McKenzie, M., and Petts, G. (2017). "The complexities of measuring fine sediment accumulation within gravel-bed rivers." *River Research and Applications*, 33(10), 1575–1584.

Herrero, A., Berni, C., and Cemenen, B. (2015). "Laboratory Analysis on Silt Infiltration into Gravel Bed." *E-proceedings of the 36th IAHR World Congress*, The Hague, Netherlands.

Jalali, M. and Mohammadi, A. (2008). "Gamma ray attenuation coefficient measurement for neutron-absorbent materials." *Radiation Physics and Chemistry*, 77(5), 523–527.

Levasseur, M., Bergeron, N. E., Lapointe, M. F., and Bérubé, F. (2006). "Effects of silt and very fine sand dynamics in Atlantic salmon (*Salmo salar*) redds on embryo hatching success." *Canadian Journal of Fisheries and Aquatic Sciences*, 63(7), 1450–1459.

Mayar, M., Schmid, G., Wieprecht, S., and Noack, M. (2019). "Optimizing vertical profile measurements setup of gamma ray attenuation." *Radiation Physics and Chemistry*, 164, 108376.

Medhat, M., Demir, N., Akar Tarim, U., and Gurler, O. (2014). "Calculation of gamma-ray mass attenuation coefficients of some Egyptian soil samples using Monte Carlo methods." *Radiation Effects and Defects in Solids*, 169(8), 706–714.

Moreira, A. C., Filho, O. P., Cavalcante, F. H. d. M., and Appoloni, C. R. (2011). "Determination of Hydraulic Conductivity of Undisturbed Soil Column: a Measurement Accomplished with the Gamma Ray Transmission Technique." *Developments in Hydraulic Conductivity Research*, O. Dikinya, ed., IntechOpen, Rijeka.

Moreira, A. C., Portezan Filho, O., Cavalcante, F. H. M., Coimbra, M. M., and Appoloni, C. R. (2007). "Gamma ray transmission for hydraulic conductivity measurement of undisturbed soil columns." *Brazilian Archives of Biology and Technology*, 50(2), 321–328.

Newson, M. and Sear, D. (1994). "Sediment and gravel transportation in rivers including the use of gravel traps." *Research and Development Note C*, 5.

Niño, Y., Licanqueo, W., Janampa, C., and Tamburrino, A. (2018). "Front of unimpeded infiltrated sand moving as sediment transport through immobile coarse gravel." *Journal of Hydraulic Research*, 56(5), 697–713.

Noack, M. (2012). *Modelling approach for interstitial sediment dynamics and reproduction of gravel-spawning fish*, <http://elib.uni-stuttgart.de/handle/11682/485>.

Noack, M., Ortlepp, J., and Wieprecht, S. (2016). "An Approach to Simulate Interstitial Habitat Conditions During the Incubation Phase of Gravel-Spawning Fish." *River Research and Applications*, 33(2), 192–201.

Pires, L., Rosa, J., Pereira, A., Arthur, R., and Bacchi, O. (2009). "Gamma-ray attenuation method as an efficient tool to investigate soil bulk density spatial variability." *Annals of Nuclear Energy*, 36(11-12), 1734–1739.

Pires, L. F. and Pereira, A. B. (2014). "Gamma-Ray Attenuation to Evaluate Soil Porosity: An Analysis of Methods." *The Scientific World Journal*, 2014, 1–10.

Reginato, R. J. (1974). "Water content and bulk density changes in a soil pedon measured with dual energy gamma-ray transmission." *Canadian journal of soil science*, 54(3), 325–328.

Reikowski, A. (2015). *Betriebsanleitung FRAHM-LOT*. MBT Underwater Technology, Kiel, 1.1 edition.

Rosenbrand, E. and Dijkstra, J. (2012). "Application of image subtraction data to quantify suffusion." *Géotechnique Letters*, 2(2), 37–41.

Schälchli, U. (1992). "The clogging of coarse gravel river beds by fine sediment." *Hydrobiologia*, 235(1), 189–197.

Schälchli, U. (1995). "Basic Equations for Siltation of Riverbeds." *Journal of Hydraulic Engineering*, 121(3), 274–287.

Seydell, I., Ibisch, R., and Zanke, U. (2009). "Intrusion of suspended sediments into gravel riverbeds: influence of bed topography studied by means of field and laboratory experiments." 61, 67–85.

Sidhu, G. S., Singh, K., Singh, P. S., and Mudahar, G. S. (1999). "Effect of collimator size and absorber thickness on gamma ray attenuation measurements." *Radiation Physics and Chemistry*, 56(5), 535–537.

Tonina, D. and Buffington, J. M. (2009). "Hyporheic Exchange in Mountain Rivers I: Mechanics and Environmental Effects." *Geography Compass*, 3(3), 1063–1086.

Wilcock, P. R., Barta, A. F., Shea, C. C., Kondolf, G. M., Matthews, W. V. G., and Pitlick, J. (1996). "Observations of Flow and Sediment Entrainment on a Large Gravel-Bed River." *Water Resources Research*, 32(9), 2897–2909.

Wooster, J. K., Dusterhoff, S. R., Cui, Y., Sklar, L. S., Dietrich, W. E., and Malko, M. (2008). "Sediment supply and relative size distribution effects on fine sediment infiltration into immobile gravels: Fine sediment infiltration into immobile gravels." *Water Resources Research*, 44(3), n/a–n/a.

List of Tables

TABLE 1. Boundary conditions of the flume experiments to test the repeatability of sediment infiltration experiments.

ID	d_s (mm)	M_s (kg)	Q_s (kg/min)	t_s (min)	Q (m^3/s)	h (m)	Fr $(-)$
R1	1.0 - 1.8	20	1.4	14.3	15	0.08	0.79
R2	2.0 - 3.5	20	3.7	5.4	15	0.08	0.79

TABLE 2. Comparison of infiltration masses determined gravimetrically and with the GRA method in the box experiments

ID	d_s (mm)	M_{grav} (g)	M_{GRA} (g)	absolute deviation (g)	relative deviation (%)
B1.1	1.0 - 1.8	359.10	376.3	17.2	4.8
B1.2	1.0 - 1.8		373.3	14.2	4.1
B2.1	2.0 - 3.5	359.72	355.8	3.92	-1.1
B2.2	2.0 - 3.5		367.5	7.78	2.1

TABLE 3. Comparison of the measured total infiltration masses for both repeatability tests in the flume experiments.

ID	d_s (mm)	M_{GRA} (g)	absolute deviation (g)	relative deviation (%)
R1.1	1.0 - 1.8	620.41	8.97	1.4
R1.2	1.0 - 1.8	611.44		
R2.1	2.0 - 3.5	564.90	43.72	7.7
R2.2	2.0 - 3.5	521.18		

List of Figures

files/Figure 1.jpg

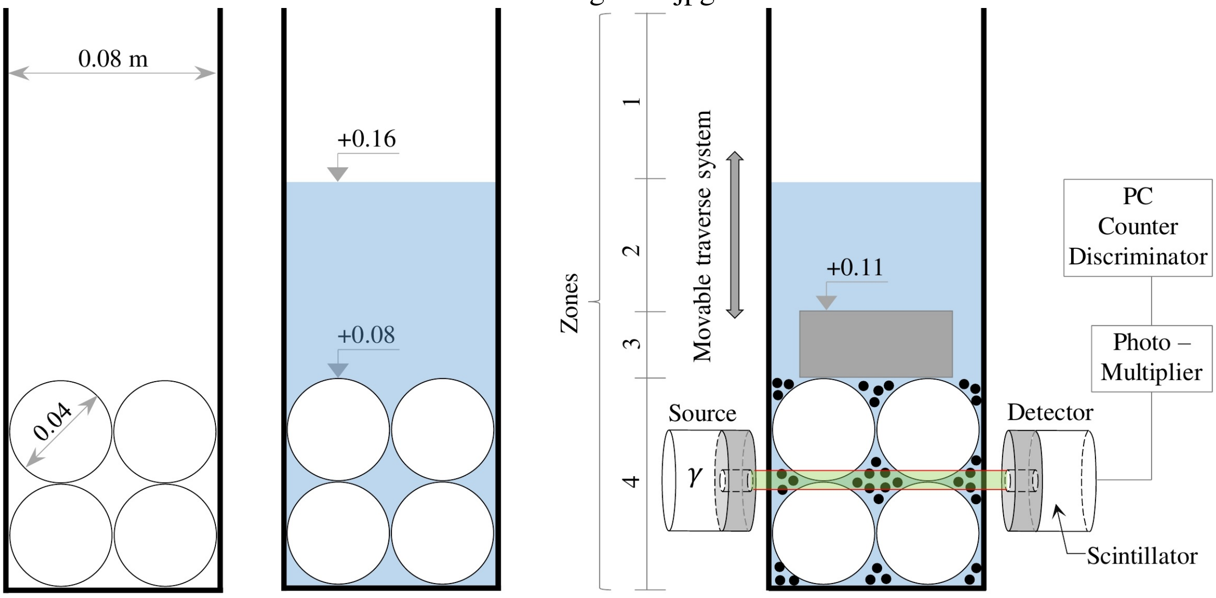

A. Empty box B. Box filled with water C. Water and sediments filled box with GRA measurement scheme

Fig. 1. Experimental setup for the box experiments including the three measurement steps and the GRA measurements setup. The empty box (a) is measured for background attenuation, while the box filled with water (b) gives the linear attenuation coefficient of water in zone 2 and total pore space in zone 4. The measurement of water and sediment filled box showed with GRA measurement scheme (c) provides linear attenuation of Aluminum equivalent to sediment and net thickness of infiltrated sediments in zone 4.

files/Figure 2.jpg

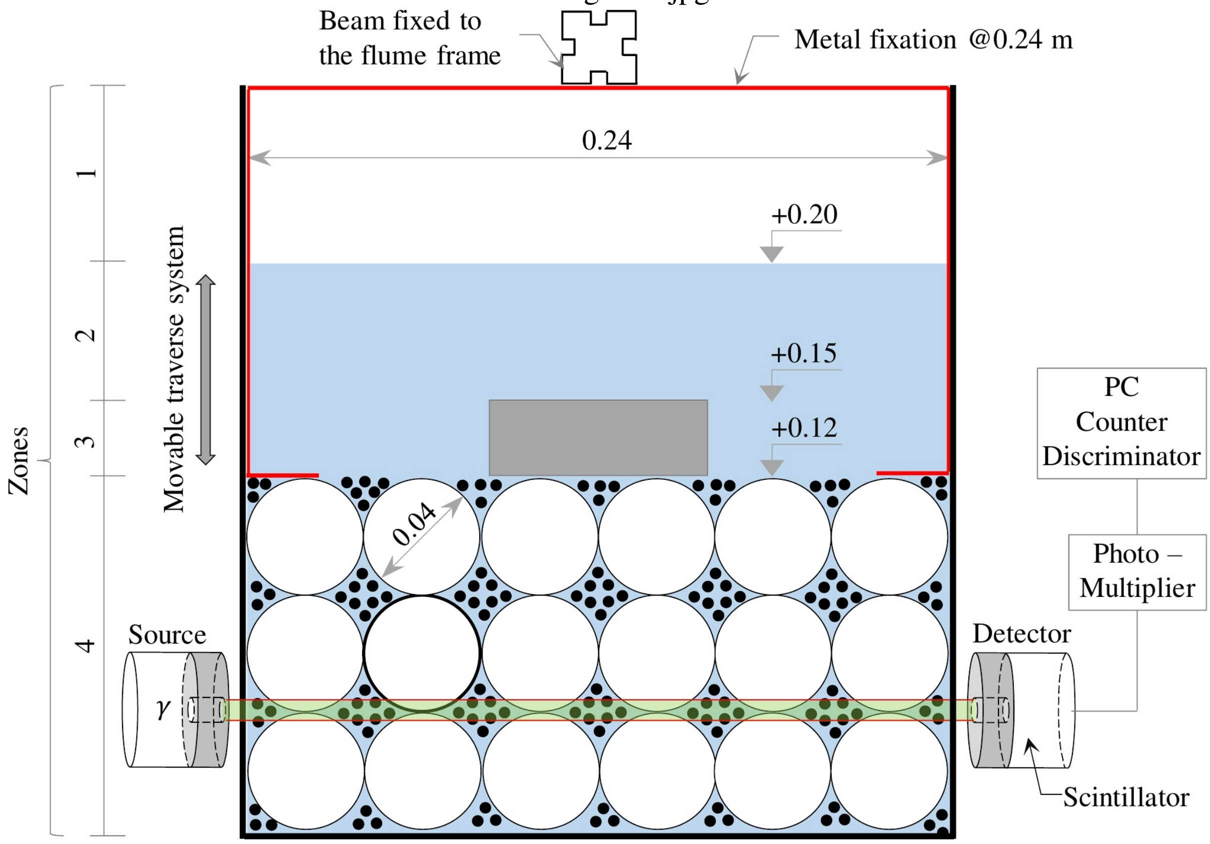

Fig. 2. Cross-sectional view of the flume including the four different vertical zones and the setup of GRA measurements. The vertical profile is measured three times: (I) flume with spheres for background attenuation profile; (II) filled with water for linear attenuation coefficient of water and total pore space in zone 4; (III) after sediment infiltration to measure the linear attenuation coefficient of Aluminum and the net thickness of infiltrated sediments in zone 4. The block of Aluminum in zone 3 is placed on top of the spheres after finishing the experiment.

files/Figure 3.jpg

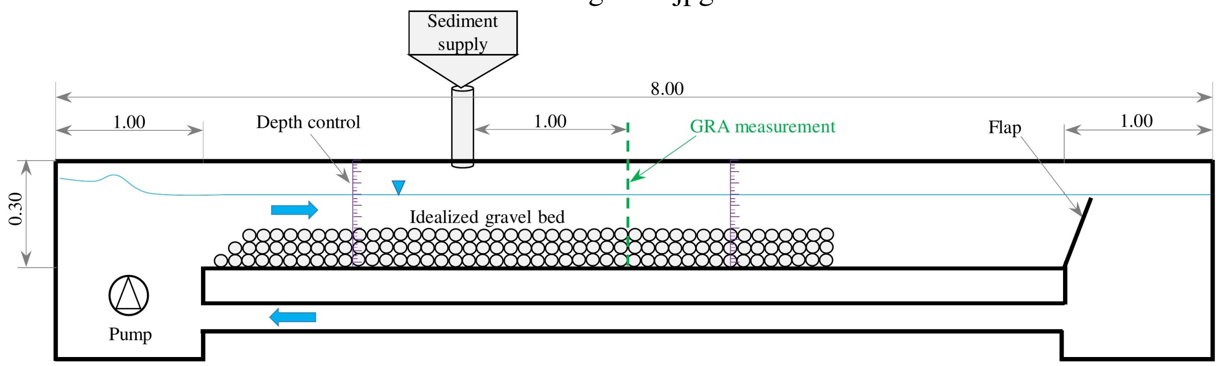

Fig. 3. Longitudinal scheme of the recirculating laboratory flume to conduct the sediment infiltration measurements showing the locations of the sediment supply and the position of the vertical profile measurements. The idealized bed is made of 0.04 m spheres (table tennis balls) in a cubic packing arrangement. The feeding machine constantly supplied sediment to the flow during the experiment.

files/Figure 4.jpg

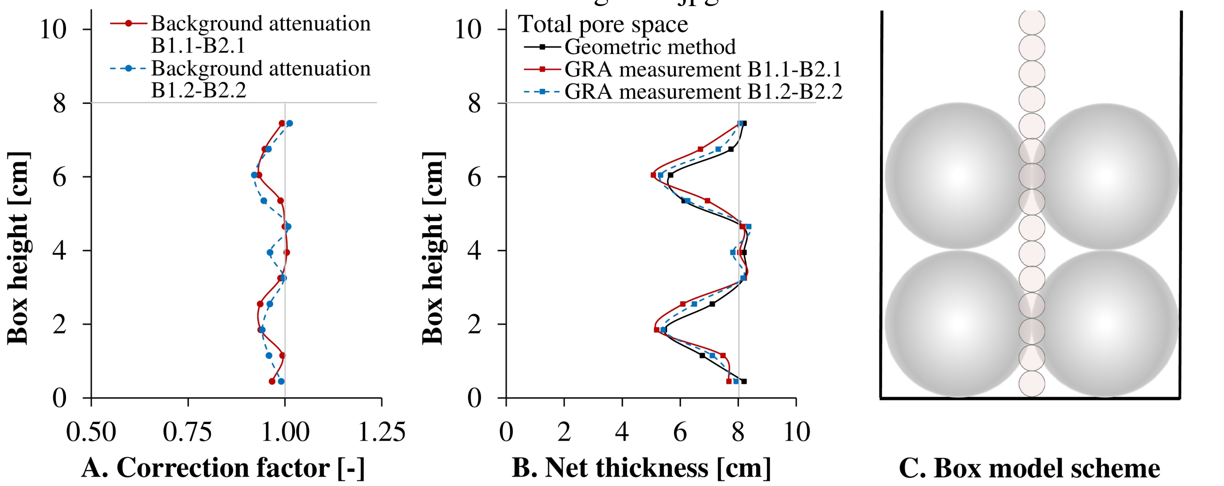

Fig. 4. Results of the box experiments showing vertical profiles of (a) the background attenuation correction factor for the box experiments (B1.1-B2.1) and the repeatability experiments (B1.2-B2.2), (b) the total pore space of box (B1.1-B2.1), repeatability experiment (B1.2-B2.2) and the geometrically determined total pore space, and in (c) the box model scheme with measuring locations.

files/Figure 5.jpg

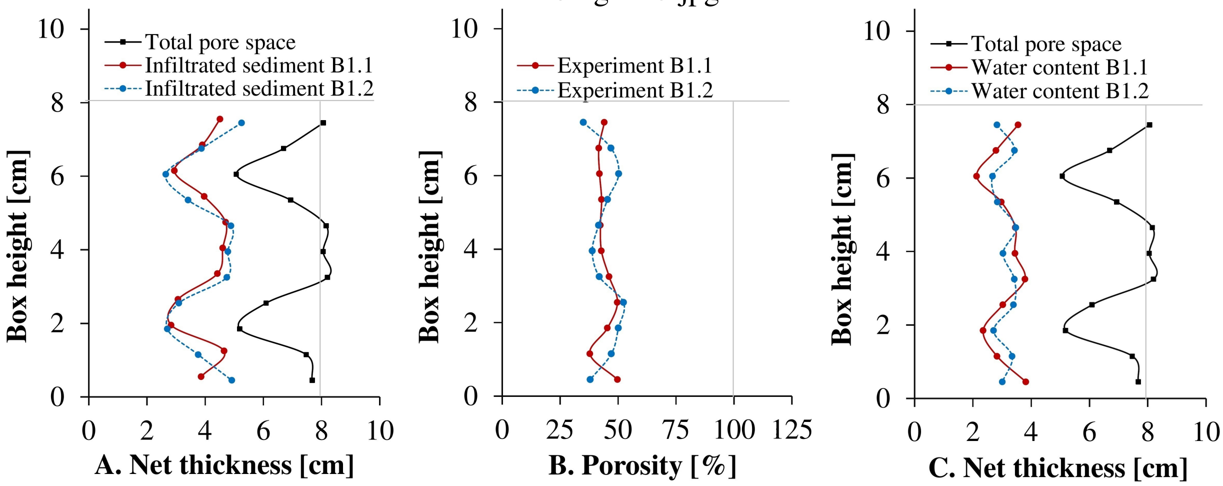

Fig. 5. Results of the box experiments showing vertical profiles of (a) the net thickness of infiltrated sediments for particle size of d_{S1} (B1.1, B1.2) in comparison to the total pore space, (b) the calculated porosities for both experiments B1.1 and B1.2 and (c) the net thicknesses of water contents after sediment infiltration for both experiments B1.1 and B1.2 in comparison to the total pore space.

files/Figure 6.jpg

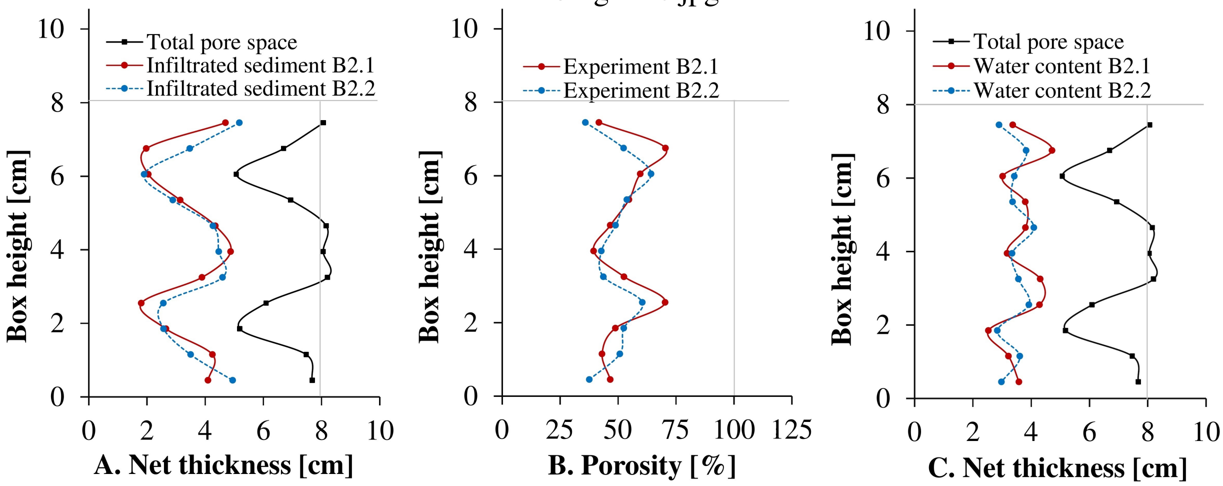

Fig. 6. Results of the box experiments showing vertical profiles of (a) the net thickness of infiltrated sediments for particle size of d_{S2} (B2.1, B2.2) in comparison to the total pore space, (b) the calculated porosities for both experiments B2.1 and B2.2 and (c) the net thicknesses of water contents after sediment infiltration for both experiments B2.1 and B2.2 in comparison to the total pore space.

files/Figure 7.jpg

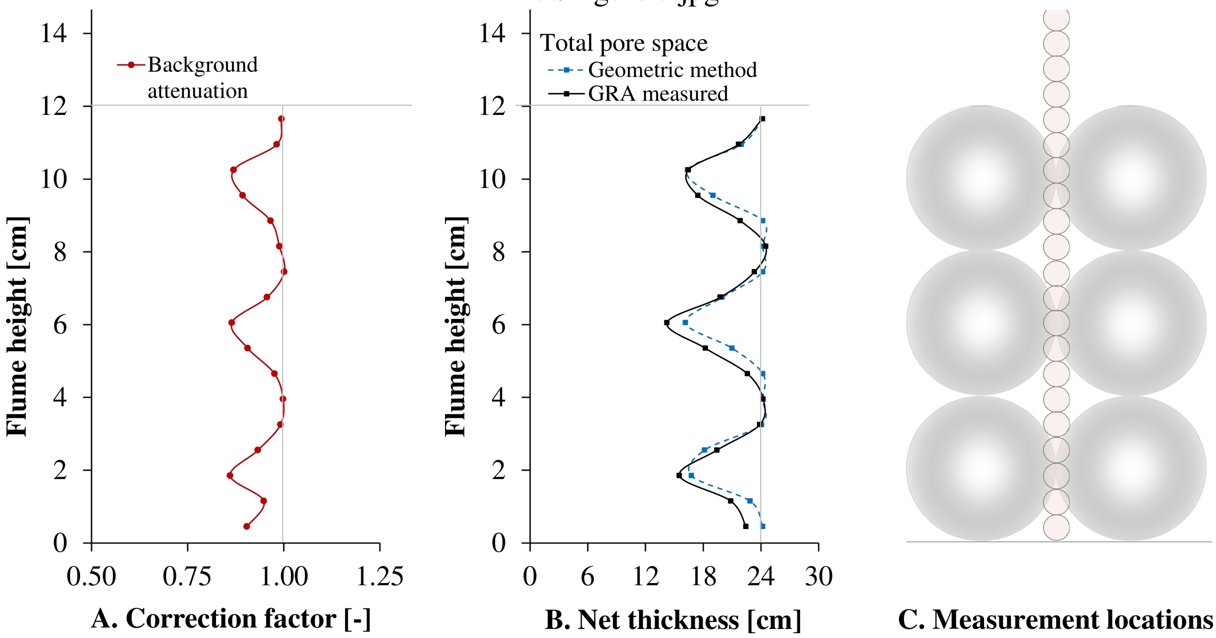

Fig. 7. Result of the flume experiment showing vertical profiles of (a) the background attenuation correction factor, (b) the total pore space and the geometrically determined total pore space, and (c) the measuring locations. Due to exactly the same structure, the profiles (a) and (b) are constant for all subsequent flume experiments.

files/Figure 8.jpg

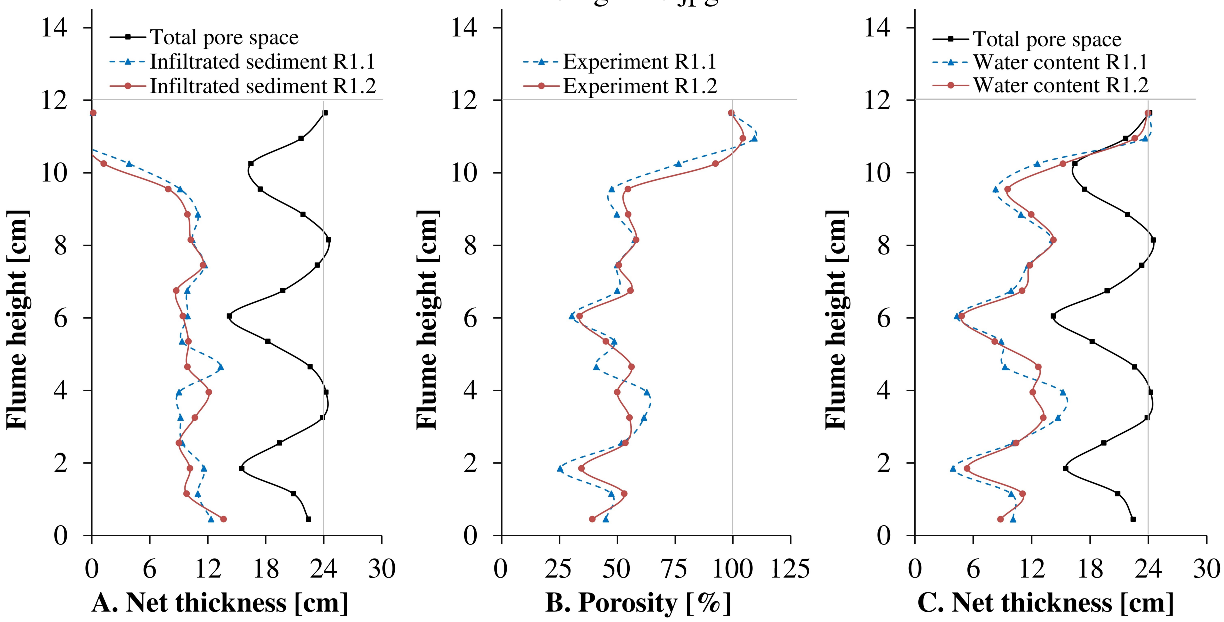

Fig. 8. Results of the repeatability experiments R1 showing vertical profiles of (a) the net thicknesses of infiltrated sediments for both experiments R1.1 and R1.2 in comparison to the total pore space, (b) the calculated porosities for both experiments R1.1 and R1.2 and (c) the net thicknesses of water contents after sediment infiltration for both experiments R1.1 and R1.2 in comparison to the total pore space.

files/Figure 9.jpg

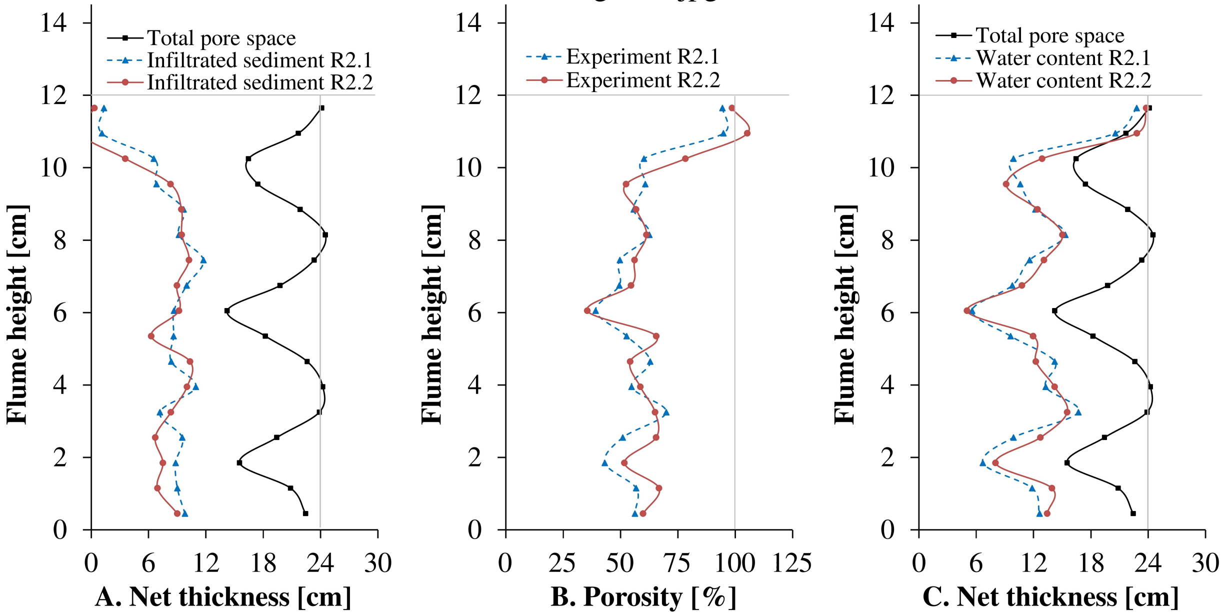

Fig. 9. Result of the repeatability experiments R2 showing vertical profiles of (a) the net thickness of infiltrated sediments for both experiments R2.1 and R2.2 in comparison to the total pore space, (b) the calculated porosities for both experiments R2.1 and R2.2 and (c) the net thicknesses of water contents after sediment infiltration for both experiments R2.1 and R2.2 in comparison to the total pore space.

Publication III.

Measuring vertical distribution and dynamic development of infiltrated sediments under laboratory conditions

Table 5.3. Metadata of publication III

Title	Measuring vertical distribution and dynamic development of infiltrated sediments under laboratory conditions
Authors	**M. A. Mayar**, S. Haun, G. Schmid, S. Wieprecht, and M. Noack
Journal	ASCE Journal of Hydraulic Engineering
Submitted	April 20, 2021
Accepted	January 25, 2022
Published	— –, 2022
DOI	https://doi.org/10.1061/(ASCE)HY.1943-7900.0001980

The final version of this article is accessed through the above DOI link.

Measuring vertical distribution and dynamic development of sediment infiltration under laboratory conditions

M. A. Mayar[1], S. Haun[2], G. Schmid[3], S. Wieprecht[4], and M. Noack[5]

[1]Ph.D. Candidate, Institute for Modeling Hydraulic and Environmental Systems, University of Stuttgart, Stuttgart 70569, Germany; Lecturer, Environmental and Water Resources Engineering Faculty, Kabul Polytechnic University, Kabul 1010, Afghanistan. Email: assem.mayar@hotmail.com

[2]Head of the Hydraulic Laboratory, Institute for Modeling Hydraulic and Environmental Systems, University of Stuttgart, Stuttgart 70569, Germany. Email: stefan.haun@iws.uni-stuttgart.de

[3]Technical Director of the Hydraulic Laboratory, Institute for Modeling Hydraulic and Environmental Systems, University of Stuttgart, Stuttgart 70569, Germany. Email: gerhard.schmid@iws.uni-stuttgart.de

[4]Professor, Institute for Modeling Hydraulic and Environmental Systems, University of Stuttgart, Stuttgart 70569, Germany. Email: silke.wieprecht@iws.uni-stuttgart.de

[5]Professor, Faculty of Architecture and Civil Engineering, Karlsruhe University of Applied Sciences, Karlsruhe 76133, Germany. Email: markus.noack@h-ka.de

ABSTRACT

The complex process of sediment infiltration in gravel beds has been widely studied. However, the temporal behavior of sediment infiltration and its clogging has not yet been sufficiently investigated. Furthermore, to understand the involved mechanisms in this phenomenon, measurements of the effect of various boundary conditions are required with a high spatial and temporal resolution. Hence, the non-intrusive and undisturbed gamma-ray attenuation method is applied in this study to establish a measuring scheme to detect the dynamic development of river bed clogging and to investigate the effects of fine sediments' particle-size distributions, total supplied mass and supply rate on the sediment infiltration process. For a series of experiments, first, vertical profiles of infiltrated sediment masses are measured at two time instants along the experiments. Second, the dynamic changes of the infiltrated sediments at a specific position of the bed are investigated using continuous measurements during the experiments. The results of the measured vertical profile show that sediment infiltration and clogging in an artificial bed match the sediment's existing bridging criterion of the porous gravel bed. Furthermore, temporal changes occur mainly in the upper layers. The continuous one-point measurements indicate almost real-time sediment accumulation development and prove that higher supply rates lead to an earlier start of the infiltration and rapid filling, while lower supply rates result in later and slower infiltration of the sediments.

INTRODUCTION

The infiltration of fine sediments into gravel beds represents a complex process, as this phenomenon is a function of several physical, chemical and biological (Schälchli, 1992) parameters. Infiltrated sediments may clog pores within the interstitial, leading to harmful ecological consequences (Schälchli, 1992; Gayraud and Philippe, 2003; Noack, 2012). Due to variations of flow and fine sediment concentrations in rivers, sediment infiltration and river bed clogging are characterized as very dynamic processes.

Sediment infiltration and river bed clogging processes have been widely studied because of their harmful effects in river ecology. However, the temporal behavior of these phenomena has not yet been sufficiently investigated, due to lack of measurement techniques, but this is necessary for understanding the mechanisms of the involved processes. Several attempts were made in the past to capture these dynamic processes in-situ. For instance, multiple sediment catch trays were deployed within river beds and extracted at certain intervals (i.e., Harper et al. 2017) for obtaining knowledge on fine sediment infiltration. However, such methods are intrusive, destructive and change the natural conditions during installation and extraction of the sampling device. Further, limitations such as the natural variation in the field and different designs of the devices need to be considered in subsequent analyses. Fletcher et al. (1995) used submersible linear displacement transducers mounted beneath a sediment catch tray to monitor fine sediment infiltration into stable gravel river beds. Although this approach gains insight into the dynamic behavior of sediment infiltration, the disadvantage is that neither the vertical distribution of infiltrated sediments over depth can be analyzed nor the sediments clogging with unhindered infiltration be differentiated.

To reduce the natural environment complexity, the temporal development of sediment infiltration has also been investigated in laboratory experiments. For this purpose, indirect methods, such as water pressure and conductivity measurements (Schälchli, 1992, 1995), monitoring of suspended sediment concentrations over time (Hamm et al., 2011), visual inspections of infiltrated sediment height evolution (Herrero et al., 2015), are used to measure the infiltrated sediment accumulation in the gravel bed. A drawback of these methods is that they are integrative and quantify the infiltrated sediments neither over depth, nor the temporal development of accumulations in a specific location. Furthermore, Niño et al. (2018) studied the infiltrated fine sediment transport in a flume with glass walls by using an image analysis technique. However, the main limitation of image analysis is that only the infiltration behavior near the wall of the flume can be investigated in which wall-friction affects the hydraulics.

The infiltration of sediments in the gravel bed strongly depends on the occurring boundary conditions. Thus, sediment particle size and shape, supply rate, amount of the supplying mass, gravel bed porosity and pore structure, and flow forces have a prominent role in the sediment infiltration and accumulation processes (Brunke, 1999; Schälchli, 1992). Some of these parameters have been investigated in the laboratory using destructive methods. For instance, Wooster et al. (2008) analyzed the effect of sediment supply rate, Gibson et al. (2009a,b) and Huston and Fox (2015, 2016) studied the mechanism and infiltration depth of sediments, leading to bridging effects. However, the spatial and temporal resolutions of the applied methods in these studies do not allow to discretize the involved mechanisms in the sediment infiltration and clogging processes, as both processes are described as highly dynamic. Hence, for an accurate understanding of the sediment infiltration and accumulation processes, measuring the effects of the boundary conditions using a non-intrusive and undisturbed measurement method with a high spatial and temporal resolution is required.

Recently, Mayar et al. (2020) introduced a novel non-intrusive and undisturbed approach using the Gamma-Ray-Attenuation (GRA) technique for measuring the infiltrated sediments in an artificial gravel bed under laboratory conditions. This method provides the opportunity to measure the sediment infiltration and the accumulation of sediments in the gravel bed with a high spatial and temporal resolution. While Mayar et al. (2020) focused on the proof-of-concept of the GRA method and its reproducibility, the aims of this study are: First, the development of a measuring scheme to account for the temporal development of pore clogging. Second, to investigate the effect of varying particle-size distributions, supply rates, and the total mass of supplied sediments during constant hydraulic conditions, on the sediment infiltration and their clogging processes, with a high spatial and temporal resolutions.

MATERIAL AND METHODS

Setup of the flume experiments

The laboratory experiments are conducted in a recirculating flume, equipped with a sediment feeding machine supplying sediments continuously for infiltration. The flume has 8.00 m length, 0.24 m width, 0.30 m height, and a constant slope of 1.35 ‰. Within the flume, a bed structure is composed of 0.04-m spheres in the upper two and the lower two layers in a rhombohedral configuration. These set-of-layers are positioned in a way to form cubic packing in the middle. 0.026-m spheres are placed separately in between the cubic packing to reduce the individual pore size. The intention of this setup is to provide an intermediate layer with smaller pores to support possible clogging effects. The spheres are arranged in 16 blocks with a total length of 3.84 m. The spheres in rhombohedral packing are glued only as a horizontal layer, while the different diameter spheres located in the cubic configuration are glued together to keep them in exact positions. The blocks are mounted to the bottom of the flume with a metal fixation at both ends. The individual pore sizes in the chosen composition, located in 45^o between the spheres, are shown in Figure 1D. The pore size is $d_1 = 6.4$ mm between the larger spheres and $d_2 = 5.3$ mm between the 0.04-m and the 0.026-m spheres. To further analyze the infiltration and accumulation behavior for this setup, the vertical profile is subdivided into three sections, namely the top, middle, and bottom section. The infiltrated sediment thickness (x) along the vertical profile is measured in the cross-sectional direction of the flume using the GRA method (Mayar et al., 2020). Figure 1B-C provides information on the vertical profile of the available total pore space geometrically calculated and measured by GRA, the bed structure and location of the measured vertical sections in the spheres arrangements. The calculated initial porosity in each section of the bed is equal to 35.4 % for the top, 26.4 % for the middle, and 36.7 % for the bottom section.

Measurement procedure

The analyses of the infiltration and accumulation behavior consist two types of measurements. The first measurement series investigates the amount and vertical distribution of infiltrated sediments at two time instants along the experiment. The measuring procedure to obtain the infiltrated sediment thickness consists of three measurements, exactly in the same vertical axis (See supplementary Figure S1): (i) The flume with its bed configuration is measured first to obtain the attenuation of the flume walls and the spheres, which is called the background attenuation, (ii) the bed configuration filled with water is measured in a second step to get the total available pore space between the spheres. Both measurements are needed only once, as the bed configuration remains the same for the whole series of experiments. In order to trace the temporal variations of infiltrated masses along the whole vertical profile, the third (iii) measurement is performed at two time instants along the experiments. The first vertical profile is measured immediately after the sediment supply is finished (T_{Exp}) and the water flow is paused. Subsequently, the discharge is gradually resumed and the experiment is continued without supplying additional sediments until the total experimental period of 28 minutes has been completed. This experimental time is chosen based on the proportionality of the sediments' supply rate and supplied masses to compare the results of infiltrated sediments for all experiments in a common duration. Thereupon, the second vertical profile (T_F) was measured. The vertical distribution of infiltrated sediments is measured using a collimator with 7 mm diameter, which defines the vertical resolution.

The second measurement series (continuous one-point measurements) is conducted at a specific position of the vertical profile during the entire experiment to monitor the dynamic behavior of sediment infiltration and accumulation. This measurement uses a collimator of 15 mm diameter, which allows shorter time-intervals (60 s), to increase the temporal resolution. The measurement principle for the second measurement type is the same as for the vertical profiles. In this measurement, the background (i) and total pore space (ii) profiles are measured for the total experimental period prior to the experiment, while the sediment infiltration (iii) profile is measured during the entire experiment. An advantage of this measurement setup is that both types of measurements can be conducted for the same experiments.

Experimental program

In total twelve experiments are conducted with different sediment related boundary conditions. Three particle-size distributions, further called fine, coarse, and mixed are investigated. The grain-size distributions of these sediments are shown in Figure 2, which indicates that the fine and coarse sediments are rather homogeneous, whereas the mixed sediment has a heterogeneous (bimodal) distribution. The average particle diameter and sorting coefficient for the fine, coarse, and mixed sediment mixtures are 1.6 mm and 1.14; 3.09 mm and 1.14; 2.02 mm and 2.0, respectively. All the three mixtures have a density of $\rho_s = 2,650 kg/m^3$ (quartz sand).

Two supply rates (Q_s) are used for each supplied sediment mixture, namely 1.4 kg/min and 3.7 kg/min. These values are average supply rates, with minor deviations in the actual sediment supply ($Q_{s,act}$) as a result of the used feeding machine performance. Finally, the total amount of each supplied sediment mixture (M_s) is varied by using 10 kg and 20 kg. Table 1 provides an overview on the experimental program.

During all the experiments the hydraulic conditions remain constant with a discharge of $Q = 16 \pm 0.2$ l/s and a flow depth of 0.08 m, leading to an average flow velocity of 0.83 m/s, a Froude-number of 0.93, and a Reynolds-number of 122,465.

Uncertainties in GRA measurements

Due to the three-fold (i - iii) GRA measurements, three statistical errors occur in this configuration. The vertical profile of the infiltrated sediments (iii) leads to the highest statistical error due to the highest attenuation of gamma quants. Therefore, according to Mayar et al. (2019), a measuring time of 240 seconds for each position of the vertical profiles is chosen, resulting in a maximum statistical error of less than 3.3 % in the infiltrated sediment vertical profile measurement.

To minimize the statistical error in the one-point measurements, a 120-second time-step is used for the (i) and (ii) profiles measurements. A 60-second time-step is used for the sediment infiltration (iii) profile measurement, which results in a higher temporal resolution of the measurements. Hence, the resulted maximum statistical error of one-point measurements is up to 4.4 % (for the mixed sediments). These statistical errors are also in the range of previously conducted experiments with the GRA method (i.e. Pires and Pereira 2014; Moreira et al. 2011; Pires et al. 2009). Finally, the total error in percent is transformed to sediment thickness and mass and is visualized in the relevant graphs.

Despite the statistical errors, uncertainties exist due to the alignment of the measurement positions as well as the performance of sediment supply machine. Thus, horizontal alignment of the bed structure was controlled through inspection of the measurement axis and previously marked nearby positions. To keep the vertical positions accurate, spheres were glued into the blocks, and an automatic vertical travers system with a maximum error of 1.0 mm was used for vertical positioning in this study. The uncertainties of the sediment supply machine are reflected in actual sediment supply ($Q_{s,act}$) in Table 1.

RESULTS

As a basis for the analysis of the measurements, the background attenuation profile is shown in Figure 1A. This profile shows that the measured values attenuate according to the net thickness of the spheres, which face the gamma emitting beam. The maximum values, located at the positions close to the surface and the bottom, are due to the collimated radiations not facing the spheres (Figure 1C) in these two positions. Figure 1B presents the GRA measured vertical profile of the available pore space as well as geometrically derived. Both profiles show minimum values for the pore space at z = 0.088 m (0.007 m) and z = 0.046 m (0.010 m), the center of 0.04-m spheres. However, 0.02 m upstream and downstream of these positions in the longitudinal direction of the flume, the total pore space is high that allows sediment to infiltrate towards the bottom. The depth averaged mean absolute deviation between GRA measured and geometrically derived values of the total pore space is equal to 0.012 m, resulting from the statistical error of GRA measurements and due to minor inaccuracies in the manufacturing process of the bed. Although the geometrically derived values represent the idealistic bed configuration, the GRA measured profile is used for the subsequent analyses as they represent the actual profile of the manufactured bed.

The experimental results are presented in a way that first the vertical distribution of sediments, including the infiltration masses subdivided into three vertical sections, are shown. Second, the dynamic effects (temporal changes) are analyzed by comparing vertical profile measurements at two time instants along the experiments (T_{Exp}, T_F) as well as by using the one-point measurements at a certain position. Finally, all the results are evaluated and discussed according to the effects of varying sediment boundary conditions used during the experiments.

Vertical distributions and masses of infiltrated sediments in the first measurement (T_{Exp})

Figure 3A-C shows the vertical distributions of infiltrated sediments for the three sediment mixtures. Each plot contains the measured total pore space profile, and the results of the experiments for the two supply rates and two supplied masses at the end of the sediment supply (T_{Exp}). The Sn.1-4 in the legend represent the experiment ID, in accordance to Table 1, in which "n" is the number of the sediment mixture. Figure 3D represents the infiltrated sediment masses at T_{Exp}, divided into three vertical sections. The infiltrated sediment masses are obtained through converting the measured sediment thicknesses by using the known volume of the lateral measuring locations with a collimator size of 7 mm, and a subsequent summing up for each section.

Fine-sediment mixture

For all the conducted experiments with fine sediments, it was observed that the filling of the pore space starts from the bottom until the top section is reached. Hence, Figure 3A shows a measured high net thickness in the bottom section, where sediments start to accumulate first. This is the result of the small-particle size, compared to the individual pore size, as the smallest pore size in the bed configuration is 3.25 times larger than the average particle size of fine sediment mixtures. These findings are consistent with the bridging criterion, developed by Huston and Fox (2015), in which the unimpeded static percolation occur when the $d_{ss}/d_{fs}\sigma_{ss}$ ratio, which is equal to 44.8 for fine sediment experiments, is higher than 27. The highest thickness (0.120 m) of the infiltrated fine sediment mixture is measured close to the flume bottom (z = 0.005 m), while the thickness achieves 0.094 m in the middle section (z = 0.068 m) and 0.085 m in the top section (z = 0.130 m). This almost homogeneous distribution proves that the sediments infiltrate smoothly and no bridging effects occur. The effects of the supplied sediment masses and supply rates are not reflected by the experiments of this sediment mixture.

By analyzing the sediment masses (Figure 3D) for the supplied sediment masses and supply rates minor variations of the infiltrated masses are observed in each section. The integrated sum of infiltrated masses of fine sediments in each section (averaged overall boundary conditions) results in 42.5 g, 21.6 g and 51.7 g for the top, middle and bottom sections, respectively. The reason for the lower mass of the middle section is the lower available pore volume ($12.37cm^3$) compared to the top ($34.97cm^3$) and bottom ($35.86cm^3$) sections. The calculated porosity after sediment infiltration (in the volume of the gamma-ray beams), is the lowest in the middle section with 34.1 % and significantly lower compared to the porosities of the top (54.1 %) and bottom (45.6 %) sections.

Coarse-sediment mixture

Figure 3B shows the vertical distribution profiles of the coarse sediments. Smaller thicknesses of infiltrated sediments can be seen at the bottom (0.06 m, z = 0.005 m) and in the middle section (0.06 m, z = 0.068 m), compared to the sediment thicknesses of fine sediment experiments (0.120 m and 0.094 m, respectively). However, a larger sediment thickness (0.097 m, z = 0.130 m) is observed in the top section for the coarse sediments. The differences in the middle and bottom sections are a direct result of pore clogging at z = 0.125 m and z = 0.060 m, which restricts sediments from further infiltration. This clogging of pores by coarse sediments corresponds the Huston and Fox (2015) bridging criterion, in which sediments bridge in the bed when $d_{ss}/d_{fs}\sigma_{ss}$ ratio is less than 27. This value is equal to 23.3 for coarse sediment experiments. The effects of varying supply rates are within the uncertainty of the GRA measurements in all three sections. An increase in the supplied masses reveals higher sediment thicknesses in the bottom section for 20 kg (0.045 m, z = 0.033 m) compared to 10 kg (0.013 m, z = 0.033 m). This vertical position represents the strait between the larger spheres, which indicates that for higher sediment masses accompanied by longer experimental durations, particles that infiltrate downward could be trapped in this strait and lead to clogging.

The infiltrated masses of the coarse sediments given in Figure 3D reflect, on the one hand, minor variations in sediment thicknesses for the supplied sediment masses and supply rates, and, on the other hand, significantly less infiltration masses in the middle and bottom sections compared to fine sediment experiments. The integrated sum of infiltration masses for each section (averaged overall boundary conditions) gives 44.9 g, 12.6 g, and 15.7 g in the top, middle, and bottom sections, respectively. The corresponding porosities after sediment infiltration of the coarse sediment result in 51.5 %, 61.6 %, and 83.5 % in the top, middle and bottom sections, respectively. This clearly indicates the bridging of sediments and demonstrates the trapping effect when coarse sediments clog the pores within the bed structure.

Heterogeneous-sediment mixture (mixed)

The vertical distribution profiles of infiltrated mixed sediments are shown in Figure 3C. Compared to measured sediment thicknesses of the fine and coarse sediment experiments, large variations can be seen in all three sections. The mixed sediments did not bridge in the spheres due to bimodal grain-size distribution and having a value of 35.4 for the $d_{ss}/d_{fs}\sigma_{ss}$ ratio, which is greater than 27.

The results of the experiments show that the vertical distribution of infiltrated mixed sediments is strongly influenced by the given supply rate and supplied mass boundary conditions. The maximum thickness of infiltrated mixed sediments (0.120 m) for all boundary conditions is seen close to the flume bottom (z = 0.005 m), which is a similar observation as for the experiments with fine sediments. However, this thickness of the infiltrated mixed sediments is also seen at flume heights z = 0.011 m and z = 0.116 – 0.130 m in the S3.3 and S3.4 experiments, respectively. Furthermore, the maximum thickness in the middle section (0.108 m, z = 0.068 m) is higher compared to the experiments with fine and coarse sediments. A reason for this behavior is the heterogeneity of the sediment mixture, which results in a lower porosity of the filling compared to the fine and coarse sediments. The infiltrated sediment thicknesses in the top section have strong variations and are discussed according to the boundary condition effects subsequently.

The effects of the supplied masses are very obvious in the experiments with a supply rate of 1.4 kg/min (S3.1, S3.3) on the infiltrated sediment thicknesses in the bottom section. The S3.3 experiment resulted in a considerably higher thickness at $z = 0.018 - 0.025$ m compared to the same experiment with 10 kg supplied mass of sediments (S3.1). However, the supplied mass did not influence the sediment thickness in the bottom section during the experiments with a supply rate of 3.7 kg/min. Further, the experiment with a supply rate of 3.7 kg/min (S3.4) resulted in a smaller thickness of infiltrated sediments compared to the same experiment with a supply rate of 1.4 kg/min (S3.3). The reason is twofold: first, a lower supply rate enables a smoother infiltration, leading to a lower probability of clogging. Second, with a supply rate of 1.4 kg/min, a 2.6 times longer sediment supply duration, compared to experiments with a supply rate of 3.7 kg/min, is given. This provides the opportunity for more sediments to infiltrate, especially for the particle sizes of 0.6 - 1.2 mm. Therefore, the smaller thickness of infiltrated sediments in the S3.1 experiment could be influenced by the higher infiltration of sediments in the empty volume, upstream of the measurement axis (dead storage), which results in a reduction of supplied mass for the measurement axis in this experiment. The mass of supplied sediments did not influence infiltrated sediment thicknesses in the middle section, while in the top section the higher supplied mass resulted in a higher amount of infiltrated sediments. For instance, the lower supplied mass and lower supply rate (S3.1) led to a minimum sediment thickness (0.044 m, $z = 0.108$ m), whereas a higher supplied mass and lower supply rate (S3.3) reached a maximum thickness (0.112 m at $z = 0.108$ m), although the thicknesses for $z > 0.12$ m is equivalent in both experiments. Furthermore, the supply rate of 3.7 kg/min with 20 kg feeding mass (S3.4) produced the highest sediment thickness (0.120 m at $z = 0.130$ m) compared to the thickness of 0.049 m at $z = 0.130$ m in the experiment with a similar supplying mass, but 1.4 kg/min supply rate (S3.3). The reason is that the flow conditions (shear force) were kept constant for all experiments, where the flow cannot transport sediments during a higher supply rate as in the lower one. In addition, the higher supply rate increases the probability of clogging and leads to more sediments in the surface layers. For this reason, mixed sediments did not infiltrate to the lower layers of the top section (z = 0.095 – 0.116) and middle section (z = 0.053 – 0.060) during the supply rate of 3.7 kg/min with 10 kg feeding mass (S3.2).

The infiltrated sediment masses of mixed sediments in Figure 3D also reflect the impact of changed supply rates and feeding masses on the infiltrated sediment thicknesses. The total infiltrated sediment masses in the top section range between 30.8 g (S3.1) and 58.0 g (S3.4). The infiltrated sediments in this section have a trend for both, supply mass and rates as: the higher supply mass resulted in more infiltration for both supply rates, while the infiltrated sediment masses are also high for the higher supply rate. The infiltrated mass of mixed sediments in the middle section is rather equal for the given supply rates and supplied masses (23.8 g on average). However, this value represents the highest infiltration mass in the middle section for all the sediment mixtures. The infiltration mass of mixed sediments in the bottom section ranges between 35.8 g (S3.1) and 58.7 g (S3.3) without a clear trend. The overall average infiltrated mass of mixed sediments in the bottom section is 47.3 g. The resulting porosity after infiltration of mixed sediments yields from 66.7 % in S3.1 to 37.3 % in S3.4 (average overall boundary conditions 52.1 %) in the top section, 27.3 % (equivalent for all boundary conditions) in the middle section, and from 62.2 % in S3.1 to 38.2 % in S3.3 (average overall boundary conditions 50.2 %) in the bottom section.

Temporal changes in the sediment infiltration and accumulation behavior

Vertical distributions and masses of infiltrated sediments in the second measurement (T_F):

The results of the measured infiltrated sediment thicknesses along the vertical profiles and the corresponding masses in the three vertical sections for T_F are shown in Figure 4. A comparison between the vertical profiles and infiltration masses at the two time instants along the experiments (T_{Exp} and T_F) leads to one general observation for all experiments: significant differences occur only in the top section. The reason is twofold: first, deposited sediments are washed away from the surface (0.109 m < z < 0.130 m) after the sediment supply ended at T_{Exp}. This effect is the strongest for fine sediments, followed by the mixed and coarse sediments fraction. Second, within the bed structure consolidation (re-distribution) of the sediments happens in all three sections, resulting in minor changes. However, the temporal behavior is depending on the sediment mixture. Within the lower part of the top section (z = 0.102 m) these temporal changes are within the statistical error for the fine sediments (range of error-bar). For the coarse (S2.1, S2.2, S2.4) and mixed sediment (S3.1, S3.2) experiments, a clear increase in the sediment thickness is observed at z = 0.102 m. The reason is that fine sediments uniformly filled the pores of the spheres at this position during T_{Exp}, but mixed and the coarse sediments clogged the upper pores (z > 0.109 m). During the second flow period without sediment supply (T_F), sediments at z = 0.102 m consolidated and additional sediments infiltrated from the upper layers. The overall boundary conditions averaged reductions of fine, coarse and mixed sediment masses in the top section are 15.3 g, 20.6 g, and 13.3 g, respectively, which represents a value of 36.0 %, 45.8 %, and 30.1 % of the initial infiltrated sediment masses at T_{Exp}.

The dynamic variations in the middle section for the fine and mixed sediments are in the range of the statistical error (error-bar thickness: ±0.01 m at z = 0.068 m); only additional accumulation is observed for the coarse sediment mixture until T_F (z = 0.068 m, Figure 4D). The average overall boundary conditions of absolute net and absolute relative deviations in the middle section result in 2.5 g, 4.6 g, and 2.3 g, which is equal to 11.4 %, 36.5 %, and 9.66 % for the fine, coarse, and mixed sediments, respectively. This clearly indicates that the coarse sediment mixture is most vulnerable to accumulation changes in the pores in case of no additional sediment supply. One potential reason can be higher interstitial flows occur in case of the coarse particles compared to the fine sediments that tend to consolidation effects.

In the bottom section smaller variations are observed compared to the upper sections. The fine and coarse sediments experiments with a supply rate of 3.7 kg/min (S1.2, S1.4, S2.2) received additional sediments, which can be the result of the re-distribution of infiltrated sediments during the longer flow period in the second interval (T_F). Similarly, mixed sediments show an increase of the sediment thickness for S3.1 (z = 0.011 – 0.018 m) and a decrease for S3.2, S3.3, S3.4 experiments in the bottom section. These changes could be the result of 0.6 – 1.2 mm particles displacement. The average overall boundary conditions of absolute net differences and absolute relative deviations in the bottom section are 6.25 g, 3.16 g, and 5.25 g or 12.1 %, 20 %, and 11.1 % for the fine, coarse, and the mixed sediments, respectively.

Further details on the experiments are available in the supplementary Figure S2 and Table S1. Figure S2 represents a comparison of the T_{Exp} and T_F vertical profiles for the boundary conditions discussed in Table 1. Similarly, the measured sediment masses of the first measurement (T_{Exp}), their net and relative deviations until the second measurement (T_F), at each section of the vertical profiles, are presented in the Table S1.

Continuous one-point measurements to detect the dynamic development of infiltration process

The results of the one-point measurements are presented in Figure 5A-C for all three sediment mixtures, supply rates and supplied masses of sediments. Based on the time-series, obtained with a temporal resolution of 60 s, it is feasible to detect three distinctive points and subsequent phases of the dynamic development of the infiltration and accumulation processes, namely: (I) the start of the pore-filling process, (II) the end of the pore filling, (III) the end of consolidation and re-distribution of sediments, which represents the final thickness (amount) of infiltrated sediments.

The start and the end of the pore-filling can be indicated by the steep gradient section of the time-series. Figure 5A shows that the gradient is steep for the fine sediments and rather flat for the coarse-sediment mixture, which indicates that fine sediments fill the pores suddenly. The reason for this is that the measuring pore is located horizontally. Once the lower layers have been filled, this pore fills quickly owing to the unhindered infiltration of fine sediments.

A deeper look into Figure 5A-C shows that the start of the filling process strongly depends on the supply rate. The 1.4 kg/min supply rate resulted in a later start (240 s and 180 s), while the 3.7 kg/min supply rate resulted in an earlier beginning (120 s and 60 s) of the filling, for all three sediment mixtures. Furthermore, the duration of the pore-filling phase for fine and mixed sediments is influenced by the supply rates. For the fine sediments (Figure 5A), the higher supply rate filled the pores during two measurement time-steps (120 s), while for the lower supply rate it took three time-steps (180 s). For coarse sediments such a clear trend between the two supply rates is not visible. In which for the 1.4 kg/min supply rate a time span of 60 s and 180 s is visible, for the higher supply rate (3.7 kg/min) 180 s to 240 s can be seen (Figure 5B). This is the result of bridging effects, which occur during the infiltration process. However, although bridges develop, they may also break up within this phase of the experiment and develop again. The mixed sediments' pore filling duration (Figure 5C) follows the fine sediments' trend with one additional time-step (60 s) for each supply rate. However, here also bridging effects occur, which may break up again during the filling, and result in a less smooth filling compared to the fine-sediment mixture.

The continuous one-point measurements (Figure 5A-C) show the distribution of the accumulated sediments and the subsequent consolidation. The effects of the different supplied sediment mixtures are reflected by the results, in which thicknesses and the range of fluctuations vary after the pores are fully filled. This can be seen especially for the coarse sediments (Figure 5B), which gradually rise after a first filling as a result of ongoing consolidation process, e.g., due to higher interstitial flow compared to the experiments with fine sediments. As a consequence, an ongoing change of the thickness of the infiltrated sediments can be seen also after the end of the sediment supply (T_{Exp}). However, once the available pore space is filled (Figure 5A and Figure 5C), considerable infiltration is no longer observed.

In addition, Figure 5A-C indicates that the mixed sediments have the highest accumulated thickness of 0.070 m (averaged overall boundary conditions), while the fine and coarse sediments achieved 0.065 m and 0.035 m, respectively. This also shows the clogging process generated by the coarse sediments in the upper layers. The total masses of supplied sediments have not influenced the three phases of the sediment infiltration (I - III). According to Figure 5A and 5C, the sediments reached the peak thickness prior to the 10 kg sediment supply duration (T_{Exp} – shown by vertical lines) in both supply rates.

Furthermore, the range of fluctuations after reaching the peak thickness for fine, coarse, and mixed sediments are 0.035 m, 0.030 m, and 0.050 m, respectively. These fluctuations are larger than the related statistical error-bars (average overall boundary conditions: 0.014 m), which characterize the sediment accumulation and depletion processes in a higher temporal resolution.

The one-point measurement dynamic results cannot be compared directly with the infiltrated sediment thickness measurements in the vertical profiles as a result of different collimator sizes. However, the sediment thickness variations in the one-point measurements follow the pattern of the infiltrated sediment thickness variations at z = 0.068 m of the vertical profiles between T_{Exp} and T_F.

DISCUSSION

The measured vertical profiles show that fine sediments infiltrate smoothly, start to accumulate from the bottom and progress further upwards due to an unhindered infiltration. The infiltration of coarse sediments leads to bridging and clogging effects within the pores, which prevent further infiltration downwards into the bed. The mixed sediments, despite the presence of coarse particles, did not bridge clearly. This is mainly the result of the bimodal particle mixture, where especially fine components of this mixture infiltrate all the way to the bottom. Hence, the coarser particles of this sediment mixture are unable to bridge the pores between the spheres of the artificial bed in a way that a bed clogging occurs.

In addition, the infiltration of homogeneous fine and coarse sediment mixtures had a minor dependency on the supply rates and total feeding masses. However, they have strongly influenced the results of the experiments with mixed sediments, particularly in the bottom section of the bed. In overall, the experiments with mixed sediments result in the highest sediment thickness and mass of infiltrated sediments, owing to the heterogeneous mixture with a bimodal grain-size distribution. The experiments with higher supply rates result in smaller accumulations of the infiltrated sediments in the bottom section. This clearly indicates that for high supply rates, independent of the supplied mass, a partial clogging of the pores happens, mainly driven by the coarser part of the infiltrating particles. The combination of a low supply rate and a high supplied mass results in maximum accumulation in the bottom section. The reason is twofold: the lower supply rate enables a smoother sediment infiltration and the longer experimental duration offers the opportunity for more particles to infiltrate and that the fine particles infiltrate deeper into the bed.

Furthermore, the comparison of the T_F and T_{Exp} measurements shows that dynamic changes happen mainly in the upper section of the artificial bed, as a result of washed-away sediments. However, in the lower part of the top section and in the middle and bottom sections dynamic changes occur, although they are smaller compared to changes in the top layer and are partly within the uncertainty of the GRA measuring method. These changes are the result of a re-distribution of the infiltrated sediments (consolidation) and the resulting additional pore space, which is filled by fine sediments, infiltrating from the above located middle and top sections.

The continuous one-point measurements give additional insight into the dynamic development of the sediment infiltration and accumulation processes. Due to the higher measurement resolution, the start, the duration and speed of pore-filling, as well as further consolidation processes within the measurement axis, which are also observed in the measurements of the vertical profiles at two subsequent steps, can be detected. The results of the experiments clearly indicate that higher supply rates lead to an earlier start and a more rapid filling of the pores compared to the lower supply rates. In addition, the supplied fine and mixed sediments achieve a form of dynamic steady-state condition regarding the sediment accumulation in the pores. Subsequent fluctuations in the sediment thickness reflect stochastic depletion and re-filling of the pores. This process is visible, especially for coarse sediments, which show a gradual increase of the accumulation process as a result of consolidation effects over time.

The experiments of this study were conducted in a 0.024 m wide flume with one-dimensional flow conditions. An increment of the flume width in the future studies would reduce wall effects and may result in two-dimensional flow within the flume, affecting fine sediment transport, infiltration, and accumulation processes. The vertical distribution of the infiltrated sediments, particularly the clogging depth of the coarse sediments, will be influenced. The temporal variation of the vertical profiles at two time instants along the experiment may only happen in the upper layers of the bed. Finally, the one-point measurement will represent a pore filling result proportional to the sediments' supply and available space. However, the limitations of the GRA method need to be taken into account. For a reliable measurement result in a wide flume, sufficient radiation should pass through the flume width. This is feasible by using either a very strong radioactive source or larger collimators, though the latter reduce spatial resolution. In addition, a larger detector unit is also required to collect the scattered radiation.

The measuring setup and procedure used in this study are based on only one GRA device. However, multiple devices to measure more vertical profiles and several one-point measurements at the same time would be beneficial and certainly lead to a more comprehensive understanding of the dynamics behind the sediment infiltration and accumulation processes. In addition, the choice of boundary conditions and artificial bed configurations could be improved in order to get closer to nature for further investigation of this phenomenon.

CONCLUSIONS

Sediment infiltration in porous gravel beds is a highly dynamic process. This study sets up first a measuring scheme that enables detection of the dynamic infiltration of fine sediments and the development of clogging layers with a high spatial and temporal resolution. Second, a series of experiments are conducted to capture the effects of fine sediments' particle-size distributions, total supplied mass and supply rate on the infiltration and accumulation process. Therefore, the non-intrusive and undisturbed GRA measurement method is used to investigate the vertical distribution of fine sediment accumulations and possible clogging in an artificial bed. The measuring concept includes measurement of high-resolution vertical profiles at two time instants along the experiments (right after the sediment supply - T_{Exp} and at the end of the experiment - T_F). In addition, a specific position of the vertical profile was continuously measured during the entire experiment to detect temporal changes of the infiltrated sediment thickness with a high temporal resolution. Considering the results, the following key conclusions are drawn:

- The sediment infiltration and clogging in an artificial bed match the existing sediment's bridging criterion of the porous gravel bed.
- The infiltration of homogeneous fine and coarse sediment mixtures had a minor dependency on the supply rates and total feeding masses. However, it strongly influenced the results of the experiments with mixed sediments, particularly in the bottom section of the bed.

- The comparison of the measurement results at two time instants along the experiment shows that dynamic changes happen mainly in the upper section of the bed, as a result of washed-away and consolidation of the sediments.
- The continuous one-point measurements, owing to the higher temporal resolution, determined the start, the duration and speed of pore-filling as well as further consolidation processes within the measurement axis. The results of the experiments clearly indicate that higher supply rates lead to an earlier start and a more rapid filling of the pores compared to the lower supply rates.

The developed scheme for measuring vertical profiles of infiltrated sediments, at different time instants along the experiments, combined with a continuous one-point measurement enables new insights into the infiltration and accumulation behavior of fine sediments under changing boundary conditions. By using this measurement method, it is possible, not only to understand the dynamic behavior of the sediment clogging, but also to unravel processes behind it in the future. The obtained experimental results within this study provide first data-sets with a very high spatial and temporal resolution, which may be used for the further development of numerical and mathematical modeling approaches to simulate and calculate sediment infiltration and accumulation processes.

DATA AVAILABILITY STATEMENT

The data measured by the GRA method for all experiments that support the findings of this study are available from the corresponding author upon request.

ACKNOWLEDGMENTS

The first author received financial support through a scholarship from the German academic exchange services (DAAD), for which he is grateful to this organization. The second author is indebted to the Baden-Württemberg Stiftung for the financial support by the Elite program for Postdocs. The authors also thank the hydraulic laboratory staff at the Institute for Modelling Hydraulic and Environmental Systems of the University of Stuttgart for their support during the experiments.

SUPPLEMENTARY MATERIALS

Figs. S1-S2 and Table S1 are available online in the ASCE Library (www.ascelibrary.org).

APPENDIX I. NOTATION

The following symbols are used in this paper:

d_s	diameter of sediment particle size (mm);
d_{fs}	mean diameter of fine sediments (mm);
d_{ss}	mean diameter of substrate material size (mm);
M_s	total mass of supplied sediments (kg);
Q	discharge (m^3/s);
Q_s	supply rate of sediments (kg/min);
$Q_{s,act}$	actual supply rate of sediments (kg/min);
T_{Exp}	duration of supplying sediments to the flume (min), first vertical profile measurement milestone;
T_F	duration of running flow without sediment supply to the flume (min), second vertical profile measurement milestone;
x	thickness of the infiltrated sediments (m);
z	vertical axis;
σ_{ss}	geometric standard deviation of substrate material and
ρ_s	density of the sediments (kg/m^3);

REFERENCES

Brunke, M. (1999). "Colmation and depth filtration within streambeds: retention of particles in hyporheic interstices." *International Review of Hydrobiology*, 84(2), 99–117.

Fletcher, W. K., McLean, W. E., and Sweeten, T. (1995). "An instrument to monitor infiltration of fine sediment into stable gravel stream beds." *Aquacultural Engineering*, 14(4), 289–296.

Gayraud, S. and Philippe, M. (2003). "Influence of Bed-Sediment Features on the Interstitial Habitat Available for Macroinvertebrates in 15 French Streams." *International Review of Hydrobiology*, 88(1), 77–93.

Gibson, S., Abraham, D., Heath, R., and Schoellhamer, D. (2009a). "Bridging process threshold for sediment infiltrating into a coarse substrate." *Journal of geotechnical and geoenvironmental engineering*, 136(2), 402–406.

Gibson, S., Abraham, D., Heath, R., and Schoellhamer, D. (2009b). "Vertical gradational variability of fines deposited in a gravel framework." *Sedimentology*, 56(3), 661–676.

Hamm, N. T., Dade, W. B., and Renshaw, C. E. (2011). "Fine particle deposition to porous beds." *Water Resources Research*, 47(11), W11508.

Harper, S., Foster, I., Lawler, D., Mathers, K., McKenzie, M., and Petts, G. (2017). "The complexities of measuring fine sediment accumulation within gravel-bed rivers." *River Research and Applications*, 33(10), 1575–1584.

Herrero, A., Berni, C., and Cemenen, B. (2015). "Laboratory Analysis on Silt Infiltration into Gravel Bed." *E-proceedings of the 36th IAHR World Congress*, The Hague, Netherlands.

Huston, D. and Fox, J. F. (2016). "Momentum-Impulse Model of Fine Sand Clogging Depth in Gravel Streambeds for Turbulent Open-Channel Flow." *Journal of Hydraulic Engineering*, 142(2), 04015055.

Huston, D. L. and Fox, J. F. (2015). “Clogging of Fine Sediment within Gravel Substrates: Dimensional Analysis and Macroanalysis of Experiments in Hydraulic Flumes.” *Journal of Hydraulic Engineering*, 141(8), 04015015.

Mayar, M. A., Schmid, G., Wieprecht, S., and Noack, M. (2019). “Optimizing vertical profile measurements setup of gamma ray attenuation.” *Radiation Physics and Chemistry*, 164, 108376.

Mayar, M. A., Schmid, G., Wieprecht, S., and Noack, M. (2020). “Proof-of-Concept for Non-intrusive and Undisturbed Measurement of Sediment Infiltration Masses Using Gamma-Ray Attenuation.” *Journal of Hydraulic Engineering*, 146(5), 04020032.

Moreira, A. C., Filho, O. P., Cavalcante, F. H. d. M., and Appoloni, C. R. (2011). “Determination of Hydraulic Conductivity of Undisturbed Soil Column: a Measurement Accomplished with the Gamma Ray Transmission Technique.” *Developments in Hydraulic Conductivity Research*, O. Dikinya, ed., IntechOpen, Rijeka.

Niño, Y., Licanqueo, W., Janampa, C., and Tamburrino, A. (2018). “Front of unimpeded infiltrated sand moving as sediment transport through immobile coarse gravel.” *Journal of Hydraulic Research*, 56(5), 697–713.

Noack, M. (2012). “Modelling Approach for Interstitial Sediment Dynamics and Reproduction of Gravel-Spawning Fish.” Dissertation No. 214, Institute for Modelling Hydraulic and Environmental Systems, University of Stuttgart, Stuttgart, Germany, <https://elib.uni-stuttgart.de/handle/11682/485>.

Pires, L., Rosa, J., Pereira, A., Arthur, R., and Bacchi, O. (2009). “Gamma-ray attenuation method as an efficient tool to investigate soil bulk density spatial variability.” *Annals of Nuclear Energy*, 36(11-12), 1734–1739.

Pires, L. F. and Pereira, A. B. (2014). “Gamma-Ray Attenuation to Evaluate Soil Porosity: An Analysis of Methods.” *The Scientific World Journal*, 2014, 1–10.

Schälchli, U. (1992). "The clogging of coarse gravel river beds by fine sediment." *Hydrobiologia*, 235(1), 189–197.

Schälchli, U. (1995). "Basic Equations for Siltation of Riverbeds." *Journal of Hydraulic Engineering*, 121(3), 274–287.

Wooster, J. K., Dusterhoff, S. R., Cui, Y., Sklar, L. S., Dietrich, W. E., and Malko, M. (2008). "Sediment supply and relative size distribution effects on fine sediment infiltration into immobile gravels: Fine sediment infiltration into immobile gravels." *Water Resources Research*, 44(3), n/a–n/a.

List of Tables

TABLE 1. Overview of conducted experiments, including all varying boundary conditions. Further, the actual supply rate of sediments with recorded sediment supply durations (T_{Exp}) are given.

No.	experiment ID	sediment d_s (mm)	M_s (kg)	Q_s (kg/min)	$Q_{s,act}$ (kg/min)	T_{Exp} (min)
1	S1.1		10	1.4	1.36	7.20
2	S1.2	fine		3.7	3.39	2.57
3	S1.3		20	1.4	1.42	14.05
4	S1.4			3.7	3.55	5.38
5	S2.1		10	1.4	1.31	7.38
6	S2.2	coarse		3.7	3.16	3.10
7	S2.3		20	1.4	1.52	13.09
8	S2.4			3.7	3.42	5.51
9	S3.1		10	1.4	1.76	5.40
10	S3.2	mixed		3.7	3.75	2.40
11	S3.3		20	1.4	1.64	12.13
12	S3.4			3.7	3.75	5.20

TABLE S1. Infiltrated sediment masses at T_{Exp}, their net and relative deviations until T_F, showing temporal effects of the sediment infiltration and accumulation behavior

Item	sections	experiments											
		S1.1	S1.2	S1.3	S1.4	S2.1	S2.2	S2.3	S2.4	S3.1	S3.2	S3.3	S3.4
Infiltrated	top	38.73	45.05	41.53	44.86	40.35	47.00	45.58	46.80	30.81	40.03	48.48	58.09
sediment mass	middle	21.35	22.29	20.31	22.42	15.99	11.47	9.08	13.83	23.92	23.13	23.91	24.41
at T_{Exp} (g)	bottom	51.54	49.55	57.27	48.39	11.89	11.66	22.25	17.13	35.86	49.41	58.73	45.25
Net sediment	top	-13.1	-19.7	-13.1	-15.5	-20.7	-21.4	-20.6	-19.6	-8.06	-18.64	-7.75	-18.94
mass changes	middle	-2.12	1.26	-2.51	4.00	3.18	3.73	6.89	4.60	-2.57	-4.04	1.71	0.89
until T_F (g)	bottom	-4.77	5.32	-6.05	8.87	-0.97	9.24	-0.79	1.64	4.76	-7.13	-7.14	1.97
Sediment mass	top	-33.8	-43.7	-31.4	-34.5	-51.4	-45.5	-45.3	-41.9	-26.15	-46.5	-15.99	-32.6
changes	middle	-9.91	5.67	-12.4	17.8	19.9	32.5	75.99	33.2	-10.76	-17.47	7.17	3.63
until T_F (%)	bottom	-9.26	10.75	-10.6	18.34	-8.2	79.24	-3.57	9.55	13.28	-14.42	-12.15	4.35

List of Figures

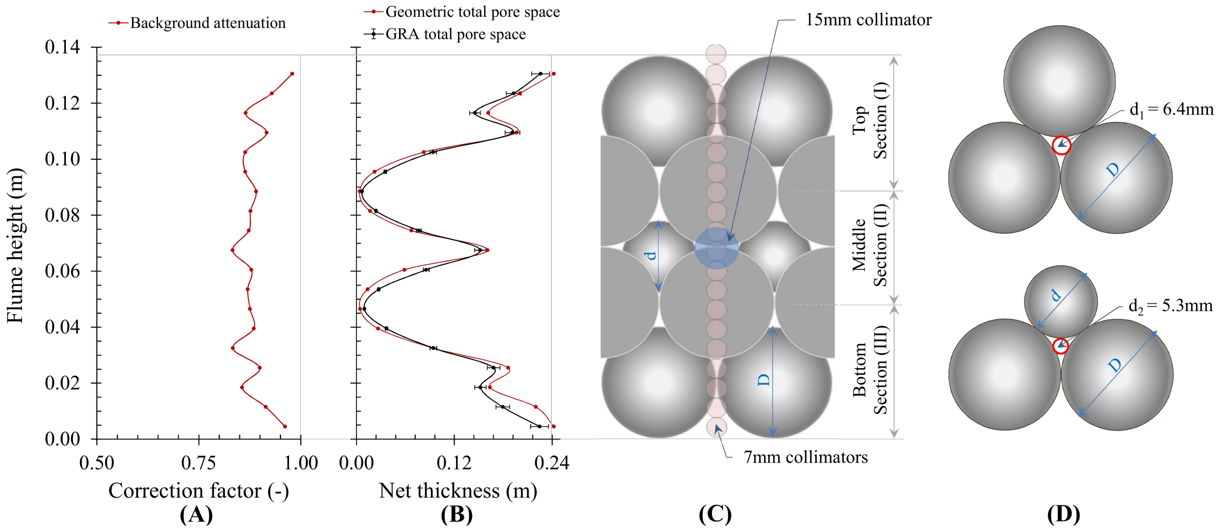

Fig. 1. (A) Vertical profile of the correction factor for background attenuation due to flume walls and spheres. (B) GRA measured total pore space in comparison with the geometrically derived total pore space. (C) Bed configuration of the large and small spheres with collimator positions for the vertical profile and dynamic measurements, and (D) individual pore sizes between the spheres.

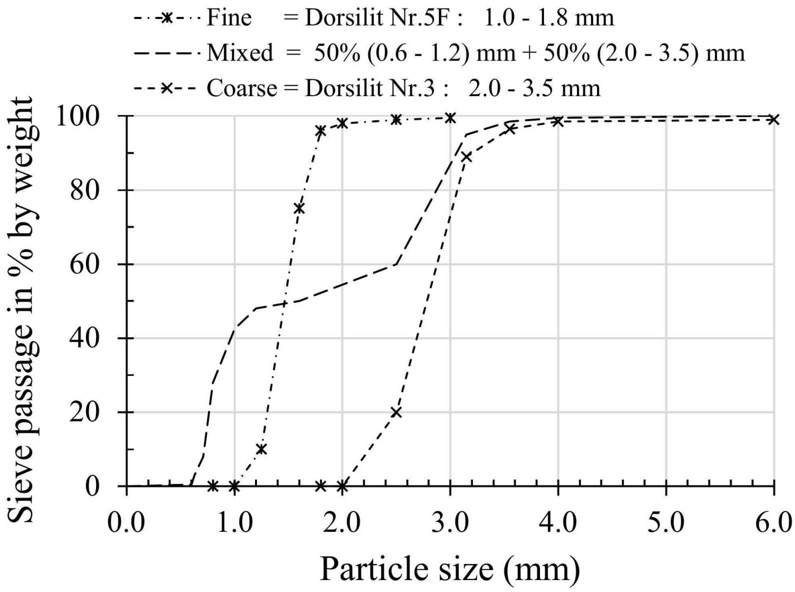

Fig. 2. Particle size distribution of supplied sediment mixtures for infiltration into the artificial bed.

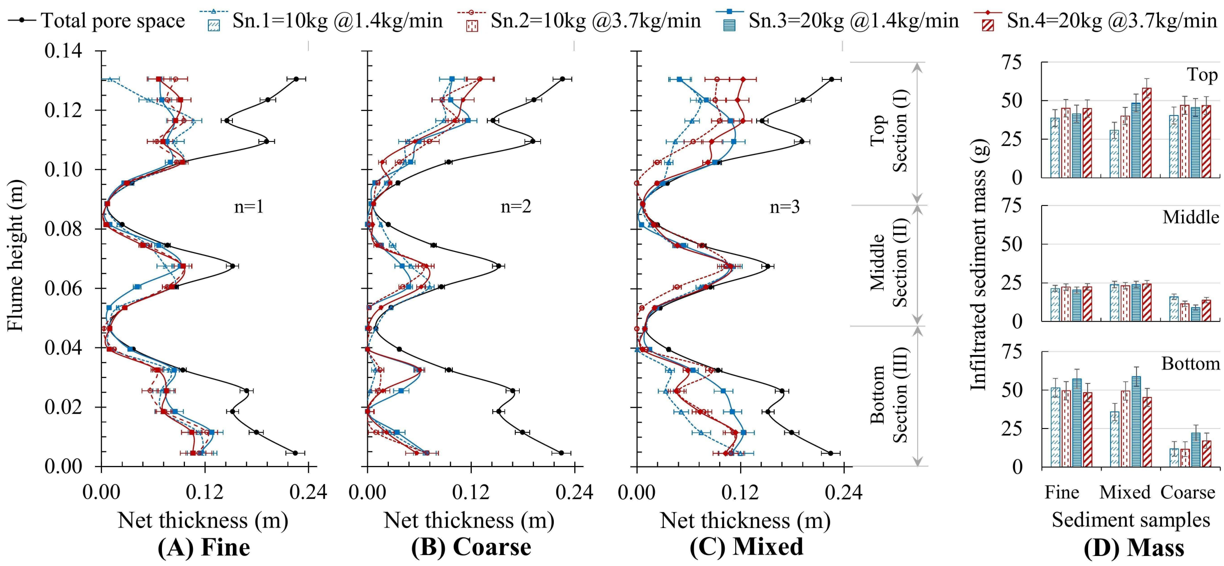

Fig. 3. Vertical distribution of infiltrated sediments, presented as sediment thicknesses, for the different boundary conditions after the end of the sediment supply (T_{Exp}) for (A) fine, (B) coarse, and (C) mixed sediment mixtures; (D) represents the integrated infiltration masses for each section (top, middle and bottom) of the vertical profile.

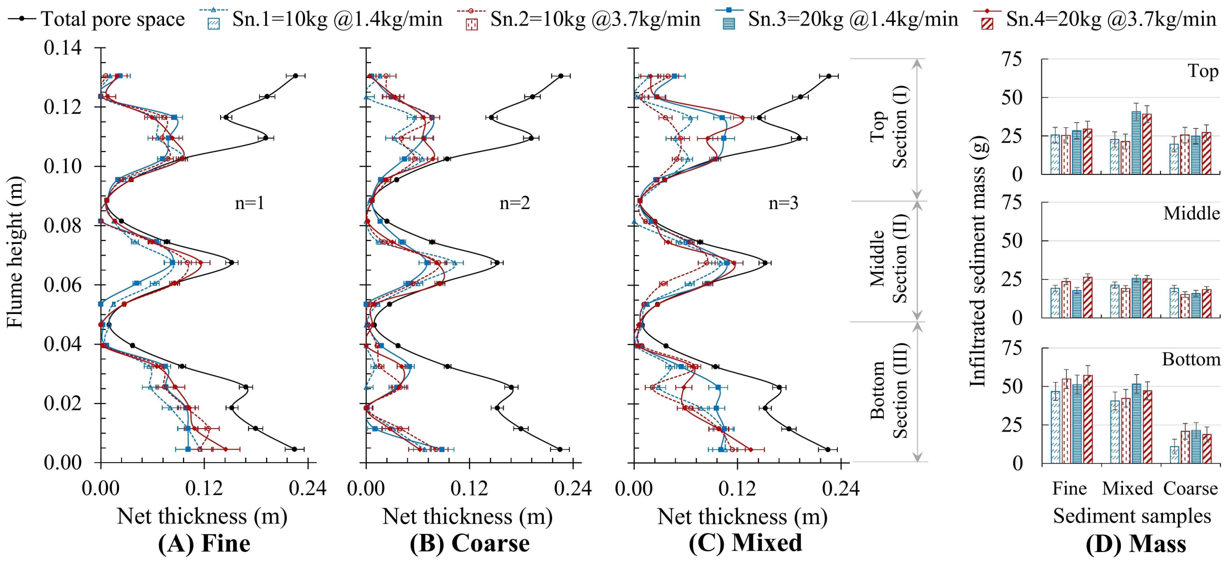

Fig. 4. Vertical distribution of infiltrated sediments, presented as sediment thicknesses, for the different boundary conditions at the end (28^{th} minute) of the experiment (T_F) for (A) fine, (B) coarse and (C) mixed sediment mixtures. (D) represents the integrated infiltration masses for each section (top, middle and bottom) of the vertical profile. A comparison of the T_{Exp} and T_F profiles for each boundary condition is available in the supplementary file (Figure S1).

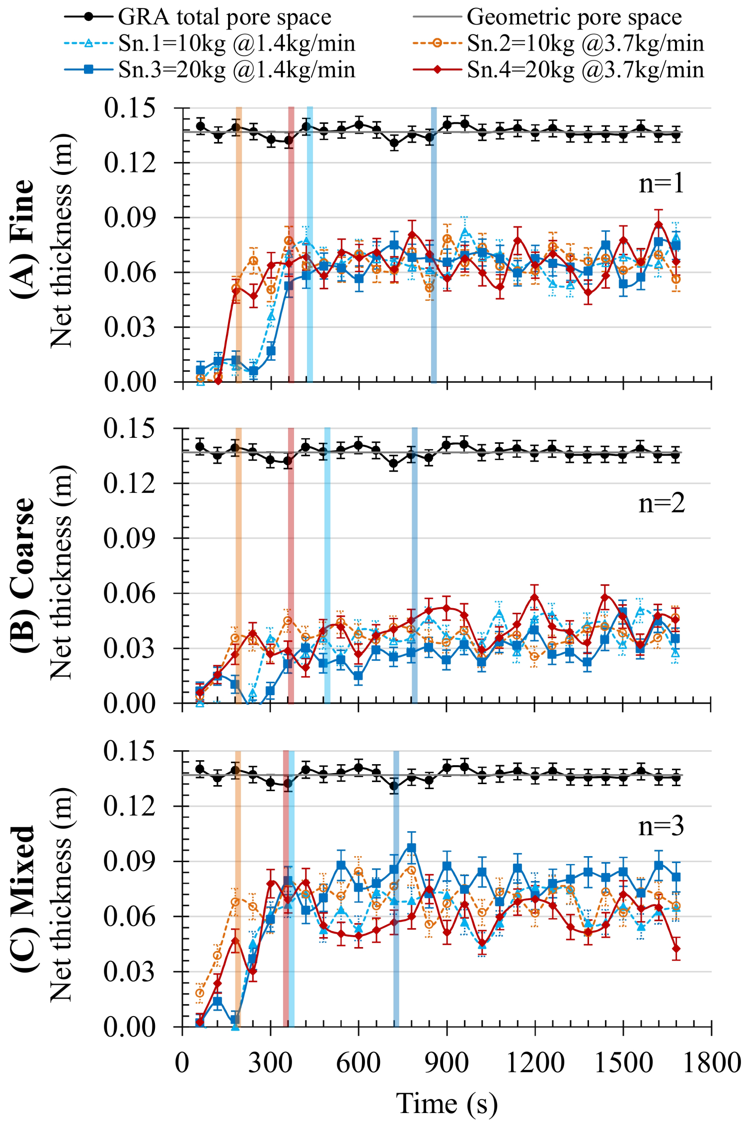

Fig. 5. Continuous one-point measurements for the three supplied sediment mixtures: (A) fine, (B) coarse, and (C) mixed, including all varied boundary conditions. The vertical lines represent the end of the sediment supply (T_{Exp}), while the end of the time-series represents T_F. Due to variations in the actual supply rate (Table 1), the vertical lines for T_{Exp} are not exactly in the same position for the experiments of the three sediment mixtures.

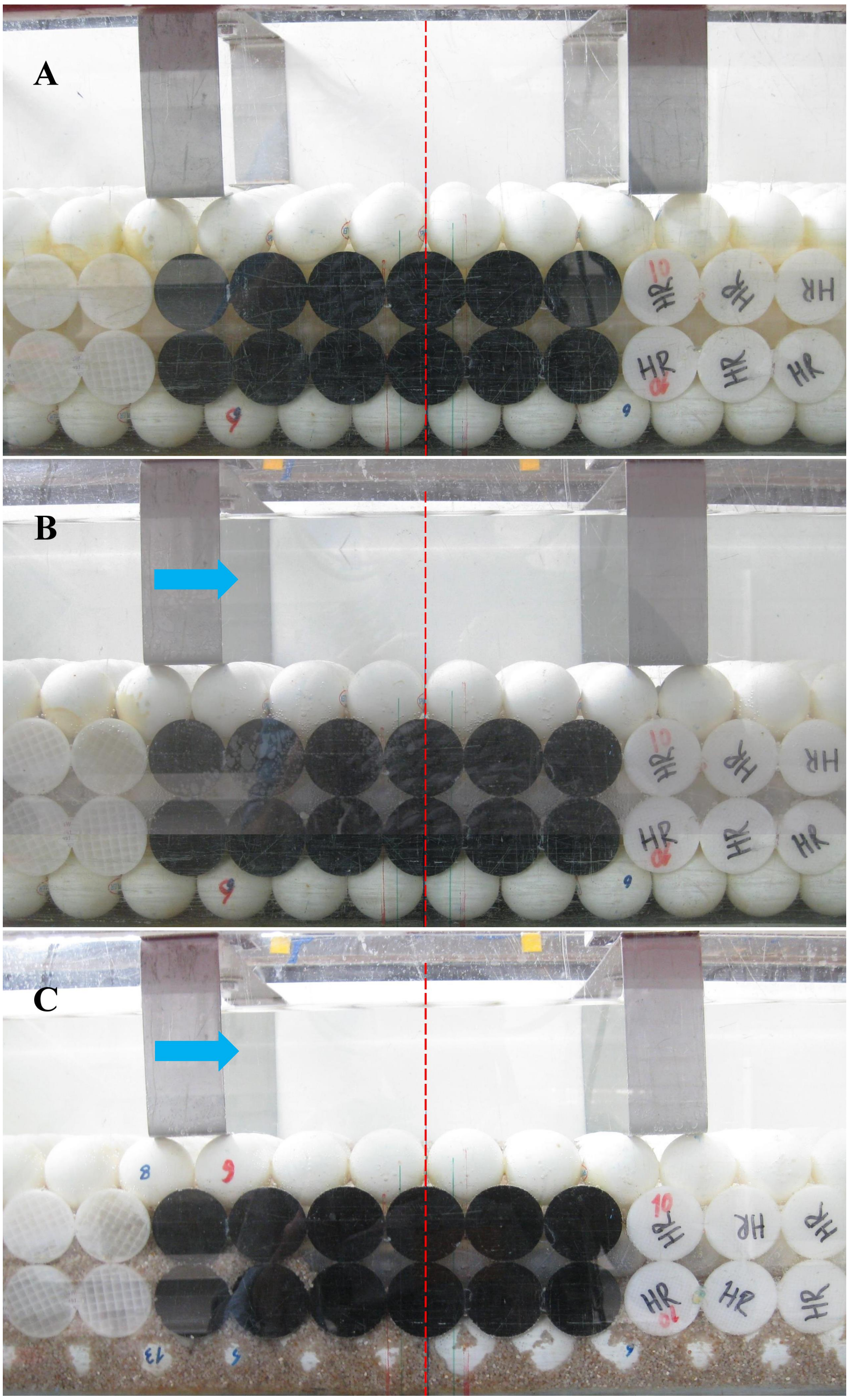

Fig. S1. Three steps of the flume experiment for measuring the infiltrated sediments using the GRA method. (A) The empty flume with bed structure (spheres) to quantify background attenuation, (B) the water-filled flume, to obtain the total pore space available for sediment infiltration, and (C) the infiltrated sediments in the bed structure, with a water layer above, to determine the amount of infiltrated sediments. The red-dashed line shows the measurement axis for the vertical profile of GRA measurements.

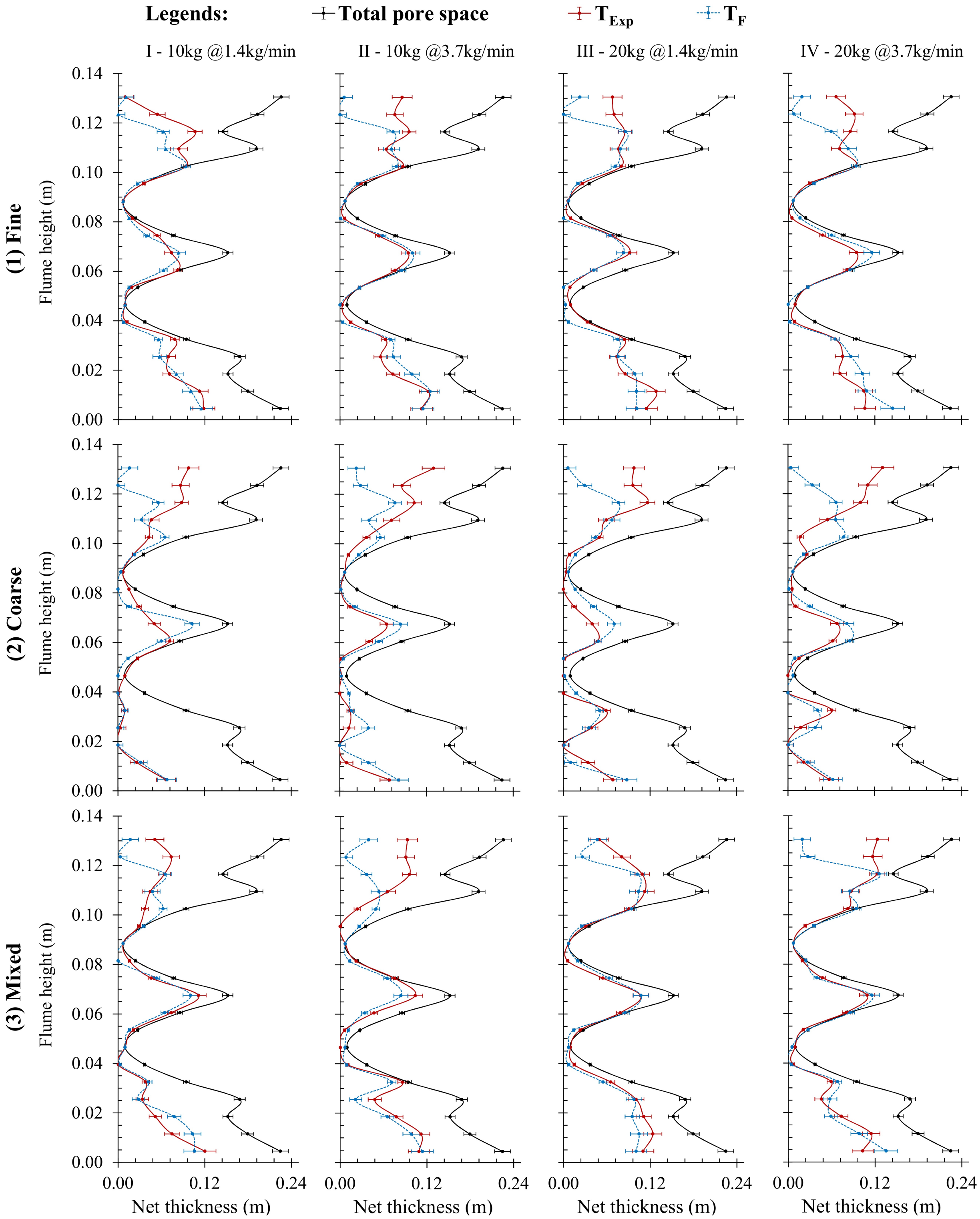

Fig. S2. The comparison of Figure 3 and Figure 4 (variation between T_{Exp} and T_F) at the infiltrated sediment vertical distributions expressed in sediment thicknesses for the four different (I - IV) boundary conditions in columns and three sediment mixtures (1 - 3) in rows.

Institut für Wasser- und Umweltsystemmodellierung Universität Stuttgart

Pfaffenwaldring 61
70569 Stuttgart (Vaihingen)
Telefon (0711) 685 - 60156
Telefax (0711) 685 - 51073
E-Mail: iws@iws.uni-stuttgart.de
http://www.iws.uni-stuttgart.de

Verzeichnis der Mitteilungshefte

1 Röhnisch, Arthur: *Die Bemühungen um eine Wasserbauliche Versuchsanstalt an der Technischen Hochschule Stuttgart*, und
Fattah Abouleid, Abdel: *Beitrag zur Berechnung einer in lockeren Sand gerammten, zweifach verankerten Spundwand*, 1963

2 Marotz, Günter: *Beitrag zur Frage der Standfestigkeit von dichten Asphaltbelägen im Großwasserbau*, 1964

3 Gurr, Siegfried: *Beitrag zur Berechnung zusammengesetzter ebener Flächentrag-werke unter besonderer Berücksichtigung ebener Stauwände, mit Hilfe von Rand-wert- und Lastwertmatrizen*, 1965

4 Plica, Peter: *Ein Beitrag zur Anwendung von Schalenkonstruktionen im Stahlwasserbau*, und
Petrikat, Kurt: *Möglichkeiten und Grenzen des wasserbaulichen Versuchswesens*, 1966

5 Plate, Erich: *Beitrag zur Bestimmung der Windgeschwindigkeitsverteilung in der durch eine Wand gestörten bodennahen Luftschicht*, und
Röhnisch, Arthur; Marotz, Günter: *Neue Baustoffe und Bauausführungen für den Schutz der Böschungen und der Sohle von Kanälen, Flüssen und Häfen; Gestehungskosten und jeweilige Vorteile*, sowie
Unny, T.E.: *Schwingungsuntersuchungen am Kegelstrahlschieber*, 1967

6 Seiler, Erich: *Die Ermittlung des Anlagenwertes der bundeseigenen Binnenschiffahrtsstraßen und Talsperren und des Anteils der Binnenschiffahrt an diesem Wert*, 1967

7 *Sonderheft anläßlich des 65. Geburtstages von Prof. Arthur Röhnisch mit Beiträgen von* Benk, Dieter; Breitling, J.; Gurr, Siegfried; Haberhauer, Robert; Honekamp, Hermann; Kuz, Klaus Dieter; Marotz, Günter; Mayer-Vorfelder, Hans-Jörg; Miller, Rudolf; Plate, Erich J.; Radomski, Helge; Schwarz, Helmut; Vollmer, Ernst; Wildenhahn, Eberhard; 1967

8 Jumikis, Alfred: *Beitrag zur experimentellen Untersuchung des Wassernachschubs in einem gefrierenden Boden und die Beurteilung der Ergebnisse*, 1968

9 Marotz, Günter: *Technische Grundlagen einer Wasserspeicherung im natürlichen Untergrund*, 1968

10 Radomski, Helge: *Untersuchungen über den Einfluß der Querschnittsform wellenförmiger Spundwände auf die statischen und rammtechnischen Eigenschaften*, 1968

11 Schwarz, Helmut: *Die Grenztragfähigkeit des Baugrundes bei Einwirkung vertikal gezogener Ankerplatten als zweidimensionales Bruchproblem*, 1969

12 Erbel, Klaus: *Ein Beitrag zur Untersuchung der Metamorphose von Mittelgebirgsschneedecken unter besonderer Berücksichtigung eines Verfahrens zur Bestimmung der thermischen Schneequalität*, 1969

13 Westhaus, Karl-Heinz: *Der Strukturwandel in der Binnenschiffahrt und sein Einfluß auf den Ausbau der Binnenschiffskanäle*, 1969

14 Mayer-Vorfelder, Hans-Jörg: *Ein Beitrag zur Berechnung des Erdwiderstandes unter Ansatz der logarithmischen Spirale als Gleitflächenfunktion*, 1970

15 Schulz, Manfred: *Berechnung des räumlichen Erddruckes auf die Wandung kreiszylindrischer Körper*, 1970

16 Mobasseri, Manoutschehr: *Die Rippenstützmauer. Konstruktion und Grenzen ihrer Standsicherheit*, 1970

17 Benk, Dieter: *Ein Beitrag zum Betrieb und zur Bemessung von Hochwasserrückhaltebecken*, 1970

18 Gàl, Attila: *Bestimmung der mitschwingenden Wassermasse bei überströmten Fischbauchklappen mit kreiszylindrischem Staublech*, 1971, *vergriffen*

19 Kuz, Klaus Dieter: *Ein Beitrag zur Frage des Einsetzens von Kavitationserscheinungen in einer Düsenströmung bei Berücksichtigung der im Wasser gelösten Gase*, 1971, *vergriffen*

20 Schaak, Hartmut: *Verteilleitungen von Wasserkraftanlagen*, 1971

21 *Sonderheft zur Eröffnung der neuen Versuchsanstalt des Instituts für Wasserbau der Universität Stuttgart mit Beiträgen von* Brombach, Hansjörg; Dirksen, Wolfram; Gàl, Attila; Gerlach, Reinhard; Giesecke, Jürgen; Holthoff, Franz-Josef; Kuz, Klaus Dieter; Marotz, Günter; Minor, Hans-Erwin; Petrikat, Kurt; Röhnisch, Arthur; Rueff, Helge; Schwarz, Helmut; Vollmer, Ernst; Wildenhahn, Eberhard; 1972

22 Wang, Chung-su: *Ein Beitrag zur Berechnung der Schwingungen an Kegelstrahlschiebern*, 1972

23 Mayer-Vorfelder, Hans-Jörg: *Erdwiderstandsbeiwerte nach dem Ohde-Variationsverfahren*, 1972

24 Minor, Hans-Erwin: *Beitrag zur Bestimmung der Schwingungsanfachungsfunktionen überströmter Stauklappen*, 1972, *vergriffen*

25 Brombach, Hansjörg: *Untersuchung strömungsmechanischer Elemente (Fluidik) und die Möglichkeit der Anwendung von Wirbelkammerelementen im Wasserbau*, 1972, *vergriffen*

26 Wildenhahn, Eberhard: *Beitrag zur Berechnung von Horizontalfilterbrunnen*, 1972

27 Steinlein, Helmut: *Die Eliminierung der Schwebstoffe aus Flußwasser zum Zweck der unterirdischen Wasserspeicherung, gezeigt am Beispiel der Iller*, 1972

28 Holthoff, Franz Josef: *Die Überwindung großer Hubhöhen in der Binnenschiffahrt durch Schwimmerhebewerke*, 1973

29 Röder, Karl: *Einwirkungen aus Baugrundbewegungen auf trog- und kastenförmige Konstruktionen des Wasser- und Tunnelbaues*, 1973

30 Kretschmer, Heinz: *Die Bemessung von Bogenstaumauern in Abhängigkeit von der Talform*, 1973

31 Honekamp, Hermann: *Beitrag zur Berechnung der Montage von Unterwasserpipelines*, 1973

32 Giesecke, Jürgen: *Die Wirbelkammertriode als neuartiges Steuerorgan im Wasserbau*, und Brombach, Hansjörg: *Entwicklung, Bauformen, Wirkungsweise und Steuereigenschaften von Wirbelkammerverstärkern*, 1974

33 Rueff, Helge: *Untersuchung der schwingungserregenden Kräfte an zwei hintereinander angeordneten Tiefschützen unter besonderer Berücksichtigung von Kavitation*, 1974

34 Röhnisch, Arthur: *Einpreßversuche mit Zementmörtel für Spannbeton - Vergleich der Ergebnisse von Modellversuchen mit Ausführungen in Hüllwellrohren*, 1975

35 *Sonderheft anläßlich des 65. Geburtstages von Prof. Dr.-Ing. Kurt Petrikat mit Beiträgen von*: Brombach, Hansjörg; Erbel, Klaus; Flinspach, Dieter; Fischer jr., Richard; Gàl, Attila; Gerlach, Reinhard; Giesecke, Jürgen; Haberhauer, Robert; Hafner Edzard; Hausenblas, Bernhard; Horlacher, Hans-Burkhard; Hutarew, Andreas; Knoll, Manfred; Krummet, Ralph; Marotz, Günter; Merkle, Theodor; Miller, Christoph; Minor, Hans-Erwin; Neumayer, Hans; Rao, Syamala; Rath, Paul; Rueff, Helge; Ruppert, Jürgen; Schwarz, Wolfgang; Topal-Gökceli, Mehmet; Vollmer, Ernst; Wang, Chung-su; Weber, Hans-Georg; 1975

36 Berger, Jochum: *Beitrag zur Berechnung des Spannungszustandes in rotationssymmetrisch belasteten Kugelschalen veränderlicher Wandstärke unter Gas- und Flüssigkeitsdruck durch Integration schwach singulärer Differentialgleichungen*, 1975

37 Dirksen, Wolfram: *Berechnung instationärer Abflußvorgänge in gestauten Gerinnen mittels Differenzenverfahren und die Anwendung auf Hochwasserrückhaltebecken*, 1976

38 Horlacher, Hans-Burkhard: *Berechnung instationärer Temperatur- und Wärmespannungsfelder in langen mehrschichtigen Hohlzylindern*, 1976

39 Hafner, Edzard: *Untersuchung der hydrodynamischen Kräfte auf Baukörper im Tiefwasserbereich des Meeres*, 1977, ISBN 3-921694-39-6

40 Ruppert, Jürgen: *Über den Axialwirbelkammerverstärker für den Einsatz im Wasserbau*, 1977, ISBN 3-921694-40-X

41 Hutarew, Andreas: *Beitrag zur Beeinflußbarkeit des Sauerstoffgehalts in Fließgewässern an Abstürzen und Wehren*, 1977, ISBN 3-921694-41-8, <u>*vergriffen*</u>

42 Miller, Christoph: *Ein Beitrag zur Bestimmung der schwingungserregenden Kräfte an unterströmten Wehren*, 1977, ISBN 3-921694-42-6

43 Schwarz, Wolfgang: *Druckstoßberechnung unter Berücksichtigung der Radial- und Längsverschiebungen der Rohrwandung*, 1978, ISBN 3-921694-43-4

44 Kinzelbach, Wolfgang: *Numerische Untersuchungen über den optimalen Einsatz variabler Kühlsysteme einer Kraftwerkskette am Beispiel Oberrhein*, 1978, ISBN 3-921694-44-2

45 Barczewski, Baldur: *Neue Meßmethoden für Wasser-Luftgemische und deren Anwendung auf zweiphasige Auftriebsstrahlen*, 1979, ISBN 3-921694-45-0

46 Neumayer, Hans: *Untersuchung der Strömungsvorgänge in radialen Wirbelkammerverstärkern*, 1979, ISBN 3-921694-46-9

47 Elalfy, Youssef-Elhassan: *Untersuchung der Strömungsvorgänge in Wirbelkammerdioden und -drosseln*, 1979, ISBN 3-921694-47-7

48 Brombach, Hansjörg: *Automatisierung der Bewirtschaftung von Wasserspeichern*, 1981, ISBN 3-921694-48-5

49 Geldner, Peter: *Deterministische und stochastische Methoden zur Bestimmung der Selbstdichtung von Gewässern*, 1981, ISBN 3-921694-49-3, <u>*vergriffen*</u>

50 Mehlhorn, Hans: *Temperaturveränderungen im Grundwasser durch Brauchwassereinleitungen*, 1982, ISBN 3-921694-50-7, <u>*vergriffen*</u>

51 Hafner, Edzard: *Rohrleitungen und Behälter im Meer*, 1983, ISBN 3-921694-51-5

52 Rinnert, Bernd: *Hydrodynamische Dispersion in porösen Medien: Einfluß von Dichteunterschieden auf die Vertikalvermischung in horizontaler Strömung*, 1983, ISBN 3-921694-52-3, <u>*vergriffen*</u>

53 Lindner, Wulf: *Steuerung von Grundwasserentnahmen unter Einhaltung ökologischer Kriterien*, 1983, ISBN 3-921694-53-1, <u>*vergriffen*</u>

54 Herr, Michael; Herzer, Jörg; Kinzelbach, Wolfgang; Kobus, Helmut; Rinnert, Bernd: *Methoden zur rechnerischen Erfassung und hydraulischen Sanierung von Grundwasserkontaminationen*, 1983, ISBN 3-921694-54-X

55 Schmitt, Paul: *Wege zur Automatisierung der Niederschlagsermittlung*, 1984, ISBN 3-921694-55-8, <u>*vergriffen*</u>

56 Müller, Peter: *Transport und selektive Sedimentation von Schwebstoffen bei gestautem Abfluß*, 1985, ISBN 3-921694-56-6

57 El-Qawasmeh, Fuad: *Möglichkeiten und Grenzen der Tropfbewässerung unter besonderer Berücksichtigung der Verstopfungsanfälligkeit der Tropfelemente*, 1985, ISBN 3-921694-57-4, <u>*vergriffen*</u>

58 Kirchenbaur, Klaus: *Mikroprozessorgesteuerte Erfassung instationärer Druckfelder am Beispiel seegangsbelasteter Baukörper*, 1985, ISBN 3-921694-58-2

59 Kobus, Helmut (Hrsg.): *Modellierung des großräumigen Wärme- und Schadstofftransports im Grundwasser*, Tätigkeitsbericht 1984/85 (DFG-Forschergruppe an den Universitäten Hohenheim, Karlsruhe und Stuttgart), 1985, ISBN 3-921694-59-0, <u>*vergriffen*</u>

60 Spitz, Karlheinz: *Dispersion in porösen Medien: Einfluß von Inhomogenitäten und Dichteunterschieden*, 1985, ISBN 3-921694-60-4, <u>*vergriffen*</u>

61 Kobus, Helmut: *An Introduction to Air-Water Flows in Hydraulics*, 1985, ISBN 3-921694-61-2

62 Kaleris, Vassilios: *Erfassung des Austausches von Oberflächen- und Grundwasser in horizontalebenen Grundwassermodellen*, 1986, ISBN 3-921694-62-0

63 Herr, Michael: *Grundlagen der hydraulischen Sanierung verunreinigter Porengrundwasserleiter*, 1987, ISBN 3-921694-63-9

64 Marx, Walter: *Berechnung von Temperatur und Spannung in Massenbeton infolge Hydratation*, 1987, ISBN 3-921694-64-7

65 Koschitzky, Hans-Peter: *Dimensionierungskonzept für Sohlbelüfter in Schußrinnen zur Vermeidung von Kavitationsschäden*, 1987, ISBN 3-921694-65-5

66 Kobus, Helmut (Hrsg.): *Modellierung des großräumigen Wärme- und Schadstofftransports im Grundwasser*, Tätigkeitsbericht 1986/87 (DFG-Forschergruppe an den Universitäten Hohenheim, Karlsruhe und Stuttgart) 1987, ISBN 3-921694-66-3

67 Söll, Thomas: *Berechnungsverfahren zur Abschätzung anthropogener Temperaturanomalien im Grundwasser*, 1988, ISBN 3-921694-67-1

68 Dittrich, Andreas; Westrich, Bernd: *Bodenseeufererosion, Bestandsaufnahme und Bewertung*, 1988, ISBN 3-921694-68-X, <u>*vergriffen*</u>

69 Huwe, Bernd; van der Ploeg, Rienk R.: *Modelle zur Simulation des Stickstoffhaushaltes von Standorten mit unterschiedlicher landwirtschaftlicher Nutzung*, 1988, ISBN 3-921694-69-8, <u>*vergriffen*</u>

70 Stephan, Karl: *Integration elliptischer Funktionen*, 1988, ISBN 3-921694-70-1

71 Kobus, Helmut; Zilliox, Lothaire (Hrsg.): *Nitratbelastung des Grundwassers, Auswirkungen der Landwirtschaft auf die Grundwasser- und Rohwasserbeschaffenheit und Maßnahmen zum Schutz des Grundwassers*. Vorträge des deutsch-französischen Kolloquiums am 6. Oktober 1988, Universitäten Stuttgart und Louis Pasteur Strasbourg (Vorträge in deutsch oder französisch, Kurzfassungen zweisprachig), 1988, ISBN 3-921694-71-X

72 Soyeaux, Renald: *Unterströmung von Stauanlagen auf klüftigem Untergrund unter Berücksichtigung laminarer und turbulenter Fließzustände*,1991, ISBN 3-921694-72-8

73 Kohane, Roberto: *Berechnungsmethoden für Hochwasserabfluß in Fließgewässern mit übeströmten Vorländern*, 1991, ISBN 3-921694-73-6

74 Hassinger, Reinhard: *Beitrag zur Hydraulik und Bemessung von Blocksteinrampen in flexibler Bauweise*, 1991, ISBN 3-921694-74-4, vergriffen

75 Schäfer, Gerhard: *Einfluß von Schichtenstrukturen und lokalen Einlagerungen auf die Längsdispersion in Porengrundwasserleitern*, 1991, ISBN 3-921694-75-2

76 Giesecke, Jürgen: *Vorträge, Wasserwirtschaft in stark besiedelten Regionen; Umweltforschung mit Schwerpunkt Wasserwirtschaft*, 1991, ISBN 3-921694-76-0

77 Huwe, Bernd: *Deterministische und stochastische Ansätze zur Modellierung des Stickstoffhaushalts landwirtschaftlich genutzter Flächen auf unterschiedlichem Skalenniveau*, 1992, ISBN 3-921694-77-9, vergriffen

78 Rommel, Michael: *Verwendung von Kluftdaten zur realitätsnahen Generierung von Kluftnetzen mit anschließender laminar-turbulenter Strömungsberechnung*, 1993, ISBN 3-92 1694-78-7

79 Marschall, Paul: *Die Ermittlung lokaler Stofffrachten im Grundwasser mit Hilfe von Einbohrloch-Meßverfahren*, 1993, ISBN 3-921694-79-5, vergriffen

80 Ptak, Thomas: *Stofftransport in heterogenen Porenaquiferen: Felduntersuchungen und stochastische Modellierung*, 1993, ISBN 3-921694-80-9, vergriffen

81 Haakh, Frieder: *Transientes Strömungsverhalten in Wirbelkammern,* 1993, ISBN 3-921694-81-7

82 Kobus, Helmut; Cirpka, Olaf; Barczewski, Baldur; Koschitzky, Hans-Peter: *Versuchseinrichtung zur Grundwasser- und Altlastensanierung VEGAS, Konzeption und Programmrahmen*, 1993, ISBN 3-921694-82-5

83 Zang, Weidong: *Optimaler Echtzeit-Betrieb eines Speichers mit aktueller Abflußregenerierung*, 1994, ISBN 3-921694-83-3, vergriffen

84 Franke, Hans-Jörg: *Stochastische Modellierung eines flächenhaften Stoffeintrages und Transports in Grundwasser am Beispiel der Pflanzenschutzmittelproblematik*, 1995, ISBN 3-921694-84-1

85 Lang, Ulrich: *Simulation regionaler Strömungs- und Transportvorgänge in Karstaquiferen mit Hilfe des Doppelkontinuum-Ansatzes: Methodenentwicklung und Parameteridentifikation*, 1995, ISBN 3-921694-85-X, vergriffen

86 Helmig, Rainer: *Einführung in die Numerischen Methoden der Hydromechanik*, 1996, ISBN 3-921694-86-8, vergriffen

87 Cirpka, Olaf: *CONTRACT: A Numerical Tool for Contaminant Transport and Chemical Transformations - Theory and Program Documentation -*, 1996, ISBN 3-921694-87-6

88 Haberlandt, Uwe: *Stochastische Synthese und Regionalisierung des Niederschlages für Schmutzfrachtberechnungen*, 1996, ISBN 3-921694-88-4

89 Croisé, Jean: *Extraktion von flüchtigen Chemikalien aus natürlichen Lockergesteinen mittels erzwungener Luftströmung*, 1996, ISBN 3-921694-89-2, vergriffen

90 Jorde, Klaus: *Ökologisch begründete, dynamische Mindestwasserregelungen bei Ausleitungskraftwerken*, 1997, ISBN 3-921694-90-6, vergriffen

91 Helmig, Rainer: *Gekoppelte Strömungs- und Transportprozesse im Untergrund - Ein Beitrag zur Hydrosystemmodellierung-*, 1998, ISBN 3-921694-91-4, vergriffen

92 Emmert, Martin: *Numerische Modellierung nichtisothermer Gas-Wasser Systeme in porösen Medien,* 1997, ISBN 3-921694-92-2

93 Kern, Ulrich: *Transport von Schweb- und Schadstoffen in staugeregelten Fließgewässern am Beispiel des Neckars*, 1997, ISBN 3-921694-93-0, vergriffen

94 Förster, Georg: *Druckstoßdämpfung durch große Luftblasen in Hochpunkten von Rohrleitungen 1997*, ISBN 3-921694-94-9

95 Cirpka, Olaf: *Numerische Methoden zur Simulation des reaktiven Mehrkomponententransports im Grundwasser*, 1997, ISBN 3-921694-95-7, vergriffen

96 Färber, Arne: *Wärmetransport in der ungesättigten Bodenzone: Entwicklung einer thermischen In-situ-Sanierungstechnologie*, 1997, ISBN 3-921694-96-5

97 Betz, Christoph: *Wasserdampfdestillation von Schadstoffen im porösen Medium: Entwicklung einer thermischen In-situ-Sanierungstechnologie*, 1998, SBN 3-921694-97-3

98 Xu, Yichun: *Numerical Modeling of Suspended Sediment Transport in Rivers*, 1998, ISBN 3-921694-98-1, vergriffen

99 Wüst, Wolfgang: *Geochemische Untersuchungen zur Sanierung CKW-kontaminierter Aquifere mit Fe(0)-Reaktionswänden,* 2000, ISBN 3-933761-02-2

100 Sheta, Hussam: *Simulation von Mehrphasenvorgängen in porösen Medien unter Einbeziehung von Hysterese-Effekten*, 2000, ISBN 3-933761-03-4

101 Ayros, Edwin: *Regionalisierung extremer Abflüsse auf der Grundlage statistischer Verfahren*, 2000, ISBN 3-933761-04-2, vergriffen

102 Huber, Ralf: *Compositional Multiphase Flow and Transport in Heterogeneous Porous Media*, 2000, ISBN 3-933761-05-0

103 Braun, Christopherus: *Ein Upscaling-Verfahren für Mehrphasenströmungen in porösen Medien*, 2000, ISBN 3-933761-06-9

104 Hofmann, Bernd: *Entwicklung eines rechnergestützten Managementsystems zur Beurteilung von Grundwasserschadensfällen*, 2000, ISBN 3-933761-07-7

105 Class, Holger: *Theorie und numerische Modellierung nichtisothermer Mehrphasenprozesse in NAPL-kontaminierten porösen Medien,* 2001, ISBN 3-933761-08-5

106 Schmidt, Reinhard: *Wasserdampf- und Heißluftinjektion zur thermischen Sanierung kontaminierter Standorte*, 2001, ISBN 3-933761-09-3

107 Josef, Reinhold: *Schadstoffextraktion mit hydraulischen Sanierungsverfahren unter Anwendung von grenzflächenaktiven Stoffen*, 2001, ISBN 3-933761-10-7

108 Schneider, Matthias: *Habitat- und Abflussmodellierung für Fließgewässer mit unscharfen Berechnungsansätzen*, 2001, ISBN 3-933761-11-5

109 Rathgeb, Andreas: *Hydrodynamische Bemessungsgrundlagen für Lockerdeckwerke an überströmbaren Erddämmen*, 2001, ISBN 3-933761-12-3

110 Lang, Stefan: *Parallele numerische Simulation instätionärer Probleme mit adaptiven Methoden auf unstrukturierten Gittern*, 2001, ISBN 3-933761-13-1

111 Appt, Jochen; Stumpp Simone: *Die Bodensee-Messkampagne 2001, IWS/CWR Lake Constance Measurement Program 2001*, 2002, ISBN 3-933761-14-X

112 Heimerl, Stephan: *Systematische Beurteilung von Wasserkraftprojekten,* 2002, ISBN 3-933761-15-8, vergriffen

113 Iqbal, Amin: *On the Management and Salinity Control of Drip Irrigation,* 2002, ISBN 3-933761-16-6

114 Silberhorn-Hemminger, Annette: *Modellierung von Kluftaquifersystemen: Geostatistische Analyse und deterministisch-stochastische Kluftgenerierung,* 2002, ISBN 3-933761-17-4

115 Winkler, Angela: *Prozesse des Wärme- und Stofftransports bei der In-situ-Sanierung mit festen Wärmequellen,* 2003, ISBN 3-933761-18-2

116 Marx, Walter: *Wasserkraft, Bewässerung, Umwelt - Planungs- und Bewertungsschwerpunkte der Wasserbewirtschaftung,* 2003, ISBN 3-933761-19-0

117 Hinkelmann, Reinhard: *Efficient Numerical Methods and Information-Processing Techniques in Environment Water,* 2003, ISBN 3-933761-20-4

118 Samaniego-Eguiguren, Luis Eduardo: *Hydrological Consequences of Land Use / Land Cover and Climatic Changes in Mesoscale Catchments*, 2003, ISBN 3-933761-21-2

119 Neunhäuserer, Lina: *Diskretisierungsansätze zur Modellierung von Strömungs- und Transportprozessen in geklüftet-porösen Medien*, 2003, ISBN 3-933761-22-0

120 Paul, Maren: *Simulation of Two-Phase Flow in Heterogeneous Poros Media with Adaptive Methods*, 2003, ISBN 3-933761-23-9

121 Ehret, Uwe: *Rainfall and Flood Nowcasting in Small Catchments using Weather Radar*, 2003, ISBN 3-933761-24-7

122 Haag, Ingo: *Der Sauerstoffhaushalt staugeregelter Flüsse am Beispiel des Neckars - Analysen, Experimente, Simulationen -,* 2003, ISBN 3-933761-25-5

123 Appt, Jochen: *Analysis of Basin-Scale Internal Waves in Upper Lake Constance,* 2003, ISBN 3-933761-26-3

124 Hrsg.: Schrenk, Volker; Batereau, Katrin; Barczewski, Baldur; Weber, Karolin und Koschitzky, Hans-Peter: *Symposium Ressource Fläche und VEGAS - Statuskolloquium 2003, 30. September und 1. Oktober 2003,* 2003, ISBN 3-933761-27-1

125 Omar Khalil Ouda: *Optimisation of Agricultural Water Use: A Decision Support System for the Gaza Strip,* 2003, ISBN 3-933761-28-0

126 Batereau, Katrin: *Sensorbasierte Bodenluftmessung zur Vor-Ort-Erkundung von Schadensherden im Untergrund*, 2004, ISBN 3-933761-29-8

127 Witt, Oliver: *Erosionsstabilität von Gewässersedimenten mit Auswirkung auf den Stofftransport bei Hochwasser am Beispiel ausgewählter Stauhaltungen des Oberrheins*, 2004, ISBN 3-933761-30-1

128 Jakobs, Hartmut: *Simulation nicht-isothermer Gas-Wasser-Prozesse in komplexen Kluft-Matrix-Systemen*, 2004, ISBN 3-933761-31-X

129 Li, Chen-Chien: *Deterministisch-stochastisches Berechnungskonzept zur Beurteilung der Auswirkungen erosiver Hochwasserereignisse in Flussstauhaltungen,* 2004, ISBN 3-933761-32-8

130 Reichenberger, Volker; Helmig, Rainer; Jakobs, Hartmut; Bastian, Peter; Niessner, Jennifer: *Complex Gas-Water Processes in Discrete Fracture-Matrix Systems: Up-scaling, Mass-Conservative Discretization and Efficient Multilevel Solution,* 2004, ISBN 3-933761-33-6

131 Hrsg.: Barczewski, Baldur; Koschitzky, Hans-Peter; Weber, Karolin; Wege, Ralf: *VEGAS - Statuskolloquium 2004,* Tagungsband zur Veranstaltung am 05. Oktober 2004 an der Universität Stuttgart, Campus Stuttgart-Vaihingen, 2004, ISBN 3-933761-34-4

132 Asie, Kemal Jabir: *Finite Volume Models for Multiphase Multicomponent Flow through Porous Media*. 2005, ISBN 3-933761-35-2

133 Jacoub, George: *Development of a 2-D Numerical Module for Particulate Contaminant Transport in Flood Retention Reservoirs and Impounded Rivers,* 2004, ISBN 3-933761-36-0

134 Nowak, Wolfgang: *Geostatistical Methods for the Identification of Flow and Transport Parameters in the Subsurface,* 2005, ISBN 3-933761-37-9

135 Süß, Mia: *Analysis of the influence of structures and boundaries on flow and transport processes in fractured porous media*, 2005, ISBN 3-933761-38-7

136 Jose, Surabhin Chackiath: *Experimental Investigations on Longitudinal Dispersive Mixing in Heterogeneous Aquifers,* 2005, ISBN: 3-933761-39-5

137 Filiz, Fulya: *Linking Large-Scale Meteorological Conditions to Floods in Mesoscale Catchments,* 2005, ISBN 3-933761-40-9

138 Qin, Minghao: *Wirklichkeitsnahe und recheneffiziente Ermittlung von Temperatur und Spannungen bei großen RCC-Staumauern*, 2005, ISBN 3-933761-41-7

139 Kobayashi, Kenichiro: *Optimization Methods for Multiphase Systems in the Subsurface - Application to Methane Migration in Coal Mining Areas*, 2005, ISBN 3-933761-42-5

140 Rahman, Md. Arifur: *Experimental Investigations on Transverse Dispersive Mixing in Heterogeneous Porous Media,* 2005, ISBN 3-933761-43-3

141 Schrenk, Volker: *Ökobilanzen zur Bewertung von Altlastensanierungsmaßnahmen,* 2005, ISBN 3-933761-44-1

142 Hundecha, Hirpa Yeshewatesfa: *Regionalization of Parameters of a Conceptual Rainfall-Runoff Model*, 2005, ISBN: 3-933761-45-X

143 Wege, Ralf: *Untersuchungs- und Überwachungsmethoden für die Beurteilung natürlicher Selbstreinigungsprozesse im Grundwasser,* 2005, ISBN 3-933761-46-8

144 Breiting, Thomas: *Techniken und Methoden der Hydroinformatik - Modellierung von komplexen Hydrosystemen im Untergrund*, 2006, ISBN 3-933761-47-6

145 Hrsg.: Braun, Jürgen; Koschitzky, Hans-Peter; Müller, Martin: *Ressource Untergrund: 10 Jahre VEGAS: Forschung und Technologieentwicklung zum Schutz von Grundwasser und Boden,* Tagungsband zur Veranstaltung am 28. und 29. September 2005 an der Universität Stuttgart, Campus Stuttgart-Vaihingen, 2005, ISBN 3-933761-48-4

146 Rojanschi, Vlad: *Abflusskonzentration in mesoskaligen Einzugsgebieten unter Berücksichtigung des Sickerraumes,* 2006, ISBN 3-933761-49-2

147 Winkler, Nina Simone: *Optimierung der Steuerung von Hochwasserrückhaltebecken-systemen,* 2006, ISBN 3-933761-50-6

148 Wolf, Jens: *Räumlich differenzierte Modellierung der Grundwasserströmung alluvialer Aquifere für mesoskalige Einzugsgebiete*, 2006, ISBN: 3-933761-51-4

149 Kohler, Beate: *Externe Effekte der Laufwasserkraftnutzung*, 2006, ISBN 3-933761-52-2

150 Hrsg.: Braun, Jürgen; Koschitzky, Hans-Peter; Stuhrmann, Matthias: *VEGAS-Statuskolloquium 2006,* Tagungsband zur Veranstaltung am 28. September 2006 an der Universität Stuttgart, Campus Stuttgart-Vaihingen, 2006, ISBN 3-933761-53-0

151 Niessner, Jennifer: *Multi-Scale Modeling of Multi-Phase - Multi-Component Processes in Heterogeneous Porous Media*, 2006, ISBN 3-933761-54-9

152 Fischer, Markus: *Beanspruchung eingeerdeter Rohrleitungen infolge Austrocknung bindiger Böden,* 2006, ISBN 3-933761-55-7

153 Schneck, Alexander: *Optimierung der Grundwasserbewirtschaftung unter Berücksichtigung der Belange der Wasserversorgung, der Landwirtschaft und des Naturschutzes*, 2006, ISBN 3-933761-56-5

154 Das, Tapash: *The Impact of Spatial Variability of Precipitation on the Predictive Uncertainty of Hydrological Models,* 2006, ISBN 3-33761-57-3

155 Bielinski, Andreas: *Numerical Simulation of CO_2 sequestration in geological formations*, 2007, ISBN 3-933761-58-1

156 Mödinger, Jens: *Entwicklung eines Bewertungs- und Entscheidungsunterstützungs-systems für eine nachhaltige regionale Grundwasserbewirtschaftung*, 2006, ISBN 3-933761-60-3

157 Manthey, Sabine: *Two-phase flow processes with dynamic effects in porous media - parameter estimation and simulation,* 2007, ISBN 3-933761-61-1

158 Pozos Estrada, Oscar: *Investigation on the Effects of Entrained Air in Pipelines,* 2007, ISBN 3-933761-62-X

159 Ochs, Steffen Oliver: *Steam injection into saturated porous media – process analysis including experimental and numerical investigations*, 2007, ISBN 3-933761-63-8

160 Marx, Andreas: *Einsatz gekoppelter Modelle und Wetterradar zur Abschätzung von Niederschlagsintensitäten und zur Abflussvorhersage, 2007,* ISBN 3-933761-64-6

161 Hartmann, Gabriele Maria: *Investigation of Evapotranspiration Concepts in Hydrological Modelling for Climate Change Impact Assessment*, 2007, ISBN 3-933761-65-4

162 Kebede Gurmessa, Tesfaye: *Numerical Investigation on Flow and Transport Characteristics to Improve Long-Term Simulation of Reservoir Sedimentation*, 2007, ISBN 3-933761-66-2

163 Trifković, Aleksandar: *Multi-objective and Risk-based Modelling Methodology for Planning, Design and Operation of Water Supply Systems*, 2007, ISBN 3-933761-67-0

164 Götzinger, Jens: *Distributed Conceptual Hydrological Modelling - Simulation of Climate, Land Use Change Impact and Uncertainty Analysis*, 2007, ISBN 3-933761-68-9

165 Hrsg.: Braun, Jürgen; Koschitzky, Hans-Peter; Stuhrmann, Matthias: *VEGAS – Kolloquium 2007,* Tagungsband zur Veranstaltung am 26. September 2007 an der Universität Stuttgart, Campus Stuttgart-Vaihingen, 2007, ISBN 3-933761-69-7

166 Freeman, Beau: *Modernization Criteria Assessment for Water Resources Planning; Klamath Irrigation Project, U.S.*, 2008, ISBN 3-933761-70-0

167 Dreher, Thomas: *Selektive Sedimentation von Feinstschwebstoffen in Wechselwirkung mit wandnahen turbulenten Strömungsbedingungen*, 2008, ISBN 3-933761-71-9

168 Yang, Wei: *Discrete-Continuous Downscaling Model for Generating Daily Precipitation Time Series*, 2008, ISBN 3-933761-72-7

169 Kopecki, Ianina: *Calculational Approach to FST-Hemispheres for Multiparametrical Benthos Habitat Modelling,* 2008, ISBN 3-933761-73-5

170 Brommundt, Jürgen: *Stochastische Generierung räumlich zusammenhängender Niederschlagszeitreihen*, 2008, ISBN 3-933761-74-3

171 Papafotiou, *Alexandros: Numerical Investigations of the Role of Hysteresis in Heterogeneous Two-Phase Flow Systems*, 2008, ISBN 3-933761-75-1

172 He, Yi: *Application of a Non-Parametric Classification Scheme to Catchment Hydrology*, 2008, ISBN 978-3-933761-76-7

173 Wagner, Sven: *Water Balance in a Poorly Gauged Basin in West Africa Using Atmospheric Modelling and Remote Sensing Information*, 2008, ISBN 978-3-933761-77-4

174 Hrsg.: Braun, Jürgen; Koschitzky, Hans-Peter; Stuhrmann, Matthias; Schrenk, Volker: *VEGAS-Kolloquium 2008 Ressource Fläche III*, Tagungsband zur Veranstaltung am 01. Oktober 2008 an der Universität Stuttgart, Campus Stuttgart-Vaihingen, 2008, ISBN 978-3-933761-78-1

175 Patil, Sachin: *Regionalization of an Event Based Nash Cascade Model for Flood Predictions in Ungauged Basins*, 2008, ISBN 978-3-933761-79-8

176 Assteerawatt, Anongnart: *Flow and Transport Modelling of Fractured Aquifers based on a Geostatistical Approach,* 2008, ISBN 978-3-933761-80-4

177 Karnahl, Joachim Alexander: *2D numerische Modellierung von multifraktionalem Schwebstoff- und Schadstofftransport in Flüssen*, 2008, ISBN 978-3-933761-81-1

178 Hiester, Uwe: *Technologieentwicklung zur In-situ-Sanierung der ungesättigten Bodenzone mit festen Wärmequellen,* 2009, ISBN 978-3-933761-82-8

179 Laux, Patrick: *Statistical Modeling of Precipitation for Agricultural Planning in the Volta Basin of West Africa,* 2009, ISBN 978-3-933761-83-5

180 Ehsan, Saqib: *Evaluation of Life Safety Risks Related to Severe Flooding,* 2009, ISBN 978-3-933761-84-2

181 Prohaska, Sandra: *Development and Application of a 1D Multi-Strip Fine Sediment Transport Model for Regulated Rivers,* 2009, ISBN 978-3-933761-85-9

182 Kopp, Andreas: *Evaluation of CO_2 Injection Processes in Geological Formations for Site Screening,* 2009, ISBN 978-3-933761-86-6

183 Ebigbo, Anozie: *Modelling of biofilm growth and its influence on CO_2 and water (two-phase) flow in porous media,* 2009, ISBN 978-3-933761-87-3

184 Freiboth, Sandra: *A phenomenological model for the numerical simulation of multiphase multicomponent processes considering structural alterations of porous media*, 2009, ISBN 978-3-933761-88-0

185 Zöllner, Frank: *Implementierung und Anwendung netzfreier Methoden im Konstruktiven Wasserbau und in der Hydromechanik*, 2009, ISBN 978-3-933761-89-7

186 Vasin, Milos: *Influence of the soil structure and property contrast on flow and transport in the unsaturated zone*, 2010, ISBN 978-3-933761-90-3

187 Li, Jing: *Application of Copulas as a New Geostatistical Tool*, 2010, ISBN 978-3-933761-91-0

188 AghaKouchak, Amir: *Simulation of Remotely Sensed Rainfall Fields Using Copulas*, 2010, ISBN 978-3-933761-92-7

189 Thapa, Pawan Kumar: *Physically-based spatially distributed rainfall runoff modelling for soil erosion estimation*, 2010, ISBN 978-3-933761-93-4

190 Wurms, Sven: *Numerische Modellierung der Sedimentationsprozesse in Retentionsanlagen zur Steuerung von Stoffströmen bei extremen Hochwasserabflussereignissen*, 2011, ISBN 978-3-933761-94-1

191 Merkel, Uwe: *Unsicherheitsanalyse hydraulischer Einwirkungen auf Hochwasserschutzdeiche und Steigerung der Leistungsfähigkeit durch adaptive Strömungsmodellierung*, 2011, ISBN 978-3-933761-95-8

192 Fritz, Jochen: *A Decoupled Model for Compositional Non-Isothermal Multiphase Flow in Porous Media and Multiphysics Approaches for Two-Phase Flow*, 2010, ISBN 978-3-933761-96-5

193 Weber, Karolin (Hrsg.): *12. Treffen junger WissenschaftlerInnen an Wasserbauinstituten*, 2010, ISBN 978-3-933761-97-2

194 Bliefernicht, Jan-Geert: *Probability Forecasts of Daily Areal Precipitation for Small River Basins,* 2011, ISBN 978-3-933761-98-9

195 Hrsg.: Koschitzky, Hans-Peter; Braun, Jürgen: *VEGAS-Kolloquium 2010 In-situ-Sanierung - Stand und Entwicklung Nano und ISCO -,* Tagungsband zur Veranstaltung am 07. Oktober 2010 an der Universität Stuttgart, Campus Stuttgart-Vaihingen, 2010, ISBN 978-3-933761-99-6

196 Gafurov, Abror: *Water Balance Modeling Using Remote Sensing Information - Focus on Central Asia,* 2010, ISBN 978-3-942036-00-9

197 Mackenberg, Sylvia: *Die Quellstärke in der Sickerwasserprognose: Möglichkeiten und Grenzen von Labor- und Freilanduntersuchungen,* 2010, ISBN 978-3-942036-01-6

198 Singh, Shailesh Kumar: *Robust Parameter Estimation in Gauged and Ungauged Basins,* 2010, ISBN 978-3-942036-02-3

199 Doğan, Mehmet Onur: *Coupling of porous media flow with pipe flow,* 2011, ISBN 978-3-942036-03-0

200 Liu, Min: *Study of Topographic Effects on Hydrological Patterns and the Implication on Hydrological Modeling and Data Interpolation,* 2011, ISBN 978-3-942036-04-7

201 Geleta, Habtamu Itefa: *Watershed Sediment Yield Modeling for Data Scarce Areas,* 2011, ISBN 978-3-942036-05-4

202 Franke, Jörg: *Einfluss der Überwachung auf die Versagenswahrscheinlichkeit von Staustufen,* 2011, ISBN 978-3-942036-06-1

203 Bakimchandra, Oinam: *Integrated Fuzzy-GIS approach for assessing regional soil erosion risks,* 2011, ISBN 978-3-942036-07-8

204 Alam, Muhammad Mahboob: *Statistical Downscaling of Extremes of Precipitation in Mesoscale Catchments from Different RCMs and Their Effects on Local Hydrology,* 2011, ISBN 978-3-942036-08-5

205 Hrsg.: Koschitzky, Hans-Peter; Braun, Jürgen: *VEGAS-Kolloquium 2011 Flache Geothermie - Perspektiven und Risiken,* Tagungsband zur Veranstaltung am 06. Oktober 2011 an der Universität Stuttgart, Campus Stuttgart-Vaihingen, 2011, ISBN 978-3-933761-09-2

206 Haslauer, Claus: *Analysis of Real-World Spatial Dependence of Subsurface Hydraulic Properties Using Copulas with a Focus on Solute Transport Behaviour,* 2011, ISBN 978-3-942036-10-8

207 Dung, Nguyen Viet: *Multi-objective automatic calibration of hydrodynamic models – development of the concept and an application in the Mekong Delta,* 2011, ISBN 978-3-942036-11-5

208 Hung, Nguyen Nghia: *Sediment dynamics in the floodplain of the Mekong Delta, Vietnam,* 2011, ISBN 978-3-942036-12-2

209 Kuhlmann, Anna: *Influence of soil structure and root water uptake on flow in the unsaturated zone,* 2012, ISBN 978-3-942036-13-9

210 Tuhtan, Jeffrey Andrew: *Including the Second Law Inequality in Aquatic Ecodynamics: A Modeling Approach for Alpine Rivers Impacted by Hydropeaking,* 2012, ISBN 978-3-942036-14-6

211 Tolossa, Habtamu: *Sediment Transport Computation Using a Data-Driven Adaptive Neuro-Fuzzy Modelling Approach,* 2012, ISBN 978-3-942036-15-3

212 Tatomir, Alexandru-Bodgan: *From Discrete to Continuum Concepts of Flow in Fractured Porous Media,* 2012, ISBN 978-3-942036-16-0

213 Erbertseder, Karin: *A Multi-Scale Model for Describing Cancer-Therapeutic Transport in the Human Lung,* 2012, ISBN 978-3-942036-17-7

214 Noack, Markus: *Modelling Approach for Interstitial Sediment Dynamics and Reproduction of Gravel Spawning Fish,* 2012, ISBN 978-3-942036-18-4

215 De Boer, Cjestmir Volkert: *Transport of Nano Sized Zero Valent Iron Colloids during Injection into the Subsurface*, 2012, ISBN 978-3-942036-19-1

216 Pfaff, Thomas: *Processing and Analysis of Weather Radar Data for Use in Hydrology*, 2013, ISBN 978-3-942036-20-7

217 Lebrenz, Hans-Henning: *Addressing the Input Uncertainty for Hydrological Modeling by a New Geostatistical Method*, 2013, ISBN 978-3-942036-21-4

218 Darcis, Melanie Yvonne: *Coupling Models of Different Complexity for the Simulation of* CO_2 *Storage in Deep Saline Aquifers*, 2013, ISBN 978-3-942036-22-1

219 Beck, Ferdinand: *Generation of Spatially Correlated Synthetic Rainfall Time Series in High Temporal Resolution - A Data Driven Approach*, 2013, ISBN 978-3-942036-23-8

220 Guthke, Philipp: *Non-multi-Gaussian spatial structures: Process-driven natural genesis, manifestation, modeling approaches, and influences on dependent processes*, 2013, ISBN 978-3-942036-24-5

221 Walter, Lena: *Uncertainty studies and risk assessment for* CO_2 *storage in geological formations*, 2013, ISBN 978-3-942036-25-2

222 Wolff, Markus: *Multi-scale modeling of two-phase flow in porous media including capillary pressure effects,* 2013, ISBN 978-3-942036-26-9

223 Mosthaf, Klaus Roland: *Modeling and analysis of coupled porous-medium and free flow with application to evaporation processes,* 2014, ISBN 978-3-942036-27-6

224 Leube, Philipp Christoph: *Methods for Physically-Based Model Reduction in Time: Analysis, Comparison of Methods and Application*, 2013, ISBN 978-3-942036-28-3

225 Rodríguez Fernández, Jhan Ignacio: *High Order Interactions among environmental variables: Diagnostics and initial steps towards modeling*, 2013, ISBN 978-3-942036-29-0

226 Eder, Maria Magdalena: *Climate Sensitivity of a Large Lake*, 2013, ISBN 978-3-942036-30-6

227 Greiner, Philipp: *Alkoholinjektion zur In-situ-Sanierung von CKW Schadensherden in Grundwasserleitern: Charakterisierung der relevanten Prozesse auf unterschiedlichen Skalen*, 2014, ISBN 978-3-942036-31-3

228 Lauser, Andreas: *Theory and Numerical Applications of Compositional Multi-Phase Flow in Porous Media*, 2014, ISBN 978-3-942036-32-0

229 Enzenhöfer, Rainer: *Risk Quantification and Management in Water Production and Supply Systems*, 2014, ISBN 978-3-942036-33-7

230 Faigle, Benjamin: *Adaptive modelling of compositional multi-phase flow with capillary pressure*, 2014, ISBN 978-3-942036-34-4

231 Oladyshkin, Sergey: *Efficient modeling of environmental systems in the face of complexity and uncertainty*, 2014, ISBN 978-3-942036-35-1

232 Sugimoto, Takayuki: *Copula based Stochastic Analysis of Discharge Time Series*, 2014, ISBN 978-3-942036-36-8

233 Koch, Jonas: *Simulation, Identification and Characterization of Contaminant Source Architectures in the Subsurface*, 2014, ISBN 978-3-942036-37-5

234 Zhang, Jin: *Investigations on Urban River Regulation and Ecological Rehabilitation Measures, Case of Shenzhen in China*, 2014, ISBN 978-3-942036-38-2

235 Siebel, Rüdiger: *Experimentelle Untersuchungen zur hydrodynamischen Belastung und Standsicherheit von Deckwerken an überströmbaren Erddämmen,* 2014, ISBN 978-3-942036-39-9

236 Baber, Katherina: *Coupling free flow and flow in porous media in biological and technical applications: From a simple to a complex interface description,* 2014, ISBN 978-3-942036-40-5

237 Nuske, Klaus Philipp: *Beyond Local Equilibrium — Relaxing local equilibrium assumptions in multiphase flow in porous media,* 2014, ISBN 978-3-942036-41-2

238 Geiges, Andreas: *Efficient concepts for optimal experimental design in nonlinear environmental systems*, 2014, ISBN 978-3-942036-42-9

239 Schwenck, Nicolas: *An XFEM-Based Model for Fluid Flow in Fractured Porous Media*, 2014, ISBN 978-3-942036-43-6

240 Chamorro Chávez, Alejandro: *Stochastic and hydrological modelling for climate change prediction in the Lima region, Peru*, 2015, ISBN 978-3-942036-44-3

241 Yulizar: *Investigation of Changes in Hydro-Meteorological Time Series Using a Depth-Based Approach*, 2015, ISBN 978-3-942036-45-0

242 Kretschmer, Nicole: *Impacts of the existing water allocation scheme on the Limarí watershed – Chile, an integrative approach*, 2015, ISBN 978-3-942036-46-7

243 Kramer, Matthias: *Luftbedarf von Freistrahlturbinen im Gegendruckbetrieb*, 2015, ISBN 978-3-942036-47-4

244 Hommel, Johannes: *Modeling biogeochemical and mass transport processes in the subsurface: Investigation of microbially induced calcite precipitation*, 2016, ISBN 978-3-942036-48-1

245 Germer, Kai: *Wasserinfiltration in die ungesättigte Zone eines makroporösen Hanges und deren Einfluss auf die Hangstabilität*, 2016, ISBN 978-3-942036-49-8

246 Hörning, Sebastian: *Process-oriented modeling of spatial random fields using copulas*, 2016, ISBN 978-3-942036-50-4

247 Jambhekar, Vishal: *Numerical modeling and analysis of evaporative salinization in a coupled free-flow porous-media system,* 2016, ISBN 978-3-942036-51-1

248 Huang, Yingchun: *Study on the spatial and temporal transferability of conceptual hydrological models*, 2016, ISBN 978-3-942036-52-8

249 Kleinknecht, Simon Matthias: *Migration and retention of a heavy NAPL vapor and remediation of the unsaturated zone*, 2016, ISBN 978-3-942036-53-5

250 Kwakye, Stephen Oppong: *Study on the effects of climate change on the hydrology of the West African sub-region*, 2016, ISBN 978-3-942036-54-2

251 Kissinger, Alexander: *Basin-Scale Site Screening and Investigation of Possible Impacts of CO_2 Storage on Subsurface Hydrosystems*, 2016, ISBN 978-3-942036-55-9

252 Müller, Thomas: *Generation of a Realistic Temporal Structure of Synthetic Precipitation Time Series for Sewer Applications*, 2017, ISBN 978-3-942036-56-6

253 Grüninger, Christoph: *Numerical Coupling of Navier-Stokes and Darcy Flow for Soil-Water Evaporation*, 2017, ISBN 978-3-942036-57-3

254 Suroso: *Asymmetric Dependence Based Spatial Copula Models: Empirical Investigations and Consequences on Precipitation Fields*, 2017, ISBN 978-3-942036-58-0

255 Müller, Thomas; Mosthaf, Tobias; Gunzenhauser, Sarah; Seidel, Jochen; Bárdossy, András: *Grundlagenbericht Niederschlags-Simulator (NiedSim3)*, 2017, ISBN 978-3-942036-59-7

256 Mosthaf, Tobias: *New Concepts for Regionalizing Temporal Distributions of Precipitation and for its Application in Spatial Rainfall Simulation,* 2017, ISBN 978-3-942036-60-3

257 Fenrich, Eva Katrin: *Entwicklung eines ökologisch-ökonomischen Vernetzungsmodells für Wasserkraftanlagen und Mehrzweckspeicher,* 2018, ISBN 978-3-942036-61-0

258 Schmidt, Holger: *Microbial stabilization of lotic fine sediments*, 2018, ISBN 978-3-942036-62-7

259 Fetzer, Thomas: *Coupled Free and Porous-Medium Flow Processes Affected by Turbulence and Roughness – Models, Concepts and Analysis*, 2018, ISBN 978-3-942036-63-4

260 Schröder, Hans Christoph: *Large-scale High Head Pico Hydropower Potential Assessment*, 2018, ISBN 978-3-942036-64-1

261 Bode, Felix: *Early-Warning Monitoring Systems for Improved Drinking Water Resource Protection*, 2018, ISBN 978-3-942036-65-8

262 Gebler, Tobias: *Statistische Auswertung von simulierten Talsperrenüberwachungsdaten zur Identifikation von Schadensprozessen an Gewichtsstaumauern*, 2018, ISBN 978-3-942036-66-5

263 Harten, Matthias von: *Analyse des Zuppinger-Wasserrades – Hydraulische Optimierungen unter Berücksichtigung ökologischer Aspekte*, 2018, ISBN 978-3-942036-67-2

264 Yan, Jieru: *Nonlinear estimation of short time precipitation using weather radar and surface observations*, 2018, ISBN 978-3-942036-68-9

265 Beck, Martin: *Conceptual approaches for the analysis of coupled hydraulic and geomechanical processes*, 2019, ISBN 978-3-942036-69-6

266 Haas, Jannik: *Optimal planning of hydropower and energy storage technologies for fully renewable power systems*, 2019, ISBN 978-3-942036-70-2

267 Schneider, Martin: *Nonlinear Finite Volume Schemes for Complex Flow Processes and Challenging Grids*, 2019, ISBN 978-3-942036-71-9

268 Most, Sebastian Christopher: *Analysis and Simulation of Anomalous Transport in Porous Media*, 2019, ISBN 978-3-942036-72-6

269 Buchta, Rocco: *Entwicklung eines Ziel- und Bewertungssystems zur Schaffung nachhaltiger naturnaher Strukturen in großen sandgeprägten Flüssen des norddeutschen Tieflandes*, 2019, ISBN 978-3-942036-73-3

270 Thom, Moritz: *Towards a Better Understanding of the Biostabilization Mechanisms of Sediment Beds*, 2019, ISBN 978-3-942036-74-0

271 Stolz, Daniel: *Die Nullspannungstemperatur in Gewichtsstaumauern unter Berücksichtigung der Festigkeitsentwicklung des Betons*, 2019, ISBN 978-3-942036-75-7

272 Rodriguez Pretelin, Abelardo: *Integrating transient flow conditions into groundwater well protection*, 2020, ISBN: 978-3-942036-76-4

273 Weishaupt, Kilian: *Model Concepts for Coupling Free Flow with Porous Medium Flow at the Pore-Network Scale: From Single-Phase Flow to Compositional Non-Isothermal Two-Phase Flow*, 2020, ISBN: 978-3-942036-77-1

274 Koch, Timo: *Mixed-dimension models for flow and transport processes in porous media with embedded tubular network systems*, 2020, ISBN: 978-3-942036-78-8

275 Gläser, Dennis: *Discrete fracture modeling of multi-phase flow and deformation in fractured poroelastic media*, 2020, ISBN: 978-3-942036-79-5

276 Seitz, Lydia: *Development of new methods to apply a multi-parameter approach – A first step towards the determination of colmation*, 2020, ISBN: 978-3-942036-80-1

277 Ebrahim Bakhshipour, Amin: *Optimizing hybrid decentralized systems for sustainable urban drainage infrastructures planning*, 2021, ISBN: 978-3-942036-81-8

278 Seitz, Gabriele: *Modeling Fixed-Bed Reactors for Thermochemical Heat Storage with the Reaction System* $CaO/Ca(OH)_2$, 2021, ISBN: 978-3-942036-82-5

279 Emmert, Simon: *Developing and Calibrating a Numerical Model for Microbially Enhanced Coal-Bed Methane Production*, 2021, ISBN: 978-3-942036-83-2

280 Heck, Katharina Klara: *Modelling and analysis of multicomponent transport at the interface between free- and porous-medium flow - influenced by radiation and roughness*, 2021, ISBN: 978-3-942036-84-9

281 Ackermann, Sina: *A multi-scale approach for drop/porous-medium interaction*, 2021, ISBN: 978-3-942036-85-6

282 Beckers, Felix: *Investigations on Functional Relationships between Cohesive Sediment Erosion and Sediment Characteristics*, 2021, ISBN: 978-3-942036-86-3

283 Schlabing, Dirk: *Generating Weather for Climate Impact Assessment on Lakes*, 2021, ISBN: 978-3-942036-87-0

284 Becker, Beatrix: *Efficient multiscale multiphysics models accounting for reversible flow at various subsurface energy storage sites*, 2021, ISBN: 978-3-942036-88-7

285 Reuschen, Sebastian: *Bayesian Inversion and Model Selection of Heterogeneities in Geostatistical Subsurface Modeling*, 2021, ISBN: 978-3-942036-89-4

286 Michalkowski, Cynthia: *Modeling water transport at the interface between porous GDL and gas distributor of a PEM fuel cell cathode*, 2022, ISBN: 978-3-942036-90-0

287 Koca, Kaan: *Advanced experimental methods for investigating flow-biofilm-sediment interactions*, 2022, ISBN: 978-3-942036-91-7

288 Modiri, Ehsan: *Clustering simultaneous occurrences of extreme floods in the Neckar catchment*, 2022, ISBN: 978-3-942036-92-4

289 Mayar, Mohammad Assem: *High-resolution spatio-temporal measurements of the colmation phenomenon under laboratory conditions*, 2022, ISBN: 978-3-942036-93-1

Die Mitteilungshefte ab der Nr. 134 (Jg. 2005) stehen als pdf-Datei über die Homepage des Instituts: www.iws.uni-stuttgart.de zur Verfügung.